Promotor: Dr. B.H. Bijsterbosch, hoogleraar in de fysische en kolloïdchemie

Aan Lie,
Joris en Roeland

Omslagfoto: detail van een polystyreen prop (electronenmicroscoop, T.F.D.L., Wageningen). Deze opname is ter beschikking gesteld door Drs. Th.J.J. van den Hoven, vakgroep Fysische en Kolloïdchemie, Wageningen.

ELECTROKINETIC INVESTIGATIONS ON THE SYSTEM POLYSTYRENE/AQUEOUS ELECTROLYTE SOLUTION

Verification of model theories on dilute and concentrated dispersions

A.G. van der Put

ELECTROKINETIC INVESTIGATIONS ON THE SYSTEM POLYSTYRENE/AQUEOUS ELECTROLYTE SOLUTION

Verification of model theories on dilute and concentrated dispersions

Proefschrift
ter verkrijging van de graad van
doctor in de landbouwwetenschappen,
op gezag van de rector magnificus,
dr. H.C. van der Plas,
hoogleraar in de organische scheikunde,
in het openbaar te verdedigen
op woensdag 14 mei 1980
des namiddags te vier uur in de aula
van de Landbouwhogeschool te Wageningen

Druk: Drukkerij Presikhaaf

Ruitenberglaan 29, 6826 CC Arnhem 1980

ISN - 107584-03

STELLINGEN

I

De 4-elektroden techniek is bij uitstek geschikt voor het correct bepalen van fenomenologische coëfficiënten, van het relaxatiegedrag van een langzaam intrinsiek polarisatieproces en van transportgetallen in een prop of membraan.

Dit proefschrift, hoofdstuk 3 en 7.

II

De stelling van Saville, dat Watillon en Stone-Masui ten onrechte corrigeren voor de elektroforetische bijdrage van geladen deeltjes aan de geleiding van een dispersie, is onjuist.

- D.A. Saville, J. Colloid Interface Sci, 71 477 (1979).
- A. Watillon en J. Stone-Masui, J. Electroanal.Chem. 37, 143 (1972).
- D. Stigter, J. Phys.Chem. 83, 1662 (1979).

III

Wanneer men de invloed van diverse vormen van polarisatie op elektrokinetische verschijnselen niet onderkent, kan dat leiden tot foutieve waarnemingen, alsmede tot onjuiste conclusies met betrekking tot een gestructureerde waterlaag aan het grensvlak.

- D. Eagland, A.P. Allen, J. Colloid Interface Sci, 58, 230 (1977).
- B. Ball, D.W. Fuerstenau, "A review of the measurement of streaming potentials", Miner.Sci. Eng., 5, 267 (1973).
- Dit proefschrift hoofdstuk 3.

IV

De conclusie van De Haan, De Boer en Halma dat de fulvinezuren uit het Tjeukemeer duidelijk eiwitachtig materiaal bevatten, is op grond van het getoonde pyrolyse spektrum op zijn minst gezegd voorbarig te noemen.

M. De Haan, T. de Boer en G. Halma, Freshwater Biology, 9, 315 (1979).

V

Het adsorptiegedrag van (vrijwel) volledig gehydrolyseerd polyvinylacetaat kan in zeer belangrijke mate bepaald worden door de aanwezigheid van een slechts geringe hoeveelheid geconjugeerde carbonylverbindingen in de polymeerketens.

- C.T. de Jonge-Vleugel en B.H. Bijsterbosch, Berichte vom VI Intern. Kongr. für grenzflächenaktive Stoffe, Carl Hauser Verlag, München, Band 2, 469-82, 1973.
- B.J.R. Scholtens, proefschrift (1977), Wageningen, hoofdstuk 3, 4 en 6.

VI

Het verdient aanbeveling om thermodynamische excesfuncties, die de afwijkingen van het ideale menggedrag van binaire systemen beschrijven, weer te geven als ortogonale polynomen met de molfractie als variabele; dit ter vervanging van de algemeen verbreide Redlich-Kister excesvorm.

- N. Brouwer en H.A.J. Oonk, Z.Phys.Chem. N.F. 105, 113 (1977).
- C.W. Bale en A.D. Pelton, Metallurg.Trans. 5, 2323 (1974).

VII

Ten onrechte wordt soms bij beschouwingen over de evenwichts-elastische eigenschappen van rubbernetwerken geheel voorbij gegaan aan het intrinsiek visco-elastische gedrag van polymeren.

b.v. L.R.G. Treloar in 'The Physics of Rubber Elasticity' third edition, Clarendon press, Oxford (1975).

VIII

In het Hoger Beroepsonderwijs voor laboratoriumpersoneel dient de docent bij de behandeling van de basisvakken de bruikbaarheid voor het latere beroepsveld en niet de opbouw van de eigen discipline als uitgangspunt te nemen.

IX

HBO instellingen in Wageningen en omgeving zijn bij uitstek geschikt om samen met de Landbouwhogeschool nieuwe programma's te ontwikkelen op het grensvlak van HBO en WO. Dergelijke programma's zijn onmisbaar om de noodzakelijke differentiatie in het "Hoger onderwijs voor Velen" te realiseren.

X

Dat op enkele terreinen van de Landbouwhogeschool de meeste onderwijskundige activiteiten 's avonds te zien zijn in de STOVA-barakken aldaar, geeft wel aan dat nieuwbouw voor de STOVA beter te rechtvaardigen is dan voor de Landbouwhogeschool.

XI

Het blijven bestaan van actiegroepen kan men relateren aan het blijven zitten van bestuurders.

XII

Het verschil tussen de "Groene long" en een stoflong is in IJzendoorn (gemeente Echteld) maar één bestuursfout groot.

Proefschrift A.G. van der Put
Electrokinetic investigations on the system polystyrene/aqueous electrolyte solution
Wageningen, 14 mei 1980.

Voorwoord

Aan het begin van mijn proefschrift wil ik al degenen, die bij het tot stand komen van mijn werk behulpzaam waren, bedanken.

Allereerst wil ik mijn ouders bedanken voor de gelegenheid welke jullie mij geboden hebt om te kunnen gaan studeren. Jullie hebben het fundament gelegd voor mijn vorming.

Beste Bert, hooggeleerde promotor, jouw voorstel om in een breed opgezet elektrokinetisch onderzoek aan een modelsysteem speciale aandacht te geven aan een beschrijving van de experimenten op basis van de irreversibele thermodynamica en membraantheorieën, is zeer waardevol gebleken. Ik wil mijn waardering uitspreken voor de vrijheid in de uitwerking van de opdracht en voor je hulp in de periode van het schrijven, voor je kritische bestudering en vooral voor je grondige korrektie van het manuscript.

Met plezier denk ik terug aan de vier jaar samenwerking met vele medewerkers van de vakgroep Fysische en Kolloïdchemie gedurende de praktikumperiode. De waardevolle diskussies hebben mij het betreden van het voor mij nieuwe vakgebied van de kolloïdchemie vergemakkelijkt. Dat het verrichte onderzoek zeker geen individuele zaak was, moge blijken uit het volgende.
Willem Norde heeft mij wegwijs gemaakt in de technieken van de latexbereiding. Ronald Wegh heeft onvervangbaar werk verricht bij de opbouw van de elektronische apparatuur, waardoor het mogelijk was om in korte tijd betrouwbare experimentele gegevens te verzamelen. Simon Maasland en Henny van Beek hebben de zo belangrijke prophouder en opstelling helpen ontwikkelen. De gesprekken met Joost Mertens over het dielektrische en elektrokinetische werk gedurende de periode van samenwerken, zijn van direkt belang geweest bij het uitwerken van diverse experimentele en theoretische problemen. Herman van Leeuwen heeft bijgedragen tot het begrijpen van de polarizatieverschijnselen. Karel Peverelli heeft het komputerwerk verricht van hoofdstuk 7. Het radiochemische werk en het grootste deel van de titraties en elektrophorese experimenten werden nauwgezet uitgevoerd door Peggy Bosman. Tenslotte wil ik mijn kamergenoot Boudewijn Scholtens bedanken voor de plezierige periode alsmede Willem van Maanen, Ben Spee en het sekretariaat voor de prettige samenwerking en de vele bewezen diensten.

De figuren werden zorgvuldig getekend door Gert Buurman, die ook het fotografische werk verzorgde.

Ook buiten de vakgroep heb ik uitgebreide steun ontvangen; Peter van der Kamp, jou wil ik speciaal noemen voor de vele uren die je gestoken

hebt in het vertalen van russische artikelen en het vervaardigen van diverse rekenprogramma's.

De afdeling Tekstverwerking van de Landbouwhogeschool wordt van harte bedankt voor de vakkundige verwerking van het manuscript.

Richard Akers, I am very much indebted to you for correcting the major part of the English text in a very short time.

Enkele persoonlijke gegevens

De schrijver van dit proefschrift werd op 4 april 1947 te Rotterdam geboren. Na het behalen van het diploma H.B.S.-b aan de Christelijke H.B.S. "Henegouwerplein" te Rotterdam begon hij in september 1965 zijn chemiestudie aan de T.H. te Delft. In december 1969 werd het kandidaats examen afgelegd en in november 1971 het ingenieursexamen (fysisch-chemische richting). Het afstuderen vond plaats onder leiding van prof.dr. H.R.K.N. Janeschitz-Kriegel met als hoofdvak Macromoleculen en met de bijvakken Fysische transportverschijnselen en Tensoranalyse. Tijdens de studie en de daaropvolgende militaire dienst werden eerste-graadsbevoegdheden in scheikunde, natuurkunde en wiskunde behaald. Na het vervullen van de militaire dienst was hij van augustus 1973 tot en met juli 1977 als wetenschappelijk medewerker in tijdelijke dienst met een gedeelde onderwijs- en onderzoektaak werkzaam op het laboratorium voor Fysische en Kolloïdchemie van de Landbouwhogeschool te Wageningen.

Sins augustus 1977 is hij als docent verbonden aan de Stichting tot Opleiding van Analisten (STOVA) te Wageningen.

CONTENTS

CHAPTER 1

INTRODUCTION

1.1 *Aim of the investigation*

In and across porous media a variety of transport processes and related phenomena can take place, e.g. ion migration, diffusion and self-diffusion, osmosis, hydraulic flow, electro-osmosis, streaming potential and streaming current, salt filtration and membrane potentials. Many of these phenomena have been the subject of considerable study in physical-chemical as well as in colloid chemical literature[1-3]. All compound transport phenomena involving the diffusive and hydrodynamic flow processes depend primarily on the concentration of the dispersed phase and the electrosurface properties of the dispersed system. A typical manifestation of the electrical double layer is constituted by the electrokinetic phenomena, which result from either flow of liquid (streaming potential, streaming current) or from particle displacement as a result of an applied electrical field (electro-osmosis, electrophoresis) In recent years special attention has been given to the connection between macroscopic physico-chemical properties of a dispersion and the structure and all the relevant parameters of the material constituting the dispersion[4]. The important theoretical developments concerning the structure of the double layer and the relationships between electrical double layer properties and electrokinetic phenomena have greatly improved the understanding of transport phenomena in many field of science and engineering. Some examples may serve to illustrate this.

Electrokinetic mechanisms have been suggested to explain a variety of biological phenomena ranging from action potentials to watertransport.[3,5] The actual values of electrokinetic parameters allow estimates of the plausibility of such mechanisms, while yielding information about the membrane structure and the existence of charged aqueous channels in cell membranes.

The movement of ions through the soil pores and along the clay surfaces towards the adsorption sites of roots bears two important aspects. The first aspect relates to the tortuosity of the dispersion. Investigations to this field are a prerequisite to a quantitative study of the second aspect, namely the effects of electrically charged particles on ion movement, convection, anion exclusion (negative adsorption) and electrokinetic coupling phenomena.

Many fundamental double layer studies on model systems are partly

based on the information obtained from electrokinetic phenomena on particle dispersions (e.g. review by Bijsterbosch and Lyklema[6]). Such studies are, e.g., imperative for the understanding of the effect of surface forces in filtration processes that remove cooloidal pollutants form drinking water (e.g. Wnek et al.[7]).

Theoretical treatments have been advanced to predict the electrophoretic velocity of a single isolated sphere (Wiersema, Overbeek, Booth[8]), incorporating the polarization concept, even in combination with anomalous conduction (Dukhin, Semenikhin[9]). Particularly promessing are recent developments in the polarization theory. Dukhin and Semenikhin succeeded in deriving an analytical expression for the dipole moment of a spherical particle induced by an electric field, which allows the construction of formulae for the conductivity of particle dispersions.

It has often been established that the electrokinetic properties of a particle dispersion are sensitive to mutual interaction and cannot simply be related to the structure of the electrical double layer of an *isolated* particle[10,11]. Overbeek's work[12], e.g., stressed the uncertainty about the correction of the electrokinetic potential for surface conductance of porous plugs. A theoretical investigation of transport processes in porous media is in principle precluded by the immensely complicated, usually undefined, geometric structure of the porous medium. Hence, a geometric model for the porous medium must be introduced which simultaneously incorporates the effects of double layer interaction, double layer polarization and the possibility that conduction can take place between the shear plane and the solid surface (anomalous conduction).

For concentrated dispersions capillary and cell models have been proposed in literature. Especially Levine's cell model[13] is rather promissing because it incorporates both the effect of double layer interaction and the concept of double layer polarization.

When studying the experimental literature on the effect of solid concentration on electrokinetics, it becomes apparent that little more than qualitative and fragmentary insight has been gained. In some cases systems were too poorly defined to enable a test of recent theories; in others, the experimental situation dealt with was so complex that, in the present state of knowledge a deeper insight can hardly be reached. If we are to gain any fundamental understanding of the effect of porosity on the various transport processes within the dispersion, we need a well-defined model system and sophisticated techniques. For an modelbased theoretical investigations, important conditions are that the particles constituting the dispersion are spherical and that their surface charge density remains constant upon changes in particle- and electrolyte concen-

tration. A monodisperse polystyrene latex dispersion seems to be an ideal model system.

The aim of this thesis is to systematically investigate the factors which determine the electrokinetic and electroconducting properties in dilute and concentrated well-defined dispersions. To that purpose we prepared and characterized polystyrene latex dispersions covering an extended surface charge density range. Much attention will be given to the preparation of isotropic concentrated dispersions.

For the evaluation of the electrokinetic phenomena it is mandatory to have excess to the true values of the relevant electrical parameters. Therefore, the influence of various forms of polarization on the electrokinetic properties will by studied. In the colloid-chemical literature remarkably little attention has been given to concentration polarization phenomena, which are so well-known in membrane studies. However, we may expect that even for coarse porous systems polarization problems may arise at low ionic strength.

The experimental results will be used to analyse recent model-based theories. Special attention will be given to the applicability of theoretical formulae for the electrical conductivity of heterogeneous systems either or not comprising an electrical double layer. The model system will be critically examined and analysed with the electrophoresis technique where the influence of double layer overlap is excluded. This also allows more definite conclusions to be drawn about the theories used. Another objective is to study the hydrodynamic behaviour of the polystyrene plugs which allows an evaluation of the electroviscous effect and enables to compare the results with theoretical predictions based upon cell and capillary models. The concept of anomalous conduction will prove to be very useful.

1.2. *References*

1. J.Th.G. Overbeek, in H.R. Kruyt Ed. "Colloid Science" Vol.I, Elsevier, Amsterdam (1952)
2. S.S. Dukhin, B.V. Derjaguin, "Electrokinetic Phenomena", in Surface and Colloid Science, E. Matijević, Ed., Vol.7 (1974)
3. N. Lakshminarayanaiah, Transport Phenomena in Membranes, Academic Press, New York, (1969)
4. G.H. Neale, W. Nader, AIChE J., 19, 112 (1973); 20, 530 (1974)
5. R. de Levie, Electrochemistry of artificial ultra thin lipid membranes. A review J. Electroanal. Chem. 69, 265 (1976)
6. B.H.. Bijsterbosch and J. Lyklema, Adv. Colloid Interface Sci., 9, 147 (1978)
7. W.J. Wnek, D. Gidaspow and D.T. Wasan, Chem. Eng. Sci., 30, 1935 (1975)

8. P.H. Wiersema, Thesis, Utrecht, Netherlands, 1964; P.H. Wiersema, A.L. Loeb, J.Th.G. Overbeek, J. Colloid Interface Sci. 22, 78 (1966)

9. Ref. 6-9, chapter 6.

10. J.H.M. Möller, G.A.J. van Os and J.Th.G. Overbeek, Trans. Faraday Soc. 57, 325 (1961)

11. R.P. Long, S. Ross, J. Colloid Interface Sci. 26, 434 (1968)

12. J.Th.G. Overbeek, P.W.O. Wijga, Rec. trav. chim. 65, 556 (1946); -, W.T. van Est, ibid., 71, 97 (1952)

13. S. Levine, G. Neale and N. Epstein, J. Colloid Interface Sci. 57, 424 (1976)

CHAPTER 2

POLYSTYRENE LATICES

2.1 *Preparation and characterization*

Within the last decade a number of studies has been made on the preparation of monodisperse latices, with the purpose to obtain a wide variety in final particle charges and diameters. For this study it was mandatory that the particle charge remained constant during the storage period, the preparation of the plugs and the rather time-consuming electrokinetic investigations. The latices were therefore prepared without the addition of emulsifying agents by practically adopting the procedure of Kotera, Furusawa and Takeda[1].

By varying the polymerization conditions such as the initiator concentration and the ionic strength, the surface charge density, σ_o, could easily be varied by a factor of 10 while keeping the particle diameter fixed. A detailed description of the slightly modified procedures of Kotera et al. and the methods of characterizing the surface groups on the latices has been given by Furusawa et al.[2], Norde[3] and Bijsterbosch[4].

All latex samples have been ion-exchanged three times with extensively purified Dowex exchange resins, according to Van den Hul and Vanderhoff[5]. In case the latices had to be stored for several months, the surface groups were converted into the K^+-form by titrating just up to the equivalence point.

Conductometric and potentiometric titration of the ion-exchanged samples in a N_2-atmosphere gave evidence that the surface charge is only made up of SO_4^--groups originating from the $K_2S_2O_8$ being used for the initiation of the polymerization reaction. All titrations were performed with a solid content exceeding 6% and for each titration samples of about 70 ml were used. The reproducibility was better than 3%. Particle sizes were determined using a Philips EM 300 electron microscope. From each sample about 150 particles were sized. The dispersity of a latex sample has been expressed by the uniformity coefficient, D_{32}/D_{10}, where

$$D_{32} = \sum_i n_i D_i^3 / \sum_i n_i D_i^2 \qquad (2\text{-}1)$$

n_i is the number of particles with diameter D_i abd D_{10} is the number-average particle diameter given by:

$$D_{10} = \sum_i n_i D_i / \sum_i n_i \qquad (2\text{-}2)$$

Table 2-1 contains the pertinent data of the latices used in the electrokinetic study. All latices were periodically tested electrophoretically. Even during a 2½ year storage no change in the mobility could be detected (see chapter 6).

Table 2-1. Characteristics of the ion-exchanged surfactant-free latices

sample code	$c(K_2S_2O_8)\times10^4$ M	$c(KHCO_3)\times10^3$ M	$-\sigma_o$ μCcm^{-2}	D_{10} nm	D_{32}/D_{10}
L	3.71	-	0.91	506	1.002
M	18.5	10.0	4.00	610	1.001
H	37.4	5.0	9.21	580	1.004

2.2 *Chloride adsorption measurements**

An important condition for a quantitative electrokinetic investigation is the precise knowledge of the actual surface density. In view of the relatively low titration charge densities any small reversible or irreversible co-ion adsorption would significantly to σ_o, so its absence had to be thoroughly verified. Since in the electrokinetic studies silver-silverchloride electrodes were used, we performed adsorption measurements with chloride ions. Two analytical methods were used, viz.

1) an electrochemical method enabling to detect adsorption for concentrations up to 2 10^{-3}M KCl. This limit was determined by the solid content of the latex samples and the supposition that co-ion adsorption will not surpass some $\mu C/cm^2$.
2) a radiochemical method, enabling to detect irreversible adsorption for concentrations up to 10^{-1}M.

The procedures were as follows:

ad 1: 5 ml of the latex sample with a volume fraction of the solid, p, of about 0.08, was mixed with 5 ml of less than 10^{-2}M KCl and equilibrated for one hour. The mixture was subsequently centrifuged and 5 ml of the supernatant was pipetted into an Erlenmeyer flask containing 25 ml 1M KNO_3. The chloride concentration was determined potentiometrically using a combination of a silver-silverchloride and a calomel electrode. In order to standardize the procedure, tests were performed with blank solutions of approximately the same concentration. Thus, any deviations caused by adsorption of chloride ions on the plastic centrifuge tube were automatically corrected for.

* The radiochemical measurements were carried out in the Institute for Atomic Sciences in Agriculture (ITAL). Thanks are due to Ir.J.F. Stoutjesdijk and other institute members for their helpful remarks.

No chloride adsorption on the latex could be detected. The confidence limit was ± 0.2 μCcm^{-2} at 10^{-3}M KCl. Experiments, inwhich the rest period was substantially varied (up to 3 days), gave essentially the same results. To examine whether possible systematic errors introduced by using the salt bridge were absent, the same tests were repeated with a phtalate buffer (25g $KHC_8H_4O_4$/l) instead of the KNO_3 solution, using a glass electrode as the reference electrode. However, the results of these tests also showed that chloride ion adsorption does not have to be considered at least not at concentrations below 2 10^{-3}M.

ad 2: for the conditioning of the radiochemical experiments a 0.46 M $H^{36}Cl$ solution was used (0.05 mCi, supplied by the Radiochemical Centre, Amsterdam). Besides the direct analysis of the supernatant the sediment was also tested separately on irreversible chloride adsorption. For the first determination 1 ml of the supernatant was pipetted into an ampoule containing 20 ml scintillation liquid made up according to Bruno and Christian[5]. For the latter determination the coagulated sediment was thoroughly rinced with water and dried for the determination of its mass. Subsequently, 10 ml lumagel solution (Lumac AG, Basel) was added to suspend the sample. The radioactivity of both solutions was measured using a standard scintillation counter (Mark I, Searle). The chloride concentrations of the samples were calculated by comparison with the standard solutions. The direct measurement again showed the absence of chloride adsorption for concentrations below 2 10^{-3}M with an uncertainty limit below ± 0.1 μCcm^{-2}. The results of the analysis of the sediments, expressed as charge densities, are presented in table 2-2.
The results at high c suggest that some adsorption starts to take place;

Table 2-2. Results of the irreversible chloride adsorption measurements; c is the electrolyte concentration at which the latex samples were equilibrated

c(KCl)	$-\sigma_{Cl^-}$ $\mu C/cm^2$		
moles/l	L	M	H
10^{-1}	0.23	0.25	0.13
10^{-2}	0.02	0.04	0.04
10^{-3}	< 0.01		
5 10^{-4}			
10^{-4}			

however it may also be related to a non-complete purification of the sediment. At any rate, at low c complications due to chloride adsorption can be disregarded. Only above 2 10^{-3}M have we to be alert for a possible reversible adsorption.

2.3 *References*

1. A. Kotera, K. Furusawa, Y. Takeda, Kolloid-Z.u.Z.Polymere 239, 677 (1970); A. Kotera, K. Furusawa, K. Kudo, 240, 837 (1970)
2. K.Furusawa, W. Norde, J.Lyklema, Kolloid-Z.u.Z. Polymere 250, 908 (1972)
3. W. Norde, Mededelingen Landbouwhogeschool, Wageningen, 76-6 (1970)
4. B.H. Bijsterbosch, Colloid & Polymer Sci., 256, 343 (1978)
5. H.J. van den Hul, J.W. Vanderhoff, J. Colloid Interface Sci. 28, 336 (1968)
6. G.A. Bruno, J.E. Christian, Anal. Chem. 33, 1216 (1961)

CHAPTER 3

EXPERIMENTAL PROCEDURES FOR THE MEASUREMENT OF ELECTROKINETIC PROPERTIES OF CHARGED POROUS SYSTEMS UNDER CONDITIONS OF POLARIZATION

3.1 *Introduction*

In this chapter we will describe and summarize the mechanisms of the influence of various forms of polarization on the determination of electrokinetic properties of charged porous systems. Several electrokinetic phenomena have been extensively studied and are comparatively well understood. Summaries of the experimental observations and theories about streaming potential and electro-osmosis may be obtained in standard references[1-6].

Remarkably little attention is given in electrokinetic research to polarization phenomena resulting from discontinuities in transport numbers between a porous phase and adjacent solution. One might expect that the peculiar phenomena so well known for membranes would also manifest themselves for coarse porous systems at relatively low ionic strenghts where the effect of negative adsorption becomes important. Thus, liquid and/or current flow through the selective coarse porous system give rise to diffusion-convection or diffusion-convection-electromigration phenomena at the interfaces[7-10], consequently influencing the local interfacial concentrations. These would, in turn cause local transient osmotic flows and diffusion potential differences. This could well obscure the determination of the important quantities as streaming potential, electro-osmosis, d.c. resistance and permeability. In fact in the past this transport number effect has been neglected in electrokinetics research.

An electrokinetic property less extensively studied than other phenomena is the streaming current. At first sight, there is no definite need for studying the streaming current because an indirect determination from streaming potential and d.c. resistance renders the same information; the choice between the direct and indirect determination then being a matter of the required accuracy. In nearly all electrokinetic research the indirect method is preferred, mainly for sake of convenience. However, the required resistances were often determined at one frequency only (even in recent studies) and treated as d.c. values without any comment. In some cases[11-13], the effect of frequency on the system was investigated over a limited frequency range and the resistance was chosen at that frequency where the resistance did not change significantly or the a.c. resistances were extrapolated to infinite frequency to eliminate polarization effects at the electrode- (and plug/membrane-) solution interfaces.

It is well known from dielectric studies (e.g. Rosen[14], Schwan[15]) that high frequencies may also cause relaxation of the system under study. However, a prerequisite for testing polarization theories with respect to the electrokinetic potential and resistance is the determination of d.c. quantities. Thus the applied frequency, must be low enough to allow the development of complete (intrinsic) polarization. Generally, it is rather difficult, especially for concentrated dispersions to separate intrinsic and electrode polarization phenomena and to obtain a fully corrected resistance at zero frequency. It is clear that determination of the resistance with the direct current technique may also be obscured by a slow intrinsic polarization proces and/or by concentration polarization due to the system's selectivity. A rather extensive electrokinetic study on cellulose fiber plugs by Goring et al.[16] has clearly shown the usefulness of performing streaming current experiments. The substantial difference between the streaming current computed from an a.c. resistance and the streaming potential and the measured streaming current together with an observed frequency dispersion in the resistance pointed to the existence of a pronounced low frequency dispersion. Similar results were recently obtained by Sidorova et al.[17] using a quartz fiber system. The problem is knowing wether or not the streaming current measurement is complicated by polarization phenomena. Koszman and Gavis[18] have already pointed to the possible effect of the concentration polarization mechanism at the electrodes during charge generation. Neale and Peters[19] stated that they were able to readily detect any polarization by the current flowing in the opposite direction when the flow of the liquid was stopped. Pravdić et al.[20] noted that short liquid pulses prevented electrolysis effects in the material studied, as well as polarization of the platinum electrodes. Similar remarks were made for methods which were based on the shunt method of Eversole et al.[21]; fast measurements were required in order to reduce polarization effects. In most other studies[22-25] streaming current measurements were performed by taking the difference in the current following a pressure change. The technique however may easily mask transient phenomena. Huber et al.[26] only take note of the fact that when the electrodes are short-circuited but not attached to the plug surfaces a potential drop invariably occurs; the net current through the plug being reduced. Such an 'ohmic polarization' does not, however, give rise to transient effects. Methods based on the alternating streaming current measurements[27,28] may mask, but not eliminate the mentioned polarization effects.

There is much reason to question if real streaming currents were measured since no independent check methods were applied.

It is clear that this subject calls not only for a careful experimental technique which allows determination of all electrokinetic quantities and the influence of the various polarization phenomena, but also for an experimental technique of plug preparation.

In this chapter we will discuss, not only in which way the experimental methods must be arranged in order to get the correct (d.c.) information, but also procedures to obtain additional information about the system under investigation.

First of all we will briefly summarize the principles of the irreversible thermodynamics which will be used in the theoretical treatment of the various polarization phenomena encountered in electrokinetic measurements.

3.2 *Phenomenological relations between fluxes and forces*

Transport phenomena taking place in a two compartment system separated by a charged porous plug or membrane can often quite conveniently be characterized purely phenomenologically[29,30]. The advantage of such an approach is that one does not have to refer to model theories. The set of phenomenological equations describing the relations between driving forces and corresponding fluxes unequivocally defines the experimental conditions which have to be fulfilled in order to obtain the proper values of the coefficients. Moreover, these equations also help to draw attention to experimental irregularities which, if they are not recognized, would invalidate molecular model interpretations.

The phenomenological equations are based on the theory of thermodynamics of irreversible processes. This approach can be envisages by considering an isothermal system consisting of two aqueous solutions containing only one permeable electrolyte seperated by a membrane or porous plug. Differences in solute concentration, pressure and electrical potential result in three forces and three conjugated flows. Kedem and Katchalsky[31,32] define the flows as the macroscopic quantities: volume flow J_v, solute flow J_s, and electric current I. The conjugated driving forces are, respectively, the total "mechano-osmotic" driving force, $(\Delta P - \Delta\pi_s)$, the difference in the chemical potential of the salt, $\Delta\mu_s$, and the electromotive force E. ΔP is the hydrostatic pressure difference across the porous plug; $\Delta\pi_s$ is the osmotic pressure difference between the two solutions. It is customary to define the chemical potential difference as $\Delta\mu_s = \Delta\pi_s/\tilde{c}_s$, where $\tilde{c}_s$ is the mean solute concentration or logarithmic average concentration. For ideal solutions $\tilde{c}_s$ is defined by the expression[32]:

$$\check{c}_s = \Delta\pi_s \,/\, RT\,\Delta \ln a_s \qquad (3\text{-}1)$$

where a_s is the solute activity.

In a system not far from equilibrium the fluxes J_i are linearly dependent on the respective driving forces, X_i. Darcy's law, Ohm's law and Fourier's law are well known examples of such linear relationships between conjugated forces and fluxes. In general, allowance must be made for coupling phenomena, implying that a given flux also depends on a non-conjugated driving force. Assuming the validity of the linear superposition principle, the mathematical description of the force/flux relation then becomes:

$$J_i = \sum_{k=1}^{n} L_{ik} X_k \qquad (i,k = 1,2\ \ldots.n) \qquad (3\text{-}2)$$

where L_{ik} represents the phenomenological coefficients. L_{ii} (i=k) are the "conductivity" coefficients, whereas L_{ik} ($i \neq k$) constitute the coupling or interaction coefficients. The latter obey Onsager's well known reciprocity relation:

$$L_{ik} = L_{ki} \qquad (3\text{-}3)$$

Applying eq. (3-2) to the set of forces and fluxes given above, the following set of phenomenological flow equations is obtained:

$$\begin{aligned} J_v &= L_{11}\,(\Delta P - \Delta\pi_s) + L_{12}\,E + L_{13}\,\Delta\pi_s/\check{c}_s \\ I &= L_{21}\,(\Delta P - \Delta\pi_s) + L_{22}\,E + L_{23}\,\Delta\pi_s/\check{c}_s \\ J_s &= L_{31}\,(\Delta P - \Delta\pi_s) + L_{32}\,E + L_{33}\,\Delta\pi_s/\check{c}_s \end{aligned} \qquad (3\text{-}4)$$

Onsager's relation reduces the nine phenomenological coefficients to six independent coefficients which characterize the system completely. Because of the linear relationship of forces and fluxes, equations (3-2) - (3-4) may be transformed into expressions containing convenient experimental variables. Kedem and Katchalsky[31] have shown, for example, that the above set of equations can be written in terms of six so-called "practical" transport coefficients:

$$J_v = L_p(\Delta P - \Delta\pi_s) + \beta I - \sigma L_p \Delta\pi_s \qquad (3\text{-}5a)$$

$$J_s = \check{c}_s(1-\sigma)J_v + (t_i/v_1 z_1 F_a)I + \omega\Delta\pi_s \qquad (3\text{-}5b)$$

$$I = (\kappa^*\beta/L_p)J_v + \kappa^* E + \kappa^* t_1/(\check{c}_s v_1 z_1 F_a)\,\Delta\pi_s \qquad (3\text{-}5c)$$

where L_p denotes the filtration coefficient, σ the reflection coefficient ($o \leqslant \sigma \leqslant 1$), β the electro-osmotic permeability, ω the solute permeability, t_1 the counterion transport number and κ^* the electrical conductance at zero volume flow. The parameters ν_1, z_1 and F_a are the dissociation number and valence of the counterions, and the Faraday constant, respectively. The practical transport coefficients are mathematically related to the original set of phenomenological coefficients L_{ik}. From eq. (3-5a,b,c) it can be deduced that:

$$L_p = \left(\frac{J_v}{\Delta P - \Delta \pi_s} \right)_{\Delta \pi_s, I} \tag{3-6}$$

$$\beta = \left(\frac{J_v}{I} \right)_{\Delta P; \Delta \pi_s} \tag{3-7}$$

$$\tilde{c}_s(1-\sigma) = \left(\frac{J_s}{J_v} \right)_{\Delta \pi_s, I} \tag{3-8}$$

The subscripts in these equations indicate the variables kept constant (zero) during the measurements. The advantage of the practical transport coefficients is that they can be determined experimentally, whereas the original phenomenological coefficients cannot or only with great difficulty. In electrokinetic research we confine ourselves to an isothermal two compartment system separated by a charged porous plug, inwhich the two compartments contain solutions of the same electrolyte. In the absence of concentration differences the system's electrokinetic behaviour can be described in terms of only two driving forces, a pressure difference and an electromotive force.

The electrokinetic phenomena investigated in this study are listed in table 3-1, where we have expressed the quantities in terms of L-values and practical coefficients. The definitions prescribe the pertinent experimental conditions in an unequivocal way. Thus the permeability at zero electromotive force can in principle be obtained from the measurement of the volume flux at given ΔP provided that no streaming potential originates during the measurements. This can be realized experimentally by short-circuiting two electrodes at either side of the plug or membrane. In other words the permeability must be measured under the same conditions as the streaming current. If we are to trust measurements involving electrical currents, we must be sure that no polarization processes occur at the electrodes. In other words the charging and discharging processes at the electrodes should be fast enough to process the hydrodynamically transported net charge in the plug or membrane (convection current). This condition obviously also concerns the measurement of the streaming currents. If for some reason or another the passage of current through the electrodes is impeded - e.g. by polarization or electrode spacing -

Tabel 3.1. Some electrokinetic and transport phenomena; all relations are defined for zero $\Delta\pi_s$

name	defenition	L-coefficients	practical coef.
streaming current	$(I/\Delta P)_E$	L_{21}	
streaming potential	$(E/\Delta P)_I$	$-L_{21}/L_{22}$	$-\beta$
electro-osmotic flow	$(J_v/I)_{\Delta P}$	L_{12}/L_{22}	β
electro-osmotic pressure	$(\Delta P/I)_{J_v}$	$L_{21}^{-1}\,(1-L_{22}L_{11}/L_{12}^2)^{-1}$	$-\beta/L_p$
hydrodynamic permeability	$(J_v/\Delta P)_E$	L_{11}	
filtration coefficient	$(J_v/\Delta P)_I$	$L_{11}[1-L_{12}^2/(L_{11}L_{22})]$	L_p
electrical conductance	$(I/E)_{\Delta P}$	L_{22}	
electrical conductance at zero flow	$(I/E)_{J_v}$	$L_{22}[1-L_{12}^2/(L_{11}L_{22})]$	κ^*

a potential drop is generated across the porous phase and the convection current will partly be compensated by charge flow in the opposite direction through the plug.

When substantial coupling of ion flow and volume flow ($L_{12} \neq 0$) occurs, the filtration coefficient at zero electric current (convection current = conduction current), L_p, will differ markedly from the "straight" coefficient L_{11}. The measurement of L_{11} implies the measurement of J_v as a function of the pressure difference, while $\Delta\pi_s$ and E are kept zero. For selective systems, such as charged plugs or membranes, a pressure difference will give rise to increasing concentration differences over both plug boundaries, and consequently to an increase in $\Delta\pi_s$ and E. The primary flux resulting from the applied pressure difference generates secondary forces, $\Delta\pi_s$ and E, and consequently the measured ratio $J_v/\Delta P$ does not equal the straight coefficient L_{11}.

If for instance water is forced through a charged porous system, the secondary force E will generate a counterelectro-osmotic flow, thereby decreasing the volume flow (electroviscous effect). If an electrolyte solution is forced through a more or less selective system, filtration of the electrolyte is brought about by the operation of the Donnan principal[33] (negative adsorption; co-ions excluded from the porous phase). This salt filtration effect gives rise to a time dependent osmotic pressure difference, and a time dependent accumulation of electrolyte at the high pressure side and a depletion at the low pressure side.

3.2.1 *Non-steady state phenomena*

If the required experimental conditions cannot be held constant during the course of an experiment, non-stationary processes will occur, giving rise to time dependent electrokinetic phenomena. The reason for the occurrence of these effects is that quantities such as transport numbers and conductance are not constant throughout the system. E.g., in a streaming current experiment, the passage of current through the short circuited electrodes attached to the plug or membrane leads to concentration polarization and consequently to an increasing diffusion resistance. This means that the necessary condition for the determination of the streaming current, E = 0, cannot be realized continuously.

Of course, one could arrange such experimental methods so as to avoid spurious results. However, one can also profit from them, because they can provide us with useful additional information about the system under investigation.

3.3 *Concentration polarization phenomena in connection with streaming potential measurements*

If a pressure difference is applied to a charged plug or membrane, a streaming potential originates. In the case of a permselective membrane or porous plug ($0 < \sigma < 1$) in addition salt filtration is brought about as a result of the Donnan principle. Due to an accumulation of electrolyte at the high pressure side and a depletion at the low pressure side a concentration potential is superposed on the streaming potential and a transient rise of the potential is observed[34-37]. Even in the case of macroporous materials such as plugs formed from colloidal dispersions this effect takes place. The result of co-ion exclusion is particularly operative in a concentration range in which the double layer thickness is of the same order of magnitude as the mean pore diameter. Then the ratio of the molar salt flux (moles/s) to the volume flux of water (cm^3/s) will be less than the molar salt concentration at the high pressure side. The selectivity due to the Donnan effect is strongly dependent on the ionic strenght. Consequently, during a streaming potential experiment, the selectivity (reflection) at the high-pressure side will decrease as the salt concentration increases due to the accumulation process. The decrease in selectivity will give rise to a time dependent salt flux in the plug. At the low-pressure side the composition of the liquid leaving the plug is initially determined by the undisturbed equilibrium composition; the period for which this holds is determined by the porosity, the plug length and the volume flow rate. Within this time span the induced

concentration gradient at the low pressure side will be fully determined by the constant concentration difference between bulk and pore liquid, the liquid flux J_v and the diffusion flux from bulk to plug. Under such conditions the concentration profile at the low pressure side and its effect on the streaming potential can be calculated. The problem of a time-dependent streaming potential has been recognized by Schmid and Schwarz[38] and, more recently, treated by Brun and Vaula[35]. Brun et al. derived an equation for complete Donnan exclusion. We will extend this treatment to the case of an arbitrary but constant σ during the accumulation of electrolyte. Because for macroporous systems the selectivity depends on the negative adsorption of co-ions and is thus very sensitive to concentration changes, this treatment will only be valid for small concentration differences.

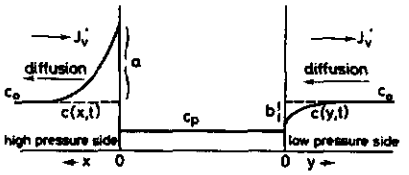

Fig. 3-1. Concentration profiles near a selective plug; the arrows indicate the directions of the volume and diffusion flows. a and b refer to accumulation and depletion respectively.

Fig. 3-1 represents schematically the concentration profile at a certain time t after the application of a constant pressure difference. As a matter of fact the profile at the high pressure side, c(x,t), and that at the low pressure side, c(y,t), are interrelated through the plugs selectivity behaviour. In the derivation of both profiles, however, we will neglect this interrelation.

3.3.1 *The concentration polarization at the high pressure side*

The non-steady state macroscopic mass balance at the high pressure side is given by the differential equation:

$$\frac{\delta c(x,t)}{\delta t} = D \frac{\delta^2 c(x,t)}{\delta x^2} + J_v^1 \frac{\delta c(x,t)}{\delta x} \qquad (3\text{-}9)$$

where
- $c(x,t)$ = electrolyte concentration of external solution
- D = diffusion coefficient of the electrolyte in the external solution
- J_v^1 = convection velocity in the external solution
- x = distance from plug boundary at high pressure side
- t = time.

The boundary conditions to be used in solving this equation are:

a. at $t = 0$ and $x \geq 0$: $c(x,t) = c_o$ (3-10)

b. at $t > 0$ and $x = \infty$: $c(x,t) = c_o$ (3-11)

c. $$D\left(\frac{\delta c(x,t)}{\delta x}\right)_{x=o} = \frac{-\sigma J_v^1}{1+\omega^*/J_v^1 - \frac{1}{2}(1-\sigma)} c(o,t) \qquad (3\text{-}12)$$

where $\omega^* = \omega^1 vRT$; $v = v^+ + v^-$

ω^1 = solute permeability per unit area

$c(o,t)$ = concentration at plug boundary.

Eq. (3-12) relates the concentration profile to the plug's selectivity properties and to the experimental conditions, as expressed by quantities σ, ω^1 and J_v^1. It is derived from the following considerations. The net solute flux density in the external solution is:

$$J_s^1(x,t) = J_v^1 c(x,t) + D\frac{\delta(x,t)}{\delta x} \qquad (3\text{-}13)$$

At the plug boundary ($x=o$):

$$J_s^1(o,t) = J_v^1 c(o,t) + D\left(\frac{\delta c(x,t)}{\delta x}\right)_{x=o} \qquad (3\text{-}14)$$

From (3-5b) $J_s^1(o,t)$ is obtained as (zero electric current):

$$J_s^1(o,t) = \tilde{c}_s(t)(1-\sigma)J_v^1 + \omega^1 \Delta\pi_s(t) \qquad (3\text{-}15)$$

Neglecting for the moment the actual concentration profile at the low pressure side we assume that the liquid leaving the plug at the low pressure side has a concentration $c^1(t)$, which will be slightly less than the value $c(o,t)$ at the high pressure side. Then $\tilde{c}_s$ reduces to the average value

$$\tilde{c}_s(t) = \frac{c(o,t) + c^1(t)}{2} \qquad (3\text{-}16)$$

The osmotic pressure difference is given by van 't Hoff's law

$$\Delta\pi_s(t) = vRT\,[c(o,t) - c^1(t)] \qquad (3\text{-}17)$$

Furthermore, the following relation holds

$$J_s^1(o,t) = c^1(t)J_v^1 \qquad (3\text{-}18)$$

Assuming that the solute flow does not vary with distance within the plug

and that $c^1(t)$ directly follows changes in the value of $J_s^1(o,t)$ (no diffusion fluxes within the plug). Combining eq. (3-14) through (3-18), eliminating $c^1(t)$ and solving $(\delta c(x,t)/\delta x)_{x=o}$, one obtains condition (3-12).

The solution of the partial differential eq. (3-9) with boundary conditions (3-10), (3-11) and (3-12) leads to the following expression for the relative concentration as a function of time and distance[o]:

$$\frac{c(x,t)}{c_o} = 1 - \tfrac{1}{2}\left\{\operatorname{erfc}\left(\frac{Pe-\tau}{2\sqrt{\tau}}\right) + \frac{\sigma^*}{1+\sigma^*}\exp(Pe)\operatorname{erfc}\frac{Pe+\tau}{2\sqrt{\tau}}\right\} +$$

$$+ \frac{2\sigma^*+1}{2(\sigma^*+1)}\exp\left\{1 - Pe\,\sigma^* + \tau\sigma^*(1+\sigma^*)\right\}\operatorname{erfc}\left(\frac{Pe-\tau(1+2\sigma^*)}{2\sqrt{\tau}}\right) \qquad (3\text{-}19)$$

in which Pe, τ and σ^* are dimensionless quantities, defined as

$$Pe = xJ_v^1/D \qquad \text{(Peclet number)} \qquad (3\text{-}20)$$

$$\tau = (J_v^1)^2 t/D \qquad (3\text{-}21)$$

$$\sigma^* = \sigma/[1+w^*/J_v^1-\tfrac{1}{2}(1-\sigma)] \qquad (3\text{-}22)$$

In ideally semipermeable plugs or membranes σ equals one and the solute permeability equals zero, which means $\sigma^*=1$. In the case of complete non-selectivity $\sigma^*=o$. In the latter case (3-19) reduces to $c(x,t) = c_o$. The time dependence of the concentration at the high pressure boundary is given by (Pe=o):

$$\frac{c(o,t)}{c_o} = 1 - \tfrac{1}{2}\left\{\operatorname{erfc}(-\tfrac{1}{2}\sqrt{\tau}) + \frac{\sigma^*}{1+\sigma^*}\operatorname{erfc}(\tfrac{1}{2}\sqrt{\tau})\right\} +$$

$$+ \frac{2\sigma^*+1}{2(\sigma^*+1)}\exp\left\{\sigma^*(1+\sigma^*)\tau\right\}\operatorname{erfc}\left\{-\tfrac{1}{2}(1+2\sigma^*)\sqrt{\tau}\right\} \qquad (3\text{-}23)$$

Series expansion and approximation for small values of τ leads to:

$$\frac{c(o,t)}{c_o} = 1 + 2\sigma^*\sqrt{\tau/\pi} \qquad (3\text{-}24)$$

The increase in concentration at the plug boundary can be inferred from the potential difference between two reversible electrodes, one of which is situated in the bulk (electrode 1) far from the polarization layer and the other is situated at the plug boundary (electrode 2)[oo]. Quite

---

o) The solution is outlined in appendix 3A.

oo) For the position of the electrodes see fig. 3-2; in the case of a difference between the potentials of the two electrodes, indicated by E(i,j), one refers to the value of a property on the right minus the value of the respective property on the left. The electrodes indicated without primes refer to the high pressure side (left) and those indicated with primes to the atmospheric pressure side (right).

generally the E.M.F. of a cell consisting of two reversible silver/silver chloride electrodes and a solution containing chloride ions, including the liquid junction potential, is given by[39]:

$$E(1,2) = E_2 - E_1 = \frac{RT}{F_a} 2t_+ \ln(a_1/a_o) \qquad (3\text{-}25)$$

where a_1 is the activity at the plug boundary and a_o the bulk activity. It is noted that this potential difference depends only on the terminal ion activities, a_o and a_1 resp., and not on the exact shape of the concentration profile in the diffusion layer. Substitution of eq. (3-24) in (3-25) and neglecting activity corrections leads to:

$$E(1,2) = \frac{RT}{F_a} 2t_+ \ln\{1+2\sigma^*\sqrt{\tau/\pi}\} \doteq \frac{RT}{F_a} 2t_+ 2\sigma^*\sqrt{\tau/\pi} = \frac{RT}{F_a} 4t_+\sigma^* J_v^1 \sqrt{\frac{t}{\pi D}} \qquad (3\text{-}26)$$

3.3.2 *The concentration polarization at the low pressure side*

By a complete analogy the time variation of the potential difference between two reversible electrodes situated at the low pressure boundary and in the corresponding bulk will yield valuable information about the neutral electrolyte content of the liquid flowing out of the pore. The average electroneutral electrolyte concetration, c_p, is defined as $\frac{1}{2}(\bar{c}_+ + \bar{c}_- - X)$ where $\bar{c}_+$ and $\bar{c}_-$ are the average molar concentrations of the mobile positive and negative ions in the porous phase, resp. and X is the equivalent molar concentration of the ions fixed on the solid matrix. For negatively charged plugs c_p equals the mean co-ion concentration. To a first approximation, we assume that the flowing mean co-ion concentration in the porous phase equals c_p. For an analysis of this supposition one is referred to section 4.8.

For the derivation of the time dependency of the E.M.F. at the low pressure side, we assume that the electrolyte concentration leaving the plug is not influenced by the non-steady state solute flux entering the plug at the other side. With this assumption, the mathematical description of the mass balance at the low pressure side resembles the preceding derivation:

$$\frac{\delta c(y,t)}{\delta t} = D \frac{\delta^2 c(y,t)}{\delta^2 y} - J_v^1 \frac{\delta c(y,t)}{\delta y} \qquad (3\text{-}27)$$

where c(y,t) = electrolyte concentration of external solution
y = distance from plug boundary at low pressure side (fig.3-1).

The boundary conditions are:

a. at $t = o$ and $y \geq o$: $c(y,t) = c_o$ (3-28)

b. at $t > o$ and $y = \infty$: $c(y,t) = c_o$ (3-29)

c. $J_v^1 c(o,t) = J_v^1 c_p + D \left(\frac{\delta c(y,t)}{\delta y}\right)_{y=o}$ (3-30)

The solution of (3-27) is:

$$c(y,t) = \tfrac{1}{2}(c_p - c_o)\left\{\operatorname{erfc}\left(\frac{Pe-\tau}{2\sqrt{\tau}}\right) - (2\tau+Pe+1)\exp(Pe)\operatorname{erfc}\left(\frac{Pe+\tau}{2\sqrt{\tau}}\right) + \right.$$
$$\left. + 2\sqrt{\frac{\tau}{\pi}}\exp\left\{-\left(\frac{Pe-\tau}{2\sqrt{\tau}}\right)^2\right\}\right. + c_o \qquad (3\text{-}31)$$

At the plug boundary where y=o:

$$c(o,t) = \tfrac{1}{2}(c_p - c_o)\left\{1-\operatorname{erf}(-\tfrac{1}{2}\sqrt{\tau}) - (2\tau+1)\left\{1-\operatorname{erf}(\tfrac{1}{2}\sqrt{\tau})\right\} + \right.$$
$$\left. + 2\sqrt{\frac{\tau}{\pi}}\exp\left(-\frac{\tau}{4}\right)\right\} + c_o \qquad (3\text{-}32)$$

For small values of τ eq. (3-32) reduces to

$$c(o,t) = 2(c_p - c_o)\sqrt{\tau/\pi} + c_o \qquad (3\text{-}33)$$

Substitution of this equation into (3-25), again neglecting activity corrections, yields:

$$E(2',1') = E_{1'} - E_{2'} = \frac{RT}{F_a} 4t_+ J_v' \frac{c_p - c_o}{c_o}\sqrt{\frac{t}{\pi D}} \qquad (3\text{-}34)$$

This equation predicts an E.M.F. increasing with the square root of time. Its determination will yield valuáble information about the pore liquid composition.

Fig. 3-2 shows a typical example of a time-dependent streaming potential for a selective porous system. Apparently, the potential difference between the plug electrodes, E(2,2'), is not only affected by the applied pressure difference ΔP, but also by the activity ratio $a_2/a_{2'}$. Summing all relevant potential differences, we obtain:

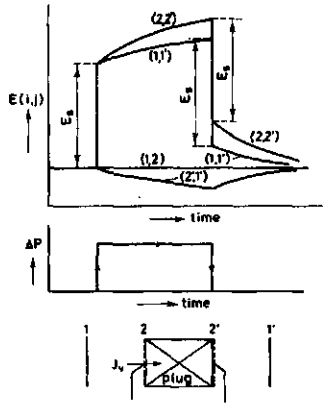

Fig. 3-2. Time-dependency of the streaming potential.
$E(i,j) = E_j - E_i$; $E(1,1') = E(1,2) + E(2,2') + E(2',1')$

$$E(2,2')_t = (E_s + E_m + E_c)_t \qquad (3\text{-}35)$$

where E_s denotes the streaming potential, E_m the 'membrane' potential, i.e. the potential difference due to a concentration difference between the two sides at the same pressure, and E_c the Nernst contributions. In principle all three contributions are time-dependent. Because of the time dependent accumulation/depletion mechanism this is evident for E_m and E_c. But E_s might also vary with time because of possible variation in the pore liquid concentration c_p, which will affect the plug's double layer properties. We will assume that the variation of E_s with concentration can be neglected over a limited range of concentration. In that case the instantaneous response of E(2,2') and for that matter of E(1,1') as well, to the application of a pressure difference is equal in magnitude to the response produced by the removal of ΔP.
With this assumption eq.(3-35) is simplified to:

$$E(2,2')_t = E_s + (E_m + E_c)_t \qquad (3\text{-}36)$$

Both cells include electrodes reversible to Cl^--ions (Ag/AgCl-el.). E_m is then given by:

$$E_m(t) = (2\tilde{t}_+^a - 1)\frac{RT}{F_a} \ln \frac{a_2(t)}{a_{2'}(t)} \qquad (3\text{-}37)$$

where $\tilde{t}_+^a$ is the average apparent transport number within the plug which takes water transport into account (see e.g. Dawson et al.[40], Staverman[41]). E_c is given by:

$$E_c = \frac{RT}{F_a} \ln \frac{a_2(t)}{a_{2'}(t)} \qquad (3\text{-}38)$$

Consequently, eq. (3-36) can be expressed as

$$E(2,2')_t = E_s + 2\,\tilde{t}_+^a \frac{RT}{F_a} \ln \frac{a_2(t)}{a_{2'}(t)} \qquad (3\text{-}39)$$

Substitution of eq. (3-24) and eq. (3-33) into the expression for $E(2,2')_t$ would lead to an explicit time dependency of the potential difference. However for actual systems, the applicability of this substition is prohibited by the fact that the accumulation at the high pressure side to a large extent takes place in the outermost layers of the plug. In other words the plug boundary concentration c(o,t) may be much lower than that behind the electrode 2. This effect is indicated in fig. 3-2 for the extreme case where E(1,2) remains practically constant during the course of an experiment.

The expression for the potential difference between the two bulk electrodes,1 and 1', includes a diffusion (junction) potential difference instead of the Nernst contribution of the previous case. This potential difference has the opposite sign of E_s and E_m and will work in the same direction in both solution layers:

$$E(1,1')_t = E_s + (E_m + E_D)_t \qquad (3\text{-}40)$$

$$\text{where } E_D = -(2t_+ - 1)\frac{RT}{F_a} \ln \frac{a_2(t)}{a_{2'}(t)} \qquad (3\text{-}41)$$

Consequently, eq. (3-40) with $E_s = -\beta\Delta P$ can be expressed as

$$E(1,1')_t = -\beta\Delta P + 2(\tilde{t}_+^a - t_+) \ln \frac{a_2(t)}{a_{2'}(t)} \qquad (3\text{-}42)$$

It is evident that penetration of accumulated salt into the plug and the decrease of its selectivity makes determination of the apparent transport number in the plug or membrane from a simultaneous determination of $E(1,1')_t$ and $E(2,2')_t$ impossible. In that case valuable information about the salt filtration effect can be obtained only from the time behaviour of E(2',1') at the low pressure side, viz. eq. (3-34).

3.4 *Concentration polarization phenomena in connection with streaming current measurements*

When a pressure difference is applied across the plug, the pore liquid is displaced, thereby carrying along a certain amount of net charge. This ion flow (convection current) causes an electric current (streaming current) in a wire short-circuiting the two electrodes that are attached to the surface of the membrane or plug. Formally the streaming current is defined by $L_{21} = (I/\Delta P)_{\Delta\pi_s,E}$. In this description any possible electrode effects are disregarded. In the ideal situation the oxidation/reduction reactions at the electrode surfaces and the diffusion of ions to and from the electrodes are fase enough to follow the rate of ion convection in the plug or membrane. If this is not the case the streaming current will decrease with time.

Time dependent streaming current

Consider a porous plug or membrane, at the surfaces of which two reversible electrodes are attached which are connected to a galvanometer, the resistance of which is negligible compared to the system's resistance. Usually, the electrolyte reservoirs at both sides of the plug contain equal concentrations of electrolyte, which are so high that no filtration effects are to be expected. Upon application of a pressure difference to

this system, the current through the plug electrodes, I(2,2'), appears to jump instantaneously to a certain value and from thereon decreases with time until a constant value is reached (see schematic representation, fig. 3-3a). Removal of the pressure difference produces the same behaviour, but with the opposite sign. A further experimental analysis of the

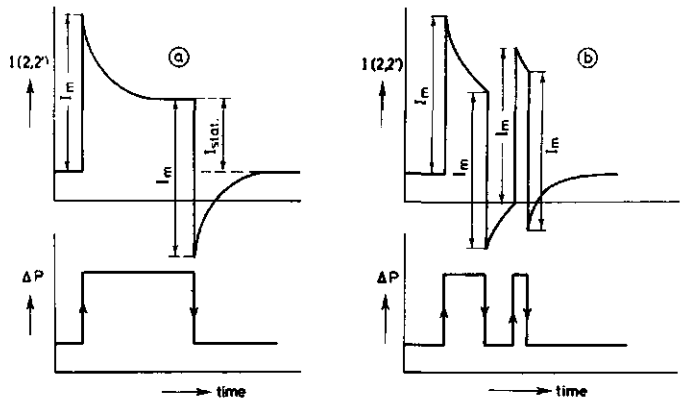

Fig. 3-3. Streaming current as a function of time.

streaming current retardation phenomena leads to the following conclusions:

1. The instantaneous value I_m is proportional to the pressure difference ΔP and is independent of the system's history (see fig. 3-3b).
2. The stationary value, $I_{stat.}$, is also proportional to ΔP.
3. The shape of the retardation curve is dependent on the history. Only when the retardation curve is recorded starting either from the equilibrium situation or from the stationary situation is the shape of the curve independent of the pressure difference.

The timedependency of the streaming current is due to an electrode effect only. The possibility of a reversible time dependent *mechanical* change in the plug can be disregarded because the streaming potential is a linear function of the pressure difference. Furthermore, permeability, a.c.- and d.c.-resistance, as measured between the plug electrodes and with the four electrode technique respectively, are both independent of pressure (see sections 3.7.2 and 3.7.4).

The occurrence of polarization phenomena at the plug electrodes (2 and 2') can also be inferred from the potential behaviour of the two reservoir electrodes (1 and 1'). Fig. 3-4 represents this behaviour; E(1,1') as recorded simultaneously with the retardation of the streaming current. The obvious conclusion is that short-circuiting the plug electrodes does not ensure that E=o, which is the condition for the measurement of the streaming current. The remarks made about the shape of the

streaming current retardation curve also apply to the time dependency of E(1,1'). In addition, E(1,1') does not depend on the electrodes' position in the reservoirs, the electrode dimensions, or the reservoir volumes.

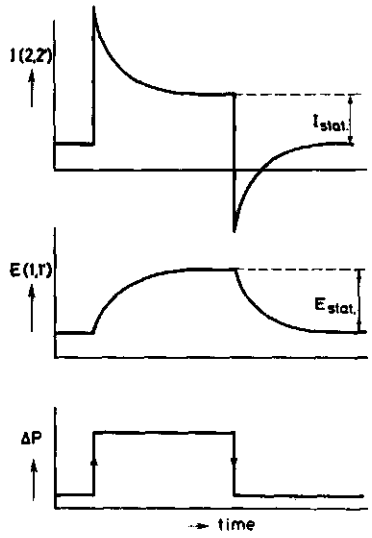

Fig. 3-4. Polarization processes during streaming current measurements.

3.4.1 *The effect of concentration polarization at the current measuring electrodes*

For a negatively charged plug or membrane the application of a pressure gradient results in positive charge being carried along to the electrode at the low pressure side. When the Ag/AgCl plug electrodes are short-circuited the following electrochemical reactions occur:

at the high pressure side (2) $\quad Ag + Cl^- \rightarrow AgCl + e^-$

at the low pressure side (2') $\quad AgCl + e^- \rightarrow Ag + Cl^-$

This electrolytic process may be imagined to occur due to the action of an "electromechanic battery" (flow driven current generator), supplying an electromotive force equal to the streaming potential. Electrolysis involves ionic transport from solution to electrode surface or vise versa. This transport is brought about by three different mechanisms:

- migration due to the electric field
- diffusion from regions of high concentration to those of low concentration
- convection of ions through the solvent motion.

The exchange current density of Ag/AgCl electrodes is so high that there is virtually no overpotential during passage of current. This means that the passage of current during a streaming current experiment will only give rise to a polarization effect that is entirely due to concentration gradients in the electrode regions. This concentration polarization can be expressed as a diffusion resistance increasing with time, $R_d(t)$.

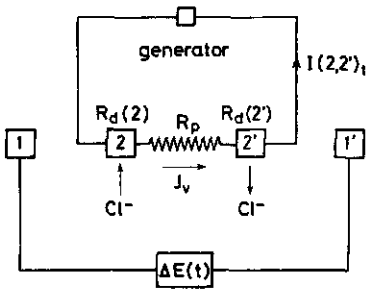

Fig. 3-5. Concentration polarization during streaming current.

The current generated by flow through the porous system can be represented as an electro-mechanic battery, supplying E_s^{em} with an internal resistance i.e. R_p[26] (see fig. 3-5). The net current through the plug $I(2,2')_t$ will be reduced as a result of an increase in $R_d(t)$. It is seen from fig. 3-5 that:

$$I(2,2')_t = \frac{E_s^{em}}{R_p+R_d(2)+R_d(2')} = \frac{E_s^{em}}{R_p+R_d(t)} \qquad (3\text{-}43)$$

$I(2,2')_t R_d(t)$ is called the effective electrolysis potential, $\Delta E(t)$:

$$\Delta E(t) = E_s^{em} - I(2,2')_t R_p \qquad (3\text{-}44)$$

In the limiting case $R_d(t) \to \infty$, the convection current is exactly balanced by back conduction through the plug, thus the net current is zero. Note that E_s^{em} represents a "hydrodynamic electromotive force", which can be regarded as the source of the convection current. E_s^{em} is defined as

$$E_s^{em} = I_s R_p \qquad (3\text{-}45)$$

E_s^{em} equals the streaming potential E_s but has the *opposite sign*, because E_s^{em} "gives rise" to a convection current I_s, whereas E_s gives rise to a conduction current in the opposite direction.

Any potential difference giving rise to conduction currents can be measured directly between the electrodes 1 and 1'. If the conduction current equals the convection current, E(1,1') equals E_s. If the conduction current is less than the convection current, corresponding to a net current in the (2,2')-circuit, E(1,1') will be less than E_s. From eq. (3-44) it can be seen that a decreasing net current, $I(2,2')_t$, corresponds to an increasing conduction current and thus to an increasing potential dif-

ference, $\Delta E(t)$. This potential difference is measured as E(1,1') (see also fig. 3-5). Because this potential difference reflects the presence of concentration gradients near the plug electrodes, removal of the pressure difference causes the (2,2')-electrode system to act as a concentration cell, causing a slowly decreasing current until the concentration differences have vanished. The sign of this current will be opposite to that of the time dependent streaming current, because the concentration gradients near the electrodes are not reduced by diffusion to or from the solution but by electrode reactions.

The concentration polarization phenomenon appearing during streaming current experiments must be considered as a secondary driving force, the osmotic pressure difference, $\Delta\pi_s$. A general treatment of the streaming current phenomena must therefore include these polarization effects.

Assuming stationary conditions at any moment, eq. (3-4) can be used:

$$I = L_{21}(\Delta P - \Delta\pi_s) + L_{22}E + L_{23}\,\Delta\pi_s/\bar{c}_s \qquad (3\text{-}4)$$

The electromotive force can be found from the schematic representation of the potential distribution during the passage of current (fig. 3-6). Because there is no externally applied potential difference, the electrical potential difference is just counterbalanced by the electrochemical potential difference. That means that E=0. We formally split up both compensating contributions to the E.M.F., in order to separate the electrical part $\Delta E(t)$, which is experimentally assessible with the other pair of electrodes (1,1') situated far from the diffusion layers at the (2,2')-electrodes:

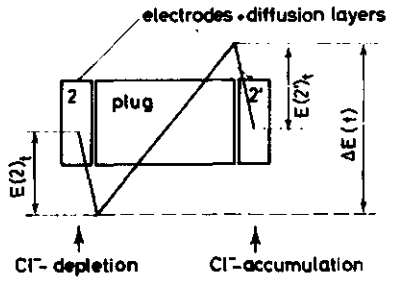

Fig. 3-6. Potential distribution during streaming current.

$$E = E(2)_t + \Delta E(t) + E(2')_t = \Delta E(t) + 2t_+ \frac{RT}{F_a} \ln \frac{a_{2'}(t)}{a_2(t)} \qquad (3\text{-}46)$$

Because the cell can be considered as a concentration cell with transference, the transport number t_+ of the ion to which the electrodes are not reversible, is involved. It is assumed that t_+ is independent of the electrolyte concentration. The osmotic term can be found from

eq. (3-4) and (3-5c). For a 1-1 electrolyte we obtain:

$$L_{23} \frac{\Delta\pi_s}{\bar{c}_s} = 2\kappa^* \tilde{t}^a \frac{RT}{F_a} \ln \frac{a_2(t)}{a_{2'}(t)} \qquad (3\text{-}47)$$

Substitution of eq. (3-46) and (3-47) into (3-4) yields:

$$I = L_{21} \Delta P + L_{22} \Delta E(t) + (2\kappa^* \tilde{t}_+^a - 2t_+ L_{22}) \frac{RT}{F_a} \ln \frac{a_2(t)}{a_{2'}(t)} \qquad (3\text{-}48)$$

where $\Delta\pi_s$ is assumed to be negligible with respect to ΔP. We will discuss this assumption later. Assuming further that $L_{12}^2/L_{11} << L_{22}$, implies (table 3-1) that $\kappa^* = L_{22}$. Then:

$$I = L_{21}\Delta P + L_{22}\Delta E(t) + 2L_{22} (\tilde{t}_+^a - t_+) \frac{RT}{F_a} \ln \frac{a_2(t)}{a_{2'}(t)} \qquad (3\text{-}49)$$

In case the concentration polarization completely develops, the current I becomes zero. Remembering that $E_s = - (L_{21}/L_{22})\Delta P$ we obtain:

$$0 = - E_s + \Delta E(t)_{I=o} + (2\tilde{t}_+^a - 2t_+) \frac{RT}{F_a} \ln \frac{a_2(I=o)}{a_{2'}(I=o)} \qquad (3\text{-}50)$$

From fig. 3-6 and eq. (3-46) it can be seen that:

$$\Delta E(t) = 2t_+ \frac{RT}{F_a} \ln \frac{a_2(t)}{a_{2'}(t)} \qquad (3\text{-}51)$$

Combining eq. (3-51) and (3-50) and rearranging yields

$$\frac{E_s - \Delta E(t)_{I=o}}{\Delta E(t)_{I=o}} = \frac{\tilde{t}_+^a}{t_+} - 1 \qquad (3\text{-}52)$$

Both E_s and $\Delta E(t)$ are defined as *differences between the high pressure and the low pressure side.* In terms of measured quantities, eq. (3-52) becomes:

$$\frac{E_s - E(1,1')_{I=o}}{E(1,1')_{I=o}} = \frac{\tilde{t}_+^a}{t_+} - 1 \qquad (3\text{-}53)$$

In order to check the validity of the assumption that $\Delta\pi_s << \Delta P$ we refer to eq. (3-51). From measured E(1,1')-values the activity ratio $a_2/a_{2'}$ can be calculated and consequently the osmotic pressure difference. In this way it is found, that for a potential difference of 100 mV the osmotic pressure correction would amount to only 1% for ΔP = 30 cm Hg.

3.4.2 *The X-Y plot*

When $I(2,2')_t$-values are plotted versus the simultaneously measured values of $E(1,1')_t$ (see fig. 3-4 and 3-7), a straight line is obtained. If this line is extrapolated to E(1,1')=o, the streaming current, I_s, is found. Extrapolation to I(2,2')=o yields the streaming potential, *provided* $\tilde{t}_+^a = t_+$ (see eq. (3-53)). Whether this provision holds can be deduced from a comparison of the extrapolated E(1,1')-value with the value found from a "classical" determination (see fig. 3-2).
From fig. 3-7 it is seen that the measured instantaneous values, I_m, however reproducible they may be, are not generally equal to the real streaming current, I_s. The instantaneous value is determined by the velocity with which the diffusion resistance manifests itself, by the speed with which the desired pressure difference can be applied, and by the speed of the recording device. When $t_+ = \tilde{t}_+^a$ (line a) the slope equals $-L_{22}$. This can be seen when eq. (3-49) for this condition is written in terms of the measured quantities:

$$I(2,2')_t = L_{21}\Delta P - L_{22}E(1,1')_t \qquad (3.54)$$

In the general case, where $t_+ \neq \tilde{t}_+^a$ and where the electroviscous effect is no longer negligible:

$$I(2,2')_t = L_{21}\Delta P - L_{22}E(1,1')_t - \frac{(\kappa^*\tilde{t}_+^a - L_{22}t_+)}{t_+}\,E(1,1')_t \qquad (3\text{-}55)$$

Thus, in the general case (b), the slope equals

$$-\,L_{22} + \frac{\tilde{t}_+^a\kappa^* - t_+L_{22}}{t_+} \qquad (3\text{-}56)$$

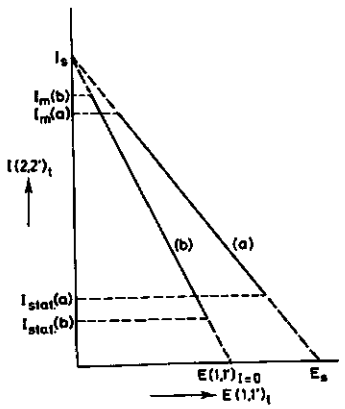

Fig. 3-7. Time dependent current through plug electrodes versus time dependent potential difference between reservoir electrodes.

a) $t_+ = \tilde{t}_+^a$; b) $t_+ < \tilde{t}_+^a$

The general expression for the shift of the extrapolated value of the streaming potential now becomes (see table 3-1):

$$\frac{E_s - E(1,1')_{I=o}}{E(1,1')_{I=o}} = \frac{\tilde{t}_+^a \kappa^*}{t_+ L_{22}} - 1 = \left(1 - \frac{L_{12}^2}{L_{11}L_{22}}\right)\frac{\tilde{t}_+^a}{t_+} - 1 \qquad (3\text{-}57)$$

When using non-reversible polarizable electrodes (e.g., platinum) the streaming current retardation phenomena can be described by incorporating in the circuit an additional resistance that increases with time (see section 3.4.4). The relation between $I(2,2')_t$ and $E(1,1')_t$ is then given by eq. (3-54); thus the X-Y plot directly reveals L_{22}.

3.4.3 *The concentration dependent retardation behaviour of the streaming current for pure concentration polarization*

If the electrochemical reaction is reversible, i.e. no other polarization is present besides the concentration overvoltage, the overvoltage will depend on the difference between bulk concentration, c_o, and the surface concentration, c_e, according to the Nernst equation and including the liquid junction potential (we are considering a silver/silver chloride electrode and a 1-1 electrolyte):

$$E(t) = 2t_+ \frac{RT}{F_a} \ln \frac{c_o}{c_e} \qquad (3\text{-}58)$$

In the general case that during electrolysis the interfacial concentration, c_e, is not zero, the expression for the current at a plane electrode under semi-infinite pure linear diffusion control is given by (e.g. Delahay[42]):

$$i(t) = \frac{F_a A D^{\frac{1}{2}}(c_o - c_e)}{\pi^{\frac{1}{2}} t_+ t^{\frac{1}{2}}} \qquad (3\text{-}59)$$

where A is the electrode's surface area. The term t_+ appears because of the migration contribution of the electroactive species to the total current. In the case of excess indifferent electrolyte the transport number of the electroactive ion (chloride in our case) is reduced to zero and a pure diffusion current remains. In electrokinetic research, however, this is generally not the case.

The diffusion resistance, R_d, is obtained by combination of eq.(3-58) and (3-59)

$$R_d = \frac{E(t)}{i(t)} = \frac{2\pi^{\frac{1}{2}} t_+^2 \, RT}{F_a^2 \, A \, D^{\frac{1}{2}}} \, t^{\frac{1}{2}} \, \frac{\ln(c_o/c_e)}{c_o - c_e} \qquad (3\text{-}60)$$

Series expansion yields the expression:

$$R_d = \frac{2\pi^{\frac{1}{2}} t_+^2 RT}{F_a^2 \, A \, D^{\frac{1}{2}}} \, t^{\frac{1}{2}} \, \frac{1}{c_o} \left\{1 + \frac{1}{2} \frac{c_o - c_e}{c_o} + \frac{1}{3} \left(\frac{c_o - c_e}{c_o}\right)^2 + \frac{1}{4} \left(\frac{c_o - c_e}{c_o}\right)^3 + \ldots\right\} \qquad (3\text{-}61)$$

Application of this analysis to the situation represented in fig. 3-6 yields expressions for $R_d(2)$ and $R_d(2')$ as a function of $c_e(2)$ and $c_e(2')$ respectively. For the high pressure side electrode (2) we can generally state that $o \leqslant c_e \leqslant c_o$, so in that case the series will be a convergent one. At the other electrode, $c_e \geqslant c_o$ during the electrolysis process. Because the current through both electrodes must be identical, the concentration difference at both electrodes must be the same, i.e. $\Delta c = c_o - c_e(2) = c_e(2') - c_o$.

In this way we are able to express $R_d(2)$ and $R_d(2')$ as well as the total diffusion resistance, $R_d(t)$, in terms of Δc.

$$R_d(2) = \frac{2\pi^{\frac{1}{2}} t_+^2 RT}{F_a^2 A D^{\frac{1}{2}}} \, t^{\frac{1}{2}} \, \frac{1}{c_o} \left\{1 + \frac{1}{2} \frac{\Delta c}{c_o} + \frac{1}{3} \left(\frac{\Delta c}{c_o}\right)^2 + \frac{1}{4} \left(\frac{\Delta c}{c_o}\right)^3 + \ldots\right\} \qquad (3\text{-}62)$$

$$R_d(2') = \frac{2\pi^{\frac{1}{2}} t_+^2 RT}{F_a^2 A D^{\frac{1}{2}}} \, t^{\frac{1}{2}} \, \frac{1}{c_o} \left\{1 - \frac{1}{2} \frac{\Delta c}{c_o} + \frac{1}{3} \left(\frac{\Delta c}{c_o}\right)^2 - \frac{1}{4} \left(\frac{\Delta c}{c_o}\right)^3 + \ldots\right\} \qquad (3\text{-}63)$$

$$R_d(t) = R_d(2) + R_d(2') = \text{const.} t^{\frac{1}{2}} \, \frac{1}{c_o} \left\{1 + \frac{1}{3}\left(\frac{\Delta c}{c_o}\right)^2 + \frac{1}{5}\left(\frac{\Delta c}{c_o}\right)^4 + \ldots\right\} \qquad (3\text{-}64)$$

Combining (3-43), (3-45) and (3-64) yields the expression

$$\frac{I(2,2')_t}{I_s} = \frac{R_p}{R_p + \text{const.} t^{\frac{1}{2}} \, \frac{1}{c_o} \left\{1 + \frac{1}{3} \left(\frac{\Delta c}{c_o}\right)^2 + \frac{1}{5} \left(\frac{\Delta c}{c_o}\right)^4 + \ldots\right\}} \qquad (3\text{-}65)$$

This equation clearly shows the factors determining the retardation behaviour. In the case of a high plug resistance and relatively short periods of measurement the polarization effect will hardly be observed.

3.4.4 *The effect of an external resistance on the determination of a streaming current complicated by concentration polarization*

Apart from the "naturally" occurring concentration polarization resistance at the electrodes one can introduce an additional resistance into the system in two other ways:

a. by incorporating an external resistance in the circuit,
b. by situating the electrodes 2 and 2' at some distance from the plug or membrane boundaries, thereby introducing additional electrolyte layers.

ad a. In the absence of concentration polarization but in the presence of an external resistance, R_e, the current through the plug is given by a modification of (3-4):

$$I(2,2)^* = L_{21}\Delta P + L_{22}\, E^* \qquad (3\text{-}66)$$

where E* represents the potential difference over the plug, corresponding to the ohmic drop over the external resistance. At very high resistances (3-66) reduces to:

$$o = L_{21}\Delta P + L_{22}\, E^*(I=o); \qquad E^*(I=o) = E_s \qquad (3\text{-}67)$$

Furthermore, by analogy with eq. (3-65):

$$I(2,2)^* = \frac{R_p}{R_p + R_e}\, I_s \qquad (3\text{-}68)$$

By introducing the definitions $R_p = 1/L_{22}$ and $R_e = 1/L_{22}{}^*$, the following relations can ultimately be derived

$$I(2,2')^* = \frac{L_{22}{}^*}{L_{22} + L_{22}{}^*}\, I_s \qquad (3\text{-}69)$$

$$E^* = \frac{L_{22}}{L_{22} + L_{22}{}^*}\, E_s \qquad (3\text{-}70)$$

Thus, by measuring both the potential drop over a known shunt resistance and the streaming potential the value of the plug conductance, L_{22}, can be determined according to eq. (3-70). This method was introduced by Eversole and Boardman[21]. In this technique the electrodes should be situated at the plug boundaries.

ad b. When an electrolyte layer acts as an additional resistance, the four electrode method can be used (2 and 2' for current measurement; 1 and 1' for potential measurement), but now the positions of 1 and 1' become extremely important. In fig. 3-8 three different positions for the potential measuring electrodes are depicted (a,a'; b,b' and c,c'). In situation a the full potential drop will be detected: $E^*_a = E^*$. Then by dividing E^* by $I(2,2')^*$ one can determine the conductance of the electrolyte layers, L^*_{22}.

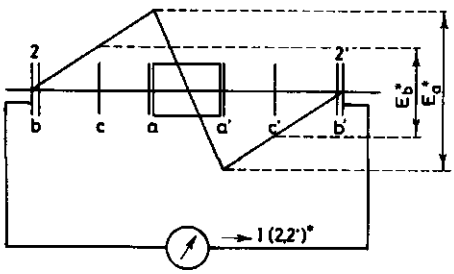

Fig. 3-8. Influence of electrolyte resistance; different electrode positions (no electrode polarization).

Additional measurement of the streaming potential will then yield the plug resistance (eq. (3-69) and (3-70)). Alternatively, measurement of two sets of I* and E*, i.e. at two different positions of the current measuring electrodes, yields two equations with two unknowns, from which L_{22} and I_s can be solved. In situation b the potential difference is almost zero. Measurement of the current and of the streaming potential will only yield the plug resistance if the resistance of the electrolyte layers is known. If the (2,2')-electrodes are situated between the plug boundaries and the (1,1')-electrodes, no potential difference is measured and again the conductance of the electrolyte layers, L^*_{22}, must be known. In the intermediate situation c, a potential difference is noticed but again additional knowledge is required in order to obtain the plug resistance.

We will now consider practical situations and will indicate in particular to what extent the combined presence of external resistances and concentration polarization can lead to erroneous results. First the simple case in which the potential measuring electrodes are situated at the plug boundaries and in which $\tilde{t}^a_+ = t_+$ (case Ia in fig. 3-9) will be considered. A sudden pressure change leads to an instantaneous change in I(2,2') from zero to point a) followed by a slow change along line Ia having a slope-L_{22}. The coordinates of a) depend on the magnitude of L^*_{22} (see fig. 3-9). Extrapolation to I=0 and E=0 yield the correct values of the streaming potential and streaming current respectively. In the more

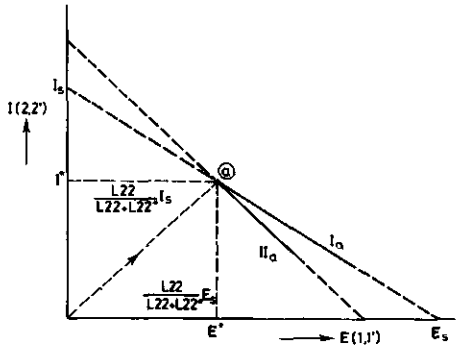

Fig. 3-9. Influence of the combined presence of external resistances and concentration polarization; X-Y plot: Ia - $\tilde{t}_+^a = t_+$, IIa - $\tilde{t}_+^a \neq t_+$.

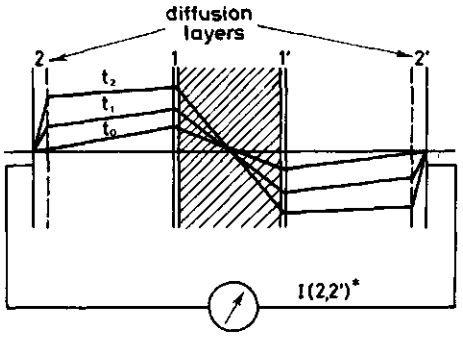

Fig. 3-10. Potential distribution as a function of time (electrode polarization included).

usual situation where $\tilde{t}_+^a \neq t_+$, the slope of the "retardation line" IIa is given by eq. (3-56). Extrapolation of this line leads to erroneous values of both streaming current (too high) and streaming potential (too low). The magnitude of the deviations depends directly on the chosen external resistance, or, alternatively, on the concentration and thickness of the electrolyte layers between plug and current measuring electrodes, because they determine the coordinates of point a) (see fig. 3-9).

Fig. 3-10 is a highly schematic represention of the potential distribution at different times. The increasing potential drops over the diffusion layers of the current measuring electrodes, 2 and 2', due to the increasing diffusion resistances, $R_d(t)$ (see eq. (3-64)), resulting in a relatively smaller potential drop over the electrolyte layers. In other words, the increase of $R_d(t)$ renders the place of the potential measuring electrodes less important. Another consequence is that, depending on the various resistances R_p, R_e and $R_d(t)$, the X-Y plot is not linear for short times.

In fig. 3-11 we have given a practical example of the case where the retardation is so fast that the $I^*_{a,c}$-value is not reached (compare with fig. 3-9). Now the magnitude of $R_d(t)$ determines whether or not a straight line is obtained with slope-L_{22} in case I or with a slope as given by eq. (3-56) in case II. The difference between $I^*_{a,c}$ and I_m has important consequences for the reliability of the shunt method, introduced by Eversole and Boardman[21]. These authors plotted the instantaneous maximum values, I_m, of the shunt current by extrapolating to zero shunt resistance. Because of the relatively low electrolyte concentrations used in their experiments only a small retardation effect is observed (about 8%) but the situation would become worse at higher electrolyte concen-

trations, as is generally the case in charged porous plugs and coarse porous membranes, characterized by relatively low resistances. Experimental results with our plugs are presented in section 3.7.2.

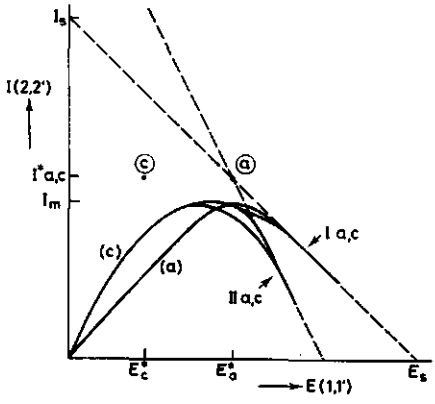

Fig. 3-11. X-Y plot, including contribution of electrolyte resistance and electrode polarization.
I: $\tilde{t}_+^a = t_+$, II: $\tilde{t}_+^a \neq t_+$; a) (1,1') at plug boundaries, c) (1,1') half-way plug boundaries/(2,2')-electrodes.

3.4.5 *Superposition principle*

In rheological theories one often refers to the well-known Boltzmann's superposition principle, which is applicable to linear retardation phenomena. The principle states that, if a system is subjected to an arbitrary, time-dependent combination of different forces the total flow at any moment equals the sum of the flows the system would exhibit if the forces would be applied separately to the system in its equilibrium position. Another way of stating the same principle is: the system's response to an applied force is at any moment independent of the system's history, i.e. it does not matter whether the system is in equilibrium or already subject to some force(s) at the moment of application of the new force. Application of this principle to the retarding streaming current leads to the following formal expression:

$$I(t) = \sum_{i=1}^{n} L_{21} (\Delta P)_i \, f(t-t_i) \qquad (3\text{-}71)$$

where $L_{21}(\Delta P)_i$ represents the streaming current resulting from the application of a pressure difference $(\Delta P)_i$. $f(t-t_i)$ represents some decay function, and t_i is the moment of application of the pressure difference $(\Delta P)_i$. Fig. 3-12 illustrates the principle for the simple case that a pressure difference is doubled after some time. I(b) would be the current

if the excess pressure difference applied at t_1 is thought to have been applied to the system in equilibrium, i.e. I(b) at time t equals I(a) at time $(t-t_1)$. The superposition principle states that I(c) = I(a) + I(b).

Two remarks have yet to be made:

a. the potential difference between the (1,1')-electrodes obeys the same superposition principle, because it depends on the same decay function as the current through the (2,2')-electrodes, as will be clear on inspection of eq. (3-54);

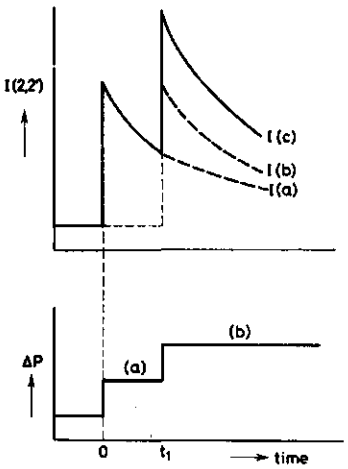

Fig. 3-12. Superposition principle. Retarding streaming current

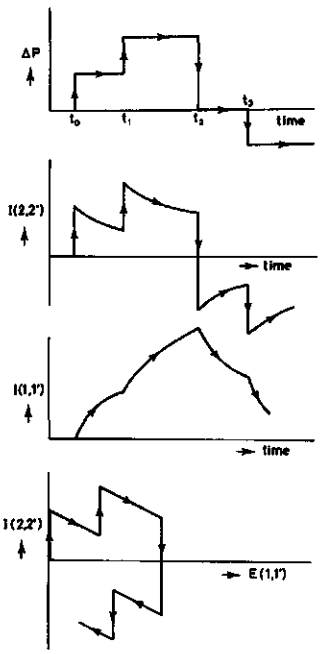

Fig. 3-13. Superposition principle. X-Y plot.

b. removal of a pressure difference ΔP at a certain moment is equivalent to applying a new pressure -ΔP at the same moment.

Fig. 3-13 represents schematically the consequences of the principle for the X-Y plot. It shows how the X-Y plot can be constructed from the two retardation curves; it represents the response of the system to the following changes: at t_o a pressure difference is applied to the system in equilibrium; at t_1 this pressure is doubled; at t_2 the total pressure is removed; at t_3 the original pressure is applied, but in the reversed direction. The retardation lines in the X-Y plot are all parallel, the slope being given by eq. (3-56) in the more general case.

3.5 *Polarization phenomena arising from an externally applied electric current through charged porous systems; the effect of low frequency dispersion*

Besides the indirect determination of the d.c. resistance of a porous system from streaming potential and streaming current, a direct determination is possible by measuring the potential difference between electrodes, attached to the surfaces of the porous system, during the passage of an externally applied current of known magnitude. In order to ensure that the diffusion profiles built up during the passage of current at the electrode interfaces do not influence the porous system and thereby the quantity to be measured, essentially the four electrode methode must be used. The electrodes producing the current are situated at a reasonable distance from the porous system boundaries.

In negatively charged porous systems exhibiting selectivity, i.e. the ionic transport numbers change at the boudaries, the passage of an electric current leads to a reduction of the electrolyte concentration at the side where the cation enters the plug and an increase at the other side[10,43,44]. This type of concentration polarization is essentially the same as at the electrode-solution interfaces[45]. The polarization process can be observed as a time dependent potential difference measured between the plug electrodes. A simple recording of this potential difference as it results from either a current interruption or a current pulse of moderate magnitude enables one to discriminate between the ohmic potential drop and the time dependent polarization potential, provided the change in concentration at the plug boundaries is not too fast.

Usually a.c. methods are preferred (measuring frequencies mostly in the kiloherz range) mainly for sake of convenience or in order to avoid polarization at electrode- and plug (or membrane)- solution interfaces. The thus determined a.c. resistance are then treated as d.c. values without any comment. In this way any low frequency dispersion of the electrical resistance is not taken into account.

In the determination of the d.c. resistance it is important to know the time of adjustment of the potential difference, caused by the sudden passage of a constant current. If a slow relaxation is involved, the adjustment cannot be considered "instantaneous" and will lay behind the "step function" current with a speed that is determined by the particular kinetics involved[15].

Where the system exhibits a dielectric dispersion behaviour the time dependent part of the polarization potential is composed of two

contributions, the "intrinsic" polarization and the concentration polarization due to plug selectivity. In practice, however, the intrinsic process is often largely overshadowed by the concentration polarization phenomena. Experimentally, the intrinsic polarization will be observed as an incorrect instantaneous value of the potential difference between the plug electrodes. The resistance determined from this instantaneous value and the applied current is then less than the value determined from streaming potential and streaming current. If low frequency measurements also lead to lower resistance values than determined from electrokinetic determinations, despite the electrode polarization contribution in this direct measurement, this will also indicate a dispersion effect.

The intrinsic effect may be so slow that it actually complicates determination of the d.c.-resistance and, as will be shown, the streaming current determination as well. Recording of the latter as a function of time will then give the opportunity to separate the intrinsic polarization from the concentration polarization.

3.5.1 *Determination of the low frequency dispersion according to the X-Y method*

At relatively low electrolyte concentrations the X-Y plot may show a feature which have not yet discussed: the first part of the I-E plot shows a curved line indicating current values exceeding those predicted from extrapolation of the straight part at high values of the potential. For the explanation of this phenomenon the following remarks are pertitent. Application of a pressure difference leads to a time dependent current through the plug electrodes which can be considered as having two components, the concentration polarization at the electrodes which we have discussed in detail and an intrinsic plug effect which we have mentioned in the discussion on impedance measurements in this section. The former contribution leads to a linear I-E relation and opens the possibility to determine the time behaviour of the "intrinsic" phenomenon (of course, the time scales of both processes should be sufficiently different). The so-called "intrinsic phenomenon" can formally be regarded as a dielectric displacement current superposed on the d.c.-currents which result from diffusion, convection and migration processes.

Fig. 3-14 shows the method by which the separation of the two contributions can be performed. In the I-E plot the dashed line, obtained from extrapolation of the linear part of the experimental curve, represents the retardation pattern if concentration polarization at the 2,2'-

electrodes would be the only mechanism of retardation. The time dependency of the intrinsic process can be found if the difference between the experimental current and the extrapolated value in the I-E plot is subtracted from the experimental value in the I-t plot. The intrinsic time dependency of the streaming current can now be formulated as:

$$I(i)_t = I_s + I(2,2')_t - I(e)_t \qquad (3\text{-}73)$$

where I_s = the d.c. streaming current
$I(2,2')_t$ = the experimental current
$I(e)_t$ = the current resulting from electrode polarization only (no intrinsic effect; see contruction)

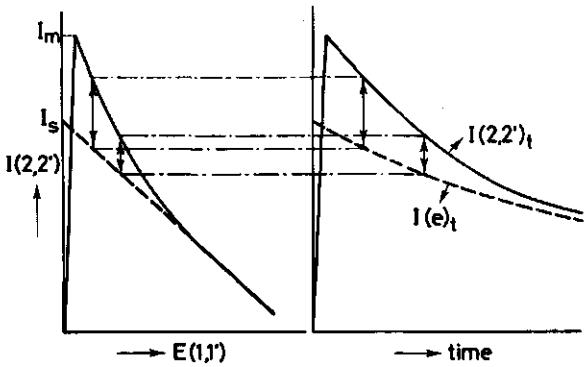

Fig. 3-14. Determination of low frequency dispersion (see text).

It is noted that for $t \to \infty$, $I(2,2')_t - I(e)_t$ equals zero and $I(i)_t$ equals I_s. The consequence of all this is that if no analysis of the time behaviour is made and the instantaneous value, I_m, is taken to be the streaming current, the real streaming current, I_s, might either exceed or be smaller than the instantaneous value, depending on wether or not a low frequency dispersion occurs, and depending on the time scales of both polarization processes as compared to that of the recorder response. Only, incidentally, might one obtain the correct value.

Under streaming potential conditions there is no net current. This means that at any moment the mechanically induced convection current equals the conduction current:

$$I(t)_{conv.} = L_{21}(t)\Delta P \qquad (3\text{-}74)$$

$$I(t)_{cond.} = L_{22}(t)E(t) \qquad (3\text{-}75)$$

Suppose the streaming potential, which is in principle a function of time (see the discussion in section 3.3), can be regarded to be constant during the period in which the intrinsic retardation of the streaming current is effective. The influence of salt filtration is still negligible. Hence, because $E(t) = E_s$, it can be concluded that the time dependence of the conductance, $L_{22}(t)$, is directly obtainable from that of the intrinsic contribution of the streaming current, $I(i)_t$. Apart from the effect of electrode polarization under streaming current conditions, short-circuiting the 2,2'-electrodes eliminates an overall back conduction through the liquid but *cannot eliminate* partial streaming potentials (and consequently conduction) at some arbitrary points in the porous phase (see section 4.2.1). Physically this means that charge is accumulated at points where the flow regime is altered as a result of expansion or contraction of the pores. In these cases the degree of charge imbalance is regulated by the flow regime at the region of disturbance. In a randomly packed bed these conditions are fulfilled, so that it is sufficient to speak of numerous regions interconnected with each other, having both ionic back conduction and partial streaming potential.

Pressure changes within short time intervals have no effect on the instantaneous current, I_m, but in some cases the rest periods between successive experiments have to be long enough to exclude possible memory effects of the preceding experiment with regard to the intrinsic retardation. If the intrinsic retardation is rather slow, the potential difference can no longer be regarded as constant. In this case the procedure for finding the intrinsic decay function must include a correction for the increasing potential difference:

$$I(i)_t - I_s = [I(2,2')_t - I(e)_t] \frac{E(I=o)}{E(I=o)-E(t)} \qquad (3\text{-}76)$$

where $I(2,2')_t$ and $I(e)_t$ are the graphically determined values and $E(I=o)$ the potential difference extrapolated to $I=o$ in the I-E plot. In the case of fast intrinsic retardation processes, where $E(t) \approx o$, eq. (3-76) reduces to eq. (3-73).

3.6 *Experimental verification of the theory developed for electrokinetic quantities complicated by polarization phenomena*

It is the purpose of this section to verify experimentally the theories and suggested methodology of measurement for a model system. It was impossible to accomplish this by using previously published data,

due to their incompleteness. It was necessary, therefore, to design an apparatus and to develop an experimental technique of plug preparation, which, while benefitting from the experience of earlier investigators, would be sufficiently improved to establish accurate and reproducible data over a wide range of system variables.

3.6.1 *Preparation of latex plugs*

Special attention has been given to the preparation of homogeneous isotropic plugs of polystyrene spheres. The plugs must be mechanically stable and have to be wetted completely in order to avoid structural changes during electrokinetic investigations. Various "wet preparation" techniques have been examined. Preparing plugs by compression of dry material must be excluded. It was found that complete displacement of air could not be achieved simply by forcing liquid through such a plug matrix at moderate pressure. The high pressure necessary would damage the electrokinetic equipment and may possible invoke irreversable deformation of the particles. Consequently, contact of the plugs with air has to be avoided. The presence of enclosed air can be detected by measuring the a.c. resistances of the plugs at atmospheric and reduced pressure.

More successfull is the filtration technique in which a latex suspension is filtered in successive stages over micropore filters. The resulting wet paste is transferred to the plugholder (see fig. 3-16b). However, plugs so obtained exhibit instability; possibly due to enclosed air, non-coagulated regions and inhomogeneities. Of course, such a plug can be stabilized by drag forces excerted by permeating liquid on the particles, causing a plug-pressure that increases in the direction of flow. But this stabilization is an irreversible process, in which particles are displaced with respect to each other (flow and pressure consolidation)[46], thereby reducing the porosity. Finally a stable, coagulated though inherently anisotropic plug results. Direct filtration in the plugholder, provided with a filter on one side, is precluded by the role of surface forces (charged particles) controlling the deposition of the particles. The necessary bridge forming of the charged particles over the pores of the filter medium is decreased by their mutual repulsion forces and partial blocking filtration occurs, thereby increasing the hydrodynamic resistance. Furthermore, the filter medium is inhomogeneous, causing the plug to be inhomogeneous in the direction perpendicular to the main flow[46,47]. Stirring the suspension during filtration can improve this situation to some extent. The deposition onto the first coagulated upper-

layer is determined by van der Waals, electrical double layer and viscous interaction forces with neighbouring moving particles. The primary structure of the plug will be determined by the first layers and micro-inhomogeneities will easily lead to macro-inhomogeneities. Upon applying a constant pressure difference, the filtration finally stops due to the increased hydrodynamic resistance of the formed plug and of the resistance of the partly blocked filter medium. Reasonably high pressure differences were required to complete the filling of the plugholder (length 1,5 cm). In most experiments this procedure failed. The plugs showed mechanically unstable behaviour during permeability experiments, especially at flow reversal and this even at relatively low pressure differences ($\Delta P \sim 15$ cmHg). Consolidation takes place in the non-coagulated regions. At the outset the densest parts are consolidated at the expense of the less dense parts. Initially, we notice an increase of permeability, indicating increased inhomogeneity, but after a long time a decrease to a constant value indicating complete consolidation.

The most succesfull preparation technique employs centrifugation, as also used for measurements of coagulation forces[48-50]. During centrifugation, at specified speed and ionic strength, the latex concentration at the bottom of the centrifuge tube increases and the lower-most layers start to coagulate whereas the non-coagulated sediment decreases in mass till the critical coagulation force is reached.

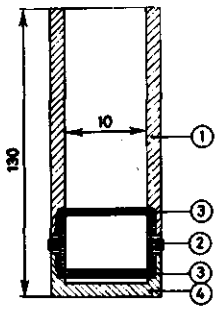

Fig. 3-15. Dimensions of the centrifuge tube
1-perspex threaded tube; 2-plugholder (see fig. 3-16b too);
3-teflon o-rings.

The deposition of the solid particles is a discontinuous process. In order to fill the plugholder completely some of the depleted supernatant is periodically replaced by original suspension; the number of replacements depends on initial concentration, centrifugation speed, ionic strength and the volume of the plugholder. The procedure is continued till the coagulation zone has passed the upper part of the plugholder to ensure complete coagulation throughout (see fig. 3-15). For that part of

the plug extending above the upper surface of the holder the maximum possible centrifuge speed is used. The threaded plugholder with the plug is then taken off by unscrewing, the protuding parts of the plug are cut off and checked for completeness of coagulation. The plug surfaces are moistened to prevent drying during their positioning between two perforated electrodes, with electrolyte-reservoirs on either side (see for the assembling prodecure section 3.6.2 and fig. 3-16b).

Table 3-2 shows that all plugs have a density far away from their state of densest packing (hexagonal close-packed: porosity $\varepsilon = 0.27$), irrespective of surface charge density, ionic strength, initial concentration and centrifugation speed. By examining electronmicrographs of coagulated latex arrays formed during measurements of interacting forces with the compression method, Barclay et al.[51] deduced a strong influence of particle size on the packing density. For small particles (radius 88 nm) the repulsive forces must have caused the particles to move around during settlement, until they attained closest packing. Compression of suspension with larger particles (550 nm) resulted in a disorded array of spheres, as in our case, which can be concluded from the relatively high ε-values. Unfortunately, the possibility of significantly exceeding the critical speed for coagulation, was limited. In one case (see table 3-2) leakage of the centrifuge tube caused an accelerated settling of particles, thereby increasing the effective number of kinetic elements in the coagulation process as can be noticed from the relatively high ε-value. The speed at which coagulation starts can be reduced by using higher initial latex concentrations. The required thickening of the suspension can be achieved by several weeks of undisturbed storage and/or by centrifuging at a speed below the critical value. It should be mentioned that association of particles increases with the solid concentration. Even small aggregates can disturb isotropic formation of the plug during centrifuging.

In table 3-3 we have summarized the critical pressures required for coagulation as calculated from the formula:

$$P_{cr} = \tfrac{1}{2} (\rho-\rho_o)(1-\varepsilon)\omega^2(r_1^2-r_2^2)/A \qquad (3\text{-}77)$$

where ρ_o and ρ denote the densities of medium and the latex particles respectively, ω the angular velocity of the centrifuge and A the cross-sectional area of the centrifugation tube, r_1, is the distance between the rotoraxis and the *upper* boundary of the coagulated plug. r_2 is the

Table 3-2. Influence of initial latexconcentration, electrolyte concentration, surface charge density and centrifuge speed on the porosity. Radius of rotation 18.7 cm. L: σ_o = 0,906 μCcm^{-2}; M: σ_o = 4.00 μCcm^{-2}; H: σ_o = 9.21 μCcm^{-2}.

plug			centrifuge speed r.p.m.	$c_{electrolyte}$	volume conc. latex %	porosity ε
I		L	2900	-	4.0	0.4085
II		H*	3800	-	4.5	0.4581
III	A,B,C	L	2800	-	4.0	0.3936
IV	A,B	H	3700	-	4.5	0.421
V	A	L	3500	2.5 10^{-2} M LiCl	2.3	0.3985
V	E	L	"	" KCl	2.3	0.3959
V	C	L	"	" CsCl	2.3	0.3985
VI	A	L	"	-	4.5	0.4120
VI	B	L	"	-	4.5	0.4112
VII	A	H	3200	-	11.0	0.4029
VII	B	H	"	-	9.4	0.3867
VII	C	H	"	-	7.5	0.3685
VIII	A	M	3500	-	6.0	0.4154
VIII	B	M	"	-	6.0	0.4049

* leakage of the end cap during centrifugation

distance of the rotoraxis to the position of the upper boundary *after* complete coagulation, which can be achieved by replacing part of the supernatant by a high concentrated electrolyte solution followed by centrifuging at the maximum speed. The porosity of the coagulated sediment layer prepared in this way with thickness (r_1-r_2) may be regarded as identical to that of the plug. Due to the moderate centrifugation speed used, the thickness of the sediment ultimately coagulated amounts to several millimeters and is consequently readily measured. When latices

Table 3-3. Some experimental coagulation pressures, P_{cr}, for three surface charge densities at different electrolyte concentrations.

	$P_{cr}.10^{-3}$ (Nm^{-2})		
c	-	10^{-3}M	2.5 10^{-2}M
L	2.4	3.4 (KCl)	2.8 (KCl)
M	4.9		
H	5.8	3.4 (KCl)	1.9 (Li,K,CsCl)

having relatively low coagulation forces are centrifuged, it is more convenient to measure the mass, m, of the non coagulated sediment (see e.g. Meyer et al.[50]). The critical force for coagulation is then calculated from:

$$F_{cr} = m\,(1-\rho/\rho_o)\,\omega r_1^2 \qquad (3\text{-}78)$$

The results of table 3-2 and 3-3 show that an attempt to vary the porosity by changing the counterion was not successfull. An explanation can be that for the radii of the particles used in our study (250-300 nm) a detectable specific ion effect will only be manifested at higher electrolyte concentration[51]. Besides, the force pressing the particles together exceeds the minimum force for coagulation; consequently kinetic elements probably mask the effects of particle size and type of counterion.

As to the mechanical stability one must realize that in general a plug is formed under pressure conditions that exceed those used in electrokinetic experiments. Consequently it normally does not exhibit unstable behaviour. In our case permeability experiments were performed at pressure differences up to 30 cm Hg ($4.0\ 10^4\ Nm^{-2}$). Even so no changes in the structure of the plug were observed which indicates complete coagulation.

3.6.2 *Electrokinetic equipment*

Fig. 3-16a and b show details of the electrokinetic equipment*. The procedure for assembling the equipment is as follows (see fig. 3-16b). The perforated electrode support (2) with the teflon o-ring (3) and plug electrode (5) are inserted as one unit into the end cap (1), after which

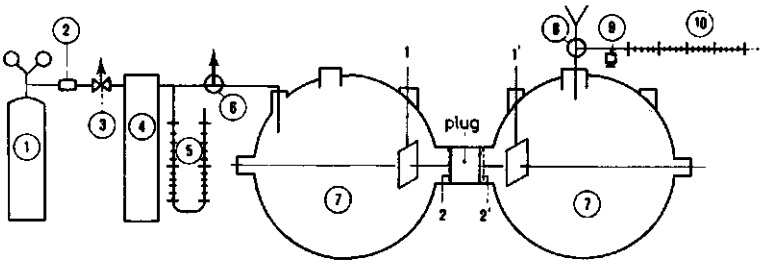

Fig. 3-16a. Equipment for measuring electrokinetic quantities.
1. cylinder with compressed N_2
2. pressure valve
3. Moore nullmatic pressure regulator (Foxboro: model 41A)
4. pressure vessel
5. mercury manometer
6. air cock
7. electrolyte reservoirs
8. filling device with air outlet for refilling
9. syringe
10. calibrated capillary tube

1,1'/2,2' - Ag/AgCl electrodes

* Designed and constructed in cooperation with S. Maasland, Laboratory for Physical and Colloid Chemistry, Agricultural University, Wageningen, The Netherlands.

the central sample holder (4) with or without a plug is screwed into the end cap. The teflonring (3) seals the threaded end cap. The other end cap with the same parts is also screwed into the plugholder until a tight fit is obtained. The connections of the electrolyte reservoirs(9) are inserted into both end gaps and fastened with the souvirel caps (6). The electrode leads, isolated in tight glass capillaries (8), enter the reservoir through the souvirel end caps. After the reservoirs have been filled with

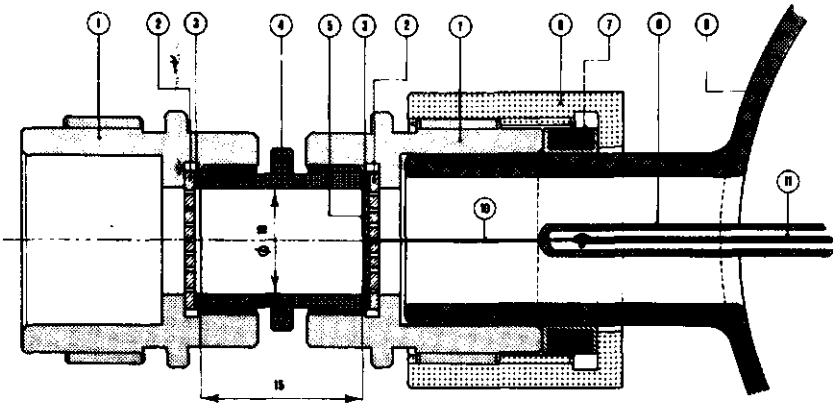

Fig. 3-16b. Dimensions of the plugholder section

1. double threaded end cap
2. perforated electrode support (teflon)
3. teflon o-ring
4. threaded plugholder
5. perforated silver-silverchloride plug electrodes (disk)
6. Souvirel connection cap with a hole for mounting the reservoirs
7. self sealing rubberring gasket covered with teflon
8. glass tubing
9. electrolyte reservoir
10. isolated platinum leads to plug electrodes
11. coaxial cable

electrolyte solution, the air is expelled from both reservoirs simultaneously (no liquid or air displacement into the plug or plugholder), in order to remove any air bubbles near the plugsurfaces.

The 1,1'-plate electrodes (surface area per electrode: 2.5 cm^2) are mounted in the reservoirs. In order to perform electro-osmotic flow and permeability experiments the filling device (8), with the calibrated capillary tube (10) is assembled. An adjustable syringe (9) is used to set the initial level in the capillary. The pressure regulator (3) is adjusted to the desired pressure (5). The aircock, placed between pressure vessel and electrolyte reservoir, permits instantaneous application of the adjusted pressure difference or a quick depressurization (< 0.2s). The symmetry of the equipment allows reversement of liquid flow by interchanging the pressure inlet with the filling device.

The optimum choie of the calibrated capillary has to be considered in relation to the system as a whole, the purpose of this capillary being to measure accurately pressure or current induced flows. The factors to be considered include the flow characteristics of the plugs, the dimen-

sions of the cell and the requirement of a negligible hydrodynamic resistance. A direct verification is obtained by measuring E_s at fixed ΔP with and without the filling device and capillary. It was found by trial and error that the optimum diameter was 0.4-0.6 mm. The capillary tube was cleaned by soaking it in chromic acid, and then rinsing it thoroughly with demineralized water prior to testing.

electrodes: each electrode is connected to the outside of the cell by a platinum wire permanently welded to the back surface of the platinum disk. In order to avoid exposure of the leads to the electrolyte solution, they have been isolated in tight glass capillaries. The degree of perforation of the plug electrodes was adapted to the permeability of the plugs. By choosing an electrode and its support having their porosity comparable to that of the plug but with pores 1000 times greater in diameter, $\emptyset$ = 0.3 mm, results in a hydrodynamic resistance that is negligible with respect to that of the plugs. The silver-silverchloride electrodes were prepared in the usual way[52], which basically consists of plating the bare platinum electrodes with high purity silver, followed by a partial conversion to silverchloride. The electrodes were aged for 3 days at 80°C in a solution of $pCl \approx 4$ and stored in the same solution, mutually short-circuited, until usage. Individual voltage readings usually differed by less than 0,5 mV.

*Electrical system**

The experiments required a sensitive and continuous reading system for rapid simultaneous measurement of current and resistance. All electrode terminals were connected to a multifunctional box, which made all electrode signals clear for recording purposes (see fig. 3-17). The leads from the electrodes to the converters are separated shielded with coaxial cables. The shields are connected to one point of the electronic box. This box contains:

- an ultra high impedance differential amplifier, serving the dual purpose of bringing the output within the operating range of the recorder device (gain select: 1x, 10x, 100x) and providing adequate high input impedance;
- a current-voltage converter of which both inputs are isolated from ground;
- a constant current source which generates currents with three ranges: 10 μA, 100 μA and 1 mA. The stability was 0.5% of the chosen range.

* The electronic part was developed and built by R. Wegh, Laboratory for Physical and Colloid Chemistry, Agricultural University, Wageningen, The Netherlands.

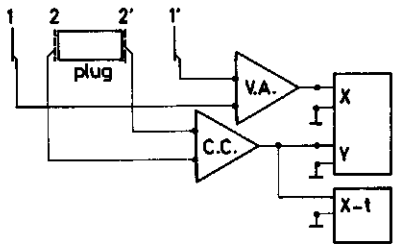

Fig. 3-17. Circuity used in streaming current experiments (see text). V.A. - ultra high impedance differential amplifier: input impedance > $10^{10}\Omega$; common mode > $10^{11}\Omega$; output impedance < 75Ω. C.C. - current-voltage converter: input impedance << 10^{-3}x source impedance; output impedance < 200Ω; selectable output 100 μV/volt, 10 μA/volt, 1 μA/volt

All terminals could be connected to any combination of Ag/AgCl-electrodes of one of four equipements by using selectors. For streaming current experiments the current-carrying electrodes are connected to the C.C. device, the potential measuring electrodes to the V.A.-device. The outputs of both converters are connected to the input of a X-Y recorder (Speedomax XL 684; Leeds & Horthrup) and one output to a X-t recorder (Kipp BD-5) in case the timedependency of the streaming current has to be measured. Since both recorders have a time constant of about 0.2 s, identical to that of the pressure device and the time constant of the electronics is negligible, any immediate changes in current and/or voltage could be measured within a fraction of a second.

Temperature regulation and measurement

The whole equipement was placed in a thermostatted box provided with a cooling thermostat, a heating element and a temperature control element connected to an electronic regulator. The temperature fluctuations in the box were held to within 0.2°C. The temperature fluctuations in the electrolyte solution in the reservoirs could be easily kept within 0.1°C.

Survey of usual combinations of electrodes in electrokinetic and control experiments

streaming potential: 1,1' or 2,2'
streaming current : mostly 2,2' for I and 1,1' for E
electro-osmosis, electro-osmotic counter pressure, d.c. resistance determination: 4-electrode technique; 1,1'-working electrodes; 2,2' for E
a.c. resistance measurements: 2,2'
salt filtration experiments; 1,1' and/or 2,2'
measurements of local concentration changes at the plug surfaces: 1,2 and/or 2',1'.

Imperfect seals may develop minute cracks giving anomalously high fluctuating potentials and a sluggish response in reaching their ultimate potentials. An imperfect electrode or rest potential can easily be detected by measuring the potential difference of the various combinations (1,2), (2,2'), (1,1') or (2',1') during a pressure change.

3.7 *Streaming potential experiments: verification of the time dependency of E_s and calculation of the electrolyte content of the porous phase*

Prior to an experimental run, the plug was permeated, until complete equilibrium was attained. A check could be made by intermittently recording one of the electrokinetic variables, suitable for this purpose. Generally, a 20-fold displacement of the interstitial liquid of the plugs (within 2 days at ΔP = 30 cm Hg) was adequate to attain steady conditions. Our "stable" reversible electrodes made it possible to obtain data at very high ionic strength. Only at c_o above about 0.3 M 1-1 electrolyte the magnitude of the streaming potential (< 0.1 mV at ΔP = 30 cm Hg) limited accurate determinations. Considerable attention was given to experimental problems such as electrode polarization and asymmetry potentials (see the review of Ball and Fuerstenau[5]). The measurements were accomplished by monitoring the change in potential between two reversible electrodes resulting from a pressure change. In the studied pressure range (30 cm Hg), for all plugs, plots of the measured potential difference against the applied pressure change gave straight lines passing through the coordinate origin. Small base-line potentials (residual potentials at ΔP=0) were automatically eliminated. It made no difference in the results if they are obtained with an increase or decrease in pressure. No hysteresis was detected. Some examples are presented in fig. 3-18. The linearity of the results indicate the absence of side-

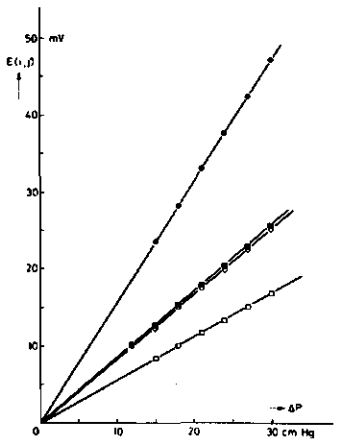

Fig. 3-18. Streaming potential vs. pressure for plug IIIB (L) ● KCl, ■ $BaCl_2$ and plug IV (H) ○ KCl, □ $BaCl_2$; $c_o = 10^{-3}$M, t = 25.0°C

effects; all plugs were studied well within creeping flow conditions (see section 3.7.4).

In the literature much attention is given to the appearance of intercepts in actual plots of recorded potentials vs. pressure differences (Ball and Fuerstenau[5]). If the same asymmetry is observed in both flow directions, the cause is supposed to be more than an "electrode effect". Recently, Eagland and Allen[53] observed a clear trend with regard to the alkali ions in the positive pressure difference corresponding to zero streaming potential for P.V.A. plugs (beads). These findings were associated with a yield stress of the boundary layer on the particles. Inspection of these and similar results reported in the literature reveals the following:

- the magnitude of the intercept tends to zero as the ionic strength is increased;
- the slope, $\delta E_s/\delta P$, of the E_s-ΔP curves remains constant despite the time dependence of the intercepts;
- in none of the cases was a transition region observed which would be typical for a yield stress of the boundary layer.

Apparently, the fact that at low ionic strength coarse porous plugs may exhibit salt rejection had been overlooked in these analysis. This phenomenon implies that during permeation, the concentrations near the plug boundaries may change. The ensuing non-steady state phenomena have been analyzed in section 3.3. The effect of development of a concentration profile on the determination of E_s was thoroughly examined. It appeared that the relatively slight rejection by our coarse porous plugs hardly influenced the magnitude of the electrokinetic quantities, even after prolonged permeation. However, they caused "erratic rest potentials" in both flow directions. Fig. 3-2 in the theoretical section 3.3 is very representative of the time dependency of E_s for all our plugs studies below about 10^{-3} M, where they become somewhat selective. When the experiments were performed in a partly systematic way, specific ionic trends were observed in the "rest potentials", at least if they were recorded after a similar period of permeation of the electrolytes involved. With the four electrode technique we could rigorously discriminate between an "electrode effect", the appearance of local concentration changes and "boundary effects" by monitoring separate potential differences, viz., E(1,1'), E(2,2') and E(2,1') during the course of an experiment. Only a time dependent concentration change at the low pressure side could be detected at relatively low ionic strengths ($\leqslant 10^{-3}$M 1-1 electrolyte).

Figures 3-19, 3-20 and 3-21 represent some experimental results for our polystyrene plugs. Fig. 3-19 shows the time dependency of E(2',1') at three different temperatures and one pressure difference. At higher temperatures the electromotive force increases. This could be anticipated from eq. (3-34); at increasing temperatures J_v' as well as D will be enhanced due to a decrease in the viscosity, but the increase of J_v' will

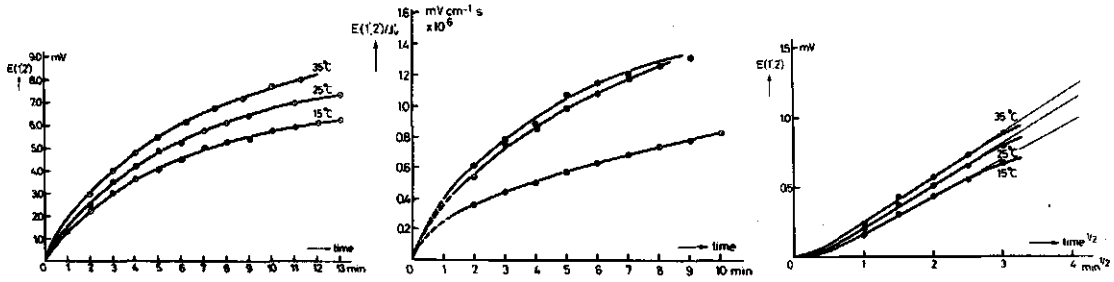

Fig. 3-19. The time variation of the potential difference $E(1',2')_t$ between to silver/silverchloride electrodes at the low pressure side at the plug boundary and in the bulk at ΔP = 30 cm Hg. Plug VIIB (H); c_o = 2.65 10^{-4}M KCl; temperature as indicated in the figure.

Fig. 3-20. $E(1',2')/J_v'$ vs time for 0.92 10^{-3}M LiCl ○, 1.00 10^{-3}M KCl ◒ and 1.00 10^{-3}M CsCl ● and plugs VIIA, VIIB and VIIC (H) resp. at 25.0°C.

Fig. 3-21. E(1',2') as a function of the square root of time for 0.92 10^{-3}M LiCl (VIIA, H) and ΔP = 30 cm Hg at three temperatures.

exceed that of $D^{\frac{1}{2}}$. In other words, both the convection flux and the diffusion flux increase with temperature, but the increase of the convection flux being more pronounced, the depletion will be faster. Fig. 3-20 shows the time dependency of the quantity $E(2',1')/J_v'$ for three different electrolytes at the same temperature and nearly the same concentration. In potential difference should be divided by the convection velocity in order to show the influence of the kind of electrolyte (see eq. (3-34)). This ratio depends on the cation transport number and the electrolyte diffusion coefficient. The former of these plays the dominant role. This is confirmed by the much slower increase in the case of LiCl.

Fig. 3-21 shows E(2',1') as a function of $t^{\frac{1}{2}}$ at three different temperatures for 10^{-3}M LiCl. The straight line predicted by the theory of concentration polarization, eq. (3-34), is confirmed, at least for short periods. For very short periods the theory is not corroborated because just after application of the pressure difference, the concentration in the liquid leaving the plug will not equal c_p, due to the gradual concentration change from c_p to c_o in the first layers of the plug. From the

slope $dE(2',1')/dt^{\frac{1}{2}}$, c_p can be calculated. This is done for various experimental parameters (kind of electrolyte, conc., temp. and surface charge density). J_v' has been determined from permeability measurements under streaming potential conditions (see section 3.7.4). It was shown that the filtration coefficient, L_p, is not influenced by induced osmotic forces that arise from concentration polarization processes. Values of c_p are presented in tabel 3.4. It is allowable to compare the results for the different plugs because their porosities differ only slightly. Three features are noticed:

Table 3-4. Calculated c_p-values according to eq. (3-34) and pertinent parameters for L, M and H. Except for III^p(A), all results correspond to plugs treated at high ionic strength. Values of t_+ and D were calculated from tabulated values (Parsons).

Plug type	c_o M x10^4	temp. °C	J_v' cms^{-1} x10^5	$-E(2',1')_t/t^{\frac{1}{2}}$ mV.min.$^{-\frac{1}{2}}$	c_p M x10^4
III A(L)	2.00 KCl	25.0	9.45	0.394	1.34
III B(L)	2.00	"	8.37	0.476	1.09
V B(L)	1.00	"	11.01	0.860	0.50
	7.65	"	11.54	0.214	6.82
VIII B(M)	2.00	"	10.82	0.856	1.04
	10.0	"	11.10	0.140	9.2
VII A(H)	2.44 LiCl	15.0	7.41	0.440	1.44
	"	25.0	9.74	-	-
	"	35.0	12.17	0.595	1.48
VII B(H)	2.65 KCl	15.0	6.89	0.620	1.26
	"	25.0	8.85	0.720	1.29
	"	35.0	11.13	0.803	1.33
VII C(H)	2.78 CsCl	15.0	6.35	0.515	1.49
	"	25.0	7.96	-	-
	"	35.0	9.68	0.648	1.50
VII A(H)	9.20 LiCl	15.0	7.79	0.075	8.6
	"	25.0	10.00	0.086	8.6
	"	35.0	12.35	0.095	8.6
VII B(H)	10.0 KCl	15.0	7.41	0.120	9.1
	"	25.0	9.33	0.138	9.0
	"	35.0	11.20	0.151	9.1
VII C(H)	10.0 CsCl	15.0	6.44	0.105	9.1
	"	25.0	7.83	0.118	9.0
	"	35.0	10.12	0.135	9.1

- c_p-values do not vary extensively, either with temperature or with the kind of electrolyte;
- c_p deviates significantly from c_o at concentrations smaller than 10^{-3}M;
- as a result of more pronounced exclusion of co-ions, high surface charge densities cause lower c_p-values.

In sector 4.7 the c_p-results will be further analysed and transformed into double layer parameters. That the moving average electrolyte concentration, c_p^{he}, may differ from the static one will also be considered there.

Fig. 3-22 presents the results of an experiment in which the pressure difference was suddenly reversed after twenty minutes. Starting from the absence of a potential difference between electrodes 1 and 2 during filtration, during the first minutes a negative potential is found indicating the passage of electrolyte that had been accumulated in the first layers of the plug at the high pressure side.

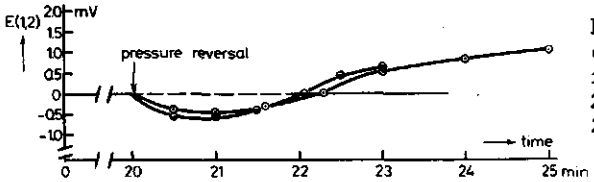

Fig. 3-22. E(1,2) vs time during application of a constant pressure (30 cm Hg) followed by a pressure reversal for c_o = $2.44.10^{-4}$M LiCl (VII A,H)○ and $2.65\ 10^{-4}$M KCl (VII B,H)● at 35.0°C.

3.7.1 *Electro-osmosis and electro-osmotic counter pressure experiments*

In order to obtain reasonably accurate values for liquid flow and counter pressure in electro-osmotic investigations, relatively high current densities have to be applied for some time. This means that the concentration polarization effects already discussed in section 3.5 are even more important here. The combined processes of electric current (through the plug), convection and diffusion give rise to time dependent concentration profiles within the plug, thereby changing the electrokinetic quantities[7,8,10,55].

In other words, the passage of an electric current gives rise to time dependent phenomenological coefficients, L_{ij}. Prolonged current of relatively high density might even lead to zero concentration at the boundary of decreasing concentration, resulting in the occurrence of additional modes of transference (Bethe and Toropoff effect[54]: concentration polarization at the anodic interface, induces the dissociation of H_2O into H^+ and OH^-, the former replacing the migrating counterion in the porous phase). Small induced external concentration changes can influence the pore liquid composition by various mechanisms. The more important effect during the

passage of an electric current is the electro-convection process giving rise to a volume flow in the direction of the cathodic side. By this process the profile at the anodic side, which is characterized by a time dependent concentration decrease, is transported into the porous phase, so that the pore liquid concentration gradually decreases. If both the electro-convective and osmotic flows can be neglected the back diffusion of electrolyte due to the induced concentration difference will cause the porous system's electrokinetic properties to change in the direction of high concentration[56,57]. The latter effect plays a dominant role in fine porous membranes and is observed during the determination of transport numbers.
From these considerations it is obvious that experimental conditions bear heavity on the determination of the phenomenological coefficients. In order to ensure a linear voltage-current and volume flow-current relationship, the current must be far below the limiting current. The solution near the membrane surfaces must be agitated if possible (when electro-convection dominates stirring of the solution at the anodic side only is sufficient). Periodic interruption of the current is also effective.

Constant currents of short duration (not more than 3 min. at a given current polarity, just the time necessary to produce a 5 cm liquid displacement) were imposed on the cell through the Ag-AgCl plate electrodes (1,1') and interrupted for 5 min. Each experiment was performed for several current densities, up to a maximum of 0.4 mA/cm^2. After each run the same procedure was applied in the reverse direction. The volume flux of the liquids was measured by the rate of advancement of the liquid meniscus in the calibrated capillary.
Control of temperature was very important as the electrolyte reservoir connecting the plug and the capillary acted as the reservoir of a thermometer. The electro-osmotic counter pressure was also measured, for a range of current strengths by applying a pressure difference such that the liquid flow just stopped. Simultaneously current-voltage characteristics were obtained by monitoring the potential difference between the plug electrodes (2,2') during a current pulse. At the same time induced concentration changes at the plug surfaces during the current pulse and the decrease due to diffusion and natural convection during the interruption periods were followed. The results shown in fig. 3-23 and 3-24 indicate that the interruption technique minimizes the influence of concentration polarization.

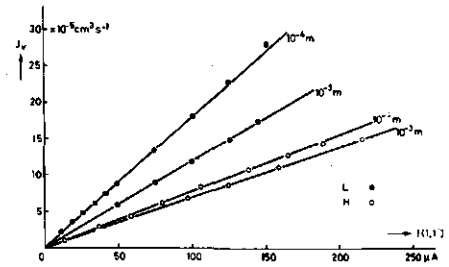

Fig. 3-23. The dependence of volume flow, J_v, on current, I(1,1') for plug I(L) and II(H) at t=25.0°C (KCl)

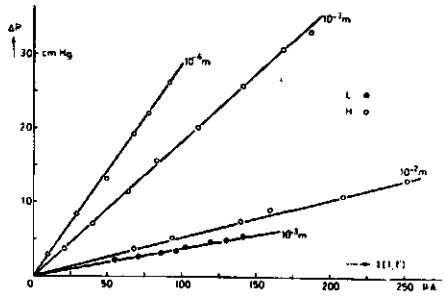

Fig. 3-24. The dependence of pressure difference, ΔP, on current, I(1,1') for plug I(L) and II(H) at t=25.0°C (KCl).

Fig. 3-25 represents an example of a characteristic *apparent* non-linear relation between volume flow and current density. The relevant electro-osmotic experiments were conducted by starting at low current densities. After some time the current was interrupted for several seconds. Then a higher current was applied for the next measurement. This was followed by another current interruption, and so on; the duration of the current

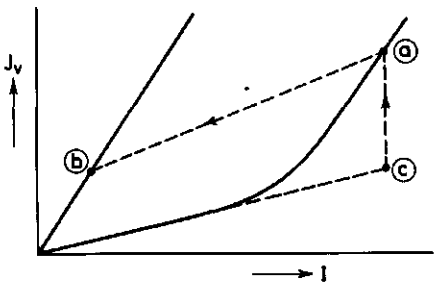

Fig. 3-25. Apparent non-linear J_v-I characteristic (see text).

interruptions was held constant. It was observed that beyond a certain value of the current density (several mA/cm²) the slope of the volume/current curve increased considerably. The location of the transition to the steeper dependence is fully determined by the experimental procedure. A sudden decrease of the current (a → b in fig. 3-25), followed by the same procedure results in the same slope as at high current values. If, starting from equilibrium the current is directly raised to high values the measured electro-osmotic displacement fits the low slope relation. If however the measurement is repeated at the same high current density, the volume flow gradually increases along the line c → a. If in situation a) a streaming potential measurement is carried out it is found that the Saxen relation (see table 3-1):

$$\left(\frac{E}{\Delta P}\right)_{I=o} = - \left(\frac{J_v}{I}\right)_{\Delta P=o}$$

holds extremely well. Furthermore, a direct resistance measurement in situation a) reveals an increased plug resistance. These findings verify the hypothesis of dominant electro-convection during electro-osmosis, leading to a time dependent concentration *decrease* of the pore liquid. The time required to reach situation a) is much smaller than the reverse process, restoration of equilibrium starting from situation a). The restoration of equilibrium can be accelerated by the following procedure: after the current has been interrupted wait some time to allow the cathodic profile to diffuse into the reservoir, and then apply pressure in such a direction that the volume flow will restore the equilibrium electrolyte concentration.

In electro-osmotic counter pressure experiments the linear relation between I and ΔP was found to hold up to much larger current densities than in the case of electro-osmotic flow. This is so because the applied pressure counteracts the concentration changes induced by electro-convection.

Finally, we draw attention to the fact that the polarization phenomena occurring during electro-osmotic experiments *carried out in a systematic way* resemble "special transitions". Additional information is needed before interpretations of non-linear J_v/I relations in terms of these transitions, as were made, e.g., by Bondarenko and Nerpin[58] can be accepted

3.7.2 *Streaming current experiments; tests of various polarization phenomena, determination of transport numbers and intrinsic relaxation phenomena from X-Y plots*

Concentration polarization at the electrodes:

The effect of concentration polarization on streaming current can be observed by applying a pressure change as discussed in detail in section 3.4.3. Fig. 3-26 represents the characteristic retardation behaviour as a function of the electrolyte concentration. At high concentrations (10^{-1} M) the retardation is very pronounced, even to the extent that in the case of fast application of the pressure difference and fast recording, the instantaneous value of I(2,2') - see fig. 3-26 - only amounts to less than half the value of the real streaming current. Going from 10^{-1} to 10^{-2} M the retardation process decreases as a result of the in-

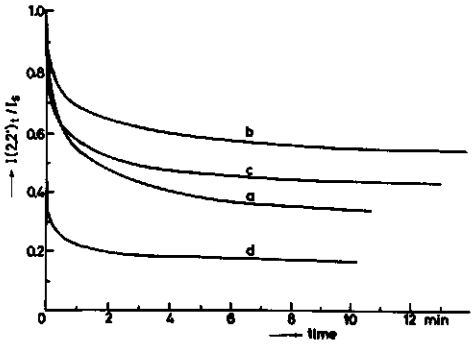

Fig. 3-26. Current retardation for short-circuited plug electrodes during pressure application (30 cm Hg). plug III A(L): a. 2 10^{-4}M; b. 10^{-3}M; c. 10^{-2}M; d. 10^{-1}M KCl. t = 25.0°C.

crease in the plug resistance, R_p. A further decrease in electrolyte concentration only slightly affects the value of R_p, because fixed charge plugs and membranes tend to exhibit constant resistances at low concentrations (see section 4.5). The diffusion resistance R_d, will however become more and more important because of the decrease in the value of c_o (see eq. (3-64) and (3-65). At the same time we notice from the reverse in sequence of the retardation curves the effect of time as predicted by eq. (3-65).

Another feature of fig. 3-26 is the ultimate steady value of the current, which can be interpreted as the result of natural and forced convection which prevents unlimited spread of the diffusion layer.

Measurement of local Cl^--concentration during retardation:

The Cl^--concentration decrease at the high pressure side and the increase at the low pressure side during pressure application (negatively charged plugs) can be followed by monitoring the potential differences E(1,2) and E(2',1'). The 1,1'-electrodes serve as reference electrodes. An example for the low pressure side is given in fig. 3-27. A pressure difference of 30 cm Hg was applied till steady state conditions were reached. In case a) the equipment was depressurized at t=o, in case b) the 2,2'-electrodes were disconnected. At t=7 min. the pressure difference ΔP = 30 cm Hg was applied again in case a) and the 2,2'-electrodes were short-circuited in case b). In both cases the potential change indicates the effect of diffusion relaxation. It is evident that the change in interfacial concentration is faster when the electrodes are short-circuited and current flow can take place. From the change to steady-state for $t \geqslant 7$ min. it can be inferred that the contribution of convective flow (ΔP = 30 cm Hg) to the interfacial concentration change is relatively small, at least for short periods. By recording the variation of interfacial potential at the high pressure side it could easily be checked

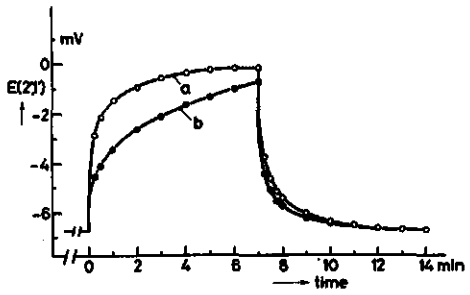

Fig. 3-27. Example of the variation in the interfacial potential of the 2'-electrode upon a) pressure change o, b) disconnection or short-circuiting of the 2,2'-electrodes at constant pressure difference ●. At $t < o$: $\Delta P = 30$ cm Hg, 2,2'-electrodes are short-circuited; at $o \leqslant t \leqslant 7$ min. a) the pressure is removed and b) the electrodes are short-circuited; at $t \geqslant 7$ min. the conditions correspond to those before t=o.
plug VII B(H): 10^{-3} M KCl, 15.0°C.

that for $R_i << R_p$ the following relation holds: $E(1,2)_t + E(2',1')_t = E(2,2')_t$.

Generally, one can test the retardation phenomena due to concentration polarization for any equipment and electrode set by applying a constant current pulse through the cell containing electrolyte enclosed by the perforated electrodes short-circuited over an amperemeter with low R_i.

The effect of an external resistance on streaming current retardation:

We now consider an experiment according to the method of Eversole and Boardman[21] at high electrolyte concentration when the retardation is expected to be pronounced. Fig. 3-28a represents the potential difference over the shunt resistance as a function of time for various values of the external resistance, ranging from 0.4 to 100 kΩ. The picture clearly shows the retardation behaviour.

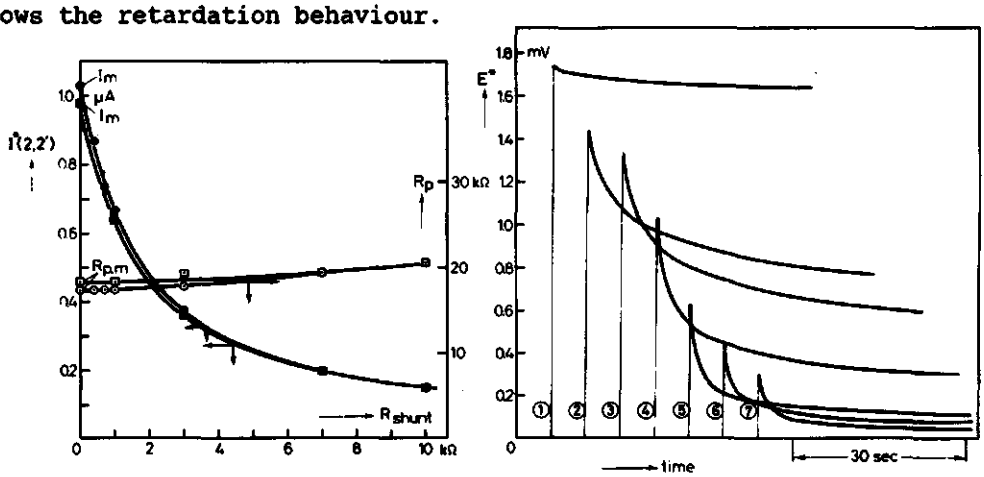

Fig. 3-28. The method of Eversole and Boardman.
a. Fast recordings of the potential difference over the plug, E*(2,2'), for various shunt resistances and $\Delta P \rightarrow 30$ cm Hg. R_{shunt}: 1-1.00 10^2; 2-10.0; 3-7.00; 4-3.00; 5-1.00; 6-0.700; 7-0.400 kΩ. The results for 6 and 7 have been multiplied by a factor 2.
b. Instantaneous maximum current, I*(2,2') and plug resistance R_p* vs. R_{shunt} calculated from max. E*-values in fig. a. according to $I^*(2,2') = E^*_{shunt}/R_{shunt}$ and eq. (3-70) resp.
plug VIII A(M); $c_o = 10^{-1}$ M LiCl; t = 25.0°C. ΔP : 30 → 0 ● ○ ; ΔP : 0 → 30 cm Hg ■ □

In fig. 3-28b the instantaneous maximum values, I_m, are plotted versus the shunt resistance. Moreover, using eq. 3-70 the plug resistance, $R_p (= L_{22}^{-1})$ was also calculated as a function of the shunt resistance. The small systematic differences between the results for $\Delta P \rightarrow 30$ cm Hg and $\Delta P \rightarrow 0$ can be attributed to the fact that at this high ionic strength the retardation is very fast. Therefore, the maximum values of I(2,2') are influenced by the speed of pressure change. The result is a more or less constant plug resistance of about 2 kΩ. So the shunt method seems to produce accurate and reproducible results. But, despite its reproducibility there is a large systematic error in the plug resistance, its true value being 865 ohms, as determined from the extrapolated values, E_s and I_s, in an X-Y plot. Admittedly, the example we have chosen is a rather extreme one because of the high electrolyte concentration (10^{-1}M), in which case the retardation is very fast. But, although at lower concentrations the deviation will be less drastic, as a rule the shunt method leads to excessively high plug resistances, or, to streaming current values that are too low. Fig. 3-29 examplifies the influence of the input impedance upon the retardation behaviour of the streaming current in an X-Y plot at a concentration, for which the selectivity is absent ($\tilde{t}_+^a = t_+$). For the X-Y plot it makes no difference if they are recorded with pressure application or removal (superposition principle). The slope of an arbitrary "retardation line" can be used for the determination of L_{22}. Extrapolation of this line to I=0 and E=0 yields correct values for E_s and I_s resp.

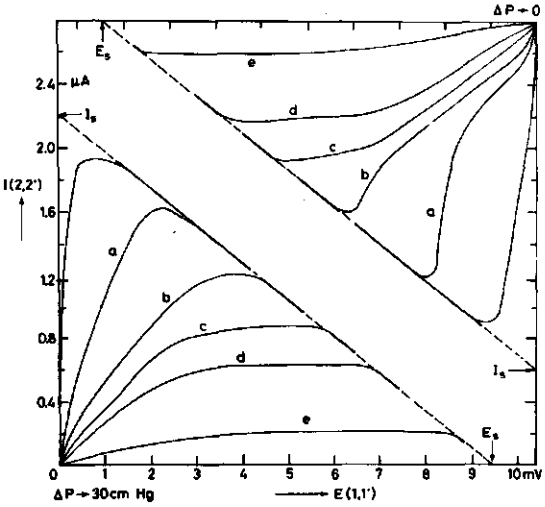

Fig. 3-29. Influence of the input impedance, R_i, on streaming current retardation for $\tilde{t}_+^a = t_+$. R_i: a-1.00; b-3.00; c-6.00; d-10.0; c-40.0 kΩ. The not-indicated curves correspond to $R_i \ll R_p$. Plug V C(L), $c_o = 10^{-2}$M CsCl, t=15.0°C.

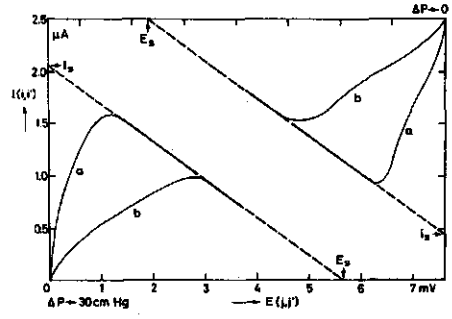

Fig. 3-30. Influence of electrode spacing on streaming current retardation for $\tilde{t}_+^a = t_+$. a. I(2,2')-E(1,1'); b. I(1,1')-E(2,2'). plug VII C(H), $c_o = 10^{-1}$M CsCl, t=35.0°C.

This plot clearly demonstrates that application of a high input impedance, yielding a relative short "retardation line", makes the extrapolation procedure less accurate. Similar results are obtained when the external resistance is introduced by electrode spacing. For this the 1,1'-electrodes were short-circuited and the 2,2'-electrodes used for the potential difference measurement. Consequently not the full potential drop is detected during the retardation (section 3.4.4). However, at the high ionic strength used in the example in fig. 3-30 ($\tilde{t}_+^a = t_+$) the extrapolation procedure yields again I_s and E_s. Fig. 3-31 is a typical example, showing the effect of the plug selectivity ($\tilde{t}_+^a \neq t_+$) on the retardation behaviour. Three situations are considered:

1. the X-Y plot is recorded using a very low R_i;
2. an external resistance is introduced by electrode spacing, using the method presented in the preceding example;
3. the Ag/AgCl-electrodes are replaced by irreversible Pt-electrodes.

In case 1. extrapolation of the retardation line gives I_s and $E(1,1')_{I=0}$. From the latter quantity and the separately measured E_s $\tilde{t}_+^a$ can be calculated, using eq. (3-57). In case 2. the same slope is obtained as in case 1. but extrapolation of I(1,1') to E(2,2')=0 leads to excessively

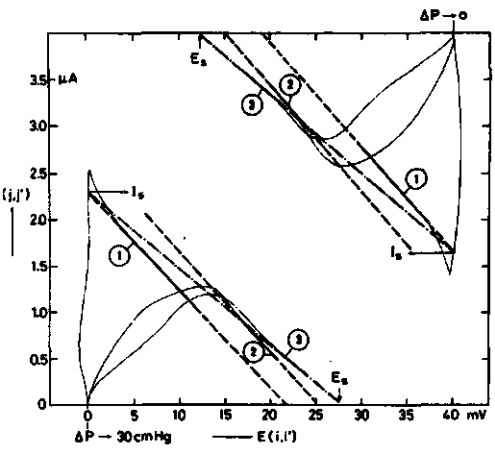

Fig. 3-31. Influence of the electrode spacing and the reversibility of the electrodes on streaming current retardation. 1. I(2,2')-E(1,1');
2. I(1,1')-E(2,2');
3. I(1,1')-E(2,2') with 1,1'-electrodes of Pt.

Plug M, 10^{-3}M KCl, t=25.0°C.

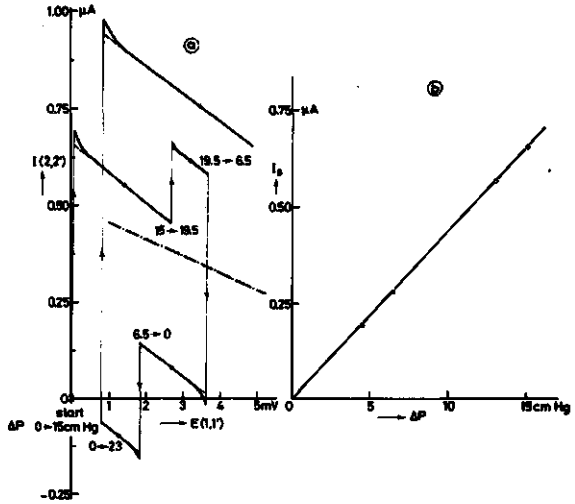

Fig. 3-32. Superposition plot.

a. I(2,2') vs. E(1,1') during application of several pressure changes at arbitrary times, as indicated in the figure. The arrows indicate the direction of the current/voltage change. The dashed line represents a slope corresponding to L_{22}.

b. Plot of extrapolated I_s-values vs. pressure difference, ΔP, determined from the superposition plot.
Plug IV(H), $c_o = 10^{-4}$M $BaCl_2$, t=25.0°C.

high streaming current values. In case 3. the use of irreversible electrodes eliminates the transport number effect; extrapolation yields directly I_s and E_s. All retardation curves show that the first part shows higher values than those corresponding to extrapolation of the linear portion, which points to a slow intrinsic relaxation contribution to the streaming current. For cases 2. and 3. this effect is seemingly less pronounced. However, as indicated in section 3.5.1, the existing and increasing potential difference present just after pressure application suppresses the intrinsic contribution to I(1,1').

Superposition principle:

Fig. 3-32a represents experimental data illustrating the superposition principle. It will be seen that the slope of the retardation lines differs from the "theoretical" quantity L_{22}. L_{22} is determined from the streaming potential and the streaming current of which the former is measured in a separate experiment and the latter is found from extrapolation of the retardation line to E=0 at the same pressure difference. The deviations in slope of the actual retardation lines indicates that the cation transport number in the plug differs from its bulk value. In fig. 3-22b we have plotted the extrapolated I_s-values versus the corresponding pressure difference. The straight line clearly shows the excellent linear dependence on pressure in the range studied.

Determination of tranport numbers from X-Y plots:

In section 3.4.2 it has been pointed out that the X-Y plot permits a direct determination of the transport number in the porous phase. In order to obtain a line of sufficient length, making the determination of the pertinent parameters, I_s and $E(1,1')_{I=o}$ accurate, the retardation line has to be monitored over an extended period and for $R_i << R_p$. An example of a series of measurements for one surface charge is given in table 3-5. All pertinent parameters have been obtained from X-Y plots, and separately performed streaming potential and permeability experiments. The $\tilde{t}_+^a$-data were calculated according to eq. (3-57), making allowance for the difference between κ^* and L_{22} (see table 3-1). The results for concentrations below 10^{-4} M LiCl and KCl, have been omitted because an extremely slow intrinsic relaxation phenomenon impedes accurate determination of $E(1,1')_{I=o}$. It can be inferred that by increasing the external concentration, counterion uptake increases and the plug loses its selectivity. Each pore of the plug becomes filled uniformly with the solution.

Table 3-5. Pertinent parameters of plug VIII A,B(M) at 25.0°C, required for calculating $\tilde{t}_+^a$. t_+ data (nearly independent of conc.) are taken at infinite dilution: $t_+(LiCl)=0.3364$; $t_+(KCl)=0.4906$. $\Delta P=30$ cm Hg

c moles/l		E_s mV	$E(1,1')_{I=0}$ mV	$\left(1 - \frac{L_{12}^2}{L_{11} L_{22}}\right)^{-1}$	$\tilde{t}_+^a$
$2\ 10^{-4}$	LiCl	44.6^5	16.1	1.023	0.954
	KCl	31.6^0	17.4	1.015	0.904
10^{-3}	LiCl	40.6^8	23.3	1.032	0.595
	KCl	27.9	21.0	1.021	0.655
10^{-2}	LiCl	14.3^6	11.4	1.012	0.429
	KCl	10.3^5	9.79	1.008	0.523
10^{-1}	LiCl	1.79^5	1.80	1.001	0.336
	KCl	1.17^8	1.18	1.001	0.491

Most of the direct measurements of ionic transport numbers in membranes which have been reported in literature have used some form of Hittorf procedure, in which the quantities transported have been determined analytically by permitting changes in the external concentrations to occur. The significance of such data and the conditions needed to obtain accurate transport numbers which refer to a definite solution concentration have been carefully considered (e.g. Kressman et al.[59]). The X-Y method involves very controlled polarization conditions and seems capable of avoiding the errors and difficulties likely to occur in the "classic methods".

The advantages are:

- exceedingly small currents flow (only some μA) during relatively short periods (several seconds), consequently only minute amounts of material are involved, part of which is again converted upon a subsequent pressure change. The influence of polarization, acting via concentration gradients to procedure retrodiffusion and osmosis, is very small;
- the slight perturbations in composition induced at the electrode surfaces do not have time to diffuse into the plug during the short period of measurement;

- a laborious analysis of the solutions after electrolyses can be omitted;
- only relatively short amounts of time are required for the analysis.

The disadvantages are:

- the electrodes have to be reversible to one of the ion constituents;
- a slow intrinsic resistance dispersion and/or the salt filtration effect may cause the $\tilde{t}_+^a$-determination to be inaccurate;
- especially for membrane systems with relatively high resistances any disturbance (convection) tending to limit the growth of the diffusion boundary layer (increase of the diffusion resistance) must be kept as small as possible. Otherwise, the resulting short retardation line makes the X-Y method inaccurate. Also, more time is needed to obtain a line of considerable length, which implies an increase of the influence of the salt filtration effect.

In order to generalize the applicability of the X-Y method, similar studies have to be performed on other systems, especially on membranes.

Determination of intrinsic retardation phenomena from X-Y plots:

As already noticed in the experimental examples at relatively low c_o, reported in this section, the first part of the retardation line shows a time dependent retardation contribution to the current. Similar observations were made at all plugs studied. Especially for $c_o<10^{-3}$M the intrinsic effect is most marked and remarkably slow. The transient phenomena were obtained by a simultaneous fast recording of I(2,2') vs. time and vs. E(1,1') using the recording device at such sensitivity as to provide full-scale deflection for the transient changes. In fig. 3-33 we have presented the time dependence of the streaming current, for three concentrations, fully corrected for electrode polarization according to the procedure depicted in fig. 3-14 and corrected with eq. (3-76). The curves show an initial rapid fall, followed by a continuous slow downward trend to $I_{s,dc}$. When adequate rest periods were taken into account, in order to exlude the influence of the "slow part" of the retardation on the subsequent experiment it appeared that the shape of the curves was independent of the pressure difference. The transient phenomena become noticeable in a c_o-range where the plugs are selective and E_s becomes time dependent (see section 3.7). However, in our case E_s hardly changes in the period that the current transient takes place. Consequently, the time dependence of the conductance can be computed from: $L_{22}(t)=I(i)_t/E_s$ (see eq. (3-73), (3-74) and (3-75). $L_{22}(t)$ thus calculated was independent of the applied pressure difference. Fig. 3-33 clearly shows that the

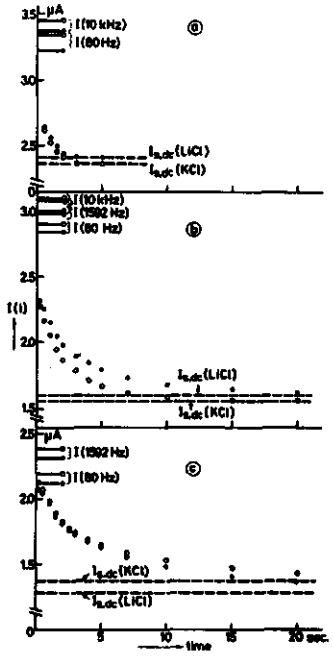

Fig. 3-33. The intrinsic time dependence of the streaming current for ΔP=30 cm Hg. plug VIII A(LiCl) ●, VIII B(KCl) ○; t=25.0°C. a. 10^{-3}M; b. 2 10^{-4} M c. 6.6 10^{-5}M LiCl, 4.0 10^{-5}M KCl. $I_{s,ac}$-values, computed from a.c. resistances, are indicated.

dispersion region shifts to longer times upon decreasing c_o. For comparison purposes we have inserted some I_s-data computed from E_s and a.c. resistance values. The substantially higher I_s (freq.)-values once more point to the presence of a low frequency dispersion. An unnoticed dispersion may invalidate much of the published data on streaming currents or resistances of plugs.

In order to determine unequivocally the physical nature of the time dependent streaming current, we have also considered possible mechanical transients, arising from an instantaneously applied pressure change.

- The transient streaming current may be related to transient velocity profiles in the pores where the excess charge is spatially distributed. Generally, the time required for the development of a steady state velocity distribution is strongly dependent on the pore radius and the kinematic viscosity (a and v*, resp.). For axial flow in a circular tube the dimensionless number v^*t/a^2 governs the deviation from steady state conditions[60]. If for our rather loosely packed plugs an average pore radius of about 25% of the particle radius is used, a velocity profile within 10% of its steady state value develops within 10^{-8} seconds. In other words, the influence of inertial effects on the streaming current can be neglected. These inertial effects do play a role, however, in alternating streaming current

measurements in capillaries with relatively large diameters[28]. In this method the maximum current will therefore depend on frequency, apart from electrode polarization complications.

- The transient streaming current may be related to a time dependent reversible compression of the plug's matrix. A change in structure would directly influence the net current flow. One would have to study then the effect of the applied pressure change on the pertinent parameters. A time dependent reversible compression or expansion, i.e. a change in packing density would cause the expulsion or uptake of water with the same time decay function which was not noticed (see section 3.7.4). The linearity of the liquid flow/pressure relation, the linear I-E-characteristics superposed at various constant pressure differences, the absence of any effect of pressure application on a.c. conductance and capacity point to the absence of compression (see section 3.7.4).

Finally, it should be stressed that the X-Y method is especially suitable to detect the time-behaviour on a time-scale which cannot normally be covered in dispersion measurements due to the effect of electrode polarization on the resistive part of the total impedance (see chapter 7).

3.7.3. *d.c. resistance experiments*

The determination of the conductance consists in principle of passing an accurately known electric current between the electrodes in the reservoirs (1,1') and determining the potential difference between the plug electrodes. Pulses of short duration and small current density ($<10\mu A/cm^2$) were used to keep polarization at the plug surfaces as small as possible. Nevertheless, recordings for $c_o \leqslant 10^{-3}M$ clearly show certain potential transients. A typical example is presented in fig. 3-34. The curve shows that initially the potential increases sharply and then slowly levels off at a finite value. The current that flows may not only comprise a conduction current but at least two other components, viz. a current induced by concentration changes at the plug-electrolyte interfaces and a dielectric displacement current. By waiting long enough the conduction-current is only obscured by the effect of concentration polarization, since the dielectric displacement component will decrease to zero while the conduction current remains constant. Due to the slow adjustment of E(2,2') it was difficult to separate these two contributions. Measurements of the local concentration changes during and after a current pulse clearly show that only a small part of the transient potential change can be attributed to the transport number effect (formation and relaxation of the concentration profile at the plug surfaces, causing a time depen-

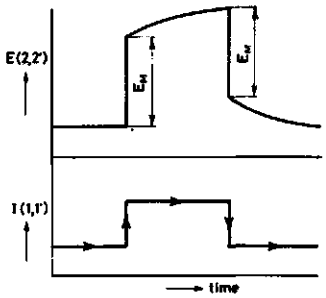

Fig. 3-34. Potential change in responce to a pulsed cell current for $c_o < 10^{-3}$M

Table 3-6. Survey of characteristic quantities of the plugs VIIIA and B(M) at 25.0°C. I_s, I_m and E_s are presented in the experimental sequence. I_s and I_m are the extrapolated and instantaneous values obtained from the X-Y plot, resp. R_m is the resistance computed from the voltage-current characteristic, using the instantaneous $E(2,2')_m$-value. The a.c. resistances have been determined using the 2,2'-electrodes

c moles/l		I_s μA	E_s mV	I_m μA	$R(E_s/I_s)$ kΩ	$R(E_s/I_m)$ kΩ	R_m kΩ	$R_{a.c.}$ (80Hz) kΩ	$R_{a.c.}$ (1592Hz) kΩ	$R_{a.c.}$ (10kHz) kΩ
10^{-3}	LiCl	2.20	46.0	2.52	20.9^1	18.2^5	18.1^3	15.3^5		14.03
	KCl	2.10	33.0	2.40	15.7^1	13.7^5	13.7^0	11.3^0		10.10
10^{-2}	LiCl	2.68	14.36	2.45	5.56^6	5.861	5.56	4.81		4.543
	KCl	2.60	10.35	2.36	4.01^2	4.386	4.02	3.47		3.213
10^{-1}	LiCL	2.07^8	1.79^5	1.66	0.86^4	1.081	0.871	0.868		
	KCl	1.92^8	1.17^8	1.55	0.61^1	0.760	0.605	0.602		
$6.6\ 10^{-5}$	LiCl	1.28	43.7^5	2.07^8	34.1^8	21.05	21.04	16.40	15.53	
$4.0\ 10^{-5}$	KCl	1.37	32.0^0	2.12^5	23.3^6	15.06	15.05	11.90	11.10	
$2.0\ 10^{-4}$	LiCl	1.59	44.6^5	2.32	28.08	19.2^5	19.08	15.70	15.00	14.89
	KCl	1.55	31.60	2.27	20.39	13.9^2	13.51	10.90	10.25	10.22
10^{-3}	LiCl	2.41	40.6^8	2.64	16.88	15.41	15.08	12.60		12.07
	KCl	2.36	27.9	2.61	11.82	10.69	10.37	8.35		8.091

dent potential difference across the plug). Even when using pulses of long duration (several minutes) the instantaneous potential change was perfectly linear with I(1,1'), indicating the small influence of the transport number effect at low current densities. A resistance determination using the instantaneous potential change, $E(2,2')_m$, seems to produce accu-

rate and reproducible results because the transport number effect is eliminated. In this connection it appears that the resistance computed from E_s and the instantaneous streaming current, I_m, yield identical values. In order to illustrate the consequences of considering the thus calculated resistance as the d.c. resistance, resistances of plug M, determined in every possible way, are presented in table 3-6 for an extended c_o-range.

It appears that at high c_o the fast retardation in a streaming current experiment gives $I_m < I_s$ and consequently $R(E_s/I_m) > R(E_s/I_s)$. However at these high ionic strengths, current-voltage characteristics can be determined without any problem. Note that $R_m(E(2,2')_m/I(1,1'))$ equals $R(E_s/I_s)$. At lower c_o the dispersion region extends to larger periods. Despite the effect of electrode polarization I_m exceeds I_s; consequently $R(E_s/I_s) > R(E_s/I_m)$. That $R(E_s/I_m)$ equals R_m results from the use of the same equipment and recording device. Some a.c. resistances have been included to show the marked decrease in resistance if a.c. values are used, despite the contribution of electrode polarization in the direct measurement. In section 7 we will briefly discuss possible causes underlying the dispersion phenomenon.

3.7.4 *Permeability experiments, electroviscous retardation*

Introduction

The fundamental variables governing fluid flow through porous media have been the subject of extensive experimental and theoretical studies[61]. For many systems it has proved possible to correlate a number of physical properties of the permeating solution and porous solids with experimentally determined permeabilities. The permeability is indispensable in studying several transport processes simultaneously, in particular interstitial diffusion, electrical conduction and fluid flow[62]. One example has already been given in section 3.7. There is a direct advantage in using the permeability method in model considerations, provided the hydrodynamic and electrokinetic characteristics are determined simultaneously. Discrepancies between experiment and predictions of thoroughly tested theories provide additional information for the interpretation of the electrokinetic results (chapter 4). Deviations from 'normal' permeability behaviour fall into two basic categories. One group, A, attributes permeability 'abnormalities' to changes which are brought about during the formation of the particle bed and/or during subsequent permeability experiments (e.g. van den Hul[63]). The other group, B, ascribes these abnormalities, especially when they are concentration dependent, to ionic or molecular forces

acting on the permeating fluid concentrated at the solid-liquid interfaces[64]. The factors of group A controlling the permeability, include:

1. Reversible and/or irreversible (time dependent) deformation of the particles during flow; this may result in non-linear flow-pressure dependencies and pressure dependent phenomenological coefficients. A rigorous direct control involves the determination of an a.c. or d.c. resistance at different pressures at an ionic strength not corresponding with the isoconductivity point (conductivity of the particle system + continuous phase equals that of the continuous phase; section 5.4.1).
2. Small traces of air, that drastically influence electrical and hydrodynamical characteristics and are often responsible for a pressure dependent resistance (decrease upon pressure application, irrespective of ionic strength, contrary to the effect mentioned under 1.)and a non-linear permeability characteristic.
3. Repeptisation and channeling effects; as discussed previously (section 3.6.1) upon flow reversal, non-coagulated regions can reveal a sudden increase of the permeability followed by a slow decrease to complete consolidation. It is clear that repeptisation processes occurring in those parts of the plugs that are coagulated in the secondary minimum, may increase anisotropic structuring. These effects often coincide with bad adhesion qualities at the wall of the plugholder and the appearance of microcracks.

A proper choice of the centrifuging conditions for the plug preparation can eliminate the afore-mentioned effects completely.

The factors of group B include:

1. The effect of a boundary layer that causes an abnormally high viscosity of the permeating fluid near the solid surface e.g. water structuring near the surface can control the location of the hydrodynamic shear plane. Increased electrolyte concentration opposes structuring[65] (except for certain ionic species).
2. The electroviscous retardation that results when a streaming potential has developed (section 3.2). When a rather concentrated aqueous solution of a strong electrolyte is caused to flow through the particle bed, the high conductivity of the solution will cause this effect to be virtually zero. The measurement of the coefficient $L_{11} = (J_v/\Delta P)_{E,\Delta\pi_s}$ implies the measurement of J_v, while $\Delta\pi_s$ and E are kept zero. As has been proved streaming currents will give rise to the appearance of concentration polarization at the electrodes. Over a relatively short period the development of substantial diffusion resistances impedes the determination of L_{11} (see section 3.7.2).

3. At low ionic strengths a possible salt filtration gives rise to a time dependent accumulation and depletion of electrolyte at the high and low pressure sides, resp. (see section 3.3 and 3.7). This effect can experimentally be determined or estimated. In our case it was found that the filtration coefficient, $L_p=[J_v/(\Delta P-\Delta\pi_s)]_{\Delta\pi_s,I}$, was hardly influenced by induced osmotic forces, due to the concentration polarization processes at the plug surfaces under the applied experimental conditions.
4. The electrolyte causes some shrinkage of the particle, especially for colloids of a macromolecular nature.

Experimental procedure

The construction of the permeability cell has been described in section 3.6.2. The conditioning of the plugs was described in section 3.7. The experimental runs and sequences are the same as reported for the electrokinetic measurements. Only a small pressure range was investigated. At pressure differences up to 30 cm Hg the Reynolds number, defined as $Re = D_p J_v \rho/(\eta A p)$, does not exceed 0.1, corresponding the conditions far within the creeping flow regime[60]. D_p is the mean particle diameter, J_v the volume flow, A the cross-sectional area of the particle bed and p the volume fraction solid of the plug. Since the spheres were very small, the ratio of the diameters of plugholder and particle remained very large. Consequently, no effort was made to correct for wall effects (uneven packing adjacent to the wall). Data for a particular run were rejected because of the appearance of bad adhesion on the perspex wall of the plugholder or micro-cracks within the plug. It is noteworthy, however, that even when these irregularities are present and induce permeability changes of 10-20%, these are hardly reflected in the electrical conductance and streaming potential, even for conditions far removed from the isoconductivity point. This illustrates the high sensitivity of the flow in comparison with the other electrokinetic quantities to packing parameters.

The permeabilities of the plugs were calculated from the displacement of the liquid meniscus in the capillary connected with the streaming cell (fig. 3-16a). Plots of the displacement versus time became linear after a short interval. L_p was determined from linear plots of volume flow versus pressure difference. The porosities of the plugs were always determined from the volume of the plugholder and the weight and density of the latex particles constituting the plug.

Results

Table 3-7 is a compilation of most of the experimental 'permeability dependent flow rate' data for KCl. The results for LiCl and CsCl show the same trend and have been omitted. The results are presented according to the actual experimental sequence. All the plugs, irrespective of their surface charge density, temperature and kind of electrolyte, generally show a small but significant decrease in J_v upon decreasing c. The observed changes are significantly greater than the experimental error (±5%). We did not observe any irreversibility in these observations; in other words, the permeability at an arbitrary concentration is independent of the history of the plugs. If the decrease were caused by a change in structure or by other irregularities pertaining to group A, the permeability change would not be reversible and no linear J_v-Δp plots would be obtained. The values in parentheses are fully corrected for the electroviscous retardation by dividing the experimental permeability by the factor $[1-L_{12}^2/(L_{11}L_{22})]$. For L_{11} the experimental value was used and subsequently improved by successive approximations. From the differences it can be concluded that the (calculated) electroviscous retardation

Table 3-7. Volume flow, J_v, at pressure difference Δp=30 cm Hg under zero current condition. The plugs indicated with L, M and H were V B(0.6041), VIII B(0.5951) and VII B(p=0.6133) resp. The values in parentheses have been corrected for the electroviscous effect.

	$J_v \times 10^5$ cm³/s						
c	L			M	H		
moles/l	15°C	25°C	35°C	25°C	15°C	25°C	35°C
10^{-1}	7.51(7.51)	9.31(9.31)	11.0(11.0)	8.79(8.80)			
10^{-2}	- -	9.38(9.44)	10.7(10.8)	8.66(8.73)	6.02(6.08)	8.07(8.14)	10.30(10.39)
5 10^{-3}					5.72(5.80)	8.13(8.24)	9.87(10.01)
1.25 10^{-3}	6.86(7.06)	8.77(9.02)	10.2(10.5)				
10^{-3}				8.26(8.43)	5.16(5.29)	7.41(7.60)	9.49(9.75)
7.65 10^{-4}	7.02(7.34)	8.81(9.10)	10.7(11.0)				
2.65 10^{-4}					5.60(5.72)	7.22(7.39)	9.26(9.45)
2 10^{-4}				7.89(8.01)			
10^{-4}	6.77(6.92)	8.43(8.65)	9.94(10.2)				

contributes a small but just detectable resistance to solute permeation if no concentration polarization at the electrodes occurs. From the results it is clear that the electroviscous retardation contributes only a small factor to the observed permeability. Thus the observed permeabi-

lity reduction probably results from the two remaining factors of group B (1 and/or 4).

The term $L_{12}^2/(L_{11}L_{22})$, appearing in the permeability relation $L_p=L_{11}[1-L_{12}^2/(L_{11}L_{22})]$, can in principle be determined directly by measuring the potential difference E as a function of the electric current I a zero volume flow: $(I/E)_{Jv}=L_{22}[1-L_{12}^2/(L_{11}L_{22})]$. Qualitatively, the effect of suppressing the electro-osmotic flow by a compensating pressure difference ΔP was clearly noticeable in our experiments (see section 3.7.1). However, in the c-range of interest, a time dependent concentration polarization at the plug/solution boundaries is significant and hardly to eliminate, and thus impedes accurate determination of this relatively small effect.

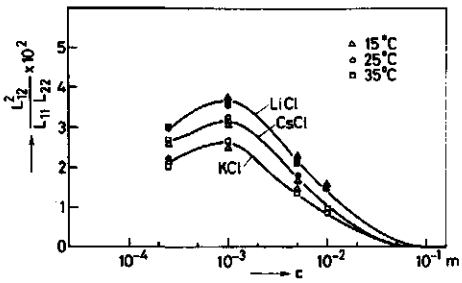

Fig. 3-35. The factor $L_{12}^2/(L_{11}L_{22})$vs. c for LiCl, KCl and CsCl at three different temperatures. plug VII A,B,C (H)

In fig. 3-35 data for $L_{12}^2/(L_{11}L_{22})$ is plotted as calculated from the component phenomenological quantities. The values of the various phenomenological coefficients, viz. L_{11}, L_{12} and L_{22}, are determined from the slopes of straight lines for the volume flow, streaming current and streaming potential versus pressure difference. Successfull experimental checks on criteria such as linearity, superposition principle and Saxén relation, demonstrate the validity of the postulates of irreversible thermodynamics. This in turn implies that the coefficients are invariant and also stresses the correctness of the method of calculating the electroviscous effect. All curves in fig. 3-35 show maxima independent of the conditions. In chapter 4 we will analyse the electroviscous effect in relation to recent theoretical models and interpret the permeability 'abnormality' in terms of the factors 1 and 4 of group B.

3.7.5 *Summary*

In order to describe the influence of all possible forms of polarization on phenomenological coefficients the theory of irreversible thermodynamics was modified.

The effects of concentration polarization on streaming potential, electro-osmosis electro-osmotic counter pressure and current-voltage curves were studied. It was shown that they could easily be minimized

and even eliminated, if experimental conditions were chosen such as to suppress interfacial concentration changes. The four-electrode technique was used to verify these predictions. It was also examined that moderate or high current densities applied in electro-osmosis experiments, when carried out in a systematic way, could lead to an apparent non-linear flow-current characteristic. Much attention has been given to the time-dependency of the streaming potential, as it occurs at relatively low ionic strengths. From the experimental data it was concluded that it is hardly possible to determine the non-steady salt accumulation process for porous systems, because the selectivity, exclusively a result of negative adsorption, decreases during the accumulation. On the other hand it was shown that an analysis of the depletion process at the low pressure side opens perspectives, experimentally as well as theoretically. The ensuing concentration gives information about the electrolyte content of the 'pore liquid', a relevant colloid-chemical quantity. A quantitative expression for the depletion process was derived and experimental data, proving the validity of the method, have been presented.

The separate and combined effects of either concentration polarization at the electrodes and/or a resistance in the electrical circuit (externally) or by electrode spacing (internally), on the streaming current, were theoretically and experimentally studied. The employment of a new experimental method, using the four-electrode apparatus permits experimental verification of the diffusion-relaxation processes occurring at the electrodes and the determination of the d.c. streaming current. A detailed study in the general framework of irreversible thermodynamics showed that the 'X-Y method' permits the determination of the transport number of counterions in the porous system under study. These numbers, which were measured under very controlled and 'soft' polarization conditions, are presented. It is likely that the methods developed here are also suitable for other systems such as membranes.

It has been demonstrated that for our systems at low ionic strengths the combination of a slow intrinsic polarization process and the transport number effect complicates determination of the d.c. resistance. However, determination of the streaming current retardation with the four electrode technique not only enabled the determination of the d.c. streaming current and thus the d.c. resistance, but also the slow part of the time behaviour of the involved intrinsic process.

Special attention have been given to the preparation of stable, isotropic plugs of polystyrene latices. The permeability measurements show that if appropriate centrifuging conditions were chosen for the plug preparation a mechanically stable system could be obtained. The fil-

tration coefficients, L_p, were determined over a wide concentration range. The observed increase of L_p with ionic strength could not be explained by the electroviscous effect, which was calculated from independently determined phenomenological coefficients. An analysis of all the factors possibly concerned reveals that two flow retarding effects could serve as an explanation viz. a concentration dependent water structuring near the surface of the particles and/or a shrinkage of the particles upon increase of the electrolyte concentration.

3.7.6 *References*

1. J.Th.G. Overbeek, "Elektrokinetic Phenomena". Colloid Science, Vol. I, H.R. Kruyt, Editor, Elsevier Publishing Co., 1952.
2. J.T. Davies and E.K. Rideal, Interfacial Phenomena, Academic Press, New York, 1963.
3. M. Bier, editor, Electrophoresis. Theory, Methods and Applications, Vol. I and II, Academic Press, 1959 and 1967.
4. D.J. Shaw, Electrophoresis, Academic Press, New York, 1969.
5. B. Ball, D.W. Fuerstenau, "A review of the measurement of streaming potentials", Miner.Sci.Eng., 5, 267 (1973).
6. B.V. Derjaguin, S.S. Dukhin, in "Surface and Colloid Science", Vol. 7, E. Matijević (Ed.), Wiley, New York, (1974).
7. R. Paterson, C.R. Gardner, J.Chem.Soc.A 2254 (1971).
8. J.H.B. George and R.A. Courant, J.Phys.Chem. 71, 246 (1967).
9. K.S. Spiegler and M.R.J. Wyllie, 'Electrical Potential Differences' Chapter 7 in Physical Techniques in Biological Research, 2nd. ed., Vol. II, part A, D.H. Moore (ed.), Acad.Press, New York, 1968.
10. N. Lakshminarayanaiah, Transport Phenomena in Membranes, Academic Press, New York, 1969.
11. S.D. James, J.Phys.Chem. 70, 3447 (1966).
12. H.F. Holmes, C.S. Shoup, C.M. Secoy, J.Phys.Chem. 69, 3148 (1965).
13. V. Subrahmanyan, N. Lakshminarayanaiah. J.Phys.Chem. 72, 4314 (1968).
14. D. Rosen, in "A laboratory manual of analytical methods of protein chemistry", Vol. 4, P. Alexander, H.P. Lundgren (Eds.), Pergamon Press, Oxford (1966).
15. H.P. Schwan, Biophysik 3, 181 (1966).
16. D.A.I. Goring and S.G. Mason, Can.J.Res., 28b, 323 (1950).
17. M.P. Sidorova, M. Fazylova, D.A. Fridrikhsberg, Proceedings of an International Conference on Colloid and Surface Science, Vol. I, Budapest, september 15-20 (1975); M.P. Sidorova, D.K. Tasev, M. Fazylova, Kolloidn.Zh., 38, 723 (1976).
18. I. Koszman, J. Gavis, Chem.Eng.Sci. 17, 1013 (1962).
19. S.M. Neale, R.H. Peters, Trans.Faraday Soc. 42, 478 (1946).
20. V. Pravdić, Croat.Chem. Acta 35, 233 (1963).
    J. Jednacak, V. Pravdić, W. Haller. J.Colloid Interface Sci. 49, 16 (1974).
21. W.G. Eversole, D.L. Deardorff, J.Phys.Chem. 45, 236 (1941); W.G. Eversole, W. Boardman. J.Phys.Chem. 46, 941 (1942).
    R.M. Hurd, N.Hackerman, J.Electrochem.Soc. 102, 594 (1955); 103, 316 (1956).
22. A. Watillon, R. de Backer, J.Electroanal.Chem. 25, 181 (1970).
    R. de Backer, Thesis, Brussels, (1966).
23. A.A. Boumans, Physica 23, 1007 (1957).
24. P.O.W. Wijga, Thesis, Utrecht (1946).
25. J.A. Ciriacks and D.J. Williams, J.Colloid Interface Sci., 26, 446 (1968).
26. P.W. Huber, A.A. Sonin, J.Colloid Interface Sci., 52 415 (1975).
27. W.F. Gerdes, 12th National USA Analysis Instrumentation Symposium, Houston, Texas, May 11-13, 1966.
28. J.M. Groves, A.R. Sears, J.Colloid Interface Sci., 53, 83 (1975).

29. J.Th.G. Overbeek. J.Colloid Sci 8, 420 (1953).
30. A.J. Staverman, Trans.Faraday Soc. 48, 176 (1952).
31. O. Kedem, A. Katchalsky, Trans.Faraday Soc. 59 1918 (1963); 59, 1941 (1963).
32. A. Katchalsky, P.F. Curran, Non-equilibrium thermodynamics in biophysics, Harvard University Press, Cambridge, Mass., 1965.
33. J.G. Mc Kelvey, K.S. Spiegler, M.R.J. Wyllie, Chem.Eng.Progr.Ser. 55, 199 (1959).
34. C.P. Minning, K.S. Spiegler, Charged Gels and Membranes I, 277 (1976).
C.P. Minning, 'Streaming potentials in hyperfiltration (reverse osmosis) of saline waters', Ph.D.Thesis, College of Engineering, University of California, Berkeley (1973).
35. T.S. Brun, D. Vaula, Ber.Bunsenges. Phys.Chem. 71, 824 (1967);
T.S. Brun, Arbok Univ.Bergen 1957, Naturv.r.Nr.8.
36. G. Jacazio, R.F. Probstein, A.A. Sonin, D. Yung. J.Phys.Chem. 76, 4015 (1972).
37. G.B. Tanny, E. Hoffer, J.Colloid Interface Sci. 44, 21 (1973).
38. G. Schmid, H. Schwarz, Z.Elektrochemie, 54 424 (1950); 55, 229,295,684; 56, 35.
39. K.S. Spiegler, M.R.J. Wyllie, 'Electrical Potential Differences', Chapter 7 in Physical techniques in biological research, 2nd.ed., Vol.II, part A, Dan H.Moore (ed.), Acad.Press, New York, 1968.
40. D.G. Dawson, P. Meares, J.Colloid Interface Sci. 33, 117 (1970).
41. A.J. Staverman, Trans.Faraday Soc. 48, 176 (1952).
42. P. Delahay, New instrumental methods of analysis, Willey (Interscience), New York (1954).
43. M. Block, J.A. Kitchener, J.Elektrochem.Soc. 113, 947 (1966).
44. K.S. Spiegler, Desalination 9, 367 (1971).
45. E.J. Fenech, C.W. Tobias, Electrochim.Acta 2, 311 (1960).
46. P.M. Heertjes, Trans.Instn.Chem.Engrs., 42, T266 (1964).
47. W.J. Wnek, D. Gidaspow, D.T. Wasan, Chemical Engineering Science, 30, 1035 (1975).
48. J.B. Melville, E. Willis, A.L. Smith, Trans.Faraday Soc. 68, 45 (1972).
49. M.S. El-Aasser, A.A. Robertson, Kolloid-Z.u.Z.Polym. 251, 241 (1973).
50. A.E.J.Meyer, W.J. van Megen, J. Lyklema, to be published.
51. L. Barclay, A. Harrington, R.H. Ottewill, Kolloid-Z.u.Z.Polymere 250, 655 (1972).
52. A.S. Brown, J.Am.Chem.Soc. 56, 646 (1934); D.J.G. Ives, G.J. Janz: Reference electrodes, theory and practice Academic Press (1961), p. 179.
53. D. Eagland, A.P. Allen, J.Colloid Interface Sci. 58, 230 (1977).
54. A. Bethe, T. Toropoff, Z.Physik.Chem. 88, 686 (1914); 89, 597 (1915).
55. P.H. Barry, A.B. Hope, Biophysical J. 9, 700 (1969).
56. T.R.E. Kressman, F.L. Tye, Trans.Faraday Soc. 55, 1441 (1959).
57. R. Schlögl, Stofftransport durch Membranen, Steinkopf Verlag, Darmstadt, 1964.
58. N.F. Bondarenko, S.V. Nerpin, Collection: Trudy po Agronomicheskoi Fizike, no. 11, Hydrometeoizdat, Leningrad, 1965, p. 11; see ref. 6, p. 174.
59. T.R.E. Kressman, I.R.E. Stanbridge, F.L. Tye, Trans.Faraday Soc. 59, 2129 (1963).
60. R.B. Bird, W.E. Stewart, E.N. Lightfood, 'Transport phenomena', J. Wiley and Sons Inc., New York (1960), p. 126.
61. A.E. Scheidegger, The physics of flow in porous media, University of Totonto, 1957.
62. G. Neale, W. Nader, AIche J., 19, 112 (1973); G. Neale, 20, 530 (1974).
63. H.J. van den Hul, Thesis, Utrecht (1966); Commun.Agric.Univ.Wageningen, 66-2.
64. Ref. 6, p. 118; p. 169.
65. F. Franks, Chem.Ind. 1968, 560 (1968).

*APPENDIX 3A: Equations for the depletion of local concentration at a plane surface**

The differential equations and the boundary conditions considered in section 3.3.2 are:

$$\frac{\delta c}{\delta t} = D \frac{\delta^2 c}{\delta x^2} - J \frac{\delta c}{\delta x} \text{ with } J = J_v \qquad \text{(A-1)}$$

$$c(x,o) = c_o \text{ for } x \geqslant o \qquad \text{(A-2)}$$

$$\lim_{x \to \infty} c(x,t) = c_o \text{ for } t \geqslant o \qquad \text{(A-3)}$$

$$D \frac{\delta c}{\delta x}(o,t) - J\, c(o,t) = - J\, c_p \text{ for } t > o \qquad \text{(A-4)}$$

Solution: Let $c(x,t) = u(x,t)\, e^{\alpha x + \beta t}$ (A-5)

then substituting (A-5) in (A-1) gives:

$$\frac{\delta u}{\delta t} + \beta u = D \frac{\delta^2 u}{\delta x^2} + (2\alpha D - J) \frac{\delta u}{\delta x} + (D\alpha^2 - J\alpha)u$$

α and β are chosen so that: $2\alpha D - J = o$ and $\beta = D\alpha^2 - J\alpha$

Thus $\alpha = \frac{J}{2D} > o$, (A-6)

$$\beta = - \frac{J^2}{4D} < o \qquad \text{(A-7)}$$

Introducing foregoing equations into eq.(A-1) through (A-4) yields:

$$\frac{\delta u}{\delta t} = D \frac{\delta^2 u}{\delta x^2} \qquad \text{(A-8)}$$

$$u(x,o) = c_o\, e^{-\alpha x} \text{ for } x \geqslant o \qquad \text{(A-9)}$$

$$\lim_{x \to \infty} u(x,t) = o \qquad \text{(A-10)}$$

$$\frac{\delta u}{\delta x}(o,t) - \alpha u(o,t) = - 2\alpha c_p e^{-\beta t} \qquad \text{(A-11)}$$

Taking the Laplace transform of the diffusion equation and the boundary conditions we can write for eq. (A-8):

---

* The author is indebted to Ir. M.H. Hendriks of the Department of Mathematics, for his help in obtaining the solution

$s\tilde{u} - u(x,o) = D\frac{d^2\tilde{u}}{dx^2}$; according to eq. (A-9) it becomes:

$$D\frac{d^2\tilde{u}}{dx^2} - s\tilde{u} = -c_o e^{-\alpha x} \qquad \text{(A-12)}$$

where $\tilde{u}(x,s) = \int_o^\infty e^{-st}u(x,t)dt$; s is the Laplacian operator.

Eq. (A-10) becomes: $\lim_{x \to \infty} \tilde{u}(x,t)=o$ (A-13)

Eq. (A-11) becomes: $\frac{d\tilde{u}}{dx}(o,s) - \alpha\tilde{u}(o,s) = -\frac{2\alpha c_p}{s+\beta}$ (A-14)

Suppose $\tilde{u} = k\, e^{-\alpha x}$ is the solution of eq. (A-12), then the general solution of eq. (A-12) becomes:

$$\tilde{u} = A\, e^{x\sqrt{s/D}} + B\, e^{-x\sqrt{s/D}} + \frac{c_o}{s+\beta} e^{-\alpha x} \qquad \text{(A-15)}$$

From (A-13) it can be shown that A=o

Thus $\tilde{u} = B\, e^{-x\sqrt{s/D}} + \frac{c_o\, e^{-\alpha x}}{s+\beta}$ (A-16)

With eq. (A-14) we get for B:

$$B = \frac{2\alpha\sqrt{D}\ (c_p-c_o)}{(\sqrt{s}+\alpha\sqrt{D})(s+\beta)}$$

Let $\frac{J}{2\sqrt{D}} = \beta_1$, then $\beta = -\beta_1^2$ and $\alpha\sqrt{D} = \beta_1$ (A-17)

After rearrangement eq. (A-16) becomes:

$$\tilde{u} = \frac{c_p-c_o}{2\beta_1}\frac{e^{-x\sqrt{s}/\sqrt{D}}}{\sqrt{s}-\beta_1} - \frac{c_p-c_o}{2\beta_1}\frac{e^{-x\sqrt{s}/\sqrt{D}}}{\sqrt{s}+\beta_1} - (c_p-c_o)\frac{e^{-x\sqrt{s}/\sqrt{D}}}{(\sqrt{s}+\beta_1)^2} + \frac{c_o\, e^{-\alpha x}}{s+\beta} \qquad \text{(A-20)}$$

Evaluating the inverse Laplace transforms (see Roberts-Kaufman: Table of Laplace transforms) and introducing eq. (A-17), (A-5), (A-6) and (A-7) into the solution of eq. (A-20) one finally gets after some rearrangements the complete time dependency of the concentration at arbitrary distance from the plug surface at the low pressure side:

$$c(x,t) = \tfrac{1}{2}(c_p-c_o)\left[\operatorname{erfc}\frac{x-Jt}{2\sqrt{Dt}} - \left(\frac{2J\sqrt{t}}{\sqrt{D}} + \frac{J}{D}x + 1\right) e^{\frac{J}{D}x}\operatorname{erfc}\left(\frac{x+Jt}{2\sqrt{Dt}}\right) + \right.$$

$$\left. + \frac{2\ J\sqrt{t}}{\sqrt{\pi D}}\right] + c_o \qquad \text{(A-21)}$$

CHAPTER 4

CONVERSION OF ELECTROKINETIC PARAMETERS OF CONCENTRATED DISPERSIONS INTO DOUBLE LAYER CHARACTERISTICS; CAPILLARY MODELS AND CELL MODELS

4.1 *Introduction*

Interpretation of electrokinetic data of porous media requires the introduction of a geometric model in order to compute correction factors to be applied to Smoluchowski's classical equations. The model-based theoretical investigations described in the literature are limited to capillaries or cells. In this chapter the consequences of such approximations of the microstructure of real plugs will be discussed. Next, we will analyse our electrokinetic results on polystyrene plugs in terms of some recent theoretical representations. Special attention will be given to the effective boundary layer thickness as it is evaluated from the hydrodynamic experiments and from the electroviscous effect. For that purpose the capillary model is extended to incorporate the possibility that the shear plane does not coincide with the particle surface and tangential ion transport can take place through the layer near the surface (anomalous conduction). The cell model will be used in assessing the hydrodynamically effective charge density from the observed time-dependency of the streaming potential, using the theory of negative adsorption.

4.2 *Problems involved in studying electrokinetic phenomena in porous media; complications due to surface conductance*

At high electrolyte concentrations, i.e. thin double layers, electrokinetic effects are confined to an area that is relatively close to the charged surface. This condition is characterized by a relatively high value of the reciprocal double layer thickness, κ, which is defined by[1]:

$$\kappa^2 = \sum_i c_i z_i F_a^2 / \varepsilon_o \varepsilon_r RT \qquad (4\text{-}1)$$

c_i and z_i are the bulkconcentration and valency of ion i, resp.. F_a is the Faraday constant, ε_r the relative permittivity, ε_o the permittivity of free space, R the gas constant and T the absolute temperature. Under these conditions, electrokinetic data of porous systems can be interpreted using the classical formulae of Helmholtz and Smoluchowski[1,2].

In the more general interpretation of streaming potential or electroosmosis experiments, one has to be aware of complications that can arise from the occurrence of surface conductance. The critical importance of

this phenomenon, which is especially crucial for dilute electrolyte solutions, was already recognized by Briggs[3] and has since been subjected to many investigations. Another complicating factor in the theoretical and experimental approaches is contributed by the circumstance that, also depending on the value of the pore or particle radius, at low ionic strength double layer overlap and double layer polarization cause serious corrections to the classical formulae (e.g. Dukhin[4]).

In order to obtain fully reliable values of the zeta-potential, one can either select the conditions in such a way that specific surface conductance and double layer polarization can be ignored or corrected properly for these phenomena. In the latter case the numerical value of the specific surface conductance has to be determined experimentally from the total conductance, which can only be done unambiguously for well-defined systems as single capillaries[5] or parallel plates[6] having perfectly smooth surfaces, so that the double layer is not polarized by an electric or hydrodynamic field.

The impossibility of calculating the true zeta-potential from experimental electrokinetic parameters of charged porous systems in the presence of a non-negligible specific surface conductance, has in the literature often been considered as an accepted fact even for the case of a thin double layer. This judgement is partly based on experimentally observed large differences between zeta-potentials obtained with a glass capillary and with a plug of small particles of the same material under identical conditions[7,8]. However, this experimental evidence is not convincing, because the plug resistance was measured by the shunt method, thus it is quite possible that part of the apparent zeta-potential depression has to be attributed to polarization effects at the electrodes (see sections 3.4.4 and 3.7.2).

The theoretical study of electrokinetics in porous systems has gained impetus from model approaches to hydrodynamic problems. We can classify theoretical studies in this field into:

a) traditional theories in which the porous system is modelled to a network of capillaries. The most simple model viz. an equivalent bundle of capillaries of equal diameter is of direct importance for estimating the effect of a thick double layer. In several theoretical analyses considering a thin double layer, it is proved that a network with cylindrical capillaries even with only slightly varying diameters and lengths will display a reduced zeta-potential. The first theoretical analysis of the surface conductance problem in terms of capillary models was presented by Overbeek and Wijga[8]. Their treatment of two simple models, dealing with an arrangement of capillaries in

series and in parallel, has shown, that for porous beds, the mere measurement of total conductance is totally inadequate. Direct substitution of this value in the Helmholtz-Smoluchowski equations for electro-osmosis or streaming potential leads to zeta-potentials that may strongly deviate from the true values. Tikhomolova[9] approached this problem theoretically and experimentally by relating the electro-osmotic volume rate to the varying structural and double layer characteristics of layers associated with the different particle sizes that compose the dispersed medium. The generation of interlayer pressure differences during electro-osmosis is responsible for an apparent zeta-potential depression. The so-called 'hydraulic effect' should not be significant when measurements are carried out on homogeneous porous media made up of particles of equal size. However, the fact that every individual particle can be polarized by the applied electrical field was not taken into account.

b) theories which describe the porous system as an array of charged spheres, often presented as the cell-type model. It is clear that cell models and also particle models are more suitable for incorporating the concept of 'particle polarization' and the effect of a relatively thick double layer *simultaneously*. The particle models, however, can only be used to predict the electrical conductivity of a particle dispersion and are therefore separately treated in chapter 5. It will be shown that the cell model is eminently suitable to relate the electrolyte content of the interstitial phase, determined from the time-dependency of the streaming potential, to double layer characteristics.

In the following sections recent theoretical results, dealing either with the 'single capillary model', including surface conductance and thick double layers, or with the cell model, will be briefly reviewed. The results are presented in terms of the phenomenological coefficients occurring in the theory of irreversible thermodynamics.

4.2.1 *Surface conduction in relation to streaming current*

It has often been suggested[10] (mostly implicit in the theoretical model[11-14]), that short-circuiting the electrodes attached to the interfaces of the porous system eliminates the influence of surface conductance. However, short-circuiting the end electrodes does not eliminate at all local ionic conduction (thus partial streaming potential conditions) at intermediate points in the porous system, as will be shown in the following example. For this we will use the same capillary model as taken by Over-

beek and Wijga[8]. In the upper part of fig. 4-1 a two-capillary system with circular cross-section is presented; for convenience both sections have been given the same length l. We will assume that the Helmholtz-Smoluchowski model can be used, with incorporation of the specific surface conductivity, κ^{σ}. Under streaming current conditions with volume flow J_v, the net current in section I, composed of a convection and a conduction part, can be written as:

$$I_I = 8\varepsilon_o\varepsilon_r\tilde{\zeta}J_v a_1^{-2} + \pi K(a_1^2 + \alpha a_1)\, E_{AB}\, l^{-1} \qquad (4\text{-}2)$$

and for section II as:

$$I_{II} = 8\varepsilon_o\varepsilon_r\tilde{\zeta}J_v a_2^{-2} + \pi K(a_2^2 + \alpha a_2)\, E_{BC}\, l^{-1} \qquad (4\text{-}3)$$

with $\alpha = 2\kappa^{\sigma}/K$. K denotes the specific conductivity of the equilibrium electrolyte in the capillary system. E_{AB} and E_{BC} are the potential differences $E_B - E_A$ and $E_C - E_B$, resp. The steady-state streaming current condition is given by $I_I = I_{II} = I_s$ and $E_A = E_C$. This identity of eq. (4-2) and (4-3) allows us to formulate E_{AB} (= $- E_{BC}$) explicitly. The sign of E_{AB} depends on the sign of the zeta-potential and the sequence of the two capillaries. The streaming current with the short-circuited (non-polarizable) electrodes can be obtained from either eq. (4-2) or (4-3) in combination with the explicit expression for E_{AB}:

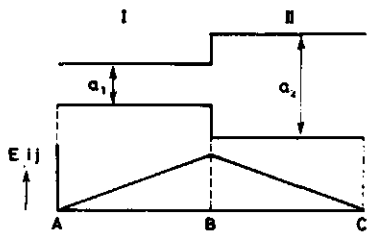

Fig. 4-1. A two-capillary system with the corresponding potential profile under streaming current condition.

$$I_s = \frac{8\varepsilon_o\varepsilon_r\tilde{\zeta}J_v}{a_1^2 a_2^2}\,\frac{a_1^4 + a_2^4 + \alpha(a_1^3 + a_2^3)}{a_1^2 + a_2^2 + \alpha(a_1 + a_2)} \qquad (4\text{-}4)$$

where ΔP and η denote the pressure difference and the viscosity resp. and $J_v = \pi a_1^4 a_2^4 \Delta P/\{8\eta l(a_1^4 + a_2^4)\}$. The streaming potential can either be calculated from the condition $I_I = I_{II} = 0$, or via the total electrical resistance of the capillary system and I_s. By substituting the expression for J_v into eq. (4-4) and by using the geometric cell constant of the capillary system, c, for the streaming current we can formally write:

$$I_s = \frac{\varepsilon_o \varepsilon_r \zeta}{\eta} \frac{\Delta P}{C} \frac{1}{Z} \qquad (4\text{-}5)$$

in which Z is a correction factor, which must be applied in a calculation of the zeta-potential from the Smoluchowski-formula. C is defined by $C = 1(a_1^2 + a_2^2)/\pi a_1^2 a_2^2$, and is usually determined at high ionic strength. With $a_1 = xa_2$, Z transforms into:

$$Z = \frac{(x^2 + 1)(x^4 + 1) + (x + 1)(x^4 + 1)\alpha/a_2}{(x^2 + 1)(x^4 + 1) + (x^2 + 1)(x^3 + 1)\alpha/a_2} \qquad (4\text{-}6)$$

For $x \neq 1$ and finite values of κ^σ, Z exceeds 1. As depicted in fig. 4-1 a potential profile with corresponding migration currents will develop in order to compensate charge accumulation/depletion. The final streaming current equation only contains the correction factor in the presence of a non-negligible κ^σ. Calculation of Z as a function of the heterodispersity of the capillary diameters, x, reveals the influence of the dimensionless parameter α/a_2. This parameter is twice the Rel concept of Dukhin for a capillary, expressing the contribution of κ^σ to the total conductance of the capilllary. For small x-values Z increases substantially with Rel (e.g. x = 2; Rel = 1: Z = 1.032, Rel = 5: Z = 1.112). For a large diameter ratio, however, Z becomes insensitive to the presence of surface conductance, because the relatively high conductance of the bigger capillary suppresses the potential difference E_{AB} (e.g. for Rel = 5, x = 20: Z = 1.016). The conclusion of this analysis must be that:

a) when considering the streaming current in network models such as that of Overbeek et al.[15], a non-negligible surface conductance leads to a zeta-potential depression. The amount of depression increases with increasing Rel and is sensitive to the degree of heterodispersity of the capillary system.

b) it is of interest to study the effect of the type of counterion on I_s. An increase in the molar conductivity of the ions decreases Rel. Determination of I_s for series of alkali ions may give direct information about the polarization effect in case no anomalous conduction takes place and no specific adsorption effects occur.

In order to verify the effect of double layer overlap similar calculations were performed using the physically unrealistic fixed charge density theory (often used in membrane literature), which assumes the capillaries to be homogeneously charged[16]. It can be shown that in this case

under streaming current conditions no conduction takes place in the capillary system. However, for moderately charged pores, even at pronounced double layer overlap ($\kappa = 0$), the charge distribution is by no means homogeneous since the charge excess is substantially localized near the surface (see sections 4.5 and 4.5.1) so that a zeta-potential depression remains to be expected.

4.3 *The specific surface conductance: defining equations and explanation of terms*

In descriptions of systems with enhanced conductivity due to the presence of a charged interface the term surface conductance is often used. Any expression for this quantity should include the contribution of the excess of counterions, σ_+, as well as the deficit of co-ions, σ_-, near the charged surface which contribute positively resp. negatively to the surface conductance (Bikerman[17]; see also Watillon et al.[18]). Moreover, the electro-osmotic displacement of ions in the double layer should also be included. For a negatively charged surface and a symmetrical z-valent electrolyte the general expression for κ^σ for a diffuse double layer is given by:

$$\kappa^\sigma = \frac{1}{F_a}\{\sigma_+\Lambda_+ - \sigma_-\Lambda_- + \sigma_+ \frac{2\varepsilon_r\varepsilon_o RT}{\eta z_+} - \sigma_- \frac{2\varepsilon_r\varepsilon_o RT}{\eta z_-}\} \qquad (4\text{-}7)$$

Λ_+ and Λ_- are the molar conductivities of the counter- and co-ions, resp. The first two terms in eq. (4-7) represent the conductive contribution and the last two terms the superimposed electro-osmotic (convective) contribution. For spheres, at any κa the σ_+ and σ_- values can be calculated from the reduced quantities $I_\pm(\psi_d, \kappa a)$ of the L.O.W. tables[19] by the relation:

$$\sigma_\pm(\psi_d, \kappa a) = \varepsilon_r\varepsilon_o RT\kappa I_\pm(\psi_d, \kappa a)/F_a \qquad (4\text{-}8)$$

where ψ_d is the potential of the diffuse part of the double layer corresponding to a surface charge density σ_o, and a is the particle radius. The condition for electroneutrality prescribes that $\sigma_o = -(\sigma_+ + \sigma_-)$. For relatively high κa and/or ψ_d values the ionic components of charge, $\sigma_\pm$, can be expressed as a function of the electrokinetic potential, ζ, just as if one is dealing with the theory of flat electrical double layers. For a system containing a monovalent electrolyte eq. (4-7) then transforms into:

$$\kappa^{\sigma} = (2\varepsilon_r\varepsilon_o RTc/F_a^2)^{\frac{1}{2}} \{(\exp(-\tilde{\zeta}/2) - 1)(\Lambda_+ + 2\varepsilon_r\varepsilon_o RT/\eta) + (\exp(\tilde{\zeta}/2) - 1)(\Lambda_- + 2\varepsilon_r\varepsilon_o RT/\eta)\} \qquad (4\text{-}7a)$$

where $\tilde{\zeta}$ is the reduced electrokinetic potential: $\tilde{\zeta} = F_a\zeta/RT$. It is assumed that the particle surface and the shear plane coincide, thus $\zeta = \psi_d$.

Surface conductance data obtained on many systems have revealed large discrepancies with values calculated according to eq. (4-7a) when using experimentally determined zeta-potentials. These discrepancies may be related to the presence of a conducting layer between the solid surface and the shear plane. Assuming that the potential distribution in this layer can still be described by the Gouy-Chapman theory, and taking into account the fact that the molar conductivities of the ions do not necessarily have to be equal to their values in the bulk, the Bikerman equation can be modified to:

$$\kappa^{\sigma} = (8\varepsilon_r\varepsilon_o RTc/F_a^2)^{\frac{1}{2}} \{\Lambda_{\pm}^{\Delta}(\cosh \tilde{\psi}_d/2 - \cosh \tilde{\zeta}/2) + (\Lambda_{\pm} + 2\varepsilon_o\varepsilon_r RT/\eta)(\cosh \tilde{\zeta}/2 - 1)\} \qquad (4\text{-}7b)$$

where Λ_+ and Λ_- have been taken as identical. The same assumption holds for the molar conductivities of the ions in the Δ-layer, $\Lambda_{\pm}^{\Delta}$. A similar expression can be obtained for the case $\Lambda_+ \neq \Lambda_-$ and $\Lambda_+^{\Delta} \neq \Lambda_-^{\Delta}$. Using additiona experimental data on the electrokinetic potential and the surface charge density, from eq. (4-7b) one can evaluate $\Lambda_{\pm}^{\Delta}$, ψ_d and ζ and from the combination of the latter quantities $\Delta(\psi_d, \zeta)$. In table 4-1 some κ^{σ} results are presented in order to show the dependency of κ^{σ} on σ_o, c and the kind of electrolyte. The effect of ignoring the electro-osmotic contribution (ζ=0) on κ^{σ} is rather sensitive to σ_o and c, but is independent of the

Table 4-1. Some κ^{σ}-values calculated according to eq. (4-7a) at 25.0°C. The result for ζ = 0 were obtained by ignoring the electro-osmotic terms.

$\kappa^{\sigma} \times 10^{10}$ Ω^{-1}

	LiCl				KCl			
	σ_o=1 μC/cm²		σ_o=8 μC/cm²		σ_o=1 μC/cm²		σ_o= 8 μC/cm²	
c moles/l	ψ_d=ζ	ζ=0	ψ_d=ζ	ζ=0	ψ_d=ζ	ζ=0	ψ_d=ζ	ζ=0
10^{-1}	-0.901	-1.16	25.1	14.8	1.12	0.854	48.8	38.5
10^{-2}	0.980	0.241	39.2	25.4	3.45	2.71	65.9	52.2
10^{-3}	3.59	2.20	45.2	27.9	6.66	5.26	73.4	58.1
$5\ 10^{-5}$	5.37	3.52	47.5	31.6	8.83	6.99	76.2	60.3

nature of the electrolyte. Furthermore, it may be noticed, that κ^{σ} becomes negative when σ_+ and σ_- are of the same magnitude (low σ_o, high c) and the counterions are less mobile than the co-ions. It is important to realize that a constant surface charge density does not imply an invariable surface conductance. Without any knowledge of ζ, σ_o and $\Lambda_{\pm}^{\Delta}$ can be determined from experimental κ^{σ} data by assigning different values to the thickness and $\Lambda_{\pm}^{\Delta}$, to a first approximation assuming them to be independent of c, and minimizing the mean square deviation between calculated and experimental values of the surface conductance[20]. An experimental check on this method is the determination of the influence of the nature of the counterion on surface conductance. However, various factors often discussed in the literature, such as surface roughness, specific adsorption of ions, variation of ε_r and η within the double layer, etc. invalidate the presented formulae[4]. Most of the many possible sources of error in determining the double layer parameters will be discussed in relation to our experimental results.

4.4 *Survey of recent theories of electrokinetic phenomena for the capillary model and the cell-model*

a. *The capillary model*

Describing a steady-state electrokinetic flow involves constructing and solving model equations (Poisson-Boltzmann, Navier-Stokes) with the proper boundary conditions. Recent mathematical (numerical) treatments as those of Anderson[31] or Levine[30] are hardly limited with regard to the magnitude of the potential (charge) and the electrokinetic radius, κa. Nevertheless, they are subjected to some restrictions that are rather important in view of practical applicability:

I it is assumed, that both monovalent ions, which constitute the electrolyte, have the same molar conductivity ($\Lambda_+ = \Lambda_-$).

II any contribution to the surface conductance residing inside the shear plane is disregarded (no anomalous conduction). The shear plane is treated as a discrete slipping plane[32].

Despite these restrictions, the relations for the several electrokinetic effects as obtained by Levine et al. extend and/or complete older results[21-29] significantly. Levine's theory refers to the constant potential case, whereas Anderson et al.[31] presented their (mainly numerical) results for constant charge conditions. We summarize the more accessible results of Levine in terms of phenomenological coefficients containing the factors that must be applied to Smoluchowski's classical results. The coupling coefficient L_{21}, which characterizes the convection current, may be expressed by:

$$L_{21} = \frac{\varepsilon_o \varepsilon_r \zeta}{\eta} \frac{(1 - G)}{C} \text{ , where} \qquad (4\text{-}9)$$

$$G = G(\kappa a, \tilde{\zeta}) = \frac{2}{(\kappa a)^2 \tilde{\zeta}} \int_o^{\kappa a} R \, \tilde{\psi}(R) dR \qquad (4\text{-}10)$$

C denotes the cell constant of the capillary, (1-G) the correction factor and $R = \kappa r$ the dimensionless radial coordinate. $\tilde{\psi}$ and $\tilde{\zeta}$ are the dimensionless potentials within the capillary and at the shear plane, resp. The correction factor will be used in evaluating our streaming current data. Comparison of (1-G) with the numerical results of an earlier study of the streaming current by Oldham et al.[21] for an extended potential and κa-range reveals no difference.

The coefficient characterizing the conductance of the capillary is given by:

$$L_{21} = \frac{K}{C} \frac{(1-G)}{F_C} \text{ with} \qquad (4\text{-}11)$$

$$F_C = F_C(\kappa a, \zeta, \beta^*) = \frac{\frac{1}{3}(\kappa a)^2 (1-G)}{\int_o^{\kappa a} R \cosh \tilde{\psi}(R) dR + \beta^* \int_o^{\kappa a} R \left(\frac{d\tilde{\psi}(R)}{dR}\right)^2 dR} \qquad (4\text{-}12)$$

where

$$\beta^* = \frac{(\varepsilon_o \varepsilon_r k \kappa)^2 T}{\eta K e_o^2} \qquad (4\text{-}13)$$

is a dimensionless parameter, that depends solely on electrolyte properties. The enhanced conductivity of the pore liquid at low κa-values, with complete incorporation of the effect of negative adsorption is given by $(1-G)/F_C$. For a discussion and calculation of the correction factors F_C and (1-G) one is referred to the original article[30].

Combining the equations (4-9) and (4-11) one gets for streaming potential and electro-osmosis:

$$\left(\frac{E_s^*}{\Delta P}\right)_{I=0} = -\left(\frac{J_v}{I}\right)_{\Delta P=0} = \left(\frac{\varepsilon_o \varepsilon_r \zeta}{K \eta}\right) F_C \qquad (4\text{-}14)$$

where $F_C = \zeta_a/\zeta$. ζ_a denotes the apparent zeta-potential, thus the non-corrected value obtained from the Smoluchowski equation.

In electrokinetic research the phenomenon of flow retardation is of

special interest. The decrease in volume velocity due to the electroviscous effect is given by the relation (see section 3.2):

$$\frac{(J/\Delta P)_{I=0}}{(J/\Delta P)_{E=0}} = \left(1 - \frac{L_{12}^2}{L_{11}L_{22}}\right) = \left(1 - \frac{8\beta^*(1 - G)F_c}{(\kappa a)^2}\right) \qquad (4\text{-}15)$$

with

$$L_{11} = a^2/(8\eta C) \qquad (4\text{-}16)$$

Numerical results can be evaluated for every combination of κa and ζ. For the constant charge case we first compute the potential at the various surface charge densities according to the Gouy-Chapman theory and then calculate the phenomenological coefficients as a function of κa or the external electrolyte concentration.

For sufficiently low potentials ($|\zeta| \leqslant 25$ mV) or charge densities, i.e. in the range of the Debye-Hückel approximation, Rice and Whitehead[25] presented analytical expressions for the correction factors in terms of the zeta-potential:

$$G = \frac{2I_1(\kappa a)}{\kappa a\, I_o(\kappa a)} \quad \text{and} \qquad (4\text{-}10a)$$

$$F_c = \frac{1 - G}{1 - (\varepsilon_o \varepsilon_r \tilde{\zeta}\kappa)^2/(\eta\kappa c).[1 - G - I_1^2(\kappa a)/I_o^2(\kappa a)]} \qquad (4\text{-}12a)$$

where I_o and I_1 are modified Bessel functions of the first kind of zero and first order, respectively. The denominator of F_c equals 1 as $\zeta \to 0$; consequently F_c equals $(1 - G)$ as $\tilde{\zeta} \to 0$. Sørensen and Koefoed[28] presented similar approximations for L_{21} and L_{22}, but then in terms of the charge density, σ_o:

$$L_{21} = \frac{2\sigma_o}{\eta\kappa^2 a}\left\{\tfrac{1}{2}\kappa a \frac{I_o(\kappa a)}{I_1(\kappa a)} - 1\right\}\frac{1}{C} \qquad (4\text{-}9a)$$

$$L_{22} = \left\{\frac{2\pi\sigma_o^2}{\eta\kappa^2} P(\kappa a) + K\right\}\frac{1}{C} \quad \text{where} \qquad (4\text{-}11a)$$

$$P(\kappa a) = \frac{1}{I_1(\kappa a)}\left\{\kappa a\, I_o(\kappa a) - \frac{Q(\kappa a)}{I_1(\kappa a)}\right\} \quad \text{and}$$

$$Q(\kappa a) = \int_o^{\kappa a} R\, I_o(R)^2\, dR$$

The terms on the right-hand side of eq. (4-11a) denote the purely convective and conductive contribution to the total current respectively.

Determination of the equivalent pore radius, a

In the traditional theoretical approach of replacing the actual system by an equivalent bundle of capillary tubes, it is customary to specify an effective pore radius and an effective pore length in terms of measurable overall properties of the porous system. For that purpose we choose the widely employed Kozeny-Carman relation[33], which assumes that the pore space in a packed system is equivalent to a bundle of parallel capillaries with a common hydraulic radius. The permeability coefficient, k*, defined in terms of Darcy's law:

$$J' = \frac{k^*}{\eta} \frac{\Delta P}{h} \tag{4-17}$$

may be evaluated experimentally. Here J' denotes the volume flow rate per unit cross sectional area of the uncharged porous plug and h the thickness of the plug. The K-C relation in the terminology used here, takes the form:

$$k^* = K_c \frac{\varepsilon^3}{S_o^2(1-\varepsilon)^2} \tag{4-18}$$

where S_o is the surface area exposed to the fluid per unit volume of solid and K_c the Kozeny constant. For capillaries of length l and radius a through which the fluid is transported by Poisseuille flow, the permeability coefficient reads:

$$k^* = \frac{1}{2}\left(\frac{h}{l}\right)^2 \frac{\varepsilon^3}{S_o^2(1-\varepsilon)^2} \tag{4-18a}$$

where S_o is related to the porosity and the capillary radius by:

$$S_o = \frac{2}{a}\frac{\varepsilon}{1-\varepsilon} \tag{4-19}$$

The capillary model can be matched with the K-C relationship by defining the effective length as $l = h/\sqrt{2K_c}$. The effective pore radius then becomes:

$$a_{K-C} = 2\left(\frac{k^*}{\varepsilon K_c}\right)^{\frac{1}{2}} \tag{4-20}$$

For our packed beds of uniform latex spheres we use the Kozeny constant $K_c = 1/5$, as determined empirically[33] in the porosity range $\varepsilon = 0.26$ to 0.8. The effective radius expressed in the particle diameter, D, according to eq. (4-19) or (4-20) amounts to:

$$a_{K-C} = \frac{\varepsilon}{3(1-\varepsilon)} D \qquad (4\text{-}20a)$$

In order to analyse the sensitivity of the correction factors for the magnitude of the effective radius, we also introduce the radius calculated from the simple Bjerrum-Manegold model[34], in which the porous bed is considered as a bundle of equivalent capillaries with length h. The radius then obtained is related to a_{K-C} by:

$$a_{B-M} = \frac{1}{5}\sqrt{10}\, a_{K-C} \qquad (4\text{-}21)$$

b. The cell-model

The experimentally observed variations of electrophoretic mobility with the concentration of charged particles stimulated the experimental and theoretical study of diffuse double layer interaction in homogeneous swarms of particles[35,36]. A first theoretical approach for $\kappa a \ll 1$ was made by Möller et al.[35], who used a cell-model. In this model each particle is enclosed within a spherical shell of electrolyte, containing just enough ions to neutralize the surface charge. The particles and their surrounding shells are considered to be of uniform size, each one being equal to the total volume of the suspension divided by the number of particles. In terms of porosity this model can be related to the particle radius a and the radius b of the particle with the shell:

$$\varepsilon = 1 - (a/b)^3 \qquad (4\text{-}22)$$

The distortion of the applied field around the particle was considered negligible. Consequently, application to the important κa-range, $1.0 \leqslant \kappa a \leqslant 100$, where the relaxation and retardation effects are particularly pronounced for moderately charged spheres, is excluded. Further, hydrodynamic interaction was not incorporated, so in principle this cell-model can only be used to examine double layer interaction.

Ciriacks et al.[11] incorporated the hydrodynamic interaction in the derivation of a relationship between zeta-potential and streaming current for mats of cylindrical fibers by using the cylindrical cell-model developed by Happel[37]. Apart from the effect of linearization of the Poisson-Boltz-

mann equation for practicability, the neglect of double layer polarization makes their theory less useful than Levine's treatment of the capillary model.

Following Möller et al., Levine et al.[38] studied electrokinetic phenomena of particle dispersions resulting from an externally applied electric field using the same cell-model for an extended κa and porosity range ($0 \leqslant \varepsilon \leqslant 0.4$). The hydrodynamic interaction was now incorporated by using Happel[37] and Kuwabara's[39] hydrodynamic boundary conditions. The electrical considerations were based on Henry's classical treatment of electrophoresis of a single isolated spherical particle. Consequently, the effects of surface conduction and double layer polarization are not considered. Moreover, the linearized Poisson-Boltzmann equation was used, reducing the applicability to small zeta-potentials. The electrophoretic (electro-osmotic) velocity was characterized by the factor $f(\kappa a,\varepsilon)$ with which Smoluchowski's expressions have to be multiplied. This factor, including several complicated integrals, can be evaluated for any ε and κa, for which we refer to the original article[38]. $f(\kappa a,\varepsilon)$ predicts the correct trend for electrophoresis and electro-osmosis within multiparticle systems. For $\kappa a \to \infty$, $f(\kappa a,\varepsilon) \to 1$ and for $\kappa a \to 0$, $f(\kappa a,\varepsilon) \to 0$. Increase of double layer interaction due to changes in κ and/or ε may result in a considerable deviation from Smoluchowski's equation. In a subsequent paper Levine et al.[40], again using the cell-model, developed a modified and generalized theory, covering the interrelated phenomena of sedimentation potential and streaming potential within swarms of spherical particles. The distortion from spherical symmetry of the charge partition within the shell (relaxation effect), due to an electric field, was described by a simple approximation. Just as in the treatment of the electrophoretic velocity of a particle swarm, the hydrodynamic considerations were based on the Kuwabara hydrodynamic cell-model. A crucial point in their theory, apart from the restriction to low zeta-potentials, is the way in which the 'streaming potential' condition was formulated. It appears that the relaxation effect in the convection current is neglected (see their equations (3-14) through (3-17)). In reality, liquid flow also deforms and polarizes the double layer, leading to an angular dependence of the volume charge density. Their expression for the internally induced macroscopic electric field, E^*, in the Dorn effect reads:

$$E^* = \frac{9\varepsilon_r\varepsilon_o\zeta v(1-\varepsilon)}{2Ka^2}\,\gamma(\kappa a,\varepsilon) \qquad (4\text{-}23)$$

where v is the sedimentation velocity of the particles and γ a complicated

correction factor, which has to be applied to the classical result of Smoluchowski. This factor equals 1, and thus the S. formula is obtained, for $\kappa a \to \infty$ and $\varepsilon \to 1$. The (primary) electroviscous effect, responsible for a retarded sedimentation velocity, was presented in the form:

$$\frac{v_o}{v} = 1 + \frac{\beta^* \tilde{\zeta}^2}{(\kappa a)^2} H(\kappa a, \varepsilon) \qquad (4\text{-}24)$$

where v_o denotes the sedimentation velocity of an uncharged swarm and $H(\kappa a, \varepsilon)$ the correction factor that equals 1 for high κa and ε. The velocity ratio can also be expressed in the apparent viscosity η_a and the true viscosity η as η_a/η. The functions $\gamma(\kappa a, \varepsilon)$ and $H(\kappa a, \varepsilon)$ were numerically evaluated for discrete values of ε (0.5 - 1.0) and graphically displayed for an extended κa-range ($10 \leqslant \kappa a \leqslant 10^4$). The predictions of the theory can be verified experimentally by a rather cumbersome determination of settling velocity and electric field strength of a suspension. All relevant physical parameters have to be known and association of particles, increasing with concentration of the solid, must be avoided. A much simpler experimental verification is feasible, however, by determination of the related phenomenon of streaming potential, combined with permeability experiments on plugs composed of charged spheres. At the same time, immobilization of the particles in the plug eliminates the necessity of incorporating the extremely difficult secondary electroviscous effect which was not considered in their theory. For this purpose we transform the formula for the settling velocity to flow through fixed beds caused by an applied pressure gradient. In terms of Darcy's law we get:

$$J'(=v) = \left(1 - \frac{L_{12}^2}{L_{11}\, L_{22}}\right) \frac{k^*}{\eta} \frac{\Delta P}{h} \qquad (4\text{-}17a)$$

The 'free surface' cell-model of Happel[37] and the 'zero-vorticity' cell-model of Kuwabara[39], describing the hydrodynamic flow field in the spherical shell of associated pore space, provide analytical expressions for the permeability constant k*. We restrict ourselves to Happel's predictions (k_H^*), which are more satisfactory than those of Kuwabara:

$$k_H^* = \frac{2a^2}{9(1-\varepsilon)\Omega_H(y)} \qquad (4\text{-}25)$$

with $\Omega_H(y) = \dfrac{2(3 + 2y^5)}{3(1-y)^3(1+y)(2+y+2y^2)}$ and $y = (1 - \varepsilon)^{1/3}$

An expression for the streaming potential (or electro-osmosis) can be obtained by combining equations (4-17a), (4-23) and (4-24) and the relation $E_s = E^*h$:

$$\left(\frac{E_s}{\Delta P}\right)_{I=0} = \frac{9\varepsilon_r\varepsilon_o\zeta(1-\varepsilon)}{2\eta\kappa a^2}\,\gamma(\kappa a,\varepsilon)\,k_H^*\left(1+\frac{\varepsilon_r\varepsilon_o\tilde{\zeta}^2}{\eta\kappa a^2}\,H\right) \qquad (4\text{-}26)$$

This expression allows a quantitative comparison between the cell-model and the experimental results obtained with our polystyrene plugs.

In an attempt to consider three-dimensional membrane effects on a microscopic scale, Metha and Morse[14] modelled the membrane by a lattice of charged uniform spheres, thus essentially employing the cell-model. They formulated the flux equations by averaging the flow over the cell volume. The convection current obtained by integration of the flow velocity and the equilibrium volume charge density over the cell yields a volume averaged current flow lower than the net flow of electric current formulated by Ciriacks[11] or Levine[40]. It will be clear that such an averaging procedure also disregards the effect of double layer polarization.

4.5 *Evaluation of electrokinetic effects in constant charge systems*

Almost all published formulae and figures related to electrokinetic phenomena enable the conversion of an experimentally measured quantity into the electrokinetic potential, which can be defined as the potential difference between the shear plane inside the porous system and the electroneutral electrolyte solution beyond. It is obvious that with increasing double layer overlap the potential in the symmetry plane in a parallel plate system, at the axis of a capillary or on the outer envelope of the cell in a cell-model will increasingly diverge from zero. In those cases we cannot simply interpret the corrected electrokinetic potential without considering the effect of interaction. In the case of constant surface charge the electrokinetic potential must increase, possibly even to infinity, when $\kappa \to 0$. However, if in practical aqueous systems dissociation of water molecules is taken into account, the Debye length is limited to a maximum value. For weakly overlapping double layers the charge (potential) partition near the surface will hardly be influenced for moderately charged surfaces. However, increase of overlap finally results in a shift of the whole potential profile relative to the reference potential in the electroneutral region beyond the interacting system. It will be clear that in this case a transformation of electrokinetic potentials into charge densities offers more direct information. We also have to consider the influence of curvature of the surface on the potential-charge relationship

together with the superimposed effect of double layer overlap. Fortunately the effect of curvature is rather limited. In mutually converting potential and charge, the error made while using the non-linearized P.B. equation for a flat double layer, although actually dealing with spherical or cylindrical geometry, is small for charge densities and/or κa-values[30,41,42] that are not too low. For a capillary with σ_o = 1 μC cm^{-2} and κa = 1 (c = 10^{-5}M 1-1 electrolyte, $\Psi_d \approx 8$) the error amounts to about 8%, while for the same capillary for σ_o = 10 μC cm^{-2} the error does not exceed 0.2%. Thus the error decreases sharply with increasing σ_o. The same trend is noticed in the case of double layer overlap. If the charge of, for example, plates is assumed to be constant, the dependency of the ratio $\Psi_d(\kappa h)/\Psi_d(\kappa h=\infty)$ on the distance h between the plates indicates the extent of overlap[43]. For σ_o = 1 μC cm^{-2} at 5 10^{-5}M 1-1 electrolyte and κh = 2 this ratio amounts to 1.005; even at κh = 0.2 it does not exceed 1.04. Summarizing, it can be stated that a corrected electrokinetic potential at moderate κa and σ_o values can be regarded as being identical to that of a 'free' surface.

4.5.1 *The $\breve{\kappa}$-concept*

A useful concept related to an analytical solution of the Poisson-Boltmann non-linear equations is that of Möller et al.[35,44] for the cell-model. They presented an alternative definition of κ in which the total surface charge was incorporated. Their parameter $\breve{\kappa}$ is based on the arithmetic mean $(\bar{C}_+ + \bar{C}_-)/2$, where $\bar{C}_+$ and $\bar{C}_-$ are the average molar concentrations of the positive and negative ions in the liquid phase. $\breve{\kappa}$ is defined by:

$$\breve{\kappa}^2 = \frac{2F_a^2}{\varepsilon_r \varepsilon_o RT} (\bar{C}_+ + \bar{C}_-) \qquad (4\text{-}27)$$

This implies that $\breve{\kappa}$ increases with increasing σ_o and/or with increasing volume fraction of the solid at constant surface charge.

We will use this concept to evaluate the phenomenological coefficients for the cylindrical geometry. An approximate solution of the P.B. equation can then be obtained by using the Debye-Hückel approximation. For this geometry the, negative, surface charge density can be incorporated by the relation: $\bar{C}_- - \bar{C}_+ = 2\sigma_o/aF_a$. The calculation of the coefficients involves a similar mathematical treatment as used by Sørensen and Koefoed[28]. In their final results, our eqs. (4-9a) and (4-11a), only κ has to be replaced by $\breve{\kappa}$. The function $Q(\breve{\kappa}a)$ can be approximated by $\frac{1}{2}\breve{\kappa}a$ for $\breve{\kappa}a \geqslant 10$ ($\breve{\kappa}a$ = 10: error $\frac{1}{2}$%); in practice $\breve{\kappa}a$ = 10 does not mean a severe

limitation for constant surface charges. The expression for L_{22} can then be simplified. For a negatively charged surface, we obtain

$$L_{22} = \{\sigma_o^2/\eta\tilde{\kappa}a + \Lambda_+(c_p - 2\sigma_o/a) + \Lambda_- c_p\}/C \qquad (4\text{-}28)$$

where c_p is the average electroneutral electrolyte concentration in the capillary, defined as $\frac{1}{2}(\bar{c}_+ + \bar{c}_- + 2\sigma_o/aF_a)$. To a first approximation, we assume that c_p equals the electrolyte concentration outside the capillary (see also section 4.8). An interesting consequence of the $\tilde{\kappa}$-concept is that one notices directly that a decrease of the external electrolyte concentration, even to zero, does not ultimately eliminate $\tilde{\kappa}$ and consequently neither the electrokinetic effects; in other words, the charge distribution at low ionic strengths is *only determined by the surface charge density and the geometry of the system*[45,46]. Another consequence of the constant charge concept is that upon decreasing the external concentration all phenomenological coefficients approach asymptotically to constant finite values. In the constant potential concept e.g. L_{21} exhibits a maximum value[30] and finally becomes zero as $c \to 0$, because ultimately the surface charge tends to zero. Comparing results of L_{21} and L_{22} for cylindrical geometry according to the *modified* analytical formulae of Sørensen et al. (κ replaced by $\tilde{\kappa}$) with numerical ones according to Levine, reveals a substantial improvement over the *unmodified* counterparts (see table 4-2 on next page).

We would also expect that in the cell-model for concentrated systems of constant charge, or more generally for an actual particle system, polarization becomes constant upon decreasing the electrolyte concentration. For $\tilde{\kappa}$-values roughly exceeding 10κ the charge partition in the double layer hardly changes any more and consequently the distortion of the double layer remains constant upon further decrease of κ.

4.6 *Survey and discussion of experimental results; interpretation in terms of the capillary-model and the cell-model*

An attempt will be made to analyse experimental data obtained by different techniques and under widely different conditions of electrolyte concentration, nature of electrolyte and temperature. The discussion will be related to recent theoretical model representations. This approach enables us to obtain the general characteristics of our geometric model system.

It has already been shown that in our studies all possible sources of error, including effects of low frequency dispersion, concentration polarization at the electrodes and the plug surfaces, can be properly cor-

Table 4-2. The phenomenological coefficients for a cylindrical capillary and KCl solutions as calculated from the various approximate expressions and the numerical approach according to Levine.

Sm.-Smoluchowski: eq. (4-9) and (4-11) with G=0 and F_c=1; Le-Levine: eq. (4-9) and (4-11); Ri-Rice and Whitehead: see Le, with G from eq. (4-10a) and F_c from eq. (4-12a); Sø-Sørensen and Koefoed: eq. (4-9a) and (4-11a); $\tilde{\kappa}$-$\tilde{\kappa}$ concept: eq. (4-9a) with κ replaced by $\tilde{\kappa}$ and eq. (4-28). t = 25.0°C; σ_o = 4.00 μC cm^{-2}.

$L_{12}.C \times 10^9$: A kg^{-1}s^2

c(KCl) moles/l	κa	$\tilde{\kappa}$a	Sm.	Le.	Ri.	Sø.	$\tilde{\kappa}$
10^{-1}	104	107	39.6	39.6	38.8	52.9	51.8
10^{-2}	32.9	40.6	85.6	82.2	80.5	162	133
10^{-3}	10.4	25.9	132	116	108	469	204
10^{-4}	3.29	24.0	178	130	87.9	10.3 10^2	220
10^{-5}	1.04	23.7	224	135	26.4	13.9 10^3	222
0	0	23.7					222

$L_{12}/L_{22} \times 10^9$: A^{-1}m^{3}s^{-1}

c(KCl) moles/l	Sm.	Le.	Ri.	Sø.	$\tilde{\kappa}$
10^{-1}	266	253	256	347	323
10^{-2}	57.4 10^2	34.4 10^2	47.1 10^2	68.7 10^2	44.9 10^2
10^{-3}	88.3 10^3	97.1 10^2	40.4 10^3	16.4 10^3	10.2 10^3
10^{-4}	11.9 10^5	11.9 10^3	12.4 10^4	12.9 10^3	11.2 10^3
10^{-5}	15.0 10^6	12 10^3	44.4 10^4	10.8 10^3	11.3 10^3
0					11.3 10^3

rected for. Details of the experimental procedures and techniques have been given in the experimental chapter 3.

4.6.1 *Irreversible behaviour of polystyrene plugs*

With regard to the reproducibility of our experiments, the experimental sequence appeared to be of vital importance. Prior to the experimental runs most plugs were thoroughly equilibrated at ionic strengths substantially higher than those used in the preparation of the plugs ($\geq 10^{-1}$M 1-1 electrolyte). After the determination of the electrokinetic quantities at these high concentrations, the plug was permeated thoroughly

with the lowest electrolyte concentration to be studied, until complete equilibrium was obtained. The electrokinetic measurements at this low concentration were followed by successive experiments with solutions of progressively higher concentrations ending with the initial high concentration. Many tests were duplicated with different plugs to verify the results, especially if any question existed as to the validity of the test. The precision was satisfactory and most experiments could be reproduced with another plug to within a few per cent. In a few cases plugs were tested, starting at once at low electrolyte concentration. Comparison of the results obtained with these 'untreated' plugs with those initially equilibrated at high c ('treated' plugs) reveals significant differences in the electrokinetic quantities, in the c-range up to about 10^{-2}M 1-1 electrolyte, irrespective of the nature of the electrolyte (LiCl, KCl, CsCl), surface charge density (L, M, H) and temperature (15, 25, 35°C). In the following the term 'untreated' is restricted to latices, which have not been exposed to c's exceeding 5 10^{-3}M 1-1 electrolyte, neither at the preparation stage nor at the centrifugation to plugs. A plug treated at high c exhibits complete reversibility. The electrokinetic data of treated plugs at arbitrary c's could always be reproduced. The irreversible behaviour of untreated plugs obviously reflects an irreversible change in electrochemical properties of the polystyrene surface and/or the bulk phase, induced at high c. It goes without saying, that these findings have been thoroughly tested by applying rinsing times sufficiently long to ensure complete equilibrium.

4.6.2 *Plug resistance: experimental and theoretical results*

It was necessary to measure the d.c. resistance of all plugs, since a pronounced dispersion effect at low ionic strength yields a.c. resistance values which are in considerable error. At low electrolyte concentration ($c < 5\ 10^{-3}$M) the X-Y method offers the opportunity to eliminate the effects of electrode polarization and low frequency dispersion (see sections 3.5 and 3.7.2). At higher c the direct determination from uncomplicated current-voltage characteristics, measured with the four-electrode technique, and the calculation from the streaming current and streaming potential experiments render the same information; the choice between them being a matter of required accuracy. At relatively high c ($\geq 10^{-1}$M) the sensitivity of the X-Y method drops considerably, so that the direct method is to be preferred. The general agreement between the two methods indicates that the directly determined d.c. resistance is essentially equal to the resistance being operative when a streaming potential is generated. The results of the low frequency dispersion will be discussed in chapter 7.

Examples of plug resistances vs. KCl concentration at 25°C are given in fig. 4-2a for three surface charge densities. This figure illustrates the observed irreversible behaviour. In all cases the R_p values of the untreated plugs are significantly higher than those of the treated ones. Increase of c causes a drastic drop in R_p at about 10^{-3}M. Above 10^{-2}M the full an broken lines converge, reflecting increasing coincidence of the electrical properties. At higher c's for each plug all experimental curves converge to one single curve; the influence of surface charge density becomes negligible and the conductance properties are only determined by the ionic strength and the mutually hardly different porosities and plug dimensions.

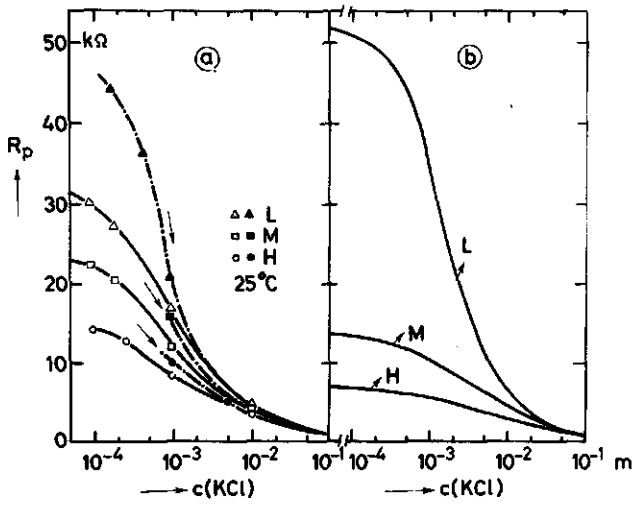

Fig. 4-2a,b. Experimental (a) and theoretical (b) plug resistances as a function of ionic strength for L(III, A,B), M(VIIIB) and H(VIIB) at 25.0°C. The experimental curves of the untreated plug are represented by broken lines and filled symbols; the arrows indicate the experimental sequence. The theoretical curves are computed according to Levine et al. with eq. (4-11), using the experimentally determined σ_o values.

At low c for each charge density the curves show different plateaus, reflecting a constant contribution of the mobile excess charge to the flow of electricity by migration and convection. Without the double layer contribution, R_p would continue to vary in an inversely proportional way to the specific conductivity of the bulk electrolyte, K; in that case R_p would exceed 5 $10^4\Omega$ at 10^{-4}M KCl.

The irreversible behaviour indicates a charging process. At this stage it is perhaps worthwhile to note that an irreversible co-ion adsorption cannot be responsible for this effect. Adsorption measurements

with radioactively labelled Cl^- yield an increase in σ_o which does not exceed -0.2 $\mu C\ cm^{-2}$. The differences in R_p at low c between the untreated and treated plugs M and H correspond to about ten times this value. Apparently, at the first treatment with high ionic strength, irreversible rearrangements of the polystyrene surface occur; this may be accomplished by exposure of a larger fraction of negatively charged groups being located close to the surface. This results in an increase of the effective charge and consequently in lower R_p values. One should take into consideration that the surface charge densities of the latices, as determined conductometrically, are evidently associated with the untreated plugs. Here we will restrict ourselves to some general aspects of this charging process; a more elaborate and quantitative analysis will be given in section 5.8.

The theoretical R_p values (fig. 4-2b) have been computed for an 'equivalent' capillary model with eq. (4-11). In the calculation the physical properties were assigned to an aqueous potassium chloride solution. The functions $G(\kappa a,\psi_d)$ and $F_c(\kappa a,\psi_d)$ in eq. (4-11) were evaluated on basis of κa- and ψ_d-data estimated by means of eq. (4-20a), yielding the equivalent pore radius and surface charge densities, respectively. As was to be expected, the values calculated at high c coincide with the experimental curves, because the experimental cellconstants were used. At lower concentrations the theoretical predictions do not agree with the experimental ones. Inspection of the plateau values, for instance, reveals marked differences. This disagreement stems mainly from the fact that the capillary model does not allow for double layer polarization.

The theoretical predictions include a complete electro-osmotic contribution ($\psi_d = \zeta$). By assuming complete absence of this effect, a small shift to higher R_p values results, which, however, reduces the differences between theory and experiment only slightly. It illustrates that the information obtained on basis of R_p measurements alone is rather limited. The apparent better correspondence with the curves of the treated plugs M and H results from the charging process; increase of effective mobile charges partly compensates the effect of double layer polarization. It is noted that the deviating relative position of the theoretical and experimental curves for L reflects the sensitivity for a small increase of σ_o; an increase with about 1 $\mu C\ cm^{-2}$ halves the theoretical plateau value.

4.6.3 *Streaming current: experimental and theoretical results*

At high electrolyte concentration (> 5 10^{-2}M) it was difficult to accurately determine the streaming current from the X-Y plot because of fast retardation. In those cases the d.c. streaming current can be com-

puted accurately from streaming potential and d.c. resistance. In discussing the consequences of the constant charge concept for electrokinetics (section 4.5.1), the conclusion was drawn, that all electrokinetic phenomena, even when complicated by double layer polarization, gradually approach finite values as $c \to 0$. This fact is illustrated by the theoretical predictions of Levine for I_s in fig. 4-3b and R_p and fig. 4-2b. The experimental curves in fig. 4-3a reveal several conspicuous features:

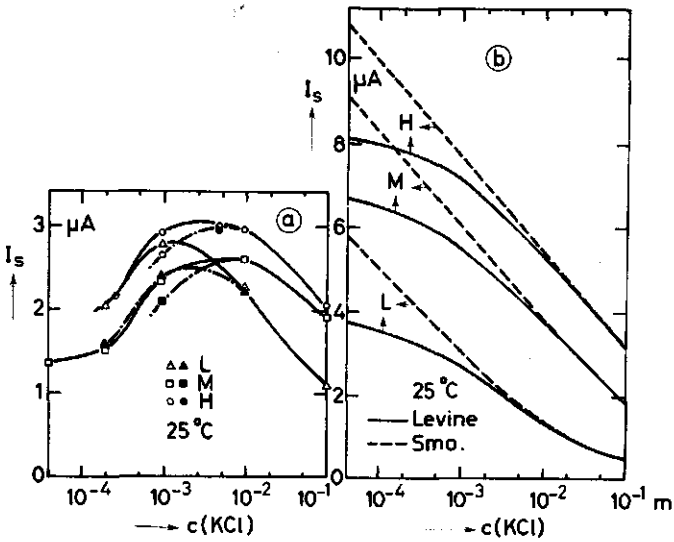

Fig. 4-3a,b. Experimental (a) and theoretical (b) streaming current characteristics for L(IIIA,B), M(VIIIB) and H(VIIB) at 25.0°C and ΔP = 30 cm Hg. The experimental results of the untreated plugs are indicated by broken lines and filled symbols.

a) all experimental curves pass through a maximum at intermediate concentration, reflecting an anomalous behaviour, irrespective of the surface charge density;

b) at low c's I_s tend to approach a constant value; the marked drop to constant values occurs over a small c-range. We have previously shown that upon variation of the bulkconcentration at low c and moderate σ_o-values, so that $\tilde{\kappa} \approx 10\kappa$, a redistribution of the charge excess in the double layer is small. Consequently, I_s will not vary significantly with c, certainly not in the observed direction;

c) the almost identical positions and shapes of the I_s curves below about 10^{-3}M point to the fact that nearly the same amount of excess charge is effectively conveyed by the mass flow irrespective of σ_o;

d) a marked deviation of the mutually hardly different experimental plateau values with the predicted ones indicates that for all σ_o's only

a strikingly small part of the excess charge is convected;

e) the irreversible charging process is less pronounced than in its effect on R_p; apparently nearly all the new charges are hydrodynamically inactive.

A mutual comparison of the trend and the position of the experimental and theoretical curves gives insight in the concentration dependency of the hydrodynamically effective charge density. The substantial decrease of this charge density would imply an anomalous behaviour, e.g. a structural rearrangement, of the surface layer, in which a redistribution of the fixed charge on the latex surface is responsible for a reduction of the excess charge carried by mass movement. Consequently, the charge transmitting the electric field to the surrounding fluid medium must also decrease. This could suggest that the anomalous findings must be reflected in the R_p-characteristics too. However, only a small part of the maximum possible convection current contributes to the total plugconductance, so that a sudden decrease of this contribution will be hardly noticeable.

In computing the theoretical I_2 values the same κa and $G(\kappa a,\psi_d)$ were taken as used in the R_p-calculations. The classical Smoluchowski predictions in the same figure illustrate especially for high constant σ_o, the good predicting trend as compared to the Levine prediction, even for low c-values. It should be recalled that this is a typical consequence of the constant charge concept. It is noted that the correction factor $G(\kappa a,\psi_d)$, that must be applied to Smoluchowski's equation, is based on a Gouy-Chapman ionic atmosphere. Consequently the I_s predictions are independent of the nature of the monovalent electrolyte.

No allowance could be made for the possible influence of double layer polarization on the streaming current. If the excess charge moves along with the lines of flow along a curved surface, it will give rise to a substantial volume charge density outside the double layer. Consequently, redistribution of ions due to the locally induced polarization field occurs by processes of diffusion and migration. A locally opposite current, gradually increasing with decreasing concentration, partly compensates the convective current, resulting in a smaller streaming current. This effect will only be substantial for not too small convective currents and curvature values that are moderate in comparison to the double layer thickness. In section 4.2.1 we have already noticed that for a two capillary system a non-negligible surface conductance leads to a depression of the streaming current. For a particle system we can express this effect more quantitatively by modifying the Rel concept of Dukhin (see chapter 5):

$$Rel(I_s) = \kappa^{\sigma}_{ek}/K_p a$$

where κ^{σ}_{ek} is the specific surface conductance beyond the plane of shear, K_p is the specific conductivity of the pore fluid and a the particle radius. A small value of Rel corresponds to a weak polarization effect on I_s. This is the case for low κ^{σ}_{ek} and/or high K_p.

In case of anomalous conduction ($\kappa^{\sigma} > \kappa^{\sigma}_{ek}$) the amount of depression of the polarization field will be strongly dependent on the actual mobility of the ions in the immobilized layer which is reflected in $K_p(\kappa^{\sigma},K)$. It is clear that for a lyotropic sequence the difference in ion mobility and thus in $Rel(I_s)$ leads to a lyotropic sequence in I_s and can misleadingly be interpreted in an ion-specificity of the zeta-potential (see chapter 6 too). In all probability the polarization effect on streaming current is insignificant for our plugs. If the smallness of I_s at low ionic strength is just a result of substantial polarization, than the influence of the mobility of the counterions must be distinguishable. The comparatively small effect that results from variation of the nature of the ionic solute and the surface charge density point to a small effect of polarization on I_s. These findings will be exemplified in table 4-3. A quantitative interpretation of the results in terms of a boundary concept is postponed for the time being. It will be shown later that an analysis of the electroviscous effect offers more direct insight into all anomalous effects connected with an 'immobilized' water layer.

4.6.4 *Streaming potential: experimental and theoretical results*

The measurements of streaming potential, contrary to those of electro-osmosis, show a high degree of reproducibility.

The effect of an intrinsic dielectic dispersion on I_s and R_p, observed at low c, completely cancels for E_s. The influence of the relatively slight rejection properties of our coarse porous plugs on the determination of the electrokinetic quantities was thoroughly examined. Extensive theoretical and experimental details have been given in sections 3.3 and 3.7.

For the sake of clarity we have presented the experimentally obtained and the theoretically calculated streaming potential results in separate figures. In fig. 4-4a the experimental results for KCl at 25°C are plotted. The effect of irreversible charging on the streaming potential values of the untreated plugs is indicated by the broken and full lines. The gradual increase of E_s to plateau values, observed for all curves in case of decreasing c, does not reflect the anomalous findings for I_s. A substantial increase of R_p in the c-range involved masks the change of I_s. In general, a streaming potential characteristic does not lend itself very well to conclusive interpretation because all possible effects separately percep-

tible in I_s and R_p are now incorporated in one quantity. For a brief discussion we present three model calculations which should permit interpretation of the experimental data. In fig. 4-4b we have plotted E_s vs. c at ΔP = 30 cm Hg according to the capillary model of Levine, eq. (4-14), for the particular case $\psi_d = \zeta$. In fig. 4-4c results for the same capillary model are presented, but are now calculated using the analytical expressions for the correction factors of Rice and Whitehead, as defined in eqs. (4-10a) and (4-12a). In these calculations the physical properties and capillary dimensions are the same as used in calculating R_p. In fig. 4-4d we have plotted the result for the cell-model, where the polarization concept is approximated. The expressions of Levine et al., as adapted for the streaming potential phenomenon in a fixed bed of spherical particles, are given in eq. (4-26). Evaluation of the expressions for $\gamma(\kappa a,\varepsilon)$ and $H(\kappa a,\varepsilon)$, presented in the original article[40], entail numerical integration. The experimentally determined porosities and particle radii have been used. It is recalled that the last two models are both subjected to the Debye-Hückel approximation.

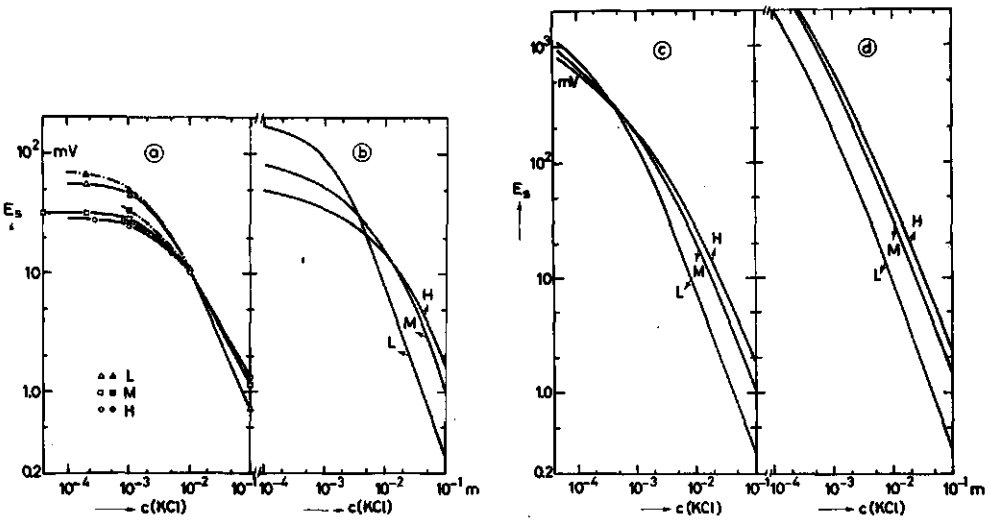

Fig. 4-4a,b,c,d. E_s vs. c curves for KCl solutions at 25°C and ΔP = 30 cm Hg. (a) experimental results for L(IIIA,B), M(VIIIB) and H(VIIB); the results of the untreated plugs are indicated by broken lines and filled symbols, (b) the theoretical predictions for the capillary model of Levine et al., (c) the theoretical results for the capillary model of Rice and Whitehead subjected to the Debye-Hückel approximation, (d) the theoretical results for the modified cell-model, according to Levine et al.

A comparison of the different trends in figs. 4-4c and 4-4d, considering the influence of polarization on $E_s/\Delta P$, may yield valuable informa-

tion for an analysis of the experimental results on the basis of the capillary model (fig. 4-4b) in the 'high potential' range. At low c the specific conductivity of the pore and shell liquid for the cases c and d resp. is miscalculated when extending the calculations past the 'low potential' range, due to the D-H approximation. However, an overestimation of the convective contribution partly compensates the underestimated conduction contribution to the total conductance. Comparison of figs. b and c clearly shows the severe low potential restriction in the E_s calculations. The divergence between the two predictions is already apparent at relatively high c. A comparison of figs. c and d reveals the typical consequence of double layer polarization on streaming potential. With increased surface charge density and decreased ionic strength the polarization field increasingly reduces the effectiveness of the mobile charge. This may result in a significant shift of the mutual intersections of the E_s-c curves to lower c values and the appearance of higher plateau values. The relatively increasing contributions of excess ions to the conductance upon decreasing c is responsible for the reversal of the sequence of the E_s-c curves with respect to the charge density. Applying similar reasoning with respect to the effect of polarization to the results in fig. 4-4b, the supposition is justified that an incorporation of double layer polarization will shift the plateau region to higher E_s-values and the mutual intersections to lower ionic strengths. This will increase the divergence between the theoretical predictions and experimental results. The observed trend agrees very well with the general anomalous findings of I_s. From the position of the plateau in fig. 4-4b it is clear that varying σ_o hardly decreases the gap between theory and experiment. Apparently, in the low c-range a marked difference between ψ_d and ζ must be considered.

4.6.5 *Evaluation of a) the zeta-potential and b) the total charge density from electrokinetic data with the capillary model*

a) The procedure to correct the zeta-potential for the effect of a thick double layer was as follows: firstly the classical value of the zeta-potential was calculated from the streaming current, using the Smoluchowski prediction, eq. (4-9) with G=0, and the experimentally determined cell constant, C. With this apparent zeta-potential, ζ_a, and the κa value, obtained from the electrolyte concentration and the capillary dimensions obtained from eq. (4-20a), a value of $G(\kappa a,\zeta_a)$ was calculated. A first corrected zeta-potential, ζ_1, is obtained again using eq. (4-9) and the calculated $G(\kappa a,\zeta_a)$. With ζ_1 a second value of $G(\kappa a,\zeta_1)$ was obtained and compared with the preceding estimate of G. This successive approximation

method was used till the difference between two subsequently corrected zeta-potentials was negligible. Usually three cycles were required to obtain an accurate corrected value. To facilitate this laborious procedure the presented procedure can also be performed graphically. To that end plots of (1-G) versus κa have to be constructed for various values of the parameter $\tilde{\zeta}$ (see Levine et al.[30]: their fig. 4). A similar procedure was already given by Oldham et al.[21].

Table 4-3a. Some corrected zeta-potentials of treated plugs for three surface charge densities at 25.0°C. The ζ_a and ζ_c^* data correspond to the apparent zeta-potentials and the values corrected on basis of the Bjerrum-Manegold radius. The actual ζ-values are negative and are expressed in mV.

c	L(V)			M(VIII)		H(VII)				
								$-\zeta_a$	$-\zeta_c^*$	
moles/l	LiCl	KCl	CsCl	LiCl	KCl	LiCl	KCl	KCl	KCl	CsCl
$2\ 10^{-1}$						45.7	43.3	43.3	43.3	37.3
10^{-1}	29.1	20.8	25.6	51.7	48.0	54.3	50.1	50.1	50.1	45.9
10^{-2}	61.2	55.8	56.3	68.5	66.4	77.5	76.6	74.2	79.0	74.3
$5\ 10^{-3}$						80.8	79.4	74.9	82.5	82.0
$1.25\ 10^{-3}$		77.9	78.1							
10^{-3}				67.7	66.5		83.2	74.1	91.0	88.9
$9.55\ 10^{-4}$	81.5									
$9.2\ 10^{-4}$						84.6				
$7.5\ 10^{-4}$*	80.7	81.6	80.3							
$2.6\ 10^{-4}$*						76.6	72.3	54.2	85.1	77.4
$2\ 10^{-4}$				53.5	52.1					
10^{-4}	68.6	75.8	75.8							

* average c-values for L and M (Li,K,Cs); for the calculations the actual values as given in Appendix 5A were used.

In table 4-3a we have summarized the most important corrected zeta-potentials, ζ_c, at 25.0°C. The results at other temperatures are presented as σ_{ek}-values in appendix 5A. Despite the correction, there is still a maximum in ζ_c as a function of c, pointing to a drastic drop of σ_{ek} with decreasing c. Even, taking a 40% lower B-M radius in the correction procedure hardly changes the overall picture, as exemplified by the ζ_c^*-values. The relatively small effect of the correction is to be expected, because at 10^{-4}M κa_{K-C} still amounts to about 10 (see the ζ_a and ζ_c values of sample H). As already suggested, the shear surface shifts outwardly on

decreasing c, probably connected with a change in the double layer structure. From the ζ_c-results we notice a small alkali-ion specificity the sequence of which reverses in going from high to low c. As already discussed, the polarization of the ion-atmosphere increases with decreasing c and decreasing molar conductivity of the counterions, Λ_+. For a polarized diffuse double layer we may, therefore, expect the sequence: $|\zeta(Li^+)| < |\zeta(K^+)| < |\zeta(Cs^+)|$. The relatively slight ion-specificity observed at low c probably points to a less different effective Λ_+ of the counterions as a result of specific double layer effects and/or an alkali-ion specificity in the concentration dependent location of the shear surface. To show the slight effect of treatment on ζ_c, the following ζ_c-values of untreated plugs at 10^{-3}M KCl may serve: L -77.0 mV; M -61.8 mV and H -64.8 mV. A more general discussion will be given in combination with surface conductance and electrophoresis results and is therefore postponed to section 5.8 and chapter 6.

b) The procedure for calculating the effective charge density, σ_t, according to the capillary model of Levine et al.[30] is as follows: in the c- and σ_o-range of interest L_{22}-σ_o plots were calculated for chosen c-values, according to eq. (4-11). For this purpose bulk values were assigned to the constants and Λ_+ and the same parameters as used for the ζ_c calculations were taken. It is recalled that in Levine's model no anomalous conduction takes place and $\Lambda_+ = \Lambda_-$, so the calculations are restricted to KCl. From L_{22}-σ_o curves corresponding with the actual concentration the σ_o corresponding to the experimentally obtained L_{22} was assessed and this value is the sought σ_t. Some σ_t-values are presented together with σ_{ek}-values in table 4-3b. Despite the severe restrictions of the capillary model with

Table 4-3b. σ_{ek} and σ_t results (the latter between parentheses) of untreated and treated plugs evaluated according to the capillary model of Levine et al.[30]; t = 25.0°C. The actual σ values are negative and are expressed in $\mu C\ cm^{-2}$.

c(KCl)	L(IIIA,B)		M(VIIIB)		H(VIIB)	
moles/l	untreated	treated	untreated	treated	untreated	treated
$2\ 10^{-1}$		2.42				4.90
10^{-1}		2.27		4.00		4.38
10^{-2}	1.84(2.95)	1.89(2.95)		1.98(4.30)		2.50(6.70)
$5\ 10^{-3}$					1.80(5.60)	1.94(6.00)
10^{-3}	0.78(1.60)	1.01(2.00)	0.531(2.24)	0.63(3.20)	0.74(3.95)	0.93(5.00)
$2.6\ 10^{-4}$						0.37(3.60)
$2\ 10^{-4}$	0.26(1.08)	0.38(1.65)		0.20(2.20)		
$4\ 10^{-5}$				0.11(1.95)		

respect to the σ_t-values, this procedure may give a general impression of our model system.

A substantial decrease of σ_t with decreasing c accompanies a decrease in σ_{ek}; the former decrease, however, is mainly a result of the fact that the capillary model ignores double layer polarization and is for a small part caused by the incorporation of a maximum electro-osmotic contribution in the theoretical L_{22}-σ_o calculations ($\psi_d = \zeta$). The increasing difference between σ_{ek} and σ_t upon decreasing c points to an increasing anomalous conduction. Apparently, the shear surface shifts outwards upon decreasing c and/or specific adsorption increases to such an extent that the anomaly of our model system is not masked by any deficiency in the conversion model. It is clear that a correction for polarization and anomalous conduction will increase the σ_t-values, especially at low c and high σ_o. A comparison of the σ_{ek} and σ_t data before and after treatment at high c shows that the new or activated charge carriers are hydrodynamically immobile. In chapter 5 we will analyse these results more extensively in terms of particle models which include the polarization concept.

4.7 *Permeability: experimental and theoretical results*

In the experimental section 3.7.4 all factors which could possibly explain the observed dependency of the permeability upon c have been analysed. Calculation of the electroviscous retardation indicates that this effect contributes only to a small extent. Apparently, the observed reduction is caused by the same phenomenon that is operative in the assessment of the electrokinetic quantities. In order to give an impression of the effective thickness of the boundary layer involved (immobilized water and/or swollen surface layer) the variation of the permeability must be transformed into a shift of the hydrodynamically effective surface. The effective thicknesses can then be compared with those ensuing from electrokinetic predictions.

4.7.1 *Computation of the location of the effective hydrodynamic plane*

The location of the *effective* hydrodynamic surface does not necessarily have to coincide with the position of the shear plane, the plane of zero fluid velocity. It is possible that the position of the shear plane is not affected by decreasing c, but only the hydrodynamically effective surface (slipping layer concept[32]). In that case a complete description including permeation within the boundary layer region, possibly attended by fluid-slip phenomena, cannot be achieved without introducing empirical parameters. The effect on the external flow of a flow field within the pe-

riphery or the boundary layer of the particle can become significant and a knowledge of it is very important for interpretation of electrokinetic results. In this framework it is realistic to treat the viscosity close to the surface as a gradually decreasing function of the double layer field strength, but quantitative verification is hardly possible because the viscoelastic constant of water is not known[32,47,48].

Transforming permeabilities into particle radii and effective hydrodynamic layers can, of course, best be afforded by application of theoretical models, which have prove to provide satisfactory agreement with experimental data over an extended porosity range. We shall apply the widely quoted 'free-surface' cell-model of Happel[37]. The coefficient L_{11} according to Happel's cell-model reads:

$$L_{11} = \left(\frac{J_v}{\Delta P}\right)_E = \frac{2a^2}{9(1-\varepsilon)\Omega_H \eta C} \qquad (4\text{-}25a)$$

C denotes the cell constant of the plug (length/surface area) and Ω_H is the function previously given in combination with with eq. (4-25):

$$\Omega_H = \frac{2 + 4/3\ y^5}{2 - 3y + 3y^5 - 2y^6} \quad \text{with} \quad y = \frac{a}{b}$$

a denotes the particle radius and b the outer radius of a concentric spherical shell of fluid. The porosity of the unit cell is equal to that of the plug, which necessitates that $\varepsilon = 1 - (a/b)^3$.

At low ionic strength the hydrodynamically effective particle radius is defined by $a^* = a + \Delta_h$ while $y^* = a^*/b$; it is noted that only a change of the particle radius is considered. The radius a, referring to the highest electrolyte concentration, is taken as the reference. The ratio of the volume flows at high c, J_v, and an arbitrary concentration, J_v^*, at the same pressure gradient yields on the basis of eq. (4-25a):

$$J_v/J_v^* = y^*\Omega_H^*/y\Omega_H \qquad (4\text{-}29)$$

With a plot of the calculated permeability ratio $J_v/J_v^*(y,y^*)$ versus $\Delta y = y^* - y$, the experimental permeability data can graphically be converted into a reduced particle radius increase, Δy. The absolute value of the effective thickness, Δ_h, is calculated using the porosity and the computed particle radius determined at high ionic strength or from electronmicroscopy provided no substantial surface area changes occur during the drying of the sample. It is of special interest to check the particle and

pore radii as calculated for high ionic strength, as these have to be used for determination of the effective hydrodynamic thickness and calculation of the double layer overlap, respectively. Comparison of the calculated diameters in table 4-4 with those determined by electronmicroscopy reveals a consistent trend, the calculated diameters being greater. It is possible that some shrinkage of the particles occurs during the drying process, but it is more likely that these differences are due to some heterogeneity of the particle bed. No significant plug shrinkage was found to occur on drying which would be required if the calculated differences were caused by compaction of the plug.

Table 4-4. Experimental and theoretical particle diameters and capillary radii: D_H, diameter calculated with Happel's cell-model, eq. (4-25); D_{K-C}, calculated with the Kozeny-Carman, eqs. (4-20) and (4-20a); D_{em} is the diameter obtained by electronmicroscopy; $a^{exp.}_{K-C}$, the effective pore radius, calculated from the experimentally determined permeability coefficient, k*; a^{em}_{K-C}, the radius calculated with D_{em}, eq. (4-20a). The L and M results are determined at 10^{-1}M; the H results at $c = 10^{-2}$M.

	ε	½D_H nm			½D_{K-C} nm			½D_{em} nm	$a^{exp.}_{K-C}$			a^{em}_{K-C}
		15°	25°	35°C	15°	25°	35°C		15°	25°	35°C	
L	VA 0.3985	284	284	279	299	299	294		131	131	129	112
	VB 0.3959	313	308	301	329	324	317	253	145	143	139	110
	VC 0.3985	288	282	283	302	297	297		132	130	130	112
M	VIIIA 0.4154		262			357		305		162		144
	VIIIB 0.4049		286			303				137		138
H	VIIA 0.4029	277	280	278	272	275	274		122	124	123	130
	VIIB 0.3867	298	305	310	315	322	327	290	132	135	137	122
	VIIC 0.3685	314	317	308	331	334	325		128	130	126	113

Furthermore, it is known from the literature that for latices the average particle size obtained by the dry method is in good agreement with that from the wet method[49-51]. Additional light is thrown on these observations by comparison with the formation factors determined by electrical measurements (see section 5.6). The latter method, which is based on statistical considerations, gives a closer agreement with electronmicroscope data which substantiates once again the higher sensitivity of the permeability method to a slight heterogeneity of the pore size. The anisotropy may result from using the centrifugation technique, where one is likely to get a plug of graded porosity, i.e., the plug can be imagined to consist of a large number of slices of varying porosity arranged in series.

However, it is evident that the relatively low overall porosity of the plug and the high degree of monodispersity prevent substantial differences in packing characteristics within one plug. Finally, it is clear that the observed trends are also reflected in the effective radii $a^{exp.}_{K-C}$ and a^{em}_{K-C} calculated from permeability, eq. (4-20), and electronmicroscopy results, eq. (4-20a), respectively. The slightly smaller a^{em}_{K-C} value will be used in all the electrokinetic capillary model calculations.

4.7.2 *The effective boundary layer thickness from hydrodynamic experiments:* Δ_h

The effective layer thickness, Δ_h, is calculated according to the Happel model with the procedure described in the preceding section. For plug VII permeability results at 10^{-1}M were lacking. The standard was therefore taken at 10^{-2}M, which may lead to a slight underestimation of the Δ_h values. To get insight in the concentration dependency, we have plotted the temperature-averaged values in fig. 4-5. From that figure it is obvious

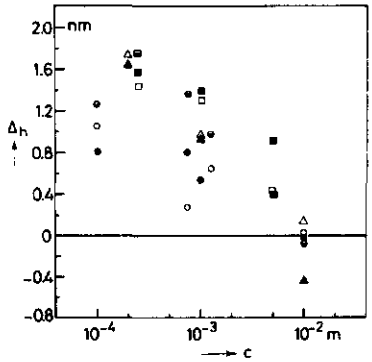

Fig. 4-5. The boundary layer thickness, Δ_h, versus electrolyte concentration for a number of counterions. L ● (LiCl), ○ (KCl), ◒ (CsCl); M ▲ (LiCl), △ (KCl); H ■ (LiCl), □ (KCl), ▬ (CsCl).

that, independent of the nature of the cation, Δ_h increases with decreasing ionic strength. Furthermore, there is a slight tendency for the plugs with the highest surface charges to produce bigger Δ_h-values, especially at relatively high c. It is noted that on the basis of these results alone no conclusions can be drawn with respect to the nature of the observed effect (particle swelling, hairyness, water structuring). However, the magnitude on the effective Δ_h-values in combination with other data may be used to elucidate the structure and properties of the boundary layer. This is particularly important in view of the anomalous findings in the electrokinetic phenomena observed in the same concentration range.

4.7.3 *Electroviscous effect*

It has already been demonstrated that plots of $L^2_{12}/L_{11}L_{22}$ vs. c(Li, K,CsCl) show a maximum for plug M (see fig. 3-35). Similar plots for L

and H for the same temperatures and electrolytes also show maxima. As argued earlier, for a system of constant charge and without a boundary layer, the coefficients L_{21} and L_{22} are expected to increase gradually to limiting values upon decreasing ionic strength, irrespective of possible double layer polarization effects ($\tilde{\kappa}$-concept). Due to the quadratic dependency of the retardation upon L_{21}, the anomalous behaviour of the streaming current is clearly noticeable. Furthermore, from fig. 3-35 it is observed that the molar conductivity of the counterion, Λ_+, has a strong influence upon the retarding flow. It is noted that a difference in Λ_+ is only reflected in L_{22}, because L_{21} is practically independent of the nature of the ions. The streaming current data show that a boundary layer effect at low ionic strength reduces L_{21} markedly, irrespective of the nature of the cation. Consequently, the observed increase in retardation in passing from Cs^+ to Li^+ was to be expected.

The absence of any temperature dependence on the retardation indicates that the part of the charge transfer that takes place through the boundary layer is hardly affected by varying the temperature in the studied range.

In fig. 4-6a,b,c experimental and theoretical retardation data are plotted as a function of the surface charge density. The experimental results in fig. 4-6a refer to σ_o's determined by the conductometric titration method. A comparison of the analytically computed and the experimentally determined apparent viscosities serves to show the influence of other phenomena than those expressed by the basic electrokinetic parameters used.

In fig. 4-6b the retardation characteristics are plotted according to the cell-model of Levine et al. as defined by eq. (4-24). A comparison of our results with those of the cell-model reveals the inconsistency of the predictions, which is due to the severe restriction to small potentials and moderate κa-values. The fact that upon decreasing c the ratio η_a/η shows a maximum for moderate *constant* σ_o-values is consistent with the underestimation of the shell conductivity by extending the 'low potential approximation'. Unfortunately, this limitation masks the improvement gained by incorporating double layer polarization.

In fig. 4-6c we have plotted the data according to the capillary model, computed with eq. (4-15) for KCl at 25°C. It should be noted, however, that conduction inside the shear plane is not considered and that the calculations are confined to monovalent electrolytes with $\Lambda_+ = \Lambda_-$. Of particular interest are the maxima for relatively low ionic strengths. This is a result of the combination of two trends that may be anticipated: an increase of L_{21} with σ_o is accompanied by an increase in fluid conduction,

but the latter eventually overcompensates the increase in L_{21}, thus reducing the retardation effect. At higher ionic strength the maximum value of the retardation is shifted to higher σ_o-values. Despite the marked effect of charge transfer in a boundary layer suppressing the total retardation effect and reversing the sequence at low concentration, a comparison of the general features of the experimental results and the capillary prediction is quite striking. We will now quantitatively illustrate the effect of charge transfer in the immobilized layer on electroviscous retardation.

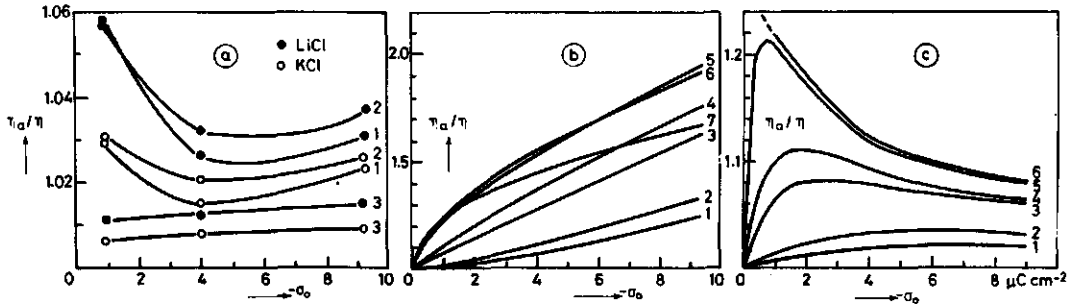

Fig. 4-6a,b,c. Experimental and theoretical electroviscous retardation ratios, $\eta a/\eta$, versus the surface charge density, σ_o. *a*) exp. results for LiCl and KCl solutions: 1) 2.5 10^{-4}M, 2) 10^{-3}M, 3) 10^{-2}M. b) results according to the cell-model theory of Levine et al. Curves 1-7 correspond with concentrations of 10^{-1}, 5 10^{-2}, 10^{-2}, 5 10^{-3}, 10^{-3}, 5 10^{-4} and 10^{-4}M KCl resp. c) results as calculated for a capillary according to the theory of Levine et al. Curves 1-6 correspond with concentrations 10^{-2}, 5 10^{-3}, 10^{-3}, 5 10^{-4}, 10^{-4} and 10^{-5}M KCl resp. An immobilized layer is not considered. The calculations are performed only at discrete values; therefore the precise maxima are uncertain. t = 25.0°C.

4.7.3.1 *The boundary layer thickness as inferred from the electroviscous effect:* Δ_{ev}

Figs. 4-7a,b,c summarize calculations of the electroviscous effect for the capillary model incorporating the concept of anomalous conduction. We shall demonstrate that when the shear plane does not coincide with the particle surface the electroviscous effect may decrease due to charge transfer in the immobilized layer, an effect not incorporated in the Levine treatment. In calculating the various effects of an immobilized layer, we have used the flat-plate approximation which introduces less than 1% error even for 10^{-4}M 1-1 electrolyte and $\sigma_o \geqslant 0.5$ μC cm^{-2} (see section 4.4.1). The extent of electromigration in the Δ-layer is indicated by the parame-

ter $p_\Delta = D_\Delta^\pm / D^\pm$, where $D_\Delta^\pm$ denotes the ionic diffusion coefficient in a boundary layer of thickness $\Delta(\psi_d, \zeta)$ and $D^\pm$ refers to the bulk. The first step in determining the electroviscous retardation is to select a value of Δ for a chosen σ_o. The charge density at the shear plane, σ_{ek}, was calculated according to Gouy-Chapman and the retardation is again evaluated according to the rigorous quantitative approach of Levine as defined by eq. (4-15). For one particular σ_o the retardation was calculated for Δ = 0.5; 1.0; 5.0 and 10 nm. L_{11} was, of course, corrected for the reduction of the capillary radius. Knowing which part of the excess charge resides in the Δ-layer, thus in the space between two coaxial cylinders, the outer one representing the charged interface and the inner one the plane of shear, the decrease of the electro-osmotic contribution to the total conductance can be fully accounted for. It will be clear that in computing the conduction of the Δ-layer, assuming $p_\Delta = 1$, knowledge of the precise ion distribution is not required because the electro-osmotic contribution does not have to be considered. In calculating the influence of a deviating diffusion coefficient in the Δ-layer, it is important to realize that the charge density of the Δ-layer, σ_Δ, consists of an excess charge σ_Δ^+ due to the counterions and a charge deficit σ_Δ^- due to the co-ions: $\sigma_\Delta = \sigma_\Delta^+ + \sigma_\Delta^-$. In other words, one has to take into account possible anomalous effects on both ions. Only for relatively low $\kappa\Delta$ values can the contribution of the anions to the conduction of the Δ-layer and therefore any change in D_Δ^- be neglected.

From fig. 4-7a,b and c it is obvious that the reducing effect is highly sensitive to the thickness, Δ, the surface charge density, σ_o, and the ionic strength. At 10^{-2}M (fig. c) and moderate Δ-values the reduction is mainly cuased by the decrease of the charge excess that is hydrodynamically effective; the relatively small contribution of the excess charge to L_{22} is of minor importance at high c. On the other hand, at low c, the latter effect dominates, because nearly the whole conduction is provided by the charge excess; however, the relatively smaller part of the charge excess which is hydrodynamically effective for the same Δ drastically compensates the former effect.

In order to illustrate the effect of p_Δ we suppose $p_\Delta = 2$. For Δ = 5 nm and $\sigma_o = 1$ μC cm^{-2} at 10^{-4}M ($\sigma_\Delta = 0.596$ μC cm^{-2}) this doubling of p_Δ results in a reduction of the relative retardation, $\eta_a/\eta - 1$, of 28%. At 10^{-2}M it amounts to only 17%. For $\sigma_o = 9$ μC cm^{-2}, when the contribution of the excess charge to L_{22} is still substantial at 10^{-2}M, we find a reduction of 70%. At 10^{-4}M it amounts to 53%. It will be obvious that a reverse effect will be observed when considering $p_\Delta < 1$. We must, however, distinguish between the effect of a Δ-layer with a possible change in mo-

bility ($p_\Delta \neq 1$) and the mere effect of specific adsorption on the electroviscous retardation, although both effects may result in identical L_{22} values. For a chosen σ_o and for $p_\Delta > 1$, the introduction of a Δ-layer with an unmodified charge partition will always lead to a reduced electroviscous effect. Specific adsorption, on the contrary, not only leads to a change in the effective excess charge, thus in L_{22}, but at the same time the charge distribution may be substantially modified. From the results at low c we notice that for σ_o exceeding $\sigma_o(\eta_a/\eta$ is max.) specific adsorption may even lead to higher retardation phenomena, ignoring, of course, any contribution of specifically adsorbed ions to L_{22}.

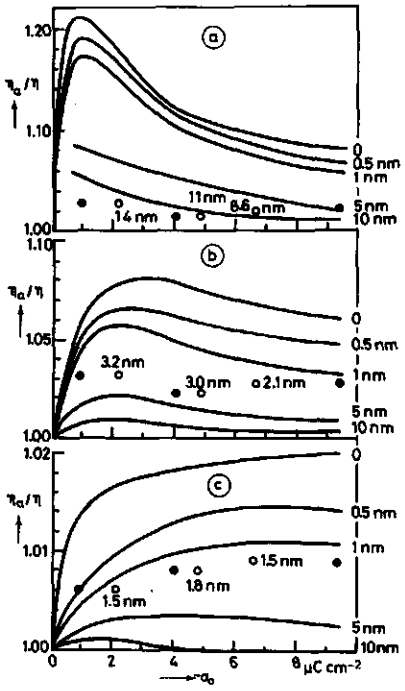

Fig. 4-7a,b,c. The effect of charge transfer through a stagnant layer on the electroviscous retardation for a. 10^{-4}M, b. 10^{-3}M and c. 10^{-2}M KCl at 25.0°C. The layer thicknesses are indicated. The filled symbols represent the electroviscous retardation of treated plugs plotted vs. the titration charge density; the open symbols correspond to the same results but now plotted vs. the charge density as calculated from surface conductance data (see text). The latter results are provided with Δ_{ev} data which were obtained by interpolation. $p_\Delta = 1$.

As pointed out before, the temperature independency of the experimental $L_{12}^2/L_{11}L_{22}$-values justifies a comparison of averaged values with theoretical predictions. Thus, besides the possibility of incorporating anomalous conduction the main advantage of using a composite quantity is because the predictions are independent of the temperature for which the numerical constants are inserted. The experimental retardation data are not only plotted vs. the titration charge densities (filled symbols), but also vs. the mean effective charge density calculated from surface conductance data (open symbols) in order to incorporate the charging and specific adsorption phenomena. For that purpose average charge densities of treated plugs calculated according to the Bruggeman model were taken from table

5A-1, viz. L(IIIB): -2.1 μC cm^{-2}; M(VIIIB): -4.8 μC cm^{-2} and H(VIIB): -6.6 μC cm^{-2}. The position of the symbols tells us that the earlier discussed charging process, induced at high c, for L and M apparently outweighs the effect of specific adsorption of the counterions. From the position of the experimental results in relation to the predicted $\eta_a/\eta(\Delta)$-σ dependencies the effective layer thickness, Δ_{ev}, may be determined. The experimental data dramatically illustrate the effect of ionic strength on the Δ_{ev}-value. Even at 10^{-2}M the interpolated values exceed 1.5 nm. From the position of the experimental values for M and H we notice that the applied correction (shift from filled to open symbols) changes the thickness only slightly. On the other hand, for 10^{-3}M and 10^{-2}M the shift of L causes a sharp increase of Δ_{ev}, causing the latter to agree better with the other Δ_{ev}-values. It has been discussed earlier that double layer polarization will be substantial at low c and high σ_o. Particularly at moderate Δ-values corresponding to a low Rel(I_s) value, a corresponding reduction of L_{22} would shift the $\eta_a/\eta(\Delta)$-σ_o curves to higher values; so we may expect that at high σ_o, Δ_{ev} is underestimated. Even at 10^{-3}M this trend can still be noticed. The Δ_{ev}-values included in fig. 4-7 indicate that the location of the shear plane is almost independent of σ_o, but extremely sensitive to c. These findings may support the concept of water structuring near the interface, which could physically control the location of the hydrodynamic plane of shear even though electrostatic conditions change drastically. Increase of ionic strength generally may disrupt the structuring or hydrogen bonding of water. Although the hydrodynamic and electrokinetic results qualitatively show the same concentration dependency, there is a large discrepancy between the absolute Δ-values. A highly c-dependent surface roughness could also account for the observation, but then in combination with specific adsorption. Apparently, only a reduction of the effective charge density to values below 1 μC cm^{-2} at 10^{-3}M and 0.5 μC cm^{-2} at 10^{-4}M would match the theoretical predictions and the observed Δ_h-values. In other words, the specific adsorption must increase upon decreasing c. In section 5.8 it will be discussed that the ionic head groups probably protrude into the aqueous phase and that this effect increases upon decreasing ionic strength resulting in a substantial modification of the charge partition near the particle surface.

In order to elaborate on the boundary layer, the time-dependency of the streaming potential was also analysed. In the next section it will be shown that this time-dependency may be used for obtaining *independent* information about the hydrodynamically effective charge density.

4.8 *Determination of the effective charge density from the time-dependency of the streaming potential of polystyrene plugs by means of the theory of negative adsorption*

Introduction

In section 3.7 it was reported that the time-dependency of the streaming potential of porous charged plugs is due to an accumulation of electrolyte at the high pressure side and a depletion at the low pressure side. For our coarse porous plugs the partial salt rejection results exclusively from negative adsorption and is consequently susceptible to variations in electrolyte concentration and double layer characteristics. It was shown that only the depletion process occurring at the low pressure side open further perspectives, experimentally as well as theoretically. Under streaming potential conditions the interfacial fluxes will inherently preserve electroneutrality, so that for a monovalent electrolyte the fluxes of positive and negative ions will be identical. In section 3.3.2 a quantitative expression has been derived for the concentration change at the low pressure side during permeation. It was expressed in terms of experimentally accessible parameters, like the ionic strength outside the plug, the electrolyte content in the porous phase and the volume flow. The experimental results were converted into average electroneutral electrolyte concentrations, c_p, defined as $\frac{1}{2}(\bar{c}_+ + \bar{c}_- - X)$, where $\bar{c}_+$ and $\bar{c}_-$ are the average molar concentrations of positive and negative ions, resp.; X is the equivalent molar concentration on the solid matrix. We will now relate c_p with the basic double layer parameters.

4.8.1 *Negative adsorption calculations for the cell-model*

For the computation of c_p as a function of surface charge density and porosity the cell-model is of direct importance. The equilibrium distribution of ions and the velocity profile within the shell are schematically given in fig. 4-8, which applies to absence of double layer overlap. The velocity distribution corresponds with the widely quoted 'free-surface' cell-model of Happel[37]. Applying proper boundary conditions (such as: the tangential shear stress component equals zero at r = b), general solutions for the r and θ components of the fluid velocity have been derived from the Navier-Stokes equations. The shell is electrically neutral, thus the charge density $\sigma(a)$ is compensated by an equal but opposite space charge (see also section 4.3). In the absence of double layer overlap, the potential at the outer radius, $\psi(b)$, equals the potential in the bulk outside the porous phase. In that case $c_+(b) = c_-(b) = c_o$, neglecting the

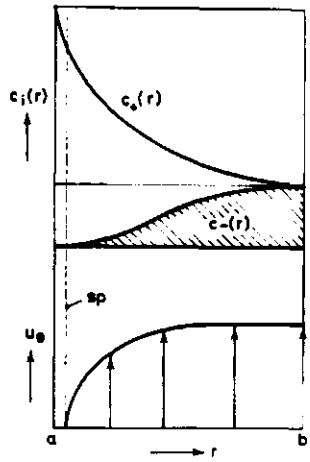

Fig. 4-8. Schematic picture of the equilibrium distribution of ions around a negatively charged sphere of radius a_o and the velocity distribution for the polar angle $\theta = 90^o$ measured from the direction of the mean fluid velocity in the entire assembly of spheres; for $\theta = 90^o$ the r-component of the fluid velocity $u_r(r,\theta)$ equals zero. b is the outer radius of the concentric spherical shell of fluid. sp: shear plane.

increase in the bulk concentration due to negative adsorption. It should be noted that the dimensions of the porous phase of our plugs are such that the liquid contained is far below 0.1% of the total volume of liquid in the system connected to them.

The total negative adsorption from the negatively charged sphere amounts to $4\pi a^2\sigma_-/F_a$ equivalents, where F_a is the Faraday constant. Without a double layer being present the total number of equivalents in the shell amounts to $4/3\pi(b^3 - a^3)c_o$ with c_o in moles/l. Thus the net mean co-ion concentration c_p in the presence of a double layer is:

$$c_p = \frac{\int_a^b c_-(r)4\pi r^2 dr}{4/3\pi(b^3 - a^3)} = c_o - \frac{3a^2\sigma_-(\kappa a)}{(b^3 - a^3)F_a} \qquad (4\text{-}30)$$

where $c_-(r)$ is the co-ion concentration, in moles/l, and $\sigma_-(\kappa a)$ the charge density deficit due to co-ions at the particle surface. The mean co-ion concentration corresponds with the shaded area in fig. 4-8. From eq. (4-30) c_p can be calculated when $\sigma_-(\kappa a)$ is known. To obtain this parameter, the numerical solutions of the Poisson-Boltzmann equation for spherical symmetry, as given by L.W.O.[19], are used. These authors express $\sigma_-(\kappa a)$ as:

$$\sigma_-(q) = \frac{\varepsilon_o\varepsilon_r kT}{e} \cdot I_-(q) \qquad (4\text{-}31)$$

In this notation the subscript - refers to negative adsorption. I_- is a function of the valencies of co- and counterions, the reduced poten-

tial, $\tilde{\psi}$, and the reduced radial distance q.*

Combination of eqs. (4-30), (4-31) and $\varepsilon = 1 - (a/b)^3$ gives an expression for the reduced mean co-ion concentration in the shell. On inserting the relevant numerical constants at 25°C the reduced electroneutral electrolyte content appears to amount to:

$$c_p/c_o = 1 - 1.823\ 10^{-7}(1 - \varepsilon)\varepsilon^{-1}a^{-1}\ c_o^{-\frac{1}{2}}\ I_-(\kappa a) \qquad (4\text{-}32)$$

4.8.2 *Discussion of experimental and theoretical results*

In table 4-5 we have presented the c_p/c_o-values, calculated according to eq. (4-32) for a wide variety of surface charge densities in the c_o-range of interest. In calculating the I_+-values from the surface charge densities a purely diffuse double layer was assumed. A porosity of 0.40 has been chosen, a value within a few per cent of the actual plug porosities. The average particle radius of the three latex samples, amounting to 282 nm, was used.

As one would expect, at higher electrolyte concentrations and lower surface charge the system becomes less selective and salt-sieving effects, expressed by the c_p/c_o ratio, will vanish. It is clear that this effect can also be achieved by increasing the porosity.

In discussing the c_p/c_o data in more detail it is necessary to consider four complicating factors:

(I) The cell model neglects that in the actual plug the latex spheres touch each other. Actually, near those contact points double layer overlap will be considerable, even at relatively high c_o. For the remaining part of the shell overlap causes, on the average, an overall depression of negative adsorption. Thus the actual (mean) c_p-value will be higher than the computed value.

(II) In calculating c_p/c_o we have used the numerical solution of the Poisson-Boltzmann equation for one isolated sphere, without taking account of neighbouring charged spheres. This must lead to erroneous results for low c_o's, where $\psi(b)$ differs from the bulk potential, so that $c_+(b)$ exceeds $c_-(b)$. Because the negative adsorption has not been calculated up to r = b but to infinity, the computed total negative adsorption will ex-

* Loeb et al.[19] define $q = \kappa a/\lambda$ where $\lambda = (z_+ + z_-)/2z_+$ with z_+ being the valency of the counterion; $\lambda = 1$ for $z_+ = z_- = 1$. Their equations refer to a positive particle. In our case the dimensionless reduced potential $\tilde{\psi} = e\psi/\kappa T$ is negative. The values for I_- are therefore taken from the table for $I_+(q) = I_+(\kappa a)$.

Table 4-5. Reduced average electroneutral electrolyte concentration, c_p/c_o, as a function of electrolyte concentration, c_o, and surface charge density, σ_o. The in brackets have been corrected for the hydrodynamic effect (see text).

c_o	$-\sigma_o$ μC/cm²					
moles/l	0.1	0.2	0.3	0.906(L)	4.00(M)	9.21(H)
$5\ 10^{-3}$	0.984 (0.999)	0.971	0.942	0.919	0.877	0.867
10^{-3}	0.926 (0.991)	0.871 (0.967)	0.785 (0.919)	0.730 (0.869)	0.690 (0.835)	0.684 (0.830)
$5\ 10^{-4}$	0.853 (0.970)	0.766 (0.904)	0.644 (0.791)	0.592 (0.721)	0.540 (0.674)	0.532 (0.664)
$2\ 10^{-4}$	0.643 (0.790)	0.513 (0.641)	0.342 (0.419)	0.288 (0.347)	0.241 (0.285)	0.227 (0.270)
10^{-4}	0.360 (0.443)	0.176 (0.202)	-0.018	-0.076	-0.154	-0.202
$5\ 10^{-5}$	-0.097	-0.371	-0.618	-0.687	-0.783	-0.824

ceed the maximum possible deficiency in the shell, resulting in negative c_p/c_o values. Generally, an overestimation of n.a. arises when interparticle distances are below $8/\kappa$ (Schofield[52], van den Hul et al.[53]). A correct computation involves incorporation of double layer overlap, but as previously noted analytical or numerical computations of the required potential distribution are still lacking. The real c_p/c_o-values will be intermediate between values computed for distances only up to $r = b$ without considering double layer overlap and values calculated for the range up to $r = \infty$ with the lower limit $c_p/c_o = 0$. As a rough estimate the calculated c_p/c_o-values below 0.2 start to underestimate the actual ones.

(III) One may question whether the computed c_p equals the actual flowing electroneutral electrolyte in the shell. Apparently, in the case of plug flow the knowledge of the precise ion partition is not required. The co-ion flux can readily be calculated from the volume flow rate and the mean co-ion concentration. For a homogeneous partition of the ions in the porous phase no knowledge of the actual velocity distribution is required, the co-ion flux being directly calculated from the volume flow rate average velocity and the co-ion concentration. For such a simple model, as put forward e.g. by Schmid et al.[16], the double layer description is completely eliminated by considering that the volume charge density will be uniform in the whole shell. However, the velocity distribution for creeping flow of an incompressible fluid obtained from the Navier-Stokes equation, using the Happel-Kuwabara cell-model, indicates a discrete velocity pattern far remote from that of a plug flow (see fig. 4-8). The contribution of the relatively high co-ion concentration near the outer ra-

dius of the shell to the total co-ion flux is promoted by the relatively high liquid velocity, so that the flowing mean co-ion concentration which we call the hydrodynamically effective mean co-ion concentration c_p^{he} exceeds c_p. A quantitative treatment of the transport processes on a microscopic scale requires the solution of the diffusion equation, the Navier-Stokes and the Boltzmann equation simultaneously, with the boundary conditions imposed by neighbouring particles. Even when the Debye-Hückel linearization is applicable the mathematics involved are formidable. Nevertheless, it is possible to estimate the salt flux by averaging sets of partial differential equations over the shell volume (Metha et al.[14]). In view of the accessibility of solutions for cylindrical symmetry, we shall derive a correction factor c_p^{he}/c_p for this geometry. It shall be assumed that the total amount of charge per unit of volume is constant, so that an equal volume-to-surface ratio for the cell and its equivalent pore may be considered. The capillary radius was calculated according to the K-C model, eq. (4-20a), for the actual average porosity and particle size as determined by electron microscopy. The ratio of the co-ion flux computed with the Poiseuille velocity profile v(r) and a plug flow profile with, of course, the same volume flow rate yields the correction factor. For cylindrical geometry we can write:

$$c_p = \frac{1}{\pi R^2} \int_o^R c_-(r) 2\pi r dr \quad \text{and} \quad c_p^{he} = \frac{\int_o^R c_-(r) v(r) 2\pi r dr}{\int_o^R v(r) 2\pi r dr}$$

where r is the radial coordinate and R the radius of the capillary. Assuming a purely diffuse double layer and introducing the Poiseuille profile, the c_p^{he}/c_p ratio can be simplified to:

$$\frac{c_p^{he}}{c_p} = \frac{\int_o^1 (1 - \bar{r}^2)\left\{1 - e^{-\bar{\psi}(\bar{r})}\right\} \bar{r} d\bar{r}}{2/3 \int_o^1 \left\{1 - e^{-\bar{\psi}(\bar{r})}\right\} \bar{r} d\bar{r}} \qquad (4\text{-}33)$$

where $\bar{r} = r/R$. The correction factor was numerically evaluated and presented in table 4-5 as the c_p^{he}/c_o-values in brackets. From a comparison of a cell-model with a capillary model representation of the same total charge and equal surface to volume ratio, Metha et al.[14] concluded that the cell-model predicts a more efficient salt rejection. Despite the extremely low charge densities used in their study ($\sigma_o < 0.2$ μC cm^{-2}) it

may be concluded that our correction factors are somewhat overestimated. The corrected values together with experimental ones are also presented in fig. 4-9. The general trend of these curves can be explained as follows.

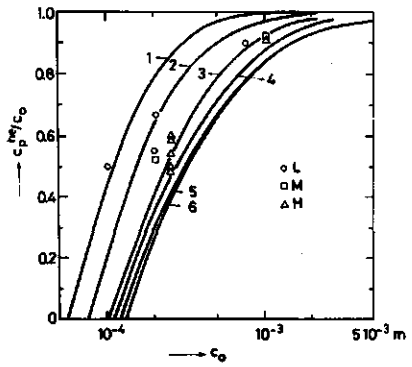

Fig. 4-9. Theoretical c_p^{he}/c_o-c_o curves for various surface charge densities. The curves 1-6 correspond with σ_o = 0.1; 0.2; 0.3; 0.906(L); 4.00(M); 9.21(H) $\mu C/cm^2$. The experimental data are taken from table 3-4.

For high ionic strengths neutral charge conditions prevail over most of the region, which is reflected by high c_p^{he}/c_o-values. Upon lowering c_o the countercharge becomes distributed over a larger part of the pore volume. For relatively high σ_o, corresponding to a sufficiently negatively charged surface, the c_p^{he}/c_o ratio becomes independent of σ_o. It would be anticipated that for any given σ_o, c_p^{he}/c_o should decrease upon lowering c_o, levelling out asymtotically to zero (S-shaped curve). The appearance of the intersections with the abscisa has already been discussed.

Combining the experimentally determined c_p^{he}-values (table 3-4) and the theoretical predictions, the effective charge density was obtained by interpolation. The results given in table 4-6 are qualitatively consistent with the σ_{ek} data, inasmuch as they also indicate a charge-reduction with decreasing ionic strength and similar substantial differences with the actual surface charge densities. These results are particularly meaningful. Factors such as the presence of a stagnant or slipping layer, which may partly explain the substantial difference between the hydrodynamically effective charge and the mobile charge effective in the conductance, are relatively unimportant in the '*dynamic negative adsorption*' method. The co-ion flux is practically independent of the presence of an immobilized layer, if its thickness is smaller than the negative adsorption depth, say about the thickness of the diffuse double layer. The thicknesses of the effective boundary layer as determined in the hydrodynamic experiments indicates that this condition is amply fulfilled. The increase in the non-uniformity of the counterion distribution upon decreasing the ionic strength means that the concept of specific adsorption is unable to explain the observed anomaly.

c moles/l	$-\sigma$ $\mu C/cm^2$ L	M	H
10^{-4}	0.1(0.24)		
$2\ 10^{-4}$	0.2	0.26(0.20)	
$2.7\ 10^{-4}$			0.3(0.37)
$7.7\ 10^{-4}$	0.25(0.76)		
10^{-3}		0.3(0.63)	0.5(0.90)

Table 4-6. Effective charge densities according to the 'dynamic negative adsorption' method. The results in brackets correspond with electrokinetic charge densities taken from appendix 5A, plugs VB, VIIIB and VIIB, at 25°C.

In all calculations we have assumed that an uniform, continuous, interfacial charge is neutralized by a space charge obeying the Poisson-Boltzmann equation. All possible variations or inhomogeneities *parallel* to the interface are ignored. Apparently, the main cause of the anomalous behaviour of our system must be sought in a strongly concentration dependent position of the fixed charges. Upon lowering the ionic strength the sulfate groups probably project out into the water phase, thereby accommodating a substantial part of the counterions in the spaces originated between the head groups. This 'hairy layer' model will be discussed extensively, along with the irreversible charging phenomenon, in section 5.8.1.

(IV) Finally, the possible influence of double layer polarization has to be investigated. The particles which form the plug matrix turn into dipoles and the total field of the polarized matrix influences the ion fluxes. The counterions 'belonging' to the particles are subjected to relaxation/retardation phenomena. The co-ions are excluded from the regions of high potential around the particles and are consequently supposedly little influenced by these effects. However, the local effective electric field strength at some distance from the surface is slightly stronger than the average field strength. This would result in a slightly increased velocity of the co-ions and causes more salt to pass through a selective porous system. However, our plugs exhibit a rather large surface conduction. At the same time an anomalous boundary layer effect is responsible for a marked reduction of the convection current. Both effects are reflected in the relatively low streaming potential values; in other words, a complicating influence of the polarized double layer on the co-ion flux is hardly to be expected.

4.9 *Summary*

Electrokinetic and fluid flow results for three types of charged plugs have been investigated experimentally and theoretically, using univalent salt solutions (LiCl, KCl, CsCl) at three temperatures (15, 25, 35°C). The general consequences of analysing experimental data on basis of the two main geometric models, viz. the single capillary and the cell-model, are discussed. It is shown that in real porous media with a non-negligible 'normal' surface conductance, evaluation of the zeta-potential from streaming current data leads to values which are essentially too low. The involved polarization may result in an apparent lyotropic sequence for the alkali cations. For our particle system we expressed the effect of relaxation on the streaming current in terms of the Rel concept of Dukhin.

The most pertinent theoretical formulae for calculating the electrokinetic quantities according to both geometric models, are shortly reviewed in terms of phenomenological coefficients. Numerical calculations, covering the actual range of charge density and ionic strength, are elaborated for the constant charge concept and tested upon their usefulness with respect to the actual system. The cell-model predictions for the sedimentation velocity in concentrated dispersions as obtained by Levine et al., are transformed into expressions for the streaming potential and the electroviscous retardation taking place in a fixed particle bed. It appears that not only the severe restriction to low potentials, but also the fact that the relaxation effect is not incorporated in the streaming current, makes the cell-model less useful than Levine's capillary model.

In order to obtain the general characteristics of our experimental system, all electrokinetic results are analysed in relation to both theoretical models. In particular a comparison of the streaming current data with the theoretical predictions clearly shows that at low ionic strength a substantial part of the counterions is hydrodynamically immobilized. The results are interpreted by an outward shift of the shear surface when decreasing the electrolyte concentration, coinciding with a change of the double layer structure. These findings are verified by calculations according to the capillary model of Levine et al. Upon decreasing the ionic strength the electrokinetic charge density and the total charge density effective in the conduction increasingly diverge.

Special attention is given to the concentration dependent thickness of the boundary layer. The concentration dependent permeability data, corrected for the electroviscous retardation effect, are transformed into effective boundary layer thicknesses according to Happel's cell-model. The boundary layer thickness is also evaluated from the electroviscous retardation results according to the capillary model of Levine et al., which

is extended for the anomalous conduction concept. Although the latter method, which is based on a Gouy-Chapman double layer, at concentrations below 10^{-3}M presents about ten times thicker layer, it becomes clear that the calculated effects have a common origin.

The effective charge densities obtained from the 'dynamic negative adsorption' measurements are not only completely consistent with the electrokinetic results, but also confirm that specific adsorption cannot account for the difference between the electrokinetic and hydrodynamic thicknesses. A 'hairy layer' model is proposed, in which a large part of the counterions is accommodated. This layer shrinks upon addition of electrolyte, causing an inward shift of the shear plane and an increase of the hydrodynamically effective part of the counterions.

4.9 *References*

1. H.R. Kruyt, 'Colloid Science', Vol. 1, Elsevier, Amsterdam (1952)
2. M. Smoluchowski, Z. Phys. Chem. 93, 129 (1918)
3. D.K. Briggs, J. Phys. Chem. 32, 641 (1928)
4. S.S. Dukhin and B.V. Derjaguin, 'Electrokinetic Phenomena', in 'Surface and Colloid Science', E. Matijević, Ed., Vol. 7 (1974)
5. A.J. Rutgers, M. de Smet and W. Rigole in 'Enriching topics from colloid and surface science', H. van Olphen and K.J. Mysels, Eds., Theorex, USA (1975)
6. A. Watillon and R. De Backer, J. Electroanal. Chem. 25, 181 (1970); R. De Backer and A. Watillon, VIth Intern. Congress Surface Active Substances, Zürich, Proceedings I, Carl Hanser Verlag, München, p. 651 (1972)
7. P.W.O. Wijga, Thesis, Utrecht (1946)
8. J.Th.G. Overbeek and P.W.O. Wijga, Rec. trav. chim. 65, 556 (1946)
9. K.P. Tikhomolova, Kolloidn. Zh. 36, 715; 36, 723; 36 1101 (1974)
10. R. De Backer, Thesis, Brussels (1966)
11. J.A. Ciriacks and D.G. Williams, J. Colloid Interface Sci. 26, 446 (1968)
12. N. Kamo, Y. Toyoshima and Y. Kobatake, Kolloid-Z. u. Z. Polymere 249, 1061 (1971)
13. P.W. Huber and A.A. Sonin, J. Colloid Interface Sci. 52, 415 (1975)
14. G.D. Metha and T.F. Morse, J. Chem. Phys. 63, 1878 (1975)
15. J.Th.G. Overbeek and W.T. van Est, Rec. trav. chim. 71, 97 (1952)
16. G. Schmid, Z. Elektrochemie 54, 424 (1950); 56, 181 (1952)
17. J.J. Bikerman, Z. Phys. Chem. A163, 378 (1933); Kolloid-Z. 72, 100 (1935); Trans. Faraday Soc. 36, 154 (1940)
18. A. Watillon and J. Stone-Masui, J. Electroanal. Chem. 37, 143 (1972); ref. 6.
19. A.L. Loeb, P.H. Wiersema and J.Th.G. Overbeek, 'The electrical double layer around a spherical colloid particle', M.I.T. Press, Cambridge, Mass. (1960)
20. N.P. Astrakhantseva and O.G. Us'yarov, Colloid J. USSR, Engl. Transl. 36, 763 (1974)
21. I.B. Oldham, F.J. Young and J.F. Osterle, J. Colloid Sci. 18, 328 (1963)
22. L. Dresner, J. Phys. Chem. 67, 1635 (1963)
23. D. Burgreen and F.R. Nakache, J. Phys. Chem. 68, 1084 (1964)
24. F.A. Morrison and J.F. Osterle, J. Chem. Phys. 43, 2111 (1965)
25. C.L. Rice and R. Whitehead, J. Phys. Chem. 69, 4017 (1965)
26. R.J. Gross and J.F. Osterle, J. Chem. Phys. 49, 228 (1968)
27. D. Hildreth, J. Phys. Chem. 74, 2006 (1970)
28. T.S. Sørensen and J. Koefoed, J.C.S. Faraday II 70, 665 (1974)
29. W. Koh and J.L. Anderson, A.I.Ch.E.J. 21, 1176 (1975)

30. S. Levine, J.R. Marriott, G. Neale and N. Epstein, J. Colloid Interface Sci. 52, 136 (1975)
31. J.L. Anderson, and W. Koh, J. Colloid Interface Sci. 59, 149 (1977)
32. J. Lyklema and J.Th.G. Overbeek, J. Colloid Sci. 16, 501 (1961)
33. P.C. Carman, 'Flow of gases through porous media', Academic Press, N.Y. (1956)
34. E. Manegold, Kapillarsysteme. Bd. 1, Heidelberg (1955)
35. J.H.M. Möller, G.A.J. van Os and J.Th.G. Overbeek, Trans. Faraday Soc. 57, 325 (1961)
36. R.P. Long and S. Ross, J. Colloid Interface Sci. 26, 434 (1968)
37. J. Happel, Amer. Inst. Chem. Eng. J. 4, 197 (1958); J. Happel and H. Brenner, 'Low Reynolds Number Hydrodynamics', Prentice-Hall, Englewood Cliffs, New Jersey (1965)
38. S. Levine and G.H. Neale, J. Colloid Interface Sci. 47, 520 (1974)
39. S.J. Kuwabara, J. Phys. Soc. Japan 14, 527 (1959)
40. S. Levine, G. Neale and N. Epstein, J. Colloid Interface Sci. 57, 424 (1976)
41. P.H. Wiersema, Thesis, Utrecht (1964); Ref. 19.
42. Ref. 4, p. 133.
43. V.L. Sigal and A.M. Alekseenko, Colloid J. USSR. Engl. Transl. 33, 614 (1971)
44. S. Levine and G. Neale, J. Colloid Interface Sci. 49, 330 (1974)
45. H. Morawetz, Macromolecules in Solution, Interscience, N.Y. (1965), p. 336.
46. L. Dresner and K.A. Kraus, J. Phys. Chem. 67, 990 (1963)
47. R.J. Hunter, J. Colloid Interface Sci. 22, 231 (1966)
48. D. Stigter, J. Phys. Chem. 68, 3603 (1964)
49. D.D. Cooke and M. Kerker, J. Colloid Interface Sci. 42, 150 (1973)
50. J.A. Davidson and H.S. Haller, 47th Natl. Colloid Symposium, Ottawa (1973), preprint.
51. A. Lecloux, H. Heyns and Y. Gobillon, Ind. Chim. Belge 35, 1 (1970)
52. R.K. Schofield, Nature 160, 408 (1947); Trans. Brit. Ceram. Soc. 48, 207 (1949)
53. H.J. van den Hul and J. Lyklema, J. Colloid Interface Sci. 23, 500 (1967)

CHAPTER 5

CONVERSION OF ELECTROCONDUCTING PARAMETERS OF CONCENTRATED AND DILUTE DISPERSIONS INTO DOUBLE LAYER CHARACTERISTICS

5.1 *Introduction*

Investigating the conductivity of a dispersion may serve as means to determine important colloid-chemical properties of the particles, constituting that dispersion. This approach not only requires an expression that relates all pertinent double layer parameters of the particles to the macroscopically measurable conductivity of the dispersion, but also such quantities as the specific conductivity of the suspending medium and the volume fraction of the solid.

Several aspects of the electrical conductance of a concentrated system of charged particles have already been treated in chapter 4. It has been shown that even the most recent cell models (Levine et al.[1]), used for the prediction of the various electrokinetic phenomena in concentrated dispersions, do not yet lead to satisfactory results. The simplified model approaches for the polarization effect (concentration polarization was not included), the limitation to low zeta-potentials (Debye-Hückel approximation) and the not-incorporated anomalous conduction concept, are severe restrictions in practice. Especially, at low ionic strength little agreement with the conductivity results on our plugs could be observed.

Particularly promising are recent developments in the polarization theory. Dukhin and Seminikhin[2] succeeded in deriving an analytical expression for the induced dipole moment of an individual charged spherical particle in an electrolyte solution. This expression enables the construction of a formula for the conductivity of a dilute particle dispersion (see also Pilgrimm et al.[3,4]). Because they considered that the actual diffuse double layer polarizes in an electric field, which enhances the polarization field, it is expected that an interpretation of conductivity data of particle dispersions on basis of their formulae is an improvement with respect to the 'classical' polarization models.

To test the predictions of Dukhin and Seminikhin, experimental methods were developed in order to obtain all pertinent parameters of dilute latex dispersions. For an analysis of the surface conductance results, we make use of the Bikerman predictions (section 4.3).

The polarization theory will also be extended to concentrated dispersions, taking into account the effect of particle interaction on the polarization field. We shall make use of the abundant experimental data

which have been accumulated for the electrical conductance of our plugs (chapter 4).

The electrokinetic parameters obtained in chapter 4 and the conducting parameters obtained in this chapter will be used to analyse the charge partition in our 'model' system. To elucidate the peculiar features of our 'model' system, as observed in chapter 4, use will be made of the combined information on the influence of the nature of the counterions and the temperature on the surface conductance.

In the following sections we will first present an outline of available theories with and without incorporation of double layer polarization; an analysis of the applicability and limitations of these theories will be given on basis of experimental evidence.

5.2 *Defining equations and explanation of terms*

Due to the presence of an electrical double layer at the fluid-solid interface, the specific conductivity of the pore fluid in a plug, K_p, can exceed the conductivity of the bulk solution, K. At sufficiently high electrolyte concentration, indicated by a superscript (^{o}), the contribution of the double layer may be disregarded, so that we can then write for the plug resistance[5]:

$$R_p^o = C_p/K_p^o \qquad (5\text{-}1)$$

with $K_p^o = K^o$, where K^o is the conductivity of the free solution and C_p the cellconstant of the plug. At an arbitrary electrolyte concentration we compute K_p from:

$$K_p = C_p/R_p = K^o R_p^o/R_p \qquad (5\text{-}2)$$

This equation merely intends to introduce an operational definition of an excess conductivity K_s (= K_p - K) in terms of two experimental quantities. It should be emphasized, however, that eq. (5-2) does not imply that the electrical conductance is identical everywhere in the plug. For arbitrary disperse systems it is more appropriate to define the excess conductivity K_s in terms of the specific conductivity of the complete disperse system, $\bar{K}$:

$$\bar{K} = (K_s + K)/F \qquad (5\text{-}3)$$

F is the structural resistance coefficient or formation factor[6] to be dis-

cussed in the following section. Both definitions can simply be related by the formalism:

$$K_p = K + K_s = \alpha K = F\bar{K} \qquad (5\text{-}4)$$

with $\alpha = 1 + K_s/K$, where the efficiency factor[7] α reflects the combined effects of the increase in conductivity due to interfacial conductivity and the decrease that results from introduction of a non-conducting solid phase into a conducting solution. Thus the contribution of the interface to the conductivity of the complete dispersion (K_s/F) can be defined as the diffference between the conductivities of the dispersion ($\bar{K}$) and the reference solution, the latter being corrected for the tortuosity of the medium (K/F). Again, this is a purely operational definition of an excess quantity, which is only feasible if F can be determined. The contribution of a charge excess near the surface can be expressed in terms of the specific surface conductance κ^σ (Ω^{-1}), the volume fraction of the dispersed phase p and the surface area S per unit volume of the particles composing the dispersion (e.g. a plug):

$$\alpha = 1 + \frac{\kappa^\sigma S}{K(1-p)} \qquad (5\text{-}5)$$

In terms of the formation factor F the equation transforms into the well-known Street equation[8], which relates the specific conductivity of a disperse system to the plug parameters:

$$\bar{K} = \frac{K}{F} + \frac{\kappa^\sigma S}{F(1-p)} \qquad (5\text{-}6)$$

Although the Street formula is generally accepted, it has features open to criticism. As pointed out by Helmy[9] and Dukhin et al.[10] the relation between the contribution of the interface to the total conductivity is expressed in terms of only one structure factor appropriate to the tortuosity of the dispersed phase. This is only justified in the case of a homogeneous spatial distribution of the counterions. Introduction of a pair of parallel conductance paths (Holmes et al.[11]), splitting the F factor up into two terms, may improve the model, but does not allow for the possible *interaction* of interfacial and volumetric currents. In other words, any contribution due to double layer polarization, particularly concentration polarization,. is ignored. This contribution will be substantial at concentrations where the effect of surface conductance on a curved or rough interface is noticeable. In this process of splitting-up,

it is supposed that the concentration of the electroneutral equilibrium electrolyte in the pores equals the bulkcomposition outside the plug. This assumption neglects the contribution due to negative adsorption, which depends on specific surface area, porosity, double layer characteristics and external electrolyte concentration. This phenomenon will usually coincide with the appearance of surface conductance when the latter is due to displacement of ions in the diffuse double layer.

The main problem we are now faced with is the determination of F that allows for the presence of the non-conducting matrix. Rephrasing the basic problem we could say that we have to determine the local flux through the pores, in order to establish the proportionality constant β in an equation of the general form: flux = $-\beta$ (gradient of a scalar). In an actual experiment, however, one observes an overall quantity. Thus to obtain the true interstitial 'velocity' one must multiply the experimental 'superficial' value by an appropriate F. In principle this factor is the ratio of the experimentally determined proportionality factors β with and without the obstructing medium.

The geometry and the volume concentration of the dispersed phase are also important in view of the conversion of the experimentally measurable contribution of the interface to the surface conductance and double layer properties.

5.3 *Theoretical aspects of conduction through an assembly of spherical particles in the absence of the complicating influence of double layer polarization: a. dilute dispersions; b. concentrated dispersions.*

Many descriptions of transport processes within isotropic porous media can be classified as extensions of reasonably well developed theories for processes occurring in capillaries. All these models are inherently anisotropic and, without exception, incorporate at least one adjustable parameter which must be determined by experiment. Here, however, we deal with isotropic dispersions composed of spherical particles, which requires another approach. Even for this geometrically simple shape the mathematics are formidable in that one requires a solution to the Laplace equation inside and outside the particles, taking into account the interaction of the electric field surrounding each particle[12]. In addition, at the boundaries of the phases, the continuity relations for potential and flux must be satisfied. Consequently, the pathways of the current should show no discontinuities. A rough classification of those theoretical formulae that express the formation factor F in terms of the porosity of systems made up of spheres, discriminates between dilute and concentrated dispersions.

If the properties of the individual phases of the dispersion are known, a simple conductivity measurement may suffice to determine its composition. Conversely, if the volume concentrations are known, a conductivity measurement of the dispersion reveals surface conductance effects or structural factors.

In the following the more important models treating the electric conduction will be reviewed briefly. The first investigations on the electrical resistance of a system of solid, (non-)conducting spheres in an electrolyte solution were carried out by Maxwell[13]. The results were applied later on to the relationship F(p) in porous media, however, without regarding Maxwell's explicit requirement that the distance between the spheres should be large compared with their diameter.

5.3.a *Dilute dispersions*

For dilute dispersions the electric field around a spherical particle, unaffected by the presence of neighbouring particles, is identified with the average field over the entire continuous phase. For a volume fraction p one then obtains Maxwell's formula:

$$\bar{K}/K = \frac{(K'/K + 2) - 2p(1 - K'/K)}{(K'/K + 2) + p(1 - K'/K)} \qquad (5\text{-}7)$$

where K' denotes the specific conductivity of the particles. Experience has shown that conductivity data may be accurately represented by Maxwell's equation for both random and ordered dispersions of spheres, provided the volume fraction of the dispersed phase remains below about 0.1[14]. In the particular case of non-conducting spherical particles (K'=0) one obtains for the formation factor:

$$F_M = \frac{2 + p}{2 - 2p} \qquad (5\text{-}8)$$

A useful form of Maxwell's equation may be obtained by expanding eq. (5-7) in a Taylor's series as $p \to 0$ and neglecting all but the first two terms:

$$\bar{K}/K = 1 - 3p\,\frac{1 - K'/K}{2 + K'/K} \qquad (5\text{-}9)$$

When dealing with non-conducting spheres in a dilute dispersion (i.e. $p < 0.1$), this relation, attributed to Wagner[15], reduces to:

$$F_W^{-1} = 1 - \frac{3}{2}\,p \qquad (5\text{-}10)$$

5.3.b *Concentrated dispersions*

Rayleigh[16] was the first to extend Maxwell's formula to ordered arrangements and higher volume fractions (close packing according to the cubic arrangement: $p = \pi/6$). He applied the principle of superposition of potentials for the dispersed and continuous phase and expressed them in terms of Legendre polynomials with interdependent coefficients. Böttcher[17] considered the surroundings of a particle as a continuum. The electrical conductivity and field strength of this continuum were identified with those of the mixture. Remarkably enough his formula is identical to Wagner's. Based on the same assumptions, but using an integration technique, Bruggeman[18] arrived at the following formula:

$$\frac{\bar{K}/K - K'/K}{(\bar{K}/K)^{1/3}(1 - K'/K)} = 1 - p \qquad (5\text{-}11)$$

For non-conducting spheres, this equation reduces to the simple structure factor:

$$F_B = (1 - p)^{-3/2} \qquad (5\text{-}12)$$

In principle this equation can also be obtained by using the linear expression that results from a series expansion of Maxwell's formula[19]. In doing so, one starts from a low volume fraction of solid that is gradually increased by adding infinitesimal fractions of the dispersed phase. After each addition the latter is considered as a continuum. This procedure is justified when the particle dimensions of each additional fraction are much bigger than those added previously. Instead of using the integral procedure it is possible to use stepwise addition of the dispersed phase. First, the conductivity of a dispersion is calculated with only half the amount of particles added. Considering this mixture as a continuum the procedure is repeated by adding the other half. In doing so, Meredith and Tobias[20] obtained the structure factor:

$$F_{M\text{-}T} = \frac{(4 + p)(4 - p)}{8(2 - p)(1 - p)} \qquad (5\text{-}13)$$

Although their derivation involved a quasi arbitrary decision (i.e. the 1:1 split of particles), they argue that the primary interaction is due to the closest neighbours. For higher p-values the equation suggested by M and T represents a convenient interpolation formula between Maxwell's and Bruggeman's equation. It is noted that all presented formulae reduce

to the Wagner formula when $p \to 0$.

A more advanced treatment of the conductivity of a monodisperse particle system, with incorporation of mutual polarization of spherical particles for an ordered and a statistical distribution, is given by Günther and Heinrich[21]. Their numerical calculations are based on the formulation of this problem by Brown[22]. Over the whole porosity range, the F-values of their statistical model coincide within 3% with the semi-empirical formula of Slawinski[23] which is given by:

$$F_S = \frac{[1.3219 - 0.3219(1-p)]^2}{1 - p} \qquad (5\text{-}14)$$

5.4 *Survey of theoretical equations for the prediction of conductivities of an assembly of spherical particles with incorporation of double layer polarization: a. concentrated dispersions; b. dilute dispersions.*

Double layer polarization results from an applied electric or hydrodynamic field and the concomittant variation in surface currents along a curved surface. The ionic transfer processes lead to deformation of the double layer and generation of a polarization field, in some cases commensurable with the externally applied one. The polarization field is opposite in direction to the external one and thus leads to a decrease of the local electric field and of the induced currents. At a flat interface with a roughness that is negligible in comparison with the double layer thickness, the double layer is not polarized.

Dukhin[24] introduced the dimensionless relaxation parameter Rel as a measure of the effect of surface conductance on electrokinetic phenomena:

$$Rel = \frac{\kappa^{\sigma}}{Ka} \qquad (5\text{-}15)$$

where a denotes the radius of curvature or radii of pores or capillaries.

It is noted that Rel can be used with two distinct meanings, viz. in indicating the degree of double layer polarization for curved surfaces and in indicating the relative contribution of surface conductance to the total conductance in non-polarized systems. An increase in the surface conductance and/or decrease in the radius results in an increase in Rel and thus in the polarization field in the direction of the induced electromigration current. In the case of a hydrodynamic field a high Rel value indicates a compensation of the convection current and thus a decrease in streaming current.

The induced tangential ionic flows near the surface have to be provided by radial ionic migration, diffusion and convection flows from be-

yond the double layer where co- and counterion concentration can differ considerably from those near the surface. The concentration polarization results in an angular dependence of the ion concentration and the potential. Dukhin et al.[25] derived analytical formulae that express these dependences for the cross section of the thin diffuse double layer ($\kappa a >> 1$) of a spherical particle. The advantage of their mathematical treatment of the polarization phenomenon, contrary to that of Overbeek, Booth and Wiersema[26], is the possibility of taking into account the effect of anomalous conduction on polarization. They could express this dependency in an analytical form. Moreover, their (Dukhin, Semenikhin) analytical expressions for the polarization potential distribution of an *isolated charged spherical particle* can be used in the computation of the dipole moment of such a particle:

$$\mu = -\frac{a^3}{2} E \left\{1 - \frac{3Rel}{1 + 2Rel - \frac{24m}{\kappa a} \ln(\cosh\tilde{\zeta}/4)}\right\} \qquad (5\text{-}16)$$

where m denotes the dimensionless parameter:

$$m = m^{\pm} = \frac{2\varepsilon_o\varepsilon_r}{3\eta D^{\pm}} \left(\frac{kT}{e}\right)^2 \quad \text{and } \tilde{\zeta} \text{ the dimensionless zeta-potential.}$$

κ is the reciprocal thickness of the diffuse part of the double layer, E the external electric field, $D^{\pm}$ the diffusion coefficient of cat- or anion. The other symbols have their usual meaning. For relatively high κa and low $\tilde{\zeta}$-values eq. (5-16) can be simplified to:

$$\mu_{D\text{-}S} = -\frac{a^3}{2} E \left(1 - \frac{3Rel}{1 + 2Rel}\right) \qquad (5\text{-}17)$$

5.4.a *Concentrated dispersions*

Dukhin[27] has already stipulated that in order to construct formulae for the electrical conductivity of a *concentrated suspension*, one also has to take into account the local environment of a particle, which changes considerably with increase of the volume fraction p. In other words, instead of $\mu(\kappa^{\sigma}, K)$ we must use $\mu(\kappa^{\sigma}, \bar{K})$, where $\bar{K}_{(p)}$ denotes the specific conductivity of the disperse system. Thus the macroscopic field determines the dipole moment. By employing the same procedure as Bruggeman[18] we consider the medium surrounding a particle (i.e. continuous phase + other particles with their double layers) as a continuum with respect to each successively added infinitesimal fraction of the dispersed phase. The field intensity of this continuum is subsequently identified with that of the mixture. In that case the change in the conduc-

tivity of the mixture by addition of the fraction dp is given by:

$$d\bar{K}_{(p)} = \bar{K}_{(p+dp)} - \bar{K}_{(p)} = \frac{4\pi\mu(\bar{K},\kappa^{\sigma})}{v\,E}\,\bar{K}_{(p)}\,\frac{dp}{1-p} \qquad (5\text{-}18)$$

where v denotes the volume of one particle. In order to illustrate the effect of concentration polarization on the effective conductivity of particle-dispersions we may begin with an expression for the dipole moment that disregards the concept of concentration polarization of a thin double layer. This expression is based on the distribution of the polarization potential as first given by Henry[28] and Booth[29]:

$$\mu_{H\text{-}B} = -\frac{a^3}{2}\,E\,\left(1 - \frac{3Rel}{1+Rel}\right) \qquad (5\text{-}19)$$

In short, the integration procedure with the condition $\bar{K}_{(p=0)} = K$ is as follows: first, we incorporate the polarization by using the two different expressions for the dipole moment of a spherical particle, represented by the abbreviations D-S (Dukhin, Seminikhin) and H-B (Henry, Booth) respectively.

Secondly, we take into account that the dipole moment of an arbitrary particle, which depends on Rel, is either determined by the mean conductivity $\bar{K}$ (procedure I) or determined by the specific conductivity of the interstitial equilibrium electrolyte K (procedure II). Integration of eq. (5-18) in combination with the above two expressions for the dipole moment and taking into account that a particle 'sees' in its vicinity a medium of conductivity $\bar{K}$ rather than K, leads to four generalized equations for $\bar{K}/K$. They are presented below, together with the explicit expressions for Rel:

$$\text{D-S I:}\quad \left(\frac{\bar{K}/K - Rel}{1 - Rel}\right)^2 \frac{1}{1-p} = (\bar{K}/K)^{4/3};\quad Rel = \frac{(1-p)^{1/2}(\bar{K}/K)^{2/3} - \bar{K}/K}{(1-p)^{1/2}(\bar{K}/K)^{2/3} - 1} \qquad (5\text{-}20)$$

$$\text{H-B I:}\quad \left(\frac{\bar{K}/K - 2Rel}{1 - 2Rel}\right) \frac{1}{1-p} = (\bar{K}/K)^{1/3};\quad Rel = \frac{(1-p)(\bar{K}/K)^{1/3} - \bar{K}/K}{2(1-p)(\bar{K}/K)^{1/3} - 2} \qquad (5\text{-}21)$$

$$\text{D-S II:}\quad \ln(\bar{K}/K) = \left(\frac{3}{2} - \frac{9}{2}\,\frac{Rel}{1+2Rel}\right)\ln(1-p);\quad Rel = \frac{\ln\{(\bar{K}/K)(1-p)^{-3/2}\}}{\ln\{(K/\bar{K})^2(1-p)^{-3/2}\}} \qquad (5\text{-}22)$$

$$\text{H-B II:}\quad \ln(\bar{K}/K) = \left(\frac{3}{2} - \frac{9}{2}\,\frac{Rel}{1+Rel}\right)\ln(1-p);\quad Rel = \frac{\ln\{(\bar{K}/K)(1-p)^{-3/2}\}}{\ln\{(K/\bar{K})(1-p)^{-3}\}} \qquad (5\text{-}23)$$

We complete this review by modifying the expressions of Street, Bruggeman, Maxwell and Meredith and Tobias[20] when the effect of surface conductance is incorporated by ascribing a specific conductivity $2\kappa^{\sigma}/a$

to the non-conducting bulk-phase of the particle (O'Konski[30]):

Street $\bar{K}/K = \frac{1}{F}\left(1 + \frac{3pRel}{1-p}\right)$; $Rel = \frac{1-p}{3p}\{F(\bar{K}/K)-1\}$ (5-24)

Bruggeman $\left(\frac{\bar{K}/K - 2Rel}{1 - 2Rel}\right)\frac{1}{1-p} = (\bar{K}/K)^{1/3}$; see H-B I, eq. (5-21) (5-25)

Meredith-Tobias $\bar{K}/K = \frac{4Rel(1+p) + 4 - 2p}{4Rel(1-p) + 4 - p} \cdot \frac{2Rel(2+p) + 4 - 4p}{2Rel(2-p) + 4 + p}$; (5-26)

Rel can easily be solved from the quadratic expression in Rel.

Maxwell $\bar{K}/K = \frac{2 + 2Rel - 2p(1-2Rel)}{2 + 2Rel + p(1-2Rel)}$; $Rel = \frac{2(1-p) - (\bar{K}/K)(2+p)}{2(1-p)(\bar{K}/K)-2(1+2p)}$ (5-27)

The general Maxwell equation was also obtained by Fricke and Curtis[31] by simplifying the Maxwell treatment for high κa.

Fig. 5-1 shows the dependence $\bar{K}/K(Rel)$ for the different generalized forms; the figure refers to p = 0.6 which corresponds to the experimentally determined porosities of the various plugs studied. Several characteristic features show up.

The D-S I, II and H-B I, II formulae all reduce to the Bruggeman formula when $\kappa^{\sigma} = 0$ (Rel = 0). On the other hand, for high Rel-values, in case of predominant surface conductance in all models, except that of Street, the ratio $\bar{K}/K$ levels off asymtotically to constant values. Moreover, the effect of incorporating the local environment disappears, so that the cases I and II coincide. The absence of a saturation effect in the Street model is typically a consequence of its basic parallel conductance path assumption.

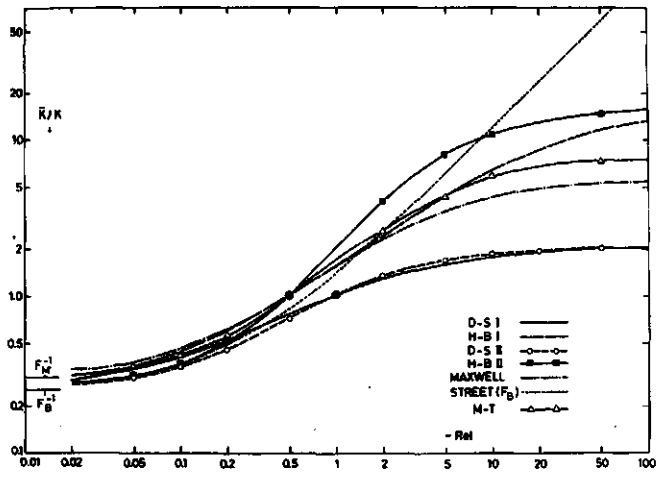

Fig. 5-1. $\bar{K}/K$ as a function of the parameter Rel, as predicted by some theoretical models. p = 0.6

The H-B I formula is identical to the modified one of Bruggeman because for a thin

double layer surface conductance without concentration polarization has the same effect on the potential distribution in an electric field and therefore on the induced dipole moment, as bulk conductivity of the particle, amounting to $2\,\kappa^{\sigma}/a$.

5.4.b *Dilute dispersions*

For low p values the D-S I and II formulae reduce to one expression linear in p. This expression, indicated with D-S, is identical to the one presented by Pilgrimm et al.[3], although they used a different derivation:

$$\text{D-S } (p\ll 1): \quad \bar{K}/K = 1 - \frac{3}{2}\,p\,\left(1 - \frac{3Re1}{1 + 2Re1}\right) \qquad (5\text{-}28)$$

It is of particular interest that in the limiting case of low p, a series expansion of all other integral forms that do not incorporate the concentration polarization concept (H-B I, II; Bruggeman, Meredith-Tobias, Maxwell), except that of Street, also lead to one expression. This equation, shown as H-B, differs from that of the foregoing expression only in a numerical coefficient:

$$\text{H-B } (p\ll 1): \quad \bar{K}/K = 1 - \frac{3}{2}\,p\,\left(1 - \frac{3Re1}{1 + Re1}\right) \qquad (5\text{-}29)$$

It may be recalled that the analytical expression for polarized spheres is restricted to the condition of a thin diffuse double layer. The H-B formula involves only a thin conducting layer without further specification. It is supposed that ion transport from the bulk on one side into the conducting layer and from that layer into the bulk on the other side is so fast that no polarization charges arise.

Conductivity measurements on dilute dispersions deserve much attention. However, the possibility of obtaining reliable quantitative information entails great experimental difficulties, as will be shown in section 5.7. On one hand, at least moderate ionic strengths are needed to guarantee a thin double layer, whereas on the other the difference between the electrical conductivity of the dilute dispersion, $\bar{K}$, and that of the continuous phase, K, must be determined accurately.

Furthermore, one has to be aware that for $Re1 \ll 1$ both expressions (D-S and H-B) coincide. This difficulty may be overcome by using dispersions of moderate p-values and relatively high surface charge densities. It is obvious that previous to any interpretation of the experimental data the linearity of the conductivity ratio $\bar{K}/K$ with p must be verified.

5.4.1 *The isoconductance point*

The isoconductance (or isoconductivity) point, ICP, is characterized by $\bar{K}/K = 1$. At this point the effects of tortuosity of the medium and surface conductance just balance. Its significance in relation to surface conductance has been discussed by Street[32]. In table 5-1 we present the Rel-values for the various integral forms at the ICP. The modified Street equation gives identical F-factors for bulk and surface conductance if it is assumed that the surface region over which the excess conductance is averaged is the same as that region through which an identical conductance would be produced by the conductance of the equilibrium solution in a geometrically identical medium having an inert surface. Introduction of F_M results in an ICP independent of p. This fact, which if necessary may be experimentally verified, does not supply evidence that the same F-factors may be used for evaluating the tortuosity effect upon surface and bulk conductance for a suspension of spherical particles, because this 'parallel conductance paths' model ignores the effect of double layer polarization.

Table 5-1. Rel-values at the isopolarization state of dispersions of charged spherical particles, according to different models.

model	Rel
D-S I	1.0
D-S II	1.0
H-B I	0.5
H-B II	0.5
Street (F_M)	0.5
Street (F_B)	$(1-p)\{(1-p)^{-3/2} - 1\}/3p$
Maxwell	0.5
M-T	0.5

The fact that higher Rel-values are necessary according to theories that include concentration polarization, means that a larger part of the mobile charge excess cannot contribute to the total conductance. At the ICP ($\mu = 0$!) the effect of incorporation of the local environment (procedure I) on the dipole moment disappears too; thus for any arbitrary particle its deficiency of bulk condition is just compensated by the excess of surface conductance, which makes $\bar{K}$ independent of p. On either side of the ICP, the concept of procedure I compared with II results in a leveling effect, thus at the low Rel-side the polarization decreases and at the high Rel-side it increases. It will be clear that increasing p to the right of the ICP increases $\bar{K}$ and to the left has a decreasing

effect on $\bar{K}$. Fig. 5-2 shows the dependency of the ratio $\bar{K}$(D-S I)/$\bar{K}$(Street, F_M) on Rel for three p values. The figure demonstrates the overwhelming effect of the 'parallel conduction paths' model of Street, especially for relatively low Rel-values. At high Rel-values the polarization concept in D-S I enhances the difference between the two models. These facts are extremely important in the interpretation of experimental $\bar{K}$/K-data of dispersions in terms of surface conductance and coherent double layer characteristics. From fig. 5-2 we also notice that under conditions of $\bar{K}/K>1$ the Rel-values differ considerably for the two models. For low p- and moderate Rel-values ($1<Rel<10$) κ^{σ} computed by the Street equation exceeds the D-S prediction by as much as 50%.

For high Rel-values the analytical predictions [Rel>>1; D-S I,II: $\bar{K} = K(1-p)^{-3/4}$; H-B I,II: $\bar{K} = K(1-p)^{-3}$] which include double layer polarization become meaningless and quantitative interpretation of experimental results becomes impossible. The reason for this is, that double layer interaction (overlap) promotes short circuiting of the ion-rich layers near the particles, thus suppressing double layer polarization and justifying more the 'parallel conduction paths' model of Street, but in this case with different F-factors.

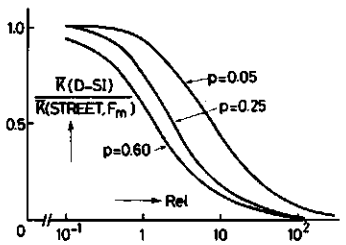

Fig. 5-2. $\bar{K}$(D-S I)/$\bar{K}$(Street, F_M) vs. Rel for three p-values.

5.4.2 *The effect of the thickness of an electroconducting layer on the conductivity of dispersions*

The extension of the theory to spherical particles covered by a spherical conducting layer (e.g. its ionic atmosphere) of non-negligible thickness embedded in the continuous phase, can be realized by adopting a triphase model. The interphase of thickness d and conductivity K_d surrounds the sphere of conductivity K'. The electrical properties of such a system can be approximated by using Maxwell's treatment, assuming that the particle and its interfacial layer can be replaced by a homogeneous sphere. It can be shown that the mean conductivity of the particle with its atmosphere, $\bar{K}_{a+d}$, is related to the conductivity of the interfacial layer, K_d, and the particle conductivity, K', by the following expression:

$$\frac{\bar{K}_{a+d} - K_d}{\bar{K}_{a+d} + 2K_d} = \left(\frac{a}{a+d}\right)^3 \frac{K' - K_d}{K' + 2K_d} \qquad (5\text{-}30)$$

Then, by applying the Maxwell equation twice (see e.g. Watillon et al.[33]) the conductivity of the whole dispersion, $\bar{K}$, can be obtained by inserting $\bar{K}_{a+d}$, computed from eq. (5-30), for the particle conductivity:

$$\frac{\bar{K} - K}{\bar{K} + 2K} = p^* \frac{\bar{K}_{a+d} - K}{\bar{K}_{a+d} + 2K} \qquad (5\text{-}31)$$

where the effective volume fraction p* is related to the volume fraction of the solid particles by $p^* = p(a + d/a)^3$.

When dealing with non-conducting spheres (K'=0) and a conducting layer of limited thickness ($p^* \cong p(1 + 3d/a)$), both relations can be deduced by using the expression $K_d = K + \kappa^\sigma/d$. Maxwell's eq. (5-27) may be rewritten as:

$$\bar{K}/K = \frac{2r + 2Rel - 2p(r - 2Rel)}{2r + 2Rel + p(r - 2Rel)} \qquad (5\text{-}32)$$

where Rel is based on the radius of the solid particle and r = 1 - d/a.

From this equation Rel can be expressed as:

$$Rel = \frac{2r(1 - p) - r(\bar{K}/K)(2 + p)}{2(1 - p)(\bar{K}/K) - 2(1 + 2p)} \qquad (5\text{-}32a)$$

By analogy with the H-B equation for dilute dispersions of spheres with thin conducting layers we can now write:

$$\bar{K}/K = 1 - \frac{3}{2} p \left(1 - \frac{3Rel}{r + Rel}\right) \qquad (5\text{-}33)$$

From this expression it will be clear that the effect of variation of the conducting layer thickness on $\bar{K}/K$ will only be substantial at low Rel-values, i.e. for small surface charge densities. For a system of particles of constant charge we may expect that with diminishing K the increase of Rel masks the effect of extension of the double layer (r < 1) to some extent.

To account simultaneously for the effect of concentration polarization, a similar approach as for the D-S expression may well give:

$$\bar{K}/K = 1 - \frac{3}{2} p \left(1 - \frac{3Rel}{r + 2Rel}\right) \qquad (5\text{-}34)$$

In fact, an analytical solution to this problem has not been proposed as yet. It is quite unlikely that analytical solution of general validity could be obtained. It should suffice to state that by using the D-S expression the condition $\kappa a >> 1$ automatically reduces r to 1. In the absence of exact theoretical results pertaining to dilute dispersions at low ionic strengths on the basis of the above eq. (5-34) an empirical equation can be postulated:

$$\bar{K}/K = 1 - \frac{3}{2} p \left(1 - \frac{3Rel}{r + sRel}\right) \qquad (5\text{-}35)$$

At low ionic strength the expansion of the diffuse double layer and a possible over- or underestimation of concentration polarization can be fitted with the variables r ($\cong 1 - (\kappa a)^{-1}$) and s.

5.4.3 *Some complicating factors concerning the measuring frequency*

A prerequisite for the experimental determination of the conductivity of plugs or dilute dispersions is that the applied frequency is low enough to allow the development of complete polarization of the particles. The frequency dispersion of the dielectric constant and the electrical conductivity of charged particle systems have recently been the subject of many investigations.[34,35] Of special interest are the studies in which surface conductance is incorporated. E.g. Schwarz[36] considers particle polarization, due to tangential migration around the particle of ions that are (partly) mobile on the surface but ultimately bound by electrostatic forces. The migration is controlled by a diffusion mechanism of these ions into a layer very close to the surface. Schurr[37], considering this model as unrealistic, reintroduces the diffuse part of the double layer, as proposed by O'Konsky. Of special interest are the results of Shilov and Dukhin[38], who consider the polarization of the diffuse part of the double layer. At high frequencies the alternating polarization field that results from the alternating electric field relaxes and the conductive currents become larger. The relaxation is essentially related to the diffusion coefficient of the ions in the double layer and the radius of the particle. The relaxation time for many theories (see Springer[34]) is given by $\tau = a^2/2D_c$, where D_c is the diffusion coefficient of the counterions. In order to allow the use of the D-S expression the measuring frequency, ν, must be low: $\nu << D_c/(2\pi a^2)$. At relatively high fre-

quency, $\nu >> D_c/(2\pi a^2)$, one can expect that the polarization field, directed opposite to the external field, breaks down. It is likely that the H-B expression becomes useful when the concentration polarization is cancelled. For a particle dispersion an increase in frequency will reduce the isoconductance condition (μ=0) from Rel = 1 to Rel = ½. For concentrated dispersions we may expect that due to interaction of neighbouring double layers a disturbance of the ion distribution is not limited to the dimensions of one particle. On concentrating a particle dispersion the frequency dispersion range may shift to lower frequencies.

Our experimental study is restricted to the measurement of the conductivity increment. Some results are reported and discussed on the basis of the D-S and H-B equations in section 5.7.7. Results of a low frequency dispersion of $\bar{K}$ of our plugs are presented and discussed in chapter 7.

5.5 *Procedure for evaluating and testing the electrokinetic results*

The following diagram summarizes the various steps involved in the conversion of $\bar{K}/K$-data into surface charge densities (or double layer potentials).

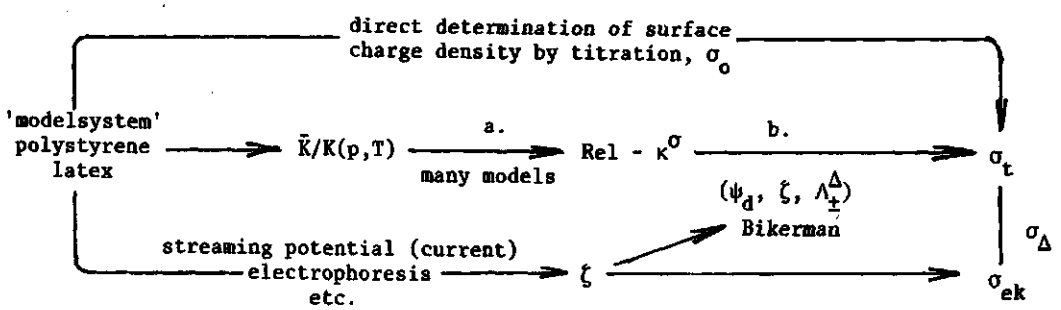

The first conversion of $\bar{K}/K$-data to Rel-values (step a) and finally to surface charge density or ψ_d-values (step b) is sensitive to the model used. It almost goes without saying that no meaningful quantitative information can be obtained if the actual mechanism of surface conductance were to be associated with a double layer structure that deviates from the assumed one or when the conditions of the polarization models used in the first conversion (step a) and the (modified) Bikerman expression (see section 4.3) in the second step b are not met. Thus interpretation of the calculated σ_t in relation to the known titration charge density, σ_o, cannot reveal quantitative information on parameters other than those presented. The finally computed σ_t can be compared with the titration charge density and the electrokinetic charge density σ_{ek}, giving the charge density, σ_Δ, or thickness Δ of the electroconducting layer, which can also

be interpreted in terms of the potential drop (ψ_d-ζ) using the Gouy-Chapman theory.

Conversion of κ^σ into σ_t or ψ_d requires independent information on the zeta-potential. This parameter can only be calculated correctly from electrokinetic experiments on the basis of formulae which incorporate the effect of possible anomalous conductance, double layer polarization and double layer overlap. Unfortunately, no theory is yet available that incorporates all of these phenomena at the same time (see chapter 4).

If σ_t computed from κ^σ remains constant over a concentration range of indifferent electrolyte it supports the model used in the first conversion. Moreover, valuable additional information can be obtained from $\bar{K}$/K-measurements for different p-values.

5.6 *Experimental results and discussion: concentrated dispersions; the formation factor*

The experimental determination of the formation factor consists of the measurement of $\bar{K}$ at such a high electrolyte concentration that the contribution of the interface and/or of the particles themselves to the total conductivity can be neglected and of the conductivity K of the same electrolyte solution in the same sample holder, but in the absence of the plug. Then we get $F = C_p/C$, where C_p and C denote the cell constants of the sample holder with and without the plug respectively. At these high electrolyte concentrations all C_p and C values were determined using simple d.c. current-voltage characteristics, measured with the four-electrode technique (see section 3.7.3). Table 5-2a presents some C_p values. From the differences in C_p at 10^{-1} and 2 10^{-1}M we notice that for sample H the relative contribution of surface conductance becomes quite small although an extrapolation of the results towards infinitely high conductivity leads, of course, to an even better estimate of F. Such an extrapolation could be performed by plotting the reciprocal of the 'apparent formation factor', R_p K, versus the conductivities of the equilibrium solutions, the intercept yielding the 'true formation factor'. For our plugs with the highest charges, it appears that a concentration of 0.3 M 1-1 electrolyte was sufficiently high.

Table 5-2b gives theoretical and experimental F-values for all the plugs used in this study. The porosities correspond mainly to structures lying between simple cubic packing with a coordination number n = 6 (p = 0.524) and primitive hexagonal packing with n = 8 (p = 0.605);thus still far from hexagonal closed packing (n = 12; p = 0.740). Almost all the experimental values show the best agreement with the statistical predictions (see the F_s-values). The experimental values are inbetween the limits pre-

Table 5-2a. Some apparent formation factors at various temperatures and types of electrolyte: A-LiCl; B-KCl; C-CsCl. The corresponding porosities of the various plugs are presented in table 5-2b.

C / M		$C_p = R_p K$ (cm^{-1}) 15.0°C	25.0°C	35.0°C	$\langle R_p K \rangle$
$2\ 10^{-1}$	VII A	7.639	7.671	7.703	7.67
	VII B	7.718	7.795	7.872	7.80
	VII C	7.912	7.988	8.070	7.99
10^{-1}	VII A	7.545	7.546	7.575	7.56
	VII B	7.588	7.650	7.750	7.66
	VII C	7.827	7.748	8.000	8.86

Table 5-2b. A comparison of the formation factor, F, according to the models of Maxwell, Meredith and Tobias, Burggeman and Slawinski, equations (5-8), (5-13), (5-12) and (5-14) respectively, with experimental results.

plug	type	p	F_M	F_{M-T}	F_B	F_S	$C_p(cm^{-1})$	$C(cm^{-1})$	F_{exp}
III	A	0.6064	3.311	3.562	4.050	3.629	7.75	2.12	3.66
(L)	B	"	"	"	"	"	7.77		3.67
	C	"	"	"	"	"	7.92		3.73
IV	A	0.579	3.063	3.273	3.661	3.343	7.04		3.32
(H)	B	"	"	"	"	"	7.19		3.39
V	A	0.6015	3.264	3.508	3.975	3.575	8.66	2.279	3.80
(L)	B	0.6041	3.289	3.537	4.014	3.604	8.67		3.81
	C	0.6015	3.264	3.508	3.975	3.575	8.61		3.78
VI	A	0.5880	3.141	3.280	3.781	3.433	8.561	2.279	3.76
(L)	C	0.5888	3.148	3.372	3.793	3.441	-		-
VII	A	0.5971	3.223	3.460	3.910	3.528	7.67	2.08	3.69
(H)	B	0.6133	3.379	3.642	4.159	3.708	7.80		3.75
	C	0.6315	3.571	3.867	4.470	3.929	7.99		3.84
VIII	A	0.5846	3.111	3.329	3.735	3.399	7.78	2.279	3.41
(M)	B	0.5951	3.205	3.438	3.881	3.507	7.71		3.38

dicted by the Bruggeman and the Maxwell equation. A remarkable feature is exhibited by the results of plug VII. An increasing p usually corresponds to an increasing deviation from the Maxwell equation, but here a reversed sequence is observed. An ordered arrangement, such as a simple cubic lattice, results in a less than average interaction between particles compared with random arrangements. Consequently, the deviation from Maxwell's equation should always be bigger for random than for ordered arrangements of spheres. Thus the expected increased deviation is probably overcompensated by a higher ordening. Deviations from the Bruggeman equation are

often found for monodisperse particles because this equation is specifically applicable to dispersions with a broad particle-size distribution. The average deviation of only about 10% from the experimental values in this particular porosity range makes the integral method (see section 5.4.a) rather attractive for incorporating phenomena like double layer polarization and surface conductance. It is clear that the equation suggested by Meredith and Tobias, representing a convenient interpolation between Maxwell's and Bruggeman's equation, is also very useful.

5.6.1 *The conversion of experimental $\bar{K}/K$-values into surface conductances: concentrated dispersions*

A representative part of the experimental $\bar{K}(K)$-values together with the κ^{σ}-values computed from them by the integral eqs. (5-20) through (5-27) for KCl at 25.0°C, is presented in table 5-3. Results at other temperatures and for other mono-valent electrolytes reveal the same trend

Table 5-3a,b,c. Experimental $\bar{K}$,K-results for KCl at 25.0°C and specific surface conductances computed according to the various indicated integral forms.
a: plug VB((L); b: plug VIIIB(M); c: plug VIIB(H). The dashes correspond to experimental $\bar{K}/K$-values exceeding the maximum possible values according to that particular equation.

a.

C	$\bar{K} \times 10^4$	$K \times 10^4$	$\kappa^{\sigma} \times 10^{10}\ \Omega^{-1}$						
M	$\Omega^{-1}cm^{-1}$	$\Omega^{-1}cm^{-1}$	DS-I	HB-I	DS-II	HB-II	Street	M-T	Maxwell
10^{-2}	4.30	13.7	10.9	10.2	20.7	19.5	14.7	8.34	2.11
$1.25\ 10^{-3}$	1.371	1.819	22.2	14.1	25.9	16.6	18.9	15.3	14.1
$7.65\ 10^{-4}$	1.193	1.112	34.2	15.8	32.9	15.2	19.0	22.0	15.8
10^{-4}	0.736	0.150	-	24.5	-	9.63	14.8	22.5	85.4

b.

10^{-2}	5.675	13.91	35.1	30.6	57.4	50.5	39.3	33.4	23.7
10^{-3}	1.926	1.490	102.	34.8	88.9	30.0	36.7	32.3	34.9
$2\ 10^{-4}$	1.116	0.347	-	37.8	-	17.9	25.0	28.4	47.4
$4\ 10^{-5}$	0.975	0.060	-	-	-	-	23.6	-	-

c.

10^{-2}	6.254	13.84	54.3	44.3	84.0	69.5	58.5	52.5	39.9
$5\ 10^{-3}$	4.365	7.082	62.0	44.0	80.8	58.0	56.5	50.1	34.6
10^{-3}	2.509	1.477	305.	49.2	230.	36.1	48.3	36.5	50.0
$2.65\ 10^{-4}$	1.634	0.403	-	52.4	-	22.8	34.9	42.2	92.7

and will be discussed later. Because the experimental a.c. $\bar{K}$-values display a time dependency in the low-frequency region, especially at low concentrations, the d.c. values will be considered. Furthermore, only the results of three plug-types (L, M and H) equilibrated at high electrolyte concentration previous to the $\bar{K}$-determinations, are given.

For analysing the usefulness of the integral forms, the various κ^{σ}-results are displayed graphically in fig. 5-3 a, b and c together with the Bikerman-predictions. The latter are calculated from eq. (4-8) for σ_o's close to those of the latex particles (1, 4 and 9 μCcm^{-2}). The upper solid curve, indicated by κ^{σ}_{B} ($\psi_d = \zeta$) presents κ^{σ}-c data based on the assumption of a fully developed electro-osmotic contribution to surface conductance, whilst the other one represents the calculated surface conductance disregarding the electro-osmotic contribution ($\zeta = 0$). Any mobility difference between ions in the boundary layer and those in the bulk is neglected at present. A value in the region endosed by the two 'theoretical' curves points to a difference between ψ_d and ζ. As can be seen, all curves for κ^{σ}(c, model) with exception of the Street prediction pass through one of the two ICP's. These important points are indicated with

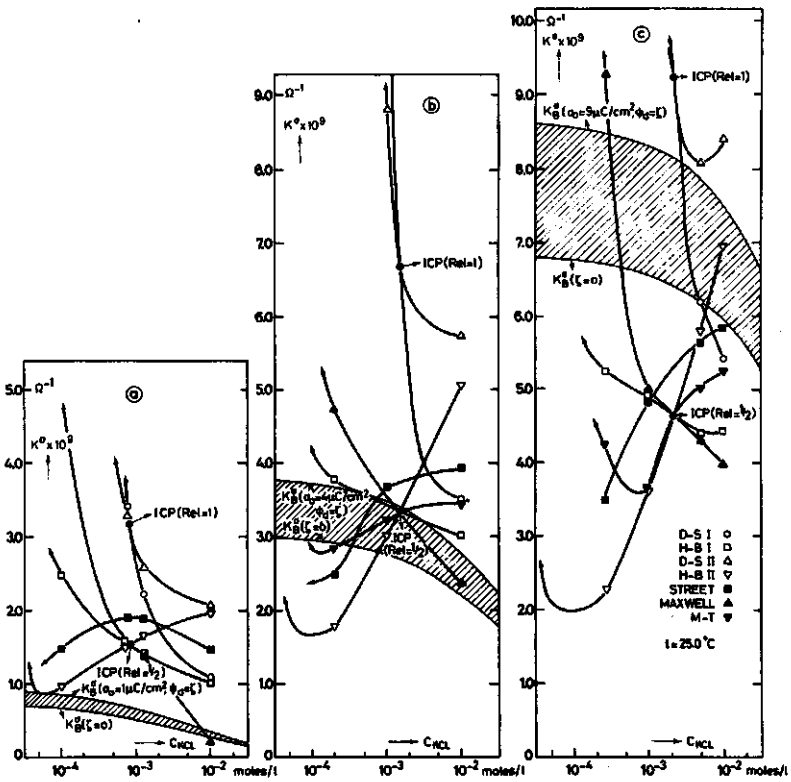

Fig. 5-3a,b,c. Theoretical and experimental values of the specific surface conductance, κ^{σ}, as a function of the KCl concentration.
a: plug VB(L); b: plug VIIIB(M); c: plug VIIB(H).

filled symbols. The exception of the Street case is caused by the application of the experimentally determined F. From the κ^{σ}-c dependency for the highest surface charge (fig. c; H) it is evident that:

1. the HB-II and Street predictions and to a lesser extent the M-T predictions show a dependency on c that is completely opposite to that in the theoretical Bikerman region ($|\psi_d| \gg |\zeta| > 0$). Considering the HB-II results, it is quite obvious that by substituting the conductivity of the continuous phase, K, into the dipole moment (μ_{H-B}) instead of the conductivity of the mixture as a whole, an even more restricted range of usefulness results. The sharp increase of κ^{σ} at low c indicates that the maximum theoretical $\bar{K}/K$ (p, Rel $\rightarrow \infty$) is exceeded.
2. already for c's below the common ICP, the DS-I and II predictions increase significantly with decreasing c and finally become undefined when the maximum theoretical $\bar{K}/K$ is exceeded; the magnitude of the experimental $\bar{K}/K$-values near the ICP already correspond to that almost horizontal part of the $\bar{K}/K$(Rel)-curve where small variations in $\bar{K}/K$ result in considerable Rel(κ^{σ}) variations (see fig. 5-1). The considerable differences between D-S I and II at high c (10^{-2}M) point to a still important surface conductance for H. Apparently, the effective conductivity of the environment surrounding the dispersed particle does not equal that of the continuous phase. The D-S I and H-B I predictions differ, which is understandable in terms of eqs. (5-20) and (5-21) as long as Rel is not sufficiently small.
3. near the ICP, the HB-I and Maxwell predictions show the same trend, but just below the ICP the Maxwell model, in contrast with H-B I, already demonstrates an unrealistic trend to infinite κ^{σ}-values.
4. the experimental data for Street, D-S I and H-B II converge at 10^{-2}M.

This apparent agreement is not particularly significant; it is mainly a consequence of compensating effects in the fundamentally different concepts. At this relatively high c the effects of surface conductance, primary double layer interaction and concentration polarization will be masked by the suspending medium because $K > \kappa^{\sigma}a$.

In view of the fact that for non-conducting particles at p = 0.10 the deviations from Maxwell's equation already become noticeable, it is clear that the usefulness of the modified prediction (eq. (5-27)), incorporating surface conductance, should decline progressively with increasing p, and decreasing c. However, the agreement of the prediction with the Bikerman region is surprisingly good.

The position of the ICP's (Rel = ½ and 1) with regard to the Bikerman region, shows a considerable shift to relatively high κ^{σ}-values upon decreasing σ_o. At high σ_o the ICP's are situated on opposite sides of the B-region, whereas for the lowest σ_o both points are situated relatively far above this region.

Overall the agreement between the positions of the curves in general and the B-region becomes poorer with decreasing σ_o. The increasing deviation is probably partly caused by the charging process discussed in chapter 4. Furthermore a reversible adsorption of co-ions, starting above about 10^{-3}M, probably contributes to the observed deviation too. These effects manifest themselves predominantly at lower σ_o's, invalidating the behaviour of our system that is supposed in the model. Moreover, the shift of the ICP to low c upon decreasing σ_o coincides with an increased violation of the condition that the conducting layer must be thin ($\kappa a \gg 1$ for a diffuse double layer).

All models, except Street, predict complete absence of conduction for $K \to 0$. More particularly, the concentration polarization concept (D-S I, II) then ceases to be meaningful. The tangential ionic flows near the particle surface, invoked under the influence of the external electric field, are maintained by ionic flows from the bulk. In the case of an isolated particle at low c diffusion flows arise beyond the double layer at a considerable distance from the particle surface. In a porous plug, however, the adjoining volume of electrically neutral electrolyte is restricted by the pore dimensions and decreases to zero for $\kappa a \to 0$ (see section 4.7.2). In other words, the outer part of the diffuse double layer, that plays an important role in the concentration polarization mechanism as described by Dukhin et al., is then actually absent. At the same time, the unavoidable contact points of the particles in the plug with locally enhanced double layer overlap, connect the ion-rich layers. Both factors suppress concentration gradients due to polarization along the external boundary of the double layer at low κa. In other words, the role of the concentration polarization on the small scale is partially cancelled. This effect and the fact that for a system at constant charge, especially for high σ_o's, the excess charge in the pore fluid remains localized close to the surface, even at very low κa (see section 4.4.1), are probably responsible for the good predictions of the HB-I (= Bruggeman) model at lower κa-values. However, the effect of short circuiting the ion-rich layer near the contactpoints makes $\bar{K}$ finite as $K \to 0$. This fact can easily be recognized by the sharp increase of κ^{σ}(HB-I) to undefined values as $c \to 0$.

Another important fact is the possible influence of the anomalous behaviour of our 'model system' at low c. From the electrokinetic and hydrodynamic experiments discussed in chapter 4 it was concluded that with decreasing c the ionic head groups increasingly project into the liquid phase. This phenomenon results in more effective shielding with decreasing c, because an increasing part of the excess charge is accomodated in spaces between the headgroups. This specific feature probably also contributes to the observed usefulness of the H-B I model over a rather extended c-range.

Before the results are discussed in terms of charge densities (step b), the experimental procedures and conductivity-results of dilute dispersions will be presented.

5.7 *Electroconductivity properties of dilute latex dispersions; experimental*

5.7.1 *Introduction*

In the literature very little experimental data are available on conductivities of particle systems that are well-defined with respect to monodispersity, surface charge density and the extent of the concentration range, that enables a critical test of all the quantitative theories. One of the major deficiencies of experimental studies of the conductivity of particle systems is an almost consistent failure to recognize that:

I κa should be the same for all particles, therefore the particle system must be monodisperse.

II the conductivity must be measured at a frequency low enough to approach static conditions; in other words, $\bar{K}$ must be measured at varying frequency to verify this. At the same time the effect of electrode polarization has to be accounted for or eliminated.

III a sufficiently extended c-range must be studied to establish the limits of applicability of theories developed for dilute systems, thus to verify experimentally qualitative theoretical conditions as $\kappa a \gg 1$.

IV all parameters characterizing the double layer under static conditions must be known to favour a quantitative comparison between theory and experiment.

V electrophoretic mobilities under the same experimental conditions have to be known because the suspension conductivity has to be corrected for the contribution of the moving particles. This information can also be obtained from other electrokinetic techniques.

Previous experimental work on this subject has been reported by Wright and James[39,40]. They measured $\bar{K}$ of a latex suspension over an extended c-range ($5\ 10^{-5}$-10^{-1}M) and studied the effect of various types of electrolytes on κ^{σ}. However, their latices were far from being monodisperse. Furthermore, all experimental data were interpreted with the Street equation. Unfortunately, they did not report any of the parameters (p, the actual values of $\bar{K}$ and K) necessary for a recalculation or a quantitative comparison with other models. One of the inconsistencies in their study is that they succeeded in evaluating surface conductances of an apparent extremely high accuracy even at ionic strenghts up to 10^{-1}M. However, the extremely high κ^{σ}-values presented with a fair degree of certainty indicate miscalculations. Watillon and Stone-Masui[33] have reported a careful study of surface conductance in dilute latex suspensions (p maximal 0.04). For their data it seems impossible to use other equations than that of Street. They reviewed older literature in which very scattered and even negative values of κ^{σ} were obtained, especially for systems with low p. In our opinion this results from their experimental conditions corresponding to Rel-values far below the ICP.

More recently (Sonntag and Pilgrimm[4]) dispersions of Aerosil (flame hydrolysed silica) were investigated conductometically, but the ψ_d's determined from $\bar{K}/K$ according to the D-S equation and calculated from σ_o, were not in good agreement.

It is clear that there is a definite need for a controlled set of $\bar{K}(K)$ experiments to enable a proper assessment of the existing theories.

5.7.2 *Experimental methods: calibration procedure of the conductivity cell; procedure for testing the polarization state of particle dispersions*

It has been shown (chapter 3) that in the extreme low frequency region measurements of $\bar{K}$ of plugs are complicated by polarization of the electrodes and by intrinsic relaxation phenomena. By using a special measuring technique it appears to be possible to separate both polarization phenomena and to obtain values of the conductivity ($\bar{K}$) at zero frequency. This result appears to be of vital importance because it enables investigations of fully polarized particle systems or membranes to be made. However, this newly developed measuring technique is restricted to immobilized systems such as plugs or membranes. Therefore, in practice the electrical properties of dilute dispersions must be determined in an alternating electric field which invariably gives rise to an electrode polarization effect and possible relaxation of the dispersion, but eliminates particle accumulation near one of the electrodes.

All measurements reported in this section were carried out using a Wayne Kerr Universal Bridge B224, the design of which is based on the transformer-ratio arm principle. This instrument which may operate at a fixed internal frequency of 1592 Hz, has a conductance range of 0-111 mMho and a capacity range of 0-11.1 μF. In essence, the measurement is made by balancing the unknown impedance with standards of conductance and capacitance in parallel. Measurements over the frequency range 200 Hz - 50 kHz were made by using a source/detector of Rhode and Schwarz in conjunction with the W.K. bridge and a digital frequency counter (TSA 6634 A/2 - Venner Electronics Ltd., England). Conductances were measured in a Philips conductance cell (type PW 9501) with platinized electrodes. The cell constant was determined at the fixed internal frequency, with dilute electrolyte concentrations in the same range as those of the experimental latex solutions ($5\ 10^{-5}$ - $7\ 10^{-3}$M). From these measurements it could be concluded that in the c-range studied the applied frequency was not high enough to eliminate electrode polarization. Furthermore, the magnitude of the electrode polarization error in determining the cell constant depends on the conductivity of the electrolyte being studied. It is possible to allow for the electrode polarization effect by calibrating the cell with standard liquids of known conductivity in the c-range being studied. In doing so, a c-dependent cell constant is obtained. Table 5-4 shows some results at three different frequencies. From this table we infer that the apparent cell constant tends towards a constant value at about 20 kHz.

C	C(v) cm^{-1}		
M	200 Hz	1592 Hz	20 kHz
$5\ 10^{-5}$	0.7049	0.7042	0.7038
10^{-4}	0.7057	0.7046	0.7039
$5\ 10^{-4}$	0.7067	0.7053	0.7038
10^{-3}	0.7077	0.7056	0.7042
$5\ 10^{-3}$	0.7085	0.7060	0.7039

Table 5-4. Variation of the apparent cell constant with frequency, v, and electrolyte concentration; KCl, 25.0°C.

At low ionic strength the magnitude of the electrode polarization effect is not substantial. It is clear that by taking one cell constant for an extended c-range the calculation of κ^{σ} may misleadingly be influenced. Measuring at higher frequencies, in order to eliminate electrode polarization, would only be correct if one assumed no frequency variation of the latex dispersion itself; such an assumption, however, is particularly questionable for our latex dispersion as will be shown later. In order to verify the relative contribution of both polarization phenomena

to the total impedance we assume that for our dilute dispersions ($p \leqslant 0.10$) the electrode polarization in the measurement of the unknown solution is the same as in the reference solution. The procedure rests on the assumption that electrode polarization impedance is solely a function of the bulk conductivity of the solution. This substitution technique (Rosen[41], Schwan[42]) is reasonably successful if the particles which give rise to unknown impedance properties are of sufficiently low volume concentration. The correction procedure means in terms of the apparent cell constant that the dispersion conductivity, $\bar{K}$, and that of the equilibrium electrolyte, K, at a certain frequency are calculated from the corresponding conductances using the same cell constant determined at that particular frequency. Fig. 5-4 illustrates the frequency dispersion

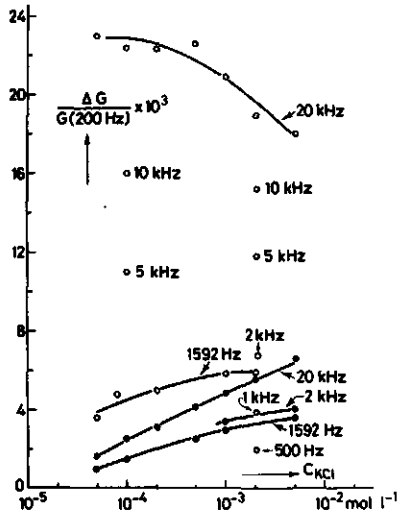

Fig. 5-4. The reduced conductance, $\Delta G/G$ (200 Hz), versus the KCl concentration for different frequencies. $\Delta G = G(\nu) - G(200\ Hz)$. The open circles represent data for the latex sample M with $p = 0.0710$, the filled circles correspond to the electrolyte solutions. $t = 25.0^{\circ}C$.

of reduced conductances as function of c_{KCl} and frequency of a dilute latex dispersion and its equilibrium electrolyte. The conductances at 200 Hz were taken as standard. From the results we immediately notice that the polarization of the metal-electrolyte interface increases with c (see also table 5-4). At the lowest concentration studied the magnitude of the electrode polarization is rather small. The relatively sharp increase of $\Delta G/G(200\ Hz)$ at $\nu = 20$ kHz for the latex dispersion compared to that of the equilibrium electrolyte reflects the relatively large contribution of the latex sample relaxation to the total impedance. In the low frequency range (below about the internal frequency: $\nu = 1592$ Hz) the onset of a relaxation contribution of the polarized particles to the resistive part of the total impedance is apparently small. A graphical extrapolation of the results obtained at $c = 2\ 10^{-3}M$ to zero and high frequency shows that

the significant change with frequency occurs within about one frequency decade (2-20 kHz). It is noted that the relaxation time calculated from $\tau = a^2/2D_c$ for KCl amounts to 2.3 10^{-5}s; this value corresponding to a critical frequency of about 6.8 kHz which is in good agreement with the observed dispersion region.

For $\omega\tau >> 1$ the ratio $\bar{K}/K$ equals 0.982 and for $\omega\tau << 1$ $\bar{K}/K$ is about 0.965 (ω is the angular frequency: $2\pi\nu$). At the internal frequency (1592 Hz) the conductivity ratio amounts to 0.967. This value hardly differs from that at zero frequency. The same indications were obtained at 10^{-4}M. Apparently, conductivity measurements carried out at frequencies below 2 kHz ensure static conditions for our latices in the c-range stu died, since below that value the ratio $\bar{K}/K$ becomes practically constant when applying the described correction method for electrode polarization.

Summarizing, we can say that these tests demonstrate the importance of studying the influence of frequency variation on dispersion conductivity.

5.7.2.1 *Titration method*

The most common technique for determination of the electrical conductivity of the equilibrium solution corresponding to a particle dispersion is by actually measuring the conductivity of the supernatant that is obtained after removal of the particles by centrifuging the dispersion. A disadvantage of this method is that the great number of involved manipulations enhances interference by atmospheric CO_2. This holds especially at low c because even a small change of the conductivity of the equilibrium electrolyte may influence the final calculations drastically. The latex dispersions and their equilibrium solutions have to be treated with scrupulous care. Furthermore, it is evident that this procedure, when carried out over an extended concentration range, requires a lot of material and time. Of more fundamental importance is the question as to whether this method provides the actual K-value, thus the *local conductivity of the interstial liquid outside the double layer of the particles*. The same applies to those methods where the suspension is equilibrated with an electrolyte solution using dialysis tubing. In those cases only the conductivities of that solution were determined. This aspect is crucial, because the actual concentration of the charge carriers along the outer double layer boundary determines the degree of double layer polarization under the influence of an electric field. One has to realize that by measuring the conductivity of the supernatant the conditions may have changed with respect to those in the dispersion. This is because the effect of negative adsorption may be reduced by partial overlapping of the

double layers in the sediment. Thus the conductivity of the supernatant is somewhat lower than that of the solution outside the double layer of the particles in the actual dispersion. It will be clear that in adopting the conductivity of the dialysate the actual saltcontent is overestimated, especially when the dialysate is diluted. To quantitatively verify the effect negative adsorption exerts on the determination of K accurate information of the actual system parameters, such as the surface charge density, are required. But the latter is just a quantity we want to establish.

As an alternative approach we used a 'continuous' titration technique to obtain relatively easily the required $\bar{K}(K)$-characteristics. Two procedures were carried out:

a) a purified saltfree latex dispersion was titrated with an accurately made-up solution of electrolyte of relatively high ionic strength.
b) one half of the saltfree latex solution was mixed with an equal volume of conductivity water and the other with an equal volume of specified eletrolyte concentration. The latter was used to titrate the first one. In order to exclude local coagulation the electrolyte concentration never exceeded $5\ 10^{-2}$M.

In method a the decrease of the solid volume fraction has to be incorporated in computing the electrolyte concentration. Upon adding an electrolyte solution of volume x and concentration c_o, the electrolyte concentration in the latex dispersion, based only on the continuous phase, c_x, becomes:

$$c_x = \frac{x}{x + x_o} \frac{c_o}{1 - p_x} \quad \text{with} \quad p_x = p \frac{x_o}{x + x_o} \tag{5-36a}$$

p_x denotes the volume fraction of the solid phase after adding the volume x and p_o is the initial volume fraction ($x = 0$); x_o is the total volume of the saltfree dispersion ($x = 0$). By taking suitable values for x_o (in our case 50 ml) and moderate values for c_o ($5\ 10^{-2}$M 1-1 electrolyte) for a concentration range up to $5\ 10^{-3}$M the change in p is rather restricted. The second method b has the advantage that the solid fraction remains constant during the titration. The actual electrolyte concentration is calculated from:

$$c_x = \frac{x}{x + x_o} \frac{c_o}{2 - p_o} \tag{5-36b}$$

where c_o denotes the concentration of the electrolyte before mixing with an identical volume of saltfree latex with volume fraction solid p_o.

The specific conductivity, K, is computed from c_x and the molar conductivity Λ which decreased with increasing c. The Λ-data for strong electrolytes are fairly well represented by the empirical relation (Parsons[43]): $\Lambda = \Lambda_o (1 - a\sqrt{c} + bc)$, where Λ_o denotes the molar conductivity at infinite dilution. The following data were used: for KCl at 25.0°C, Λ_o = 149.8 $\Omega^{-1}cm^2eq^{-1}$, a = 0.78 and b = 0.64; for LiCl at 25.0°C, Λ_o = 115.0 $\Omega^{-1}cm^2eq^{-1}$, a = 0.78 and b = 0.63. c is here in moles per liter. Then $K(\Omega^{-1}cm^{-1})$ can be calculated by multiplying Λ with c, but now c in moles cm^{-3}.

The titration procedure was checked with the values of the solute presented above by using blanks. For that purpose the conductance was measured at a fixed frequency after addition of electrolyte of known concentration and converted to a conductivity using the appropriate apparent cell constant. The resulting K-value was then compared with the computed one. It appears that below c's of 10^{-4}M the contribution of the solvent becomes noticeable and already starts to exceed 1% of that of the added electrolyte. In order to obtain good reproducibility, experimental factors as addition of the standard solution, attainment of equilibrium, determination of the volume fraction of the solid phase were carefully controlled. To measure the conductivities of the solutions as accurately as 0.1%, it was necessary to regulate the thermostat (Haake), containing the titration set up within 0.05°C. The titrations were performed in a 200 ml pyrex round bottom vessel equipped with a perspex cover with holes for the conductivity cell and in- and outlet tubes for nitrogen gas. It was essential to maintain a small nitrogen overpressure.

For this study latex, that had already been purified, was treated once more with purified ion exchange resins (Dowex 50W-X4; I-X4) according to the methods described by Van den Hul and Vanderhoff[44]. All charged surface groups were thus converted into the H^+-form. Finally, shortly before the conductometric titration, with either LiCl or KCl solutions, the latex was converted into the Li^+- or K^+-form to ensure a well-defined electrolyte composition over the whole concentration range under study. The latter conversion was achieved by a conductometric titration with LiOH or KOH till the point of lowest conductivity. This procedure is acceptable because this point differs only slightly from the equivalence point. In most cases the resulting conductivity (thus $\bar{K}$ for x = 0) was of the same order as that of the conductivity water even at moderate volume fractions (p = 0.1). This indicates the absence of free electrolyte and the small number of effective charge carriers of the highly polarized particles.

5.7.3 *Conversion of experimentally observed conductivity values, $\bar{K}_{obs.}$, to $\bar{K}$-values*

For the conversion of the conductivity of a particle system to a specific surface conductance, the following factors not incorporated in the theoretical formulae have to be considered:

I the suspension conductivity has to be corrected for the effect of electrophoresis[33,45]. The contribution of the moving particles to the suspension conductivity can be written in terms of particle charge, Q, and mobility U/X ($cm^2s^{-1}V^{-1}$):

$$\bar{K} = \bar{K}_{obs} - NQU/X \qquad (5\text{-}37)$$

where N is the number of particles per cm^3. The factor NQU/X, representing the specific conductivity of the moving particles ($\Omega^{-1}cm^{-1}$), when expressed in terms of the particle fraction p, particle radius a, and the effective or electrokinetic charge density, σ_{ek}, is given by: $3p\sigma_{ek}U/(aX)$. σ_{ek} can be evaluated from the electrophoretic mobility of individual particles, or from other electrokinetic experiments with plugs. In our case detailed information on the electrokinetic charge densities, obtained by various methods, was available. For the present purpose zeta-potentials and corresponding charge densities were evaluated from mobilities, according to Wiersema's theory of electrophoresis (see chapter 6). Despite the unmistakable presence of anomalous conduction, which according to W's theory leads to an underestimation of the charge density, it appears that the σ_{ek}'s thus calculated nearly coincide with those obtained from other electrokinetic experiments. This is merely a result of mutually compensating factors as discussed in section 6.5. The correction factors required for electrophoresis are relatively low because in the c-range, where this correction may be significant, the electrokinetic charge density was orders of magnitude lower than the surface charge density obtained by titration. In this connection it is important to realize that the mere occurrence of a common intersection point (ICP) does not offer an independent test of the correctness of the applied correction, because the factor is linear with p. An under- or overestimation of σ_{ek} (or Q) would result in a shift of the ICP to a higher resp. lower electrolyte concentration.

II an additional dipole moment originating from deformation of the double layer due to particle movement (μ_U). Its effect, relative to that due to the electric field (μ_E), can be roughly estimated from

the ratio[46]:

$$\frac{\mu_U}{\mu_E} \sim 10^{-2} \frac{\varepsilon_o \varepsilon_r \zeta^2}{(\kappa a)^2 D\eta} \sim 10^{-1} \frac{\tilde{\zeta}^2}{(\kappa a)^2} \qquad (5\text{-}38)$$

Application of the proper data shows this correction to be negligible for our particle system. Even at 10^{-4}M ($\kappa a = 10$) the value $\tilde{\zeta} = 4$ is hardly surpassed for any of the studied latices.

III the contribution of negative adsorption to the interstitial (bulk)-phase. Using our titration method, the average free electrolyte content based on the total liquid phase is exactly known. As already mentioned, the degree of polarization of the particles depends, among other things, on the interstitial saltcontent, the actual charge partition, thus the deficit of co-ions and the excess of counterions at any point in the double layer in a closed system has also to be defined with regard to the interstititial concentration. The extent to which negative adsorption enhances the bulk concentration depends on the actual double layer parameters. Assuming a purely diffuse double layer and absence of specific adsorption and double layer interaction, we can write for the increase in concentration[47]:

$$\Delta c_i = \frac{S_t \, \sigma_-(a)}{V_t \, z_i \, F_a} \quad (\text{mole } l^{-1}) \qquad (5\text{-}39a)$$

where $\sigma_-(a)$ is the deficiency of negative ions (charge density), S_t the total surface area of the spheres, V_t the total liquid volume and F_a the Faraday constant. Inserting the known relation between charge and potential (see section 4.8.1) and after evaluation of the constants, the relative increase for monovalent electrolytes at 25.0°C is given by:

$$\frac{\Delta c}{c} = \frac{S \, w \, I_-(\kappa a)}{1.644 \; 10^6 \; V_t \; c^{\frac{1}{2}}} \qquad (5\text{-}39b)$$

in which $I_-(\kappa a)$ is a quantity that for spherical particles has been tabulated by Loeb et al.[48]. S denotes the specific surface area in m^2/g, w the particle mass in g and V_t the total liquid volume in cm^3. In our case the effect of negative adsorption on K and thus on the ratio $\bar{K}/K$ was calculated using the experimentally determined charge densities. In general, however, without any knowledge of the system

involved, one has to convert the uncorrected $\bar{K}/K$-ratio into a specific surface conductance and a surface charge density and then to use the latter value to calculate the concentration rise. The final results can be improved by successive approximation. It is clear that the resulting higher K's will lead to lower Rel values, irrespective of the theoretical prediction used. The equations given above relate to systems without interacting double layers. It is easy to show that they remain valid to within a few per cent as long as the average particle separation exceeds $8/\kappa$ (Schofield[49]). The situation may be complicated by the fact that anions such as Cl^- are also adsorbed, resulting in a partial or complete masking of the anion expulsion. Further comments will have to await the experimental results. Therefore, we shall first give a short account of the titration experiments.

5.7.4 *Titration characteristics: results and discussion*

For discussing the general features of the titration curves, we have plotted in fig. 5-5 typical $\bar{K}/K$ vs. c data, corrected for the electrophoretic contribution, for three volume fractions of sample M, together with the theoretical results according D-S, H-B and Street (eq. (5-28), (5-29) and (5-24) resp.). The theoretical curves are computed for a fully developed electroosmotic contribution ($\psi_d = \zeta$). Without this contribution the $\bar{K}/K$-values will be somewhat lower for the intermediate c-range around the ICP. For the sake of clarity the prediction according to Street is only given for the highest p. This figure is representative for all titration results at other charge densities and electrolytes too. The fol-

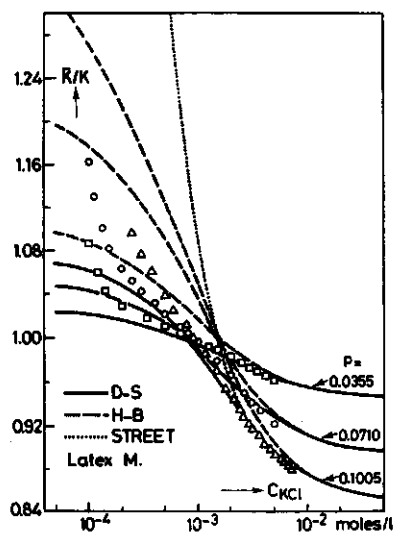

Fig. 5-5. Experimental $\bar{K}/K$-values versus c_{KCl}, corrected for electrophoresis for three volume fractions, together with theoretical results. Sample M, $t = 25.0^{o}C$.

lowing features are observed:

I the experimental points refer to different suspensions, although prepared from a given master suspension, they all fall very well on smooth curves and show similar behaviour. At high c_{KCl}, an increase in p leads to a decrease in $\bar{K}$, whereas the opposite occurs at low c. A common feature of all latices is the existence of an ICP: irrespective of the surface charge density and p (up to about 0.10) all experimental curves pass through a common intersection point with $\bar{K} = K$.

II the ICP shifts to lower c by lowering σ_o and/or by replacing the electrolyte with one having less mobile counterions.

III the experimental curves show some differences when compared to the theoretical ones. At low c especially, on the left side of the ICP, the slopes steepen upon decreasing c, whereas the theoretical $\bar{K}/K$-values tend to plateau values, at least for D-S and H-B. The initially rather convex portions of the titration curves can hardly be matched with theoretical predictions that suppose a concentration independent surface charge density. It seems useful to notice that the appearance of a mutual intersection and a subsequent divergence of a particular set theoretical and experimental curves on decreasing ionic strength, in terms of that theory, implies an increase of charge density. Where the experimental $\bar{K}/K$-data exceed the theoretical plateau values ($\bar{K}/K$ for $Rel \to \infty$, p) the corresponding charge density becomes undefined.

In testing the accuracy and reproducibility, it appears that errors accumulate at the end of the curves. At low ionic strength the sharp increase can be attributed to one or more of three factors:

a) the effect of small amounts of impurities,

b) underestimation of the electrophoretic contribution,

c) the effect of negative adsorption (n.a.).

ad a) What prevents measurement at extremely dilute electrolytes is not only that the solute conductivity is overshadowed by that of impurities but also by the contribution of the solvent itself. It was possible to keep the solvent conductivity below 1% of that of 10^{-4}M KCl and it does not seem sensible to extend the measurements far below 10^{-4}M. Even if the contribution of the conductivity water is known exactly, interpretation of the suspension conductivity in terms of specific surface conductance becomes speculative unless the precise composition of the various charge carriers is known.

ad b) Incorporation of the effect of anomalous conduction in the conversion of UX^{-1} into σ_{ek} results in somewhat higher σ_{ek}-values (see chapter 6) and a higher correction.

ad c) As will be shown in the quantitative discussion of the results, the correction for n.a. is rather important, especially for an interpretation on the basis of the D-S and H-B equations.

$\bar{K}$-p characteristics. In fig. 5-6 results of $\bar{K}$ vs. p are plotted at distinct c_{KCl}'s for three surface charge densities. The $\bar{K}$-values were obtained from accurate interpolation of titration data, corrected for the electrophoretic contribution. It is obvious that the straight lines, drawn through the experimental points, all come together at $\bar{K}/K = 1$. It can be deduced that for our dilute particle systems, even for p up to 0.1, the ratio $\bar{K}/K$ may be fairly well described by the relation: $\bar{K}/K = 1 - 3/2\ p\ f(Rel)$. Apparently, the electric fields surrounding the charged particles do not interact. Except for H at the highest p the $\bar{K}/K$-values show a positive deviation at low c, probably a result of small amounts of free electrolyte at the start of the titration. From fig. 5-6 it can be seen that the sequence of the surface charge densities is cor-

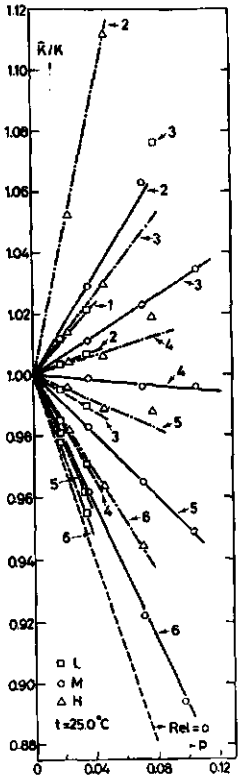

Fig. 5-6. Experimental $\bar{K}/K$-values as a function of the volume fraction, p, for some KCl concentrations and three surface charge densities.
1: 10^{-4}M, 2: 2 10^{-4}M, 3: 5 10^{-4}M, 4: 10^{-3}M, 6: 5 10^{-3}M.

rectly reflected in the slopes. Furthermore, the decreasing effect of κ^{σ} on $\bar{K}$ with increasing c, is demonstrated; at high c all lines gradually tend to converge to a single one (Rel = 0). It will be clear that such linear plots ($\bar{K}$/K-p or $\bar{K}$-p) provide independent checks on the titration procedure and on the correction procedure for electrode polarization:

I extrapolation of the observed or corrected suspension conductivity to p = 0 yield K,

II extrapolation to high c reveals the formation factor from which p can be calculated with the Maxwell equation. The latter can be compared with the value obtained by drying a known volume of suspension after correction for the saltcontent. In connection with these checks it is worth mentioning that the observed linearity does not provide any information on the correction factors used because for dilute systems they are also linear with p.

5.7.5 *The conversion of experimental $\bar{K}$/K-values to specific surface conductances: dilute dispersions*

In table 5-5 we have presented some experimental results for three surface charge densities, corrected for the effect of electrophoresis. The $\bar{K}$/K-values together with those fully corrected for the effect of negative adsorption (values in brackets) are obtained by interpolation of the titration characteristics. For the second correction, ψ_d and $I_-(\kappa a)$ were deduced from σ_o, using the L.O.W. tables[48]. In the same table the κ^{σ} results are presented according to the three basic predictions for dilute dispersions. The results according to the extended Maxwell expression are omitted because differences with the H-B results are negligible in the relevant p-range. It is seen that the apparently small effect of n.a. influences the final calculations, especially at low c, with the exception of the Street case. Whether the observed decrease of κ^{σ} is real is, of course, difficult to ascertain on account of the uncertainty about the actual charge densities. It may be added that it is not so much the surface charge itself that counts, but rather the way in which the counter charge is distributed between the Gouy and Stern layer. In this connection one has to be aware of effects, as observed with our system, that as the solution is diluted at low c, the 'immobilized part' of the counter charge apparently increases (chapter 4). Such an observation, which obviously clashes with common double layer knowledge, may invalidate the use of the D-S expression. It is worth mentioning that for the actual double layer, despite all possible non-ideal effects, a general description in terms of the concentration polarization mechanism remains valid. An assessment of the usefulness of the theoretical predictions is afforded

Table 5-5 a,b,c. Experimental $\bar{K}/K$-results for KCl at 25.0°C and specific surface conductances according to the three indicated models.
a: sample L, p = 0.0345; b: sample M, p = 0.0355; c: sample H, p = 0.0458.

a.

C_{KCl} M	$\bar{K}/K$	$\kappa^\sigma \times 10^{10}$ Ω^{-1} D-S	H-B	Street
$5\ 10^{-5}$	1.271 (1.218)	- -	- -	5.96 (5.20)
10^{-4}	1.0215 (0.994)	27.8 (2.78)	3.35 (1.62)	2.68 (1.71)
$2\ 10^{-4}$	1.007 (0.989)	11.6 (4.23)	4.57 (2.72)	4.27 (2.99)
$5\ 10^{-4}$	0.990 (0.980)	10.9 (6.51)	6.86 (4.83)	7.50 (5.72)
10^{-3}	0.971 (0.964)	7.58 (4.64)	6.27 (4.11)	7.94 (5.44)
$2\ 10^{-3}$	0.962 (0.958)	7.73 (5.10)	6.98 (4.76)	9.32 (6.45)
$5\ 10^{-3}$	0.955 (0.953)	8.11 (5.39)	7.75 (5.23)	10.5 (6.92)

b.

10^{-4}	1.087 (1.059)	-	26.0 (10.5)	6.04 (4.95)
$2\ 10^{-4}$	1.029 (1.012)	- (19.8)	9.51 (6.24)	7.03 (5.56)
$5\ 10^{-4}$	1.0117 (1.002)	48.1 (25.2)	15.4 (11.9)	13.8 (11.7)
10^{-3}	0.999 (0.992)	42.1 (29.1)	21.6 (17.6)	21.8 (18.8)
$2\ 10^{-3}$	0.983 (0.979)	36.9 (30.0)	26.0 (22.3)	30.0 (26.6)
$5\ 10^{-3}$	0.962 (0.959)	25.2 (19.2)	22.5 (17.7)	29.9 (23.7)

c.

10^{-4}	1.158 (1.115)	- -	- (26.7)	7.24 (6.08)
$2\ 10^{-4}$	1.112 (1.085)	- -	46.5 (23.7)	11.5 (10.0)
$5\ 10^{-4}$	1.029 (0.015)	164 (46.0)	19.2 (14.8)	15.3 (13.3)
10^{-3}	1.006 (0.997)	55.6 (37.6)	24.1 (20.0)	23.1 (20.4)
$2\ 10^{-3}$	0.989 (0.983)	53.9 (42.9)	32.8 (28.4)	35.3 (31.8)
$5\ 10^{-3}$	0.964 (0.960)	47.9 (39.8)	38.8 (33.3)	48.3 (42.3)

by comparing the calculated κ^σ-values with those predicted by the Bikerman-equation. As in the case of the plugs p-averaged κ^σ-values (for each charge density three fractions) are displayed in fig. 5-7 a,b,c with the Bikerman region. From the position of those curves that are not corrected for n.a. it is evident that none of them fits very well with the theoretical B-region. The Street prediction shows a similar trend as observed at high p, that on lowering the ionic strength the calculated κ^σ deviates increasingly from the B-region. The rise in κ^σ for L at c's below 10^{-4}M may in part be attributed to experimental error, since $\bar{K}_{obs}$ becomes of

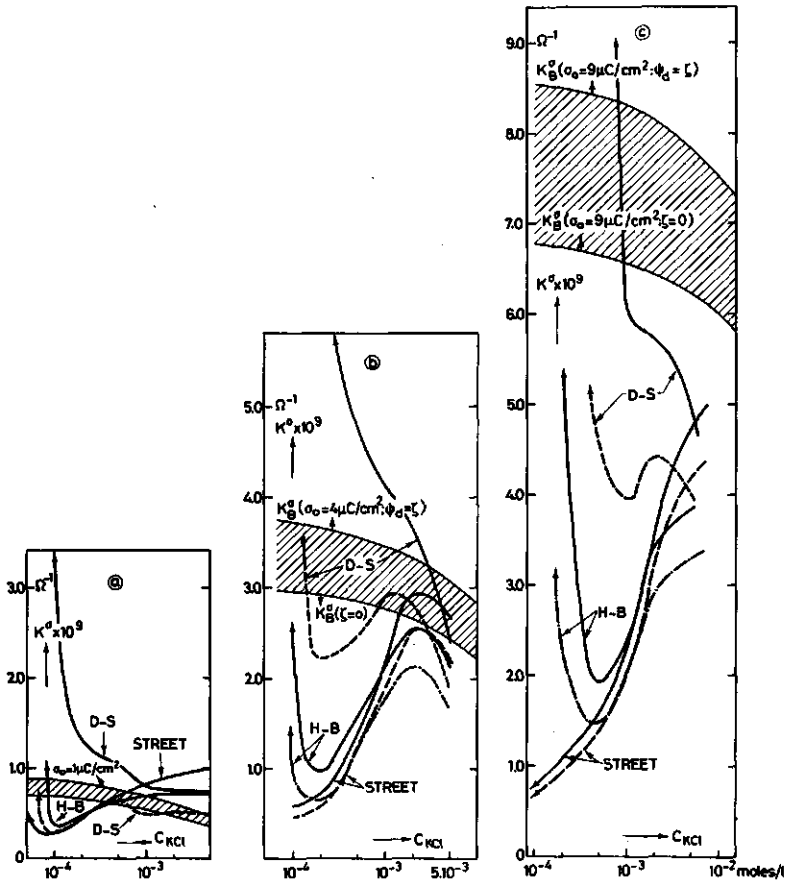

Fig. 5-7 a,b,c. Specific surface conductance, κ^{σ}, calculated from experimental $\bar{K}/K$ data for dilute dispersions according to three different models, versus the KCl concentration. The hatched area refers to the Bikerman region. a: sample L, b: M, c: H. The dashed lines show the effect of correction for negative adsorption. In case of sample L, the corrected κ^{σ} is only given for D-S for the sake of clearness.

the same order of magnitude as that of pure water, and to the fact that all uncertainties in determining the correction factors show up strongly in $\bar{K}/K$. On inspecting the shape of the κ^{σ}-c dependency as predicted by H-B (or Maxwell) it becomes clear why in the literature based on this equation, often scattered or negative values for κ^{σ} are reported. Most of that experimental work was performed in the low c-range. Incorporation of the effect of n.a. results in a shift of the whole curves to lower κ^{σ}-values. For the Street and H-B predictions this means that instead of an improvement we are faced with an even more restricted range of usefulness. On the other hand, the agreement of the D-S prediction with the B-region is closer and extends over a broader c-range. As mentioned earlier good agreement for this prediction can only be expected when $\kappa a \gg 1$. The sharp

increase in κ^σ just below 10^{-4}M ($\kappa a \sim 10$) for all σ_o's points to the fact that the D-S prediction overestimates the effect of concentration polarization (increasingly so with σ_o). From our results it is clear that the D-S prediction is the most useful for dilute dispersions. A quantitative comparison of the κ^σ-results with those obtained at high p but also at high c ($\geq 5\ 10^{-3}$M; double layer overlap reduced) gives us an overall picture of this prediction over a broad c-range. The plug results, however, are about 20% higher. This is in agreement with expectations that account for the charging effect and for the not fully eliminated double layer overlap near the contact points of the spheres in the plug. By examining the position of all curves and the ICP's with regard to the B-region at low and high p it is clear that the main effect of double layer interaction is to exclude the existence of one practical expression for all porosities. It seems quite logical to expect that upon concentrating a particle dispersion a meaningful description in terms of concentration polarization shifts to higher c, whereas an interpretation in terms of the Bruggeman model becomes more reasonable at lower c.

5.7.6 *The effect of the thickness of the double layer: results and discussion*

In order to estimate the effect of a finite thickness of the interphase on κ^σ we use the modified Maxwell eq. (5-32) and regard the thickness as identical to the double layer thickness ($1/\kappa$). The effect is illustrated on basis of the conductivity data of M not corrected for n.a. (see table 5-6). We also give the H-B results in order to illustrate the small effect of linearization even at this volume fraction solid. The

c_{KCl} M	$\tilde{K}/K$	$\kappa^\sigma \times 10^{10}\ \Omega^{-1}$ H-B	Maxwell r=1	Maxwell r=1-1/κa
10^{-4}	1.163	18.3	20.3	18.2
$2\ 10^{-4}$	1.063	10.0	10.1	9.35
$5\ 10^{-4}$	1.0023	15.3	15.3	14.6
10^{-3}	0.996	21.0	21.0	20.3
$2\ 10^{-3}$	0.965	25.4	25.4	24.8
$5\ 10^{-3}$	0.9222	22.7	19.9	19.6

Table 5-6. The influence of a finite thickness of an electroconducting layer on κ^σ according to the modified Maxwell eq. (5-32) for sample M with p = 0.0710 at 25.0°C.

main conclusion is that correction for the finite thickness of the conducting layer always leads to lower κ^σ-values; so it may give a limited improvement to the D-S prediction at low c. In the c-range studied, this

correction is only of minor importance with respect to the other factors considered in section 5.7.3.

5.7.7 *The low frequency dispersion of the conductivity: results and discussion*

From the calibration procedure of the conductivity cell it was already corroborated that the conductance of the electrolyte-particle complex can reasonably well be separated from that of the electrode-electrolyte complex. Actually, the purpose of the experiments described was to investigate the validity of the correction procedure for electrode polarization and to verify the polarization state of the particles. We have focussed our attention only on the measurement of $\bar{K}$ with the substitution technique described in section 5.7.2. For an analysis of the effect of concentration polarization on κ^{σ}-values calculated from the D-S and H-B equations, we shall limit ourselves to measurements that are carried out over a relatively extended frequency range in the immediate vicinity of the ICP, where any residual polarization effects of the electrodes on $\bar{K}/K$ must be small. To that purpose we select the results of M at 2 10^{-3}M. In table 5-7 we have presented κ^{σ}-values, calculated from $\bar{K}/K$, at various frequencies. The values corrected for n.a. are given in brackets. The non-corrected and corrected κ^{σ}-values obtained by extrapolating the D-S predictions to zero frequency agree fairly well with the H-B predictions extrapolated to infinite frequency. The same trend is observed at c = 10^{-4}M. The agreement between H-B and (not presented) Street for this

ν kHz	$\bar{K}/K$	$\kappa^{\sigma} \times 10^{10}$ Ω^{-1} D-S	H-B
∞	0.982* (0.9728)*	55.3 (43.9)	34.0 (29.2)
20	0.978 (0.969)	50.0 (39.7)	31.9 (27.3)
10	0.975 (0.966)	46.1 (36.8)	30.2 (25.9)
5	0.972 (0.963)	43.0 (34.0)	28.8 (24.5)
2	0.9678 (0.9588)	38.6 (30.5)	26.8 (22.6)
1	0.9658 (0.9568)	36.6 (28.9)	25.8 (21.7)
0.5	0.9653 (0.9563)	36.2 (28.6)	25.6 (21.5)
0.2	0.9651 (0.9561)	36.0 (28.4)	25.5 (21.4)
0	0.965* (0.956)*	35.9 (28.3)	25.4 (21.4)

note: - data obtained by extrapolation are indicated with an asterisk
- the number of decimals used in the presentation of $\bar{K}/K$ is determined by frequency dependent accuracy of the bridge.

Table 5-7. Specific surface conductance data as function of frequency, ν, according to two theoretical equations, (5-28) and (5-29), for 2 10^{-3}M at 25.0°C; the values in brackets are corrected for n.a.
sample M, p = 0.0710.

example is a consequence of the fact that the experimental conditions were close to those at the ICP. This test probably cannot be considered as fully conclusive, but it is most likely that the observed conductivity increment is primarily due to the elimination of the concentration polarization mechanism (see section 5.4.3 too). Moreover, as already noted, the calculated critical frequency falls very well within the dispersion region, underlining that the frequency dispersion is due to a diffusion-relaxation mechanism of the double layer. Moreover, it appears that an interpretation of the conductivity results at high frequencies according to H-B is reasonable; this is important from an experimental point of view because at frequencies above the dispersion region the effect of electrode polarization is seriously diminished. In order to generalize these findings, similar conductivity studies on other well-characterized model systems remain desirable.

5.7.8 *The ICP's of concentrated and dilute dispersions: results and discussion*

In table 5-8 the ICP's are given for widely different conditions of surface charge density, volume fraction solid, temperature, nature of counterion and treatment at high ionic strength (irreversible charging). The results are classified under dilute and concentrated dispersions; the latter group is subdivided into untreated and treated ones. Unfortunately, we failed to perform sucessful experiments with treated dilute dispersions for practical reasons (partial coagulation, cumbersome dialysis and ion-exchange). The concentrations corresponding with the isopolarization state of the dispersions, c_{ICP}, are obtained by careful interpolation of the $\tilde{K}/K$-c characteristics. From the c_{ICP}-results, covering a rather extended concentration range (1½ decades), the following features are observed:

1) c_{ICP} shifts to higher values on increasing σ_o; the increase of charge carriers is not fully compensated by the increased concentration polarization. This fits into the general picture of the concentration polarization mechanism.
2) treating a plug at high ionic strengths does shift c_{ICP} to higher values. The proportional increase of c_{ICP}, indicative of the increase of the effective charge, is practically the same for all σ_o's, but is slightly more pronounced for K^+ than for Li^+ (LiCl: L 21%; M 22%; H 17% and KCl: L 30%; M 31%; H 24%). This implies an alkali-ion specificity in the charging process.
3) the differences between the c_{ICP}'s for Li^+, K^+ and Cs^+ are much smaller than can be explained by an ordinary diffuse double layer struc-

Table 5-8. Experimental c_{ICP}-values of untreated dilute and concentrated dispersions and treated concentrated dispersions. The values in brackets are corrected for negative adsorption (see text).

$c_{ICP} \times 10^4$(M)

dilute dispersions: untreated

	t °C	L		M			H		
LiCl		p: 0.0420					0.0360		
	25.0	2.19 (0.776)					13.0 (8.91)		
KCl		p: 0.0172	0.0345	0.0355	0.0710	0.1057	0.0225	0.0458	0.0768
	25.0	2.75 (0.812)	2.95 (0.795)	9.33 (5.75)	9.01 (5.55)	9.12 (5.50)	14.5 (9.12)	13.2 (8.91)	12.9 (9.11)

concentrated dispersions

		untreated			treated		
	t °C	L	M	H	L	M	H
LiCl		p: 05880 (VI A)	0.5846 (VIII A)	0.5971 (VII A)	p: 0.6015 (V A)	0.5846 (VIII A)	0.5971 (VII A)
	15.0	5.77			7.07		19.2
	25.0	5.66	10.3	15.9	6.82	12.5	18.5
	35.0	6.07			6.83		18.2
KCl		p: 0.5888 (VI C)	0.5951 (VIII B)	0.6133 (VII B)	p: 0.6041 (V B)	0.5951 (VIII B)	0.6133 (VII B)
	15.0	6.45			8.68		21.0
	25.0	6.46	10.7	17.2	8.39	14.6	21.3
	35.0	6.42			8.16		21.4
CsCl					p: 0.6015 (V C)		0.6315 (VII C)
	15.0				8.11		17.7
	25.0				8.06		18.5
	35.0				8.12		18.9

ture. Moreover, the sequence is at variance with the lyotropic series in solution, so that an alkali-ion specificity seems eminently feasible.

4) c_{ICP} is temperature-indepedent, at least within experimental accuracy, for both untreated and treated plugs; the added charge carriers

after treatment at high ionic strength manifest themselves in the same way as the initial ones. In this connection, it is noted that theoretical c_{ICP}'s are temperature independent too.

In the next section all these findings will be verified and analysed more quantitatively for the complete c-range. To that purpose specific surface conductances are converted into charge densities.

In fig. 5-8 p-averaged c_{ICP}-values for KCl are plotted vs. σ_o, together with the theoretical D-S predictions for $\psi_d = \zeta$ and $\zeta = 0$. The results for LiCl reveal the same trend and are therefore omitted. We notice that the experimental results and theoretical predictions diverge with increasing σ_o, corresponding to a region of moderate κa-values (κa exceeds 30 for $c \geq 10^{-3}$M). The complexity of all factors involved as well as the uncertainty about the theoretical region, especially at low σ_o (low κa!), only allow some qualitative comments. It seems that at high σ_o some of the counterions are immobilized or exhibit a decreased mobility. However, an increase of concentration polarization in consequence of the earlier discussed increased shielding of the fixed charges by counterions ('hairy layer' model) can also contribute to the observed trend.

At low σ_o (low κa) the c_{ICP}'s corrected for n.a. are situated below the lowest possible prediction (Rel = 1; $\zeta = 0$). It is likely that as a consequence of the anomalous double layer structure, the correction for n.a. is overestimated. To verify this, we recalculated the effect of n.a. on the basis of an effective layer thickness, Δ_h, obtained from hydrodynamic experiments (section 4.7.2) and the electrokinetic charge densities. For that purpose, we used σ_{ek}-values obtained from streaming current experiments on plugs, fully corrected for double layer overlap (section 4.6.5). The Δ_h-values are taken from fig. 4-5 and are averaged over a number of temperatures (15.0, 25.0, 35.0°C) and electrolytes (LiCl, KCl, CsCl). Of course, the occurrence of an immobile layer with unmodified charge partition does not influence the extent of the n.a. correction, but the supposed unusual partition of the sulfate end-groups protruding into the aquous phase and contracting the double layer (confirmed in section 4.8.2), may lead to a smaller correction. In the calculations we assumed that the Δ-layer was co-ion free. The parameter $I_-(\kappa a)$ was calculated on basis of σ_{ek} and the specific surface area from the enlarged particle radius $(a + \Delta)$. The correction factors were obtained by interpolation of plots of the concentration rise $\Delta c/c$ vs. c. c_{ICP}-values corrected in this way are presented as broken lines in fig. 5-8.

For the lowest σ_o in particular the agreement between theory and experiment is hardly improved.

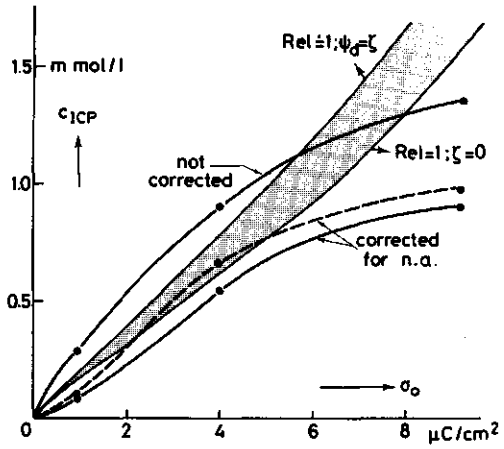

Fig. 5-8. Experimental c_{ICP}-values as a function of the surface charge density, σ_o, together with the theoretically predicted region according to D-S at 25.0°C. The upper experimental line is not corrected for n.a., the middle one is is corrected for n.a. on basis of σ_{ek} and Δ_h, the lower one on basis of σ_o.

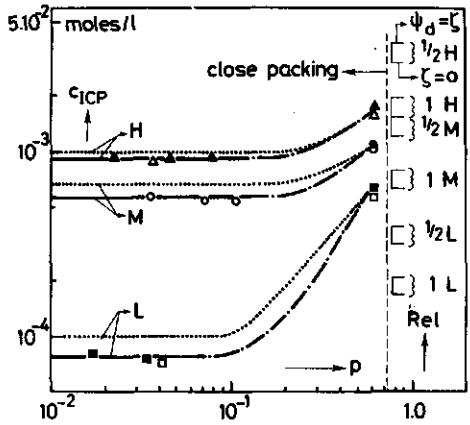

Fig. 5-9. c_{ICP} as a function of the volume fraction solid, p, at 25.0°C for three surface charge densities. The solid line and dotted lines represent the results corrected for n.a. on basis of σ_o and on basis of σ_{ek} Δ_h, resp.
The theoretical predictions according to D-S and H-B, considering the effect of anomalous conduction ($\psi_d = \zeta$; $\zeta = 0$), are inserted.
The circles refer to KCl; the squares to LiCl.

Although a positive adsorption of Cl^-ions in the very low c-range (below 10^{-3}M) could not be demonstrated (chapter 2), it is instructive to test the effect of a very small chloride adsorption. A decrease in concentration (free electrolyte) due to Cl^--adsorption ($\Delta\sigma_{Cl^-}$) can easily be computed from $-\Delta c = S_t\ \Delta\sigma_{Cl}$ w/F. For p = 0.05 and $\Delta\sigma_{Cl^-} = -0.1$ μC/cm² it already amounts to $5\ 10^{-6}$M. This would correspond to a decrease of 5% at 10^{-4}M, just the value commensurate with that computed for n.a. From these results it may be inversely concluded that below about $5\ 10^{-4}$M adsorption of moderate amounts of Cl^-ions is out of the question. It is clear that adsorption at higher σ_o, which would exceed 1 μC/cm², would shift the results into the theoretical D-S region. However, values of this magnitude could not be detected.

The effect of p. The effect of the volume fraction of the disperse phase on c_{ICP} is clearly noticed from the results of untreated dispersions, presented in fig. 5-9. The results for LiCl are inserted to express the same trend over the whole p-range. The most distinct effect is the strong increase of c_{ICP} upon concentrating the dispersion, especially for L (L fac-

tor 8.2; M and H factor 1.9).

A comparison of c_{ICP} at high p with the theoretical regions (Rel=½,1) inserted along the ordinate reveal that for high σ_o c_{ICP} is just shifted into the region Rel = 1; H. For the lower σ_o's these regions are surpassed, increasingly so with decreasing σ_o. It is essential to realize that this is not fully attributable to a decrease in polarization. The irreversible charging, starting for L about 5 10^{-4}M (for the higher σ_o's at somewhat higher c's), also contributes to the observed increase, especially for L.

5.8 *General outline of the electrokinetic and electroconducting parameters of the 'model' system*

In this section we will survey and analyse the structure of the electrical double layer of our model system on the basis of the information obtained in this and preceeding chapters. Several important features have already been discussed along with various electrokinetic models, double layer overlap corrections and the conversion models (chapter 5 and 6). The combined information on the influence of the nature of the counterions and the temperature on κ^σ will be used to analyse the peculiar features of the 'model' system. In order to facilitate the analysis, all experimental results have been transformed into charge densities.

Although the procedure for evaluating and testing the electrokinetic results has already been discussed (section 5.5), the applied procedure will be briefly reviewed in order to complete some important details. Substituting the ζ-potential, deduced from streaming current experiments and corrected for double layer overlap (section 4.6.5), and various other physical constants into the Bikerman-equation (section 4.3), the specific surface conductance associated with the plane of shear is obtained: κ^σ_{ek}. Next, the conductance contribution of the Δ-layer between particle surface and shear plane, κ^σ_Δ, is obtained as the difference of the total (model dependent) specific surface conductance, $\kappa^\sigma_{t,model}$, and κ^σ_{ek}. The charge density of the Δ-layer, σ_Δ, could be estimated from $\kappa^\sigma_\Delta/(\Lambda^+_\Delta F)$, where Λ^+_Δ denotes the molar conductivity of the counterions in that layer. This procedure is only correct if the charge deficit due to the co-ions, σ^-_Δ, is negligible as compared to the charge excess σ^+_Δ (note that $\sigma_\Delta = \sigma^+_\Delta + \sigma^-_\Delta$), a condition realized in our system. The total charge density, σ_t, is then computed as $\sigma_t = \sigma_{ek} + \sigma_\Delta$. The total, or effective, charge so obtained is identical to the 'mobile' charge σ_m. In case the aforementioned condition is not obeyed, σ_t must be determined indirectly. The procedure is then as follows: first, the electroosmotic contribution is calculated according to Bikerman and subtracted from $\kappa^\sigma_{t,model}$, giving the quantity $\kappa^\sigma_{\zeta=0}$, which

is only related to the migration contributions of counter and co-ions. σ_t can then be determined graphically (or numerically) from $\kappa^{\sigma}_{\zeta=\bar{o}}\sigma$ characteristics. In our case, the difference between the two methods does not exceed 4%.

5.8.1 *Plug results and discussion*

The main data on the charge distribution, obtained by using the H-B I (= Bruggeman) model, is tabulated in appendix 5A, table 5A-1 through 5A-3 and shown graphically for KCl at 25.0°C in fig. 5-10 a,b,c. The H-B I model was chosen because its usefulness over an extended c-range has been demonstrated in the preceding discussion. Bulk values are assigned to the molar conductivities of the ions in the whole double layer. The results obtained before treatment of the plugs with high ionic concentrations (irreversible charging) are indicated with a single arrow. The resulting reversibility of the charge distribution on varying c in an arbitrary direction is indicated by the double arrows. The following aspects are noteworthy (for other electrolytes and temperatures see appendix 5A):

I a substantial increase in the electrokinetic charge density, σ_{ek}, with increasing c_{MCl} for all three charge densities; the curves are not significantly influenced by treatment, except at relatively low c, where they are slightly shifted to larger values.

II the shape of the σ-c curves is essentially the same for the three charge densities; the same applies to the charging effect.

III for treated plugs the increase of σ_{ek} on increasing c_{MCl} accompanies a comparable decrease of σ_{Δ}; apparently, the absence of decrease of σ_{Δ} *before* complete treatment is merely a result of the charging that takes place during that treatment.

IV the charging effect is hardly reflected in σ_{ek}; thus the new or activated charge carriers are hydrodynamically immobile.

It is evident, that there is little point in attributing these findings to specific counterion adsorption, because the ratio σ_{ek}/σ_t just increases with increasing c_{MCl}. Moreover, it has often been established, for various systems, that in case of monovalent electrolytes adsorption in the outer Helmholtz plane takes place only at relatively high c (from about 10^{-2}-10^{-1}M on), depending on the nature of the counterions, the fixed charges involved and the magnitude of the charge density. Furthermore, the results of the Cl^--adsorption study (section 2.2) show that one can not refer to reversible or irreversible co-ion adsorption.

An alternative explanation could be that the shear plane shifts inwards on increasing c to such an extent that this not only masks but over-

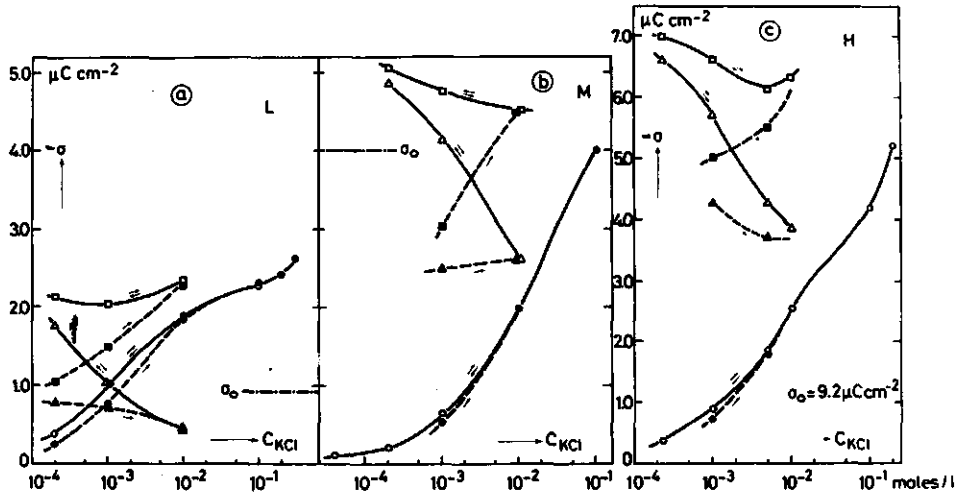

Fig. 5-10 a,b,c. The charge density distribution as a function of the electrolyte concentration (KCl) for L, M and H plugs at 25.0°C according to H-B I.

untreated: σ_t ■ , σ_Δ ▲ , σ_{ek} ● (broken lines)

treated : σ_t □ , σ_Δ △ , σ_{ek} ○ (solid lines)

compensates for the opposing effect of compression of the double layer. This shift must, therefore, be associated with the highly c-dependent location of the ionic head groups with respect to the particle surface.

5.8.1.1 *The 'hairy layer' model*

At low c the ionic endgroups of the polystyrene chains are projected out, probably with a broad range of lengths into the waterphase. Particularly at high charge densities and a low electrolyte content, a high proportion of them will be vertically oriented as a result of mutual electrical repulsion. The fixed charges may be separated from each other, to some extent, as the polystyrene chains expand when the ionic strength decreases. In consequence of the more open structure of the hairy layer with an enlarged exposure of hydrophobic groups to the water, the tendency of the hydrophobic chains to be squeezed out of the water by the hydrophobic effect is more pronounced (Tanford[50]). It is this interdependence which is mainly responsible for the extent of protrusion. Upon decreasing the ionic strength the counterions will tend to distribute themselves at larger distances from the particle surface. As a consequence of the increased spacing between the headgroups, a substantial part of the counterions is accommodated in spaces between the headgroups, a situation also encountered in micellar[51-53] and polyelectrolyte solutions[54]. At

higher c there is less repulsion between the fixed charges due to more shielding. The Δ-layer shrinks, due to the hydrophobic effect, whereby increasing parts of the protruded chains attain a more folded state and tend to lie flat on the surface in hydrophobic association with the surface, or adsorb *into* the periphery, which must not be regarded as totally rigid. Consequently, the screening of the fixed charges which is originally spherically symmetric gradually becomes perpendicular to the particle surface, mainly caused by excluded volume effects. This important factor has a positive effect on the electrokinetic charge density (zeta potential). The reduction in entropy, associated with the increasingly folded state of the polymer chains and the change in the electrical free energy due to a decrease in sphericity of the charge screening is, apparently, entirely compensated by the positive entropy change due to breakdown of ordered water structure at the hydrophobic surface. Additional contributions may arise from the redistribution of charge that involves transfer of ions to a region of higher permittivity.

The apparently important role of mutual repulsion of the fixed charges upon decreasing c, responsible for the enlarged exposure of the hydrophobic groups to the aqueous medium, suggests a substantial overlap of electric fields, so that the mutual distances of the charged heads are *small* compared to the characteristic shielding length (κ^{-1}). One may wonder whether a continuous distribution of the fixed charges still applies for our 'model' system. If they are distributed uniformly over the particle surface, their mean distance to nearest neighbours will have to be of the same order of magnitude as the shielding length at intermediate values of the studied c-range. For L the inter-charge distance amounts to 4.21 nm, for M to 2.00 nm and for H to 1.32 nm, whereas the double layer thickness at 10^{-3}M MCl, where the collapse of the Δ-layer starts, is 9.62 nm. The shielding length at 10^{-2}M (= 3.04 nm) is such that one would not expect extensive repulsion. Fig. 5-10 a,b,c, nevertheless shows that this concentration is in the middle of the transition range. An interpretation may be sought in a *patch-wise* distribution of the charged groups. The charge density (especially for L) is then high enough locally to cause the required enhanced repulsion. The close spacing creates high local potentials, so that the counterions are powerfully attracted even if the saltcontent is very low. This may also lead to the binding of counterions at specific sites, which is quite different from long-range electrostatic field effects. Thus decrease of c, starting from such a situation, has a surprisingly small effect on the charge distribution in the neighourhood of a charged patch.

5.8.1.2 *The charging phenomenon*

It is recalled that charging is only observed for plugs that have not previously been treated at high ionic strength and also that the latex particles are prepared at relatively low ionic strength.

For lattices prepared without surfactant the discrepancy between the titration charge and the charge calculated from the initiation if one end-group per chain is at the particle surface, may be due to the circumstance that not all the chains have an end-group at the particle surface. Such a conclusion arises by comparing the root-mean-square end-to-end distance of the polystyrene molecule and the particle diameter[55]. Thus part of the end-groups is buried in the particle or just in the periphery. It is clear that due to the low permittivity inside the particle and in the periphery all buried sulphate groups are associated with cations.

Upon increasing c for the *first time*, the chains are salted out. The region of high permittivity adjacent to the particle surface shifts inwardly; ion-paired groups become activated and the liberated cations contribute increasingly (in our case K^+-ions from the initiator) to the surface conductance. From the effect of treatment on σ_{ek} we conclude that the influence of ionic strength on the charge distribution of the 'new' groups is essentially the same as on the initial ones. When this would not be the case and the total increase of charge would be electrokinetically operative, the σ_{ek} curves would have been shifted to larger values in the low c-range and would have completely masked the peculiar findings at low c, especially for L where the added charge is commensurate with the initial one. It is, therefore, most likely, that new groups arise in the charged patches. In this picture, a charge increase results in an enhanced inhomogeneity of the charge distribution. The ion-paired groups, located within the particle wall and surrounded by the protruded hydrophobic chains, are not accessible for ion-exchange at low c and are therefore not included in the titration charge density.

The final location of the headgroups at high ionic strength is determined by a balance between many factors, such as the local permittivity of the micro-environment, the hydrophobic effect favouring and the heavily hydrated groups opposing close approach and the nature of the counterion (the latter in view of the extent of association of the headgroups).

Upon decreasing c for the *first time*, a larger portion of the sulphate end-groups tends to stand up on the particle surface. It is probable that some of them remain located on hydrophobic sites because the involved polystyrene chains are more strongly adsorbed onto or inserted into the particle surface. Upon protrusion of the polystyrene chains the average permittivity of the layer adjacent to the polystyrene surface

decreases. Consequently, the occurrance of a net charge in this region becomes unfavourable. The fraction of the sulphate groups fixed in that region will form ion-pairs, leading to a decrease of their contribution to the specific surface conductance. Apparently, the net result of the first treatment is still a relative increase of the 'mobile charge'. It is recalled that subsequent treatments at high ionic strength do not change at all the observed charge partition after the first treatment.

A complication in the interpretation of charge partition arises from the fact that the nearly constant σ_t for K^+ and Cs^+ after treatment, suggesting a nearly constant 'mobile charge', may be attributed to the model in the conversion (H-B I). In this connection, it may be significant to refer to the results for Li^+ which according to the same model point to an increase of the 'mobile charge' upon decreasing ionic strength.

All the anomalous findings may suggest the presence of weak acidic groups. The dissociation of such groups increases with increasing pH and/or ionic strength (e.g. Stone-Masui and Watillon[56]). However, in our case

I conductometric and potentiometric titration at low ionic strength present no evidence of weak acidic groups;

II in the pH range 4 to 10 the mobility of the latex particles at 10^{-2}M KNO_3 is independent of pH[57]. The presence of carboxyl groups, having pK_a values between about 4.0 and 4.6 would cause an increase in the electrophoretic mobility up to pH 6 (Ottewill and Shaw[58]);

III surface conductance experiments with our plugs at 10^{-3}M LiCl and KCl (within the charging range) reveal a slight increase in κ^σ (all conversion models) with increasing pH up to 9.2. According to H-B I this increase covers, however, only about 10% of the difference between κ^σ_Δ-treated and κ^σ_Δ-untreated. Moreover, dissociation upon increasing c would be reversible.

It could be that electrolyte also influences the thickness or compactness of the adhering layer of water molecules, i.e. the position of the shear plane. However, as discussed later, the observed lyotropic sequence provides evidence that the adhering water layer is thin or lacking on the hydrophobic parts of the particle. The shear surface probably coincides with the surface enveloping those hydrated end-groups which are most protruded in the charged patches. The hydroxyl groups, possibily present at the surface of the polystyrene particles[59], probably have only a slight effect on the anomalous effects.

On basis of the shape of all σ-c curves and an earlier analysis of all conversion models, it seems well founded that for the c-range studied the vast majority of the countercharge is diffusely distributed. Upon de-

creasing c an increasing part of the counterions is present inside the shear plane. This effect decreases the net electrokinetic charge of the particle.

5.8.1.3 *Ion specificity*

In order to study the influence of the nature and concentration of different electrolytes upon κ^{σ}, any possible effect of the conversion model ($\bar{K} \rightarrow \kappa^{\sigma}$) should be excluded. Therefore, ratios rather than absolute values are analysed, these are only slightly dependent on the conversion model. By way of example we compare the Street and H-B I models, which diverge substantially at low c. For H at 10^{-4}M and 25.0°C the Street model gives $\sigma_{\Delta}^{Li} : \sigma_{\Delta}^{K} : \sigma_{\Delta}^{Cs} = 1.94 : 1.24 : 1$ and H-B I leads to 2.24 : 1.33 : 1, whereas the absolute values for σ_{Δ} are about 3-fold less in the Street approach.

In fig. 5-11 we have plotted the charge density ratios $\sigma_t^{Li}/\sigma_t^{Cs}$ and $\sigma_t^{K}/\sigma_t^{Cs}$ versus c at 25.0°C. The ratios at other temperatures are hardly different (see appendix 5A). We have taken the σ_t-ratio instead of the σ_{Δ}-ratio to improve a comparison with the experimental activation energy results, which will be presented hereafter.

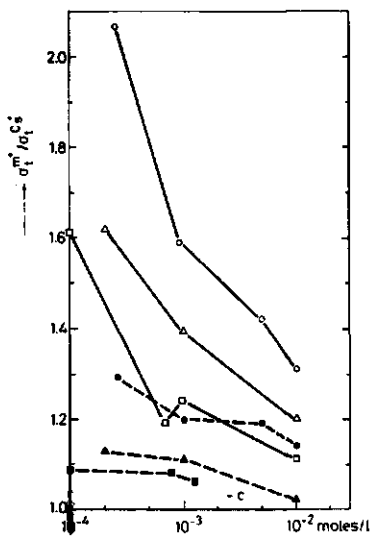

Fig. 5-11. The charge density ratio vs. the electrolyte concentration at 25.0°C.

$\sigma_t^{Li}/\sigma_t^{Cs}$: L □ , M △ , H ○

$\sigma_t^{K}/\sigma_t^{Cs}$: L ■ , M ▲ , H ●

The σ-ratios are calculated from the results tabulated in appendix 5A-1 through 3.

From fig. 5-11 we notice a conspicuous ion-specificity in the σ_t-ratio, which increases progressively upon diluting the solution and increasing σ_o. This may be caused by the joint effect of two parameters, viz. increasing adsorbability and change in mobility of the cations. While an enhanced adsorption of the counterions in the Stern layer leads to lower σ_t's, increasing mobility is the reason for an opposite effect. It is re-

called that bulkvalues are assigned in the computation of σ_t, thus without an alkali-specificity we should expect $\sigma_t^M / \sigma_t^{Cs} = 1$. For $c > 10^{-2}$M all results tend to converge to 1, either corresponding with more ideality or with an identical deviation from ideality. However, the σ_{ek} results, tabulated in appendix 5A, reveal for $c > 10^{-2}$M an increasing ion-specificity over the whole σ_o-range. At high c (10^{-1}M) the following trend is observed: $\sigma_{ek}^{Li} \geqslant \sigma_{ek}^{K} \geqslant \sigma_{ek}^{Cs}$. The lyotropic effect on the charge density at the shear plane becomes more 'visible' when the double layer is more and more located on the outer side of the charges. At the same time the collapse of the Δ-layer ensures that the masking effect of anomalous conduction on it is reduced (see section 4.6.3 and chapter 6). Apparently Cs^+, by adsorbing better than K^+ and Li^+ in the Stern layer, screens the fixed charges better and consequently less countercharge seems to be involved in the tangential movement of the solvent. The results suggest that the shear surface coincides with the OHP or is located in close proximity to it. The relative large σ_{ek} for Li^+ as compared to Cs^+, suggests that little, if any, transfer of Li^+-ions from the diffuse region of the double layer into the OHP occurs. The observed sequence in σ_{ek} has been found for hydrophobic colloids, which supports the conclusion that for our 'model' system the adhering layer is also thin[60,61].

Upon dilution we notice a more pronounced alkali-specificity in σ_t, suggesting an increasing divergence in specific adsorption of the alkali-ions. It is probable that the increased space between the headgroups, arising from decreasing c, facilitates specific interacton, especially for Cs^+. The Cs^+-ions fit better in the Δ-region of lower effective permittivity than the Li^+-ions. This may agree with a hardly changed or even increased adsorbability of Cs^+ with decreasing ionic strength. However, an increasing divergence in the ionic mobilities in the important Δ-region at low c, may also contribute to the observed trend in the σ_t-ratio. We have to regard the fact that the lower permittivity of the Δ-layer compared to that of the bulk not only influences ion-association but has a drastic effect on ion-mobility.

An increased ion-association does not necessarily have to result in a reduction of the mobility. If the adsorption is accompanied by a decrease in the degree of hydration of the cations and the distance between neighbouring charges is small (low energy barrier; non-localized adsorption) it is not improbable that these ions retain their mobility or even exhibit an increased mobility in the tangential direction. This picture is seemingly substantiated by the Li^+-results. On increasing the charge density the observed trend in the alkali-ion sequence is more pronounced.

This may point to the fact that the Cs^+-specificity is progressive with σ_o.

The effect of treatment. Because of the absence of relevant experimental results for Cs^+ we have only compared the results for Li^+ and K^+ before and after treatment. The slightly lower σ_t^{Li}/σ_t^K-data for L and M in the low c-range before treatment (lower σ_o) are in agreement with the observed effect of σ_o on ion-specificity. From the proportional increase of c_{ICP} upon treatment, discussed in section 5.7.8, a small alkali-specificity was noted. Apparently, less hydrated cations are more effective in the salting-out process and liberation of ion-paired cations. We may, therefore, expect a small alkali ion-specificity in the location of the shear surface too.

5.8.1.4 *Temperature effect; activation energy of conductance*

The activation energies* of conductance for treated plugs have been calculated from the linear relationships of log K_s (K_s is the excess conductivity defined by $F\bar{K}$-K) vs. 1/T (Arrhenius). The results are compared with those of the alkali-ion in the bulk phase. The evaulation of an excess quantity is to be preferred over that of a quantity which may be markedly influenced by the model of conversion. It is easy to verify, e.g., that an evaluation of the activation energy via κ^σ(T)-data (the usual procedure quoted), is *only* justified when the conversion of $\bar{K}$ to κ^σ is correct of the experimental Rel's are temperature independent. The activation energy indicates whether the charge carriers are involved in processes that imply some additional energy barrier. The presence and relative significance of any 'interfacial resistance' to tangential transfer can only be invoked if the involved ions of the excess charge exhibit some mobility. Detection of ions with a considerably depressed mobility is only possible if they constitute a substantial quantity of the excess charge. Of course, the distinction between ions in terms of bounded and mobile charge is entirely arbitrary in that on a time average basis, all ions contribute equally to the conductance. An interpretation of κ^σ-data in terms of an ordinary rate process may be largely specula-

* According to Arrhenius we can define the activation energy by:
$-\frac{\delta}{\delta T}(\ln D^\sigma)_p = -E_A/(RT^2)$. From eq. (5-40) we can derive:
$-\frac{\delta}{\delta T}(\ln D^\sigma)_p = (\Delta H^* + RT)/(RT^2)$. Apparently, $E_A = \Delta H^* + RT$.
The difference of E_A with ΔH^* often falls far within the experimental accuracy of the measurement of E_A.

tive. The surface diffusion coefficient, readily obtained from κ^{σ}, is related to the jumping distance d by the well-known formula[62]:

$$D^{\sigma} = A\ T\ \exp(-\Delta H^*/RT)\ \exp(\Delta S^*/R)\ d^2 \qquad (5\text{-}40)$$

where ΔS^* is the entropy of activation for the diffusion process, the activated state referring to an ion between two neighbouring sites. A is a constant and ΔH^* the activation enthalpy. As already stated it seems reasonable to suppose that an ion, adsorbed at an exchange site, is in a partially dehydrated state, in other words, the ion-solvent association is less intimate than ion solvation in the bulk. When jumping from one position to another, the ion moves through a region in which its surrounding water molecules are liable to be reoriented, the activated state corresponding to the solvated state of the ion. It seems obvious, that the loss of degrees of freedom of water, taken up by the Li^+-ion, will be smaller when the water is taken from the Δ-region, where it has already lost some degrees of freedom. Furthermore, the concept of close-packed exchange sites in the patches implies small jumping distances.

For comparison purposes experimental results of L and H are presented in fig. 5-12 as activation energy-ratios. For L at $c > 10^{-3}$M the low σ_o

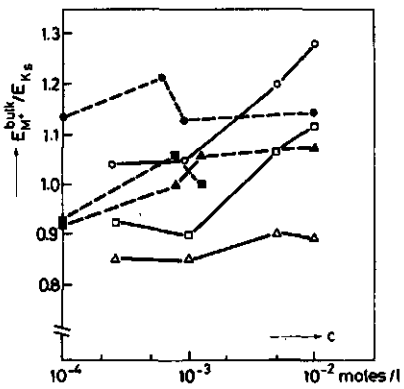

Fig. 5-12. The ratio of the activation energy of the specific ionconductivity in solution, E_M^{bulk} and of the excess conductivity E_{K_s} vs. ionic strength.

L : Li^+ ● ; K^+ ■ ; Cs^+ ▲
H : Li^+ ○ ; K^+ □ ; Cs^+ △

E_M^{bulk} is calculated from molar conductivity data, tabulated by Parsons[43].

(and therefore K_s) impedes an accurate determination of the E-ratio. These results are therefore less reliable. From the remaining results the most notable features are:

I the lyotropic sequence fits well into the specific surface conductance results given above: The relative increase of E_{K_s} with respect to the activation energy values in the bulk, observed in the sequence Li^+, K^+, Cs^+, irrespective σ_o, suggest an increase in specific adsorption of the ions going from Li^+ to Cs^+. The σ_t-values increase

also in the order given, which could in turn be attributed to the above mentioned sequence in the specific adsorption,

II increasing σ_o results in increasing E_{K_s}, suggesting enhanced counterion adsorption,

III the decrease of activation energy of the excess conductivity (rise in the E-ratio) upon increasing c for Li^+ and K^+ in case of high σ_o may be related to the shrinkage of the Δ-layer. An increase in hydration of the Li^+ and K^+ ions 'liberated' from that layer corresponds, apparently, with a less intimate interaction with the endgroups. This picture does not apply to the barely hydrated Cs^+-ions. The decrease in the σ_t-ratios noticed in fig. 5-11 may therefore also be interpreted in terms of an increased hydrodynamic radius. At higher c (> 10^{-2}M) we expect finally a decrease of the E-ratio due to an increase of specific adsorption. Low values for the activation energy of surface conductance for monovalent electrolytes are often noted in the literature. Kittaka and Morimoto found for NaCl and even $MgCl_2$ on slica, E-values less than those in the corresponding bulk solution. These results were explained by stating that high mobilities of adsorbed ions arise from their small radii in the adsorbed state in co-operation with the relatively weak adsorption forces present.

The effect of treatment. Only for L at 10^{-3}M were activation energies determined. The E-ratios are: for Li^+ 1.05 and for K^+ 0.95. Both values are lower than those of the treated plugs; however, as already stated for L the results are inaccurate for c >·10^{-3}M.

Additional modes of charge transfer. When discussing κ^σ-data one must take into consideration possible additional modes of change transfer. The L particles bear so little charge, that their surfaces, especially in view of the patch-concept, are essentially hydrophobic. The hydrophobic parts could display a charging process if 'selective adsorption' of one of the ions in the waterphase occurs[63]. A desorption rather than an adsorption is suggested by the fact that simple electrolytes raise the interfacial tension of water against organic surfaces[64,65]; consequently from the Gibbs adsorption equation negative adsorption is inferred. As cations are usually more hydrated than anions, they are unable to approach the interface as closely as the latter and a negative charge is produced at the hydrophobic sites[66]. Electrophoresis measurements seem to confirm this theory. The pH-dependence of the zeta-potential of polyethylene, teflon and paraffin points to the potential determining role of $\overset{+}{H}$ and $O\overset{-}{H}$ ions[61,67,68]. The idea that sorbed water undergoes greater dissociation

is quoted by many authors[67,69]. However, in our case specific surface conductance results at high pH did not reflect a drop in κ^{σ}, corresponding to an elimination of H^{+}-ions in close proximity to the surface.

An analysis of the actual charging mechanism is often impeded by effects of dissociation of small traces inorganic impurities (residues of polymerization catalysts, etc.) and the effect of oxygen-containing groups that result from oxidation[61]. Anyhow, in most cases conversion of the zeta-potential of 'clean' organic substances into charge densities reveals values hardly surpassing some tenths of a $\mu C/cm^2$.

A particular difference between the unsaturated benzene rings in polystyrene and saturated hydrocarbons is the slightly hydrophilic property of the former[71,72]. An interaction between the water dipoles and the induced dipoles in the benzene rings leads to mutual attraction. This may explain the relative ease with which the hydrophobic/water interphase is enlarged by the protrusion of the polystyrene chains.

Combining these facts and considerations with the findings that specific Cl^{-}-adsorption in the low c-range ($< 5\ 10^{-3}$M) is negligible justifies the above mentioned possibility of charge transfer to be not worthy of further consideration.

5.8.1.5 *The thickness of the Δ-layer*

It is possible to estimate the thickness of the Δ-layer, assuming that the potential profile in this region still obeys the Gouy-Chapman theory. For a flat double layer, Δ_{G-C} ($\tilde{\psi}_d$, $\tilde{\zeta}$) is given by:

$$\Delta_{G-C} = \ln \left\{ \frac{\tanh \tilde{\psi}_d/4}{\tanh \zeta/4} \right\} /\kappa \qquad (5\text{-}41)$$

$\tilde{\psi}_d$ and ζ are computed from the titration charge density, σ_o, and the streaming current results corrected for double layer overlap, resp. To account for the charging effect for L two σ_o-values were taken as indicated in table 5-9. The higher value gives better agreement with the electrokinetic results. The dashes correspond to σ_{ek}'s exceeding 1 μCcm^{-2}. The effect of treatment on Δ_{G-C} is illustrated for M. The Δ_{G-C} values suggest an unrealistically high thickness of the immobile layer. In section 4.7.3.1 the boundary layer thickness was estimated from the electroviscous effect ($\Delta_{e.v.}$), according to the capillary model of Levine, which was extended to take account of anomalous conduction. The double layer is assumed to be identical to that used for the computation of Δ_{G-C}, which results in a similar picture as noticed for Δ_{G-C}. The results are hardly improved by taking σ_t-values deduced from κ^{σ}, irrespective of the model

Table 5-9. Survey of the main layer thicknesses: Δ_{G-C} is calculated from σ_o-values and corrected zeta-potentials; $\Delta_{e.v.}$ is calculated from the electroviscous effect and Δ_h is determined from hydrodynamic experiments. The Δ_h-data are averaged over the temperatures (15, 25, 35.0°C) and the electrolytes (Li, K, CsCl) given in fig. 4-5. The standards (Δ_h=0) are taken for L 10^{-1}M, M 10^{-1}M and H 10^{-2}M (see section 4.7.2).

L c moles/l	Δ_{G-C} nm σ_o = -2.5 μCcm^{-2} LiCl	KCl	CsCl	σ_o = -1.0 μCcm^{-2} LiCl	KCl	CsCl	$\Delta_{e.v}$ nm KCl	Δ_h nm KCl
10^{-2}	0.53	0.76	0.74	-	-	-	1.5	0
1.25 10^{-3}		2.42	2.40		0.39	0.37		0.72
10^{-3}	2.66			0.62			3.2	
7.8 10^{-4}		2.83	2.87		0.79	0.79		0.82
6.9 10^{-4}	3.48			1.40				
10^{-4}	15.0	12.7	12.7	12.8	10.6	10.6	14	1.04

M c moles/l	Δ_{G-C} nm σ_o = -4.0 μCcm^{-2} untreated LiCl	KCl	treated LiCl	KCl	$\Delta_{e.v}$ nm KCl	Δ_h nm KCl
10^{-2}			0.74	0.82	1.8	0
10^{-3}	5.06	5.38	4.43	4.52	3.0	0.99
2 10^{-4}			15.0	15.5		1.68
10^{-4}					11	
5 10^{-5}			29.7	27.5		

H c moles/l	Δ_{G-C} nm σ_o = -9.0 μCcm^{-2} LiCl	KCl	CsCl	$\Delta_{e.v}$ nm KCl	Δ_h nm KCl
10^{-1}	0.30	0.37	0.44		
10^{-2}	0.97	1.00	1.07	1.5	0
5 10^{-3}	1.42	1.47	1.37		0.59
10^{-3}	3.38	3.46	3.07	2.1	1.21
2.6 10^{-4}	8.30	9.10	8.17		1.59
10^{-4}				8.6	

used for conversion ($\bar{K} \rightarrow \kappa^{\sigma}$). The effective hydrodynamic layer thickness, Δ_h, exhibits a much more acceptable picture at low c. However, by comparing the molecular radius of the hydrated sulphate endgroups ($OS\bar{O}_3$ 0.29 nm; H_2O 0.138 nm) with the Δ_h-values one is forced to conclude that the extent to which the polystyrene chains protrude is substantial. The patch-concept may be of importance for elucidating the hydrodynamic results. It is found that a 9-fold increase in charge density hardly affects the effective thickness Δ_h. A patchwise distribution of charged groups might be expected to produce a pronounced surface roughness and this would be particularly apparent for sample L at low c. This may increase the hydrodynamic resistance of a sphere unit more effectively than in the case of a homogeneous distribution (smooth sphere).

5.8.2 *Dilute dispersions; results and discussion*

In fig. 5-13 a,b,c the charge distribution is presented as a function of the electrolyte concentration for L, M and H, calculated according to the D-S theory. The σ_t-values were calculated from p-averaged κ^{σ}-data. The σ_{Δ}-values were obtained on the basis of the procedure outlined for plugs. The results for LiCl are tabulated in appendix 5B. The general agreement of the σ-results with those for untreated plugs is remarkably good and believed to be very meaningful, especially since the results were obtained by different methods and theories. The finding that σ_{Δ}(L) becomes negative for higher c is a result of underestimation of κ^{σ} in the D-S formula. For that particular c-range σ_{ek} surpasses the calculated σ_t-values. As already discussed, the excess conductivity for low p-

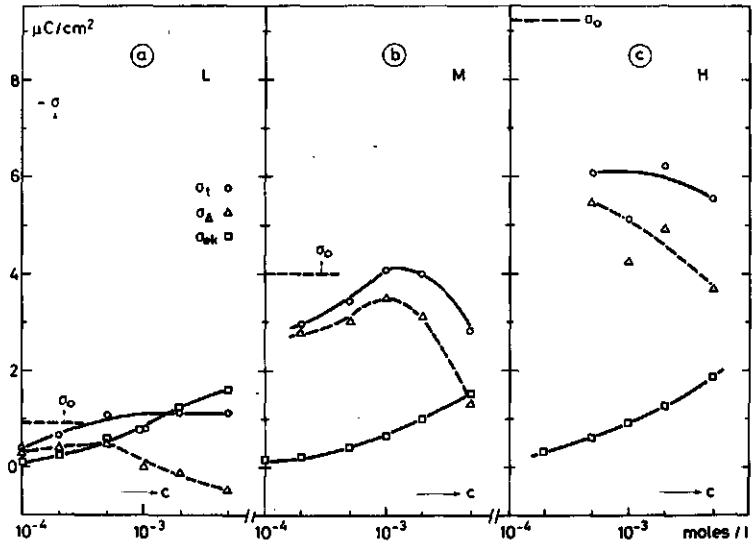

Fig. 5-13 a,b,c. The charge density distribution versus C(KCl) for dilute L, M and H dispersions ($p \leq 0.1$) according to D-S. $t = 25.0^{o}C$.

values is highly sensitive to many (systematic) errors, limiting application over a more extended c-range. It is possible that the sudden decrease of σ_t (and therefore σ_Δ) for $c > 10^{-3}$M can be attributed to some artifact in the determination of $\bar{K}$ and K. A further increase in experimental accuracy is, therefore, imperative.

To all complex factors involved in the experimental and theoretical treatment of latex dispersions we may add the patch-concept. It is clear that for a sphere, the polarized charge of which is distributed in local patches, the mobile charge is more effectively reduced. In that case the polarization intensity of the total particle should not be estimated from the parameter $Rel = \kappa^{\sigma}/(Ka)$ but from $Rel = \kappa^{\sigma}/(Ka_p)$, where a_p is related to the dimensions of the patches. A patchlike distribution enhances polarization, resulting in a decrease of the electrokinetic charge. The latter effect results in an apparent ion-specificity because the relaxation of the ion-atmosphere increases with decreasing ionic mobility, unless differences in mobility of the ions are cancelled due to specific effects in the interfacial layer, as in our case.

5.9 *Summary*

Electroconductivity results on dilute and concentrated dispersions of monodisperse polystyrene particles are analysed in terms of polarization theories and the Street equation. Some of the polarization models incorporate the double layer polarization concept of Dukhin and Seminikhin. The surface conductance data obtained from the various models are compared with the Bikerman predictions.

The presented results demonstrate, that for all three surface charge densities investigated the D-S equation, accounting for the concentration polarization effect, presents a rather satisfactory description of dilute particle dispersions ($p \leqslant 0.1$). On the other hand, the 'classical' Bruggeman equation proves to be useful for evaluation of double layer properties in concentrated dispersions ($p \approx 0.6$) over an extended electrolyte concentration range. It appears, that concentrating a particle dispersion suppresses the effect of double layer polarization. Due to overlap of the ion-rich layers near the contact points of the spheres, the particles are electrically short-circuited. This keeps the conductivity finite as the ionic strength approaches zero; consequently all polarization models finally underestimate the conductivity of a concentrated dispersion upon decreasing ionic strength.

The results of the dilute dispersions constitute fair proof for the correct evaluation of the electrode polarization and the presented titration procedure; furthermore, they demonstrate the necessity to correct

the conductivity of the suspending electrolyte solution for the effect of negative adsorption. The agreement between surface conductance data, obtained at high frequency according to the H-B equation and those obtained at low frequency according to the D-S equation, lends support to the description of the concentration polarization mechanism.

For dilute dispersions and plugs the occurrence of an isoconductance point is established. It appears that in case of untreated latex dispersions the ICP is reasonably constant for p-values up to 0.1. It is argued that the ICP increase observed upon concentrating the dispersion, is not only a result of the short-circuiting effect but for a limited part also of an additional charging effect.

The combined results of the electrokinetic, electroconducting and hydrodynamic studies clearly show the strong deviation from 'model behaviour' of our latex samples. The 'hydrodynamically immobilized' part of the countercharge *increases* upon diluting the solution, an observation clashing with common double layer knowledge. Upon decreasing the ionic strength the electrokinetic charge density decreases sharply for all latex samples, whereas the net contribution of the countercharge remains to the surface conductance more or less constant. The 'hairy layer' model (Δ-layer) is used to explain these peculiar findings. Upon increase of the ionic strength the protruding polystyrene chains are salted out; the shear surface, coinciding with the surface enveloping the endgroups of the most protruded chains, shifts inwardly; the counterions that originally are accommodated between the headgroups and chains distribute themselves increasingly on the outside of the shear plane where they become electrokinetically 'visible'. Especially for the lowest surface charge, it is assumed that the charged groups are distributed patch-wise, providing the enhanced mutual repulsion required for a substantial protrusion of the polystyrene chains.

For all three surface charge densities a remarkable charging effect was observed. A first contact with high ionic strength causes shrinkage of the charge polystyrene patches; the permittivity of the innermost regions increases, ion-paired groups are activated and contribute to the surface conductance. Irreversible structural rearrangements in the Δ-layer, accompanying this salting out process, are responsible for the fact that upon subsequent dilution of the electrolyte a larger fraction of end-groups remains active.

For the surface conductance and the activation energy of conductance an alkali-specificity is noticed. The relative increase of the activation energy in the sequence Li^+, K^+, Cs^+ is explained by an increase of specific adsorption in the same sequence. The surface conductance data confirm

the observed sequence. The concentration dependent surface diffusion of the ions, especially substantial for Li^+, is strongly related to the shrinkage of the Δ-layer. The relative large surface diffusivity of the Li^+-ions at low c is explained by the relative low permittivity of the Δ-layer. When jumping in the Δ-layer from one adsorption site to another, the loss of degrees of freedom of water, taken up by the Li^+-ions from the Δ-layer, is relatively low.

5.10 *References*

1. S. Levine, G. Neale and N. Epstein, J. Colloid Interface Sci. 57, 424 (1976)
2. S.S. Dukhin and N.M. Seminikhin, Kolloidn. Zh. 32, 360 (1970)
3. H. Pilgrimm, H. Sonntag and S.S. Dukhin, Colloid & Polymer Sci. 253, 750 (1975)
4. H. Sonntag and H. Pilgrimm, Progr. Colloid & Polymer Sci. 61, 87 (1976)
5. D.K. Briggs, J. Phys. Chem. 32, 641 (1928)
6. G.E. Archie, Trans. A.I.M.E. 146, 54 (1942)
7. P.H. Zhukov and D.A. Fridriksberg, Kolloidn. Zh. 11, 163 (1949)
8. N. Street, Aust. J. Chem. 9, 333 (1956); 10, 207 (1957)
9. A.K. Helmy, J. Electroanal. Chem. 52, 287 (1974)
10. S.S. Dukhin and B.V. Derjaguin, in 'Surface and Colloid Science' Vol. 7, E. Matijević Ed., Wiley, New York, chapter 2, p. 214 (1974)
11. H.F. Holmes, C.S. Shoup Jr. and C.H. Secoy, J. Phys. Chem. 69, 3148 (1965)
12. C.J.F. Böttcher and P. Bordewijk, 'Theory of electric polarization', Vol. I, Elsevier, Amsterdam (1978)
13. J.C. Maxwell, A treatise on electricity and magnetism, 2nd ed., Vol I, p. 435, Clarendon Press, Oxford (1881)
14. R.E. Meredith and C.W. Tobias, J. Electrochem. Soc. 108, 286 (1961)
15. K.W. Wagner, Arch. Elektrotech. 2, 371 (1914)
16. W.R. Raleigh, 'On the influence of obstacles arranged in a rectangular order upon the properties of a medium', Phil. Mag., 5th Ser., 34, 481 (1892)
17. C.J.F. Böttcher, Rec. Trav. Chim. 64, 47 (1945)
18. D.A.G. Bruggeman, Ann. Physik. 24, 636 (1935)
19. R.E. Meredith and C.W. Tobias, 'Advances in electrochemistry and electrochemical engineering', Interscience, New York, Vol. 2, Ch. II, p. 15 (1962)
20. Ref. 19, p. 24.
21. R.D. Günther and D. Heinrich, Z. Phys. 185, 345 (1965)
22. W.F. Brown, J. Chem. Phys. 23, 1514 (1955)
23. A. Slawinski, J. Chim. Phys. 23, 710 (1926)
24. Ref. 10, p. 34.
25. S.S. Dukhin and N.M. Seminikhin, Kolloidn. Zh. 32, 360 (1970); Ref. 3 and Ref. 10, chapter 3.
26. P.H. Wiersema, Thesis, Utrecht, The Netherlands, 1964; P.H. Wiersema, A.L. Loeb and J.Th.G. Overbeek, J. Colloid Interface Sci. 22, 78 (1966)
27. Ref. 10, p. 227.
28. D.C. Henry, Trans. Faraday Soc. 44, 1021 (1948)
29. F. Booth, Trans. Faraday Soc. 44, 955 (1948)
30. C.T. O'Konski, J. Chem. Phys. 64, 605 (1960)
31. H. Fricke and H.J. Curtis, J. Phys. Chem. 40, 715 (1936)
32. N. Street, Soil Sci. 95, 367 (1963)
33. A. Watillon and J. Stone-Masui, J. Electroanal. Chem. 37, 143 (1972)
34. M.M. Springer, Thesis, Wageningen (1976)
35. S.S. Dukhin and V.N. Shilov, 'Dielectric phenomena and the double layer polarization in disperse systems and polyelectrolytes', Wiley, New York (1974)
36. G. Schwarz, J. Phys. Chem. 66, 2636 (1962)
37. J.M. Schurr, J. Phys. Chem. 68, 2407 (1964)
38. V.N. Shilov and S.S. Dukhin, Kolloidn. Zh. 32, 293 (1970); Ref. 35.

39. M.H. Wright and A.M. James, Kolloid-Z. u. Z. Polymere 251, 745 (1973)
40. M.H. Wright, G.E. Nichols and A.M. James, Kolloid-Z. u. Z. Polymere 245, 525 (1971)
41. D. Rosen, in 'A Laboratory Manual of Analytical Methods of Protein Chemistry', Vol. 4, P. Alexander and H.P. Lundgren Eds., Pergamon Press, Oxford (1966)
42. H.P. Schwan, Biophysik 3, 181 (1966)
43. R. Parsons, Handbook of electrochemical constants, Butterworths, London (1959)
44. H.J. van den Hul and J.W. Vanderhoff, J. Colloid Interface Sci. 28, 336 (1968)
45. A.M. James and M.N.A. Carter, J. Colloid Interface Sci. 29, 696 (1969)
46. Ref. 10, p. 239.
47. H.J. van den Hul and J. Lyklema, J. Colloid Interface Sci. 23, 500 (1967)
48. A.L. Loeb, P.H. Wiersema and J.Th.G. Overbeek, 'The electrical double layer around a spherical colloid particle', M.I.T. Press, Cambridge, Mass. (1960)
49. R.K. Schofield, Trans. Brit. Ceram. Soc. 48, 207 (1949)
50. C. Tanford, 'The hydrophobic effect', Wiley-Interscience, New York (1973)
51. D. Stigter, J. Phys. Chem. 68, 3603 (1964)
52. J.T. Davies and E.K. Rideal, Interfacial Phenomena, Academic Press, New York (1961)
53. D.A. Haydon and F.H. Taylor, Philos. Trans. A258, 285 (1960)
54. H. Morawetz, Macromolecules in solution, Interscience Publ., New York (1965)
55. B.W. Brooks, Brit. Polymer J. 3, 269 (1971)
56. J. Stone-Masui and A. Watillon, J. Colloid Interface Sci. 52, 479 (1975)
57. W. Norde, Thesis, Agricultural University, Wageningen (1976)
58. R.H. Ottewill and J.N. Shaw, Kolloid-Z. u. Z. Polymere 218, 34 (1967)
59. Ref. 56, section 2.3.5.
60. B.H. Bysterbosch and J. Lyklema, Adv. Colloid Interface Sci. 9, 147 (1978)
61. P. Benes and M. Paulenová, Kolloid-Z. u. Z. Polymere 251, 766 (1973)
62. S. Glasstone, K.S. Laidler and H. Eyring, The theory of rate processes, Mc Graw Hill, New York (1941)
63. A.S. Taylor and F.W. Wood, Trans. Faraday Soc. 63, 523 (1957)
64. J.T. Davies and E.K. Rideal, 'Interfacial Phenomena', Acad. Press, New York and London, p. 148 (1963)
65. D.A. Haydon, 'Surface Science I', J.F. Danielli, K.G. Pankhurst and A.C. Riddiford Eds., Acad. Press, New York and London, p. 147 (1964)
66. J.E. Randles, Disc. Faraday Soc. 24, 194 (1957)
67. H.C. Parreira and J.H. Schulman, Adv. Chem. Ser. 33, 160 (1961)
68. I.A. Skulskii and V.V. Glazunov, Radiokhimiya 7, 703 (1965)
69. M. Tschapek, R. Santamaria and I. Natale, Electrochim. Acta 14, 889 (1969)
70. J.C. Kirkwood and J.B. Shumaker, Proc. Natl. Acad. Sci. U.S. 38, 855 (1952)
71. R.H. Boundy and R.F. Boyer, 'Styrene', Reinhold Publ., New York, p. 550 (1952)
72. R.F. Field, J. Appl. Phys. 17, 318 (1946)

Appendix 5A

The charge distribution as a function of the electrolyte concentrations for different conditions of surface charge density, nature of electrolyte and temperature

In table 5A-1 through 5A-3, σ_t-results according to HB-I (Bruggeman) are classified in two groups, viz. untreated and treated plugs. The sequence in concentrations does not necessarily correspond with the experimental one; in the case of untreated plugs the actual sequence is from low to high c (MCl), whereas for the treated plugs the experimental sequence appears to be unimportant.

The σ_{ek}-results are calculated from zeta-potential values obtained by the streaming current method and corrected for double layer overlap (section 4.6.5).

Table 5A-1. The charge distribution for L plugs. The results of IIIA and IIIB correspond to one plug. In all other cases different numbers correspond to different plugs. The negative values for σ_Δ in case of plug VB (10^{-2}M KCl) at 15.0°C and 25.0°C are in all probability caused by experimental errors (see for comparison all other σ_Δ-results at 10^{-2}M MCl).

	- untreated -			- treated -		
L	(IIIA): KCl 25.0°C			(IIIB) 25.0°C		
c moles/l	$-\sigma_{ek}$	$-\sigma_\Delta$	$-\sigma_t$	$-\sigma_{ek}$	$-\sigma_\Delta$	$-\sigma_t$
		$\mu C/cm^2$			$\mu C/cm^2$	
$3\ 10^{-1}$	2.62					
$2\ 10^{-1}$	2.42					
10^{-1}	2.31			2.27		
10^{-2}	1.84	0.478	2.32	1.89	0.469	2.36
10^{-3}	0.776	0.721	1.50	1.01	1.028	2.04
$2\ 10^{-4}$	0.259	0.789	1.05	0.378	1.765	2.14

- untreated -

L (VIA): LiCl	15.0°C			25.0°C			35.0°C		
c moles/l	$-\sigma_{ek}$	$-\sigma_{\Delta}$	$-\sigma_t$	$-\sigma_{ek}$	$-\sigma_{\Delta}$	$-\sigma_t$	$-\sigma_{ek}$	$-\sigma_{\Delta}$	$-\sigma_t$
$5.66\ 10^{-4}$				0.661	1.50	2.16			
10^{-3}	0.837	1.305	2.14	0.815	1.266	2.08	0.841	1.312	2.16
L (VIB): KCl									
$6.46\ 10^{-4}$				0.610	1.12	1.73			
10^{-3}	0.815	0.756	1,57	0.789	0.792	1.58	0.817	0.849	1.67

- treated -

L (VA): LiCl	15.0°C			25.0°C			35.0°C		
c moles/l	$-\sigma_{ek}$	$-\sigma_{\Delta}$	$-\sigma_t$	$-\sigma_{ek}$	$-\sigma_{\Delta}$	$-\sigma_t$	$-\sigma_{ek}$	$-\sigma_{\Delta}$	$-\sigma_t$
10^{-1}	2.18			2.22			2.24		
10^{-2}	1.89	0.869	2.76	1.75	0.065	2.62	1.73	0.898	2.63
$9.55\ 10^{-4}$	0.862	1.733	2.60	0.849	1.61	2.46	0.823	1.632	2.46
$6.86\ 10^{-4}$	0.730	1.98	2.71	0.707	1.86	2.57	0.679	1.805	2.48
10^{-4}	0.201	5.40	5.60	0.208	4.68	4.69	0.195	5.09	5.29
L (VB): KCl									
10^{-1}	2.11			2.16			2.15		
10^{-2}	1.58	-0.087	1.49	1.54	-0.393	1.15	1.55	0.432	1.98
$1.25\ 10^{-3}$	0.909	1.21	2.12	0.900	1.131	2.03	0.911	1.16	2.07
$7.65\ 10^{-4}$	0.771	1.49	2.26	0.761	1.442	2.20	0.700	1.40	2.10
10^{-4}	0.219	2.91	3.13	0.243	3.07	3.31	0.259	3.30	3.56
L (VC): CsCl									
10^{-1}	1.88			1.93			1.96		
10^{-2}	1.60	0.742	2.34	1.56	0.564	2.12	1.61	0.584	2.19
$1.25\ 10^{-3}$	0.895	1.03	1.93	0.903	1.004	1.91	0.883	1.04	1.92
$7.85\ 10^{-4}$	0.771	1.30	2.07	0.750	1.29	2.04	0.730	1.30	2.03
10^{-4}	0.209	2.41	2.62	0.243	2.79	3.03	0.258	2.74	3.00

Table 5A-2. The charge distribution for M plugs.

	- untreated -				- treated -		
M (VIIIA): LiCl 25.0°C							
c moles/l	$-\sigma_{ek}$	$-\sigma_{\Delta}$	$-\sigma_{t}$	c moles/l	$-\sigma_{ek}$	$-\sigma_{\Delta}$	$-\sigma_{t}$
10^{-1}	4.21			10^{-3}	0.643	5.34	5.98
10^{-2}	2.07	3.31	5.38	$2\ 10^{-4}$	0.206	6.70	6.91
10^{-3}	0.562	3.70	4.26	$6.6\ 10^{-5}$	0.123	15.9	16.0
M (VIIIB): KCl 25.0°C							
10^{-1}	4.00			10^{-3}	0.626	4.13	4.76
10^{-2}	1.98	2.61	4.59	$2\ 10^{-4}$	0.199	4.85	5.05
10^{-3}	0.531	2.49	3.02	$4\ 10^{-5}$	0.105	-	-

Table 5A-3. The charge distribution for H plugs.

	- untreated -					
H (VIIA): LiCl 25.0°C				(VIIB): KCl 25.0°C		
c moles/l	$-\sigma_{ek}$	$-\sigma_{\Delta}$	$-\sigma_{t}$	$-\sigma_{ek}$	$-\sigma_{\Delta}$	$-\sigma_{t}$
$5\ 10^{-3}$	1.85	3.96	5.81	1.80	3.73	5.53
10^{-3}	0.716	5.08	5.80	0.741	4.28	5.02

- treated -

H (VIIA): LiCl	15.0°C			25.0°C			35.0°C		
c moles/l	$-\sigma_{ek}$	$-\sigma_{\Delta}$	$-\sigma_{t}$	$-\sigma_{ek}$	$-\sigma_{\Delta}$	$-\sigma_{t}$	$-\sigma_{ek}$	$-\sigma_{\Delta}$	$-\sigma_{t}$
$2\ 10^{-1}$	5.25			5.31			5.27		
10^{-1}	4.72			4.70			4.49		
10^{-2}	2.61	5.11	7.72	2.52	4.72	7.24	2.47	4.48	6.95
$5\ 10^{-3}$	2.02	5.49	7.51	1.91	5.38	7.29	1.86	5.05	6.91
$0.92\ 10^{-3}$	0.897	7.79	8.69	0.889	7.87	8.76	0.943	7.69	8.63
$2.44\ 10^{-4}$	0.357	10.31	10.7	0.387	11.15	11.5	0.407	11.01	11.4
H (VIIB): KCl									
$2\ 10^{-1}$	4.90			4.97			4.81		
10^{-1}	4.38			4.22			4.20		
10^{-2}	2.50	4.08	6.58	2.47	3.86	6.33	2.42	3.86	6.28
$5\ 10^{-3}$	1.94	4.33	6.27	1.86	4.27	6.13	1.86	4.18	6.04
10^{-3}	0.927	5.59	6.52	0.900	5.71	6.61	0.961	5.83	6.79
$2.65\ 10^{-4}$	0.366	6.92	7.29	0.367	6.61	6.98	0.379	6.96	7.34
H (VIIC): CsCl									
$2\ 10^{-1}$	4.05			4.16			4.10		
10^{-1}	3.70			3.78			3.76		
10^{-2}	2.37	3.07	5.44	2.35	3.19	5.54	2.30	3.34	5.64
$5\ 10^{-3}$	1.94	3.12	5.06	1.96	3.19	5.15	1.96	3.28	5.24
10^{-3}	1.01	4.34	5.35	1.01	4.51	5.52	1.05	4.70	5.75
$2.78\ 10^{-4}$	0.410	4.66	5.07	0.420	4.98	5.40	0.417	5.17	5.59

Appendix 5B

The charge distribution for dilute dispersions.

Table 5B-1. Results for dilute untreated dispersions at 25.0°C according to D-S.
For the conversion of κ^{σ} to σ_t, p-averaged κ^{σ}-data corrected for negative adsorption (on basis of σ_o) are taken.
The dashes correspond to experimental $\tilde{K}/K$-values exceeding the maximum possible values according to the D-S equation.
The electrokinetic charge densities are in some cases determined by interpolation of results present in table 5A-1 through 3. For L the σ_{ek}-results are taken from plug IIIA. Because the σ_{ek}-results for untreated M and H do not cover the whole c-range, some values are taken from treated plugs where it is expected that they hardly differ from the untreated ones. The charge density is expressed in μCcm^{-2}.

	KCl								
	L			M			H		
c moles/l	$-\sigma_{ek}$	$-\sigma_{\Delta}$	$-\sigma_t$	$-\sigma_{ek}$	$-\sigma_{\Delta}$	$-\sigma_t$	$-\sigma_{ek}$	$-\sigma_{\Delta}$	$-\sigma_t$
$5\ 10^{-3}$	1.62	-0.49	1.13	1.52	1.30	2.82	1.86	3.66	5.52
$2\ 10^{-3}$	1.23	-0.09	1.14	0.97	3.01	3.98	1.27	4.92	6.19
10^{-3}	0.78	0	0.78	0.63	3.47	4.10	0.90	4.21	5.11
$5\ 10^{-4}$	0.60	0.488	1.09	0.40	3.01	3.41	0.61	5.45	6.06
$2\ 10^{-4}$	0.26	0.390	0.65	0.20	2.76	2.96	0.30	-	-
10^{-4}	0.10	0.294	0.39	0.14	-	-			
	LiCl								
$5\ 10^{-3}$	1.48	-0.36	1.12				1.91	5.73	7.64
$2\ 10^{-3}$	1.12	-0.27	0.85				1.28	6.89	8.17
10^{-3}	0.86	0.12	0.98				0.93	6.67	7.60
$5\ 10^{-4}$	0.58	0.42	1.00				0.64	7.64	8.28
$2\ 10^{-4}$	0.34	0.48	0.82				0.32	-	-
10^{-4}	0.21	0.45	0.66						

CHAPTER 6

ELECTROPHORESIS OF POLYSTYRENE LATICES

6.1 *Introduction*

The discussion in previous chapters has shown that there are several methods for obtaining electrokinetic potentials and charge densities. However, these quantitities can only be obtained correctly on the basis of formulae which incorporate simultaneously the effects of double layer polarization, double layer overlap and anomalous conduction. From an analysis of the electrokinetic results on plugs we can infer that the effect of double layer polarization on streaming currents is small, whereas the other two factors can be accounted for. Recent developments in the polarization theory for electrophoresis (Dukhin, Semenikhin[5-9]) allow the verification of the plug results in an independent way. The electrophoresis technique has the advantage that the effect of double layer overlap is absent.

6.2 *Basic principles and outline of the electrophoretic study*

Since the theory of electrophoresis is most thoroughly established, this technique is of primary interest for suspensions of spherical particles. In case the double layer of spherical particles can be described with sufficient rigor by the Gouy-Chapman theory and in absence of anomalous surface condition, the Wiersema-Loeb-Overbeek (W.L.O.) method[1] of determining zeta-potentials is the most complete treatment available. The absence of anomalous conduction implies that no charge transfer between the shear plane and the particle surface takes place.

In the studies of Henry[2], Overbeek[3] and Booth[4] about the variation of Smoluchowski's equation with κa, mathematical complications limited the validity of their results to low potentials ($\zeta < 25$ mV). Therefore, W.L.O. made a more detailed analysis of all the forces acting on a spherical particle during electrophoresis for moderate potentials, and they found that the relaxation and retardation effects are particularly pronounced for κa values between 0.2 and 50.* Their solutions are summarized

* At intermediate κa values, where sphere and double layer are of comparable size, the e.m. is significantly lowered by two effects. The electric field exerts on the ions in the atmosphere a force which is transferred to the solvent molecules. The resulting flow causes a retarding force on the sphere (electrophoretic retardation). The centre of the ionic atmosphere lags behind that of the moving particle, creating another retarding force (relaxation effect).

in elaborate tables and graphs. For a detailed discussion of the relevant theory and the methods of calculating zeta-potentials one is referred to Overbeek and Wiersema[1] and Dukhin[5].

The recent analytical approach for solid spherical particles with a relatively thin double layer is of special importance (Dukhin, Semenikhin[5-9]). The mathematical simplification of the thin double layer enabled D. and S.[7] also to extend their analytical approach to cases in which the shear plane does not coincide with the particle surface. They took into account the effect of tangential ion transfer through the layer near the wall upon the polarization. Furthermore, a change in mobility of the ions was considered by introduction of the parameter $p_\Delta^\pm = D_\Delta^\pm/D^\pm$, where $D_\Delta^\pm$ denotes the ionic diffusion coefficients in the boundary layer of thickness $\Delta(\psi_d, \zeta)$ and $D^\pm$ refers to the bulk. It is noted that their derivation is also based on the Gouy-Chapman model. The complete representation for the dimensionless electrophoretic mobility in case of monovalent electrolytes is given by[7]:

$$\tilde{u}_{ef}(\tilde{\psi}_d, \tilde{\zeta}, p_\Delta, \kappa a) = \frac{3}{2}\tilde{\zeta} -$$

$$\frac{3}{2}\,\frac{\tilde{\zeta}\{4(1+3m)\sinh^2\tilde{\zeta}/4 + 2g_1\}+\{2(1+3m)\sinh\tilde{\zeta}/2 - 3m\tilde{\zeta} + 2g_2\}\,4\ln(\cosh\tilde{\zeta}/4)}{\kappa a + 8(1+3m)\sinh^2\tilde{\zeta}/4 - 24m\,\ln(\cosh\tilde{\zeta}/4) + 4g_1} \qquad (6\text{-}1)$$

where $g_1 = p_\Delta\,(\cosh\tilde{\psi}_d/2 - \cosh\tilde{\zeta}/2)$; $g_2 = p_\Delta\,(\sinh\tilde{\psi}_d/2 - \sinh\tilde{\zeta}/2)$

$$p_\Delta^+ = p_\Delta^- = p_\Delta; \qquad m = m^\pm = \frac{2\varepsilon_o\varepsilon_r}{3\eta\,D^\pm}\left(\frac{kT}{e}\right)^2$$

$\tilde{u}_{ef}$ is related to the electrophoretic mobility UX^{-1} (velocity, U, per unit field strength, X) by:

$$\tilde{u}_{ef} = \frac{3\,\eta\,e}{2\varepsilon_o\varepsilon_r kT}\,\frac{U}{X}$$

The other symbols have their usual meaning.

For comparison with Wiersema's numerical results it is sufficient to substitute $\tilde{\psi}_d = \tilde{\zeta}$. Excellent agreement was already obtained for $\kappa a > 20$; furthermore, the existence of maxima in the $\tilde{u}_{ef}(\tilde{\zeta})$-curves could now be checked at higher κa-values, which was not possible with the numerical calculations[5]. Analytical formulae for $m^+ \neq m^-$ and for bivalent electrolytes are given in the original literature[5-9]. The theoretical results are rather difficult to verify quantitatively because ζ cannot be measured directly. Wiersema[1] and Dukhin and Semenikhin[7] did find some

justification for their theoretical results for $\tilde{\psi}_d = \tilde{\zeta}$ in available data on electrophoresis in the critical κa-region and in most cases this maximum was in good agreement with respect to κa and $\tilde{\zeta}$ with the maximum $\tilde{u}_{ef}$ predicted by the W.L.O. theory. However, some experiments with AgI-sols and polystyrene latices gave certain high mobilities which slightly exceeded the theoretical values. Semenikhin[9] demonstrated that the numerical results and the analytical expression underestimate $\tilde{u}_{ef}$ for $\tilde{\zeta} \geqslant 6$ ($\kappa a \geqslant 50$). In recent years experimental verifications of the effect of polarization of the double layer have much been favored by the availability of monodisperse suspensions of solid spherical particles. Since there is a minimum of two independent parameters ($\tilde{\zeta}$ and κa) in the e.m.-formula, it can be tested by varying one of these, when the other is fixed. In several studies one refers to the investigation of the relaxation effect carried out by Ottewill and Shaw[10]. In their paper three polystyrene latices of different diameters were used. In comparing experimental mobilities with theoretical ones calculated according to Wiersema's numerical method, it appeared that the three batches had approximately identical zeta-potentials over an extended κa-range. This was also corroborated by the nearly equal titration charge densities of these fractions. It was therefore concluded that only the relaxation and retardation effects of the ion atmosphere were observed. Semenikhin arrived at the same conclusion by comparing the same experimental results with the analytical formulae. However, a comparison of the experimental results converted into charge densities with the known surface charge density reveals the same peculiar trend as observed for our latices. The electrokinetic charge densities are 0.10 $\mu C\ cm^{-2}$ at $5\ 10^{-5}$ M; 0.48 $\mu C\ cm^{-2}$ at 10^{-3} M; 0.78 $\mu C\ cm^{-2}$ at 10^{-2} M and 1.05 $\mu C\ cm^{-2}$ at $5\ 10^{-2}$ M NaCl resp., whereas the titration charge density amounts to about 6 $\mu C\ cm^{-2}$. This trend is essentially the same as observed for our PS-plugs. In a combined study of surface conductance and electrophoresis on latices, Watillon and Stone-Masui[15] point already to the discrepancy between the surface conductance determined according to the Street equation and the one calculated from electrophoresis experiments. From their results it seems that the thickness of the boundary layer increases drastically with a slight decrease in ionic strength. The zeta-potentials calculated from electrophoresis experiments by Wright and James[16] show even a maximum upon decreasing c, which also points to a sharp decrease in σ_{ek} upon decreasing ionic strength. Consequently, it appeared necessary to consider the effect of anomalous conduction in the interpretation of electrokinetic results. It is tempting to conclude that the carboxylate latices of Watillon and Stone-Masui[15], and of Wright and James[16,17], as well as our sul-

phate latices exhibit the same peculiarities at low ionic strength. The causes underlying the inconsistency have already been discussed in section 5.8. Upon decreasing ionic strength the charge distribution becomes progressively different from the G-C description coinciding with an outward shift of the shear surface. One consequence is that various electrokinetic phenomena are not very sensitive to the surface charge density at low ionic strength. Despite the fact that the actual charge partition near the particle surface deviates from that used in the Dukhin-Semenikhin theory, it should be stipulated that in both cases the mechanism of anomalous conductions is associated with the presence of a boundary layer. It has already been noted that an interpretation of electroconductivity data of dilute polystyrene dispersions on basis of the D-S theory is rather consistent. Apparently the extent of perturbation of an applied electric field in the proximity of the actual particle hardly differs from that of a model particle bearing the same surface charge density and electrokinetic charge density. It is therefore rather attractive to interpret the e.m.-data also in terms of their electrophoresis theory.

6.3 *The effect of anomalous conduction on electrophoresis*

In fig. 6-1 the effect of a difference between ψ_d and ζ on e.m. is illustrated. We have computed the dimensionless electrophoretic mobility, $\tilde{u}_{ef}$, using experimental data of M (σ_o = 4 μC cm^{-2}; a = 305 nm; KCl). A

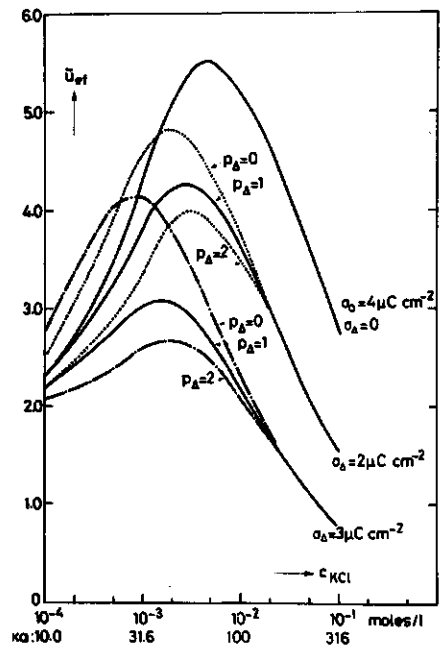

Fig. 6-1. $\tilde{u}_{ef}$ as a function of c for different values of σ_Δ and p_Δ for M at 25.0°C. m = m$^+$(K$^+$) = 0.175.

difference between ψ_d and ζ is presented in terms of σ_Δ, the charge density of the region inside the shear plane. Furthermore, the extent of electromigration in the Δ-layer is indicated with the parameter p_Δ; three cases are considered, viz.

a) all ions in the Δ-layer are immobile (the lines indicated with $p_\Delta = 0$);

b) the ionic mobilities equal those in the bulk ($p_\Delta = 1$); and

c) the mobilities are doubled.

From the latter two cases (solid and dashed lines resp.) it is noticed that tangential charge transfer between shear plane and particle surface reduces the e.m. increasingly upon increasing p_Δ.

The values of $\tilde{u}_{ef}(\tilde{\psi}_d, \tilde{\zeta}, p_\Delta=0)$ computed according to D. and S. agree well with W.'s numerical results for $\kappa a \geqslant 20$.

The following characteristic features are observed:

(i) the outward shift of the shear plane, equivalent with an increase of σ_Δ, shifts $\tilde{u}_{ef}$ to lower values when $p_\Delta \geqslant 0$ and $\kappa a > 10$; high p_Δ's having roughly the same effect as high σ_Δ. The maxima in the $\sigma_o(\sigma_\Delta, p_\Delta)$-curves shift to lower κa-values upon increase of σ_Δ. The effect of p_Δ on $\tilde{u}(\sigma_o, \sigma_\Delta, p_\Delta)$ becomes more marked for greater σ_Δ-values, especially in the intermediate κa-region.

(ii) Wiersema indicated already that at relatively low κa for $\tilde{\psi}_d = \tilde{\zeta}$ the curves $\tilde{u}(\tilde{\zeta})$ pass through maxima; thus two different values of the zeta-potential correspond to an identical value of e.m. A similar behaviour is now observed when σ_Δ is finite. It is clear that with variable p_Δ a large number of $\sigma_o(\sigma_\Delta, p_\Delta)$ combinations can fit one particular e.m. value.

(iii) the convergence of all curves for κa below about 30 makes an accurate experimental verification of relaxation effects with anomalous conduction almost impossible. Generally, when the double layer of an actual particle system cannot be described by the Gouy-Chapman theory with sufficient rigor, although p_Δ and σ_Δ are available, one cannot obtain rigorous proof for the D-S theory, especially not for $\kappa a < 30$, where the accuracy of the analytical formulae becomes unsatisfactory. For the study of the small number of parameters, necessary to describe the effect of anomalous conduction on polarization and electrophoresis, D. and S. proposed (probably inspired by the comments made by Booth[11] and the experimental work of Ottewill and Shaw[10]) a method whereby the e.m. of at least three fractions of monodisperse suspension of spherical particles must be determined at one ionic strength. These fractions must have different diameters but the same surface characteristics: ψ_d and ζ may not depend on the particle size. Then, it is in principle possible to determine simultaneously ψ_d, ζ and p_Δ. However, to obtain some accuracy the results

must cover a rather extended κa-range. The example given in fig. 6-1 clearly shows that these requirements conflict. A determination of p_Δ for κa > 50 becomes inaccurate, whereas experiments for κa < 30 must be omitted. Alternative possibilities of testing the D-S theory would be:

a) determination of $\tilde{u}_{ef}$ for three monovalent electrolytes with greatly differing counterion mobilities. In case no specific ionic effects occur and the three p_Δ's are identical, σ_{ek} and $\sigma_o(\zeta$ and $\psi_d)$ are obtained from an intersection of fitting $\sigma_o(\sigma_\Delta, p_\Delta)$-characteristics. The absence of any intersection or the appearance of additional intersections may point to specific ionic effects and/or different p_Δ-values.

b) creation of an 'artificial' boundary layer by adsorbing polymer on well-characterized particle systems. A suitable choice of polymer-particle system may minimize complicating corrections for the effect of the adsorbed polymer on the distribution of counterions (Brooks[13]);

c) In case the surface charge density is known, $\tilde{u}_{ef}(\sigma_\Delta, p_\Delta)$ characteristics can be calculated. To illustrate the procedure to evaluate $\sigma_{ek}(p_\Delta)$, used in this study, we have plotted theoretical $\tilde{u}_{ef}(\sigma_\Delta, p_\Delta)$-curves for M at 10^{-3} M (κa = 32) in fig. 6-2. From this figure we notice that even at this relatively high κa-value the mobilities as a function of σ_Δ pass through a shallow maximum for p_Δ-values close to zero. At lower κa these maxima become more pronounced; apparently, for fixed p_Δ, two different positions of the shear plane correspond to the same value of $\tilde{u}_{ef}$. At high p_Δ, $\tilde{u}_{ef}$ shifts to lower values, even at extremely small σ_Δ.

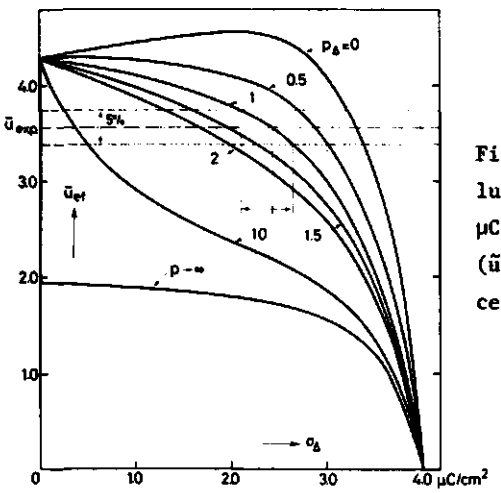

Fig. 6-2. $\tilde{u}_{ef}$ versus σ_Δ for different values of p_Δ at 10^{-2} M KCl; σ_o(M) = 4.00 μC cm^{-2}, t = 25.0°C. An experimental result ($\tilde{u}_{exp.}$) is inserted together with its uncertainty margins (dashed lines).

The effect of the polarization field limits a further decrease of $\tilde{u}_{ef}$ upon increasing σ_Δ even to rather high σ_Δ-values. In this regard it is interesting to note that the formula for the electrophoretic mobility including anomalous surface conductance, obtained by Booth[11] and Henry[12], predicts $\tilde{u}_{ef} = 0$ for $p_\Delta \to \infty$. A graphical representation facilitates the conversion of the confidence limits of the e.m.-data into those of the corresponding $\sigma_{ek}(\sigma_o, p_\Delta)$ results. The relatively low mobilities observed for our latex particles (far below the maximum theoretical values) guaranteed a relatively high accuracy of the $\sigma_{ek}(p_\Delta)$-results for p_Δ-values close to 1. These σ_Δ-values are determined from the intersections of the lines representing experimental mobilities and theoretical $\tilde{u}_{ef}(\sigma_\Delta, p_\Delta)$-characteristics using the relation: $\sigma_{ek}(p_\Delta) = \sigma_o - \sigma_\Delta(p_\Delta)$. An experimental result together with its confidence limits (95%) is shown in fig. 6-2.

6.4 *Experimental*

Measurements of electrophoretic mobilities were performed at 25.0 ± 0.2°C in a Rank Bros MK II microelectrophoresis apparatus, equipped with a thin-walled closed cylindrical cell, platinum electrodes and a constant current source. The velocities of the particles, U, were measured at the two stationary levels (van Gils and Kruyt[14]). At both levels, in both directions at least ten particles were timed and the overall average was taken as the required velocity. The field strength, X, was calculated from the constant current through the cell and the specific conductivity of the sample. The electrophoretic mobility is expressed as U/X. For concentrations of monovalent electrolyte above 5 10^{-4} M the reproducibility of the measurement was better than 95%.

6.5 *Results and discussion*

The first step in determining $\sigma_{ek}(p_\Delta)$ was to select the total charge density giving ψ_d. This value was used for the $\tilde{\zeta}$-potential and substituted in eq. (6-1) for a chosen p_Δ. Next, the calculated $\tilde{u}_{ef}$ was compared to the experimental value. When the two did not match for fixed p_Δ, a new estimate of $\tilde{\zeta}$ was tried till $\tilde{u}_{calc.}$ equalled $\tilde{u}_{exp.}$ For one particular $\tilde{u}_{exp.}$-value $\sigma_{ek}(p_\Delta)$ was calculated changing the parameter p_Δ from 0 to 2 in steps of 0.5. For L we took σ_o = 2.5 μC cm^{-2}, instead of the charge density obtained by titration (0.92 μC cm^{-2}). This value is in close agreement with the electrokinetic results on plugs and the electrophoresis results at high ionic strength. For M and H the charge densities obtained by titration were taken (4.0 and 9.0 μC cm^{-2} resp.). To allow for the effect of the actual molar conductivities of the ions it seemed correct to

Table 6-1. Results of the electrophoretic study of polystyrene latices. t = 25.0°C. Mobilities were converted into zeta-potentials using tables derived from the results of Wiersema et al. for m ≈ 0.184 by Ottewill and Shaw[10]. The charge densities deduced from streaming current data (values in brackets) of untreated plugs are taken from table 5A and partly from fig. 5-10a,b,c by interpolation. For high c the results of treated plugs were used.

sample	c	$UX^{-1} \times 10^4$ $cm^2V^{-1}s^{-1}$			$-\zeta$(W.L.O.) mV			$-\sigma_{ek}$(W.L.O.) μCcm^{-2}		
	M	LiCl	KCl	CsCl	LiCl	KCl	CsCl	LiCl	KCl	CsCl
L	10^{-1}	2.37	2.25	2.12	31.3	29.7	28.0	2.40(2.22)	2.27(2.16)	2.12(1.93)
	$5\ 10^{-2}$	3.32		2.81	43.8		37.1	2.52		2.06
	10^{-2}	5.05	4.80	4.75	71.7	66.2	65.5	2.22(1.75)	1.97(1.54)	1.94(1.56)
	$5\ 10^{-3}$	5.57	5.35		82.3	78.1		1.98	1.81(1.55)	
	10^{-3}	5.00	5.49		83.3	100.5		0.90	1.29(0.78)	
	$5\ 10^{-4}$	4.01	4.26		65.2	70.7		0.43	0.49(0.52)	
	10^{-4}		2.96			51.6			0.14(0.15)	
	$5\ 10^{-5}$		1.99			34.3			0.06	
M	10^{-1}		3.30			43.3			3.51(4.00)	
	$5\ 10^{-2}$		3.85			50.9			3.05(3.45)	
	10^{-2}		5.05			68.7			2.08(1.98)	
	$5\ 10^{-3}$		5.14			72.5			1.60(1.42)	
	10^{-3}		4.76			74.5			0.75(0.53)	
	$5\ 10^{-4}$		3.97			62.9			0.41	
	10^{-4}		3.77			68.5			0.21	
H	10^{-1}	4.22	3.84	3.60	55.2	50.3	47.1	4.80(4.70)	4.24(4.22)	3.90(4.16)
	$5\ 10^{-2}$	4.78	4.90	4.50	63.3	64.9	59.5	4.12	4.27(3.70)	3.77
	10^{-2}	5.37	5.77	5.93	74.0	80.7	83.3	2.34(2.52)	2.70(2.47)	2.85(2.35)
	$5\ 10^{-3}$	5.97	5.33		90.1	77.9		2.33(1.85)	1.80(1.80)	
	10^{-3}	4.56	4.52		70.6	69.6		0.69(0.72)	0.67(0.74)	
	$5\ 10^{-4}$	4.10	3.98		65.5	62.9		0.43	0.41	
	10^{-4}	3.42	3.37		60.6	59.4		0.17	0.17	
	$5\ 10^{-5}$		2.73			48.0			0.09	

identify m with m^+, because calculations showed that the mobility of the counterions has much more effect on the e.m. than that of the co-ions, even more so at higher surface potentials[1]. Because only experimental data for $\kappa a > 20$ can be analysed in terms of the D-S theory, the charge-potential relationship for a flat double can be used. The experimental mobility data, ζ-potentials and electrokinetic charge densities derived by W's method, are listed in table 6-1. To permit comparison, pertinent σ_{ek}-results computed from streaming current data of untreated plugs are also presented. The results of the $\sigma_{ek}(p_\Delta)$-calculations are presented graphically in fig. 6-3 abc.

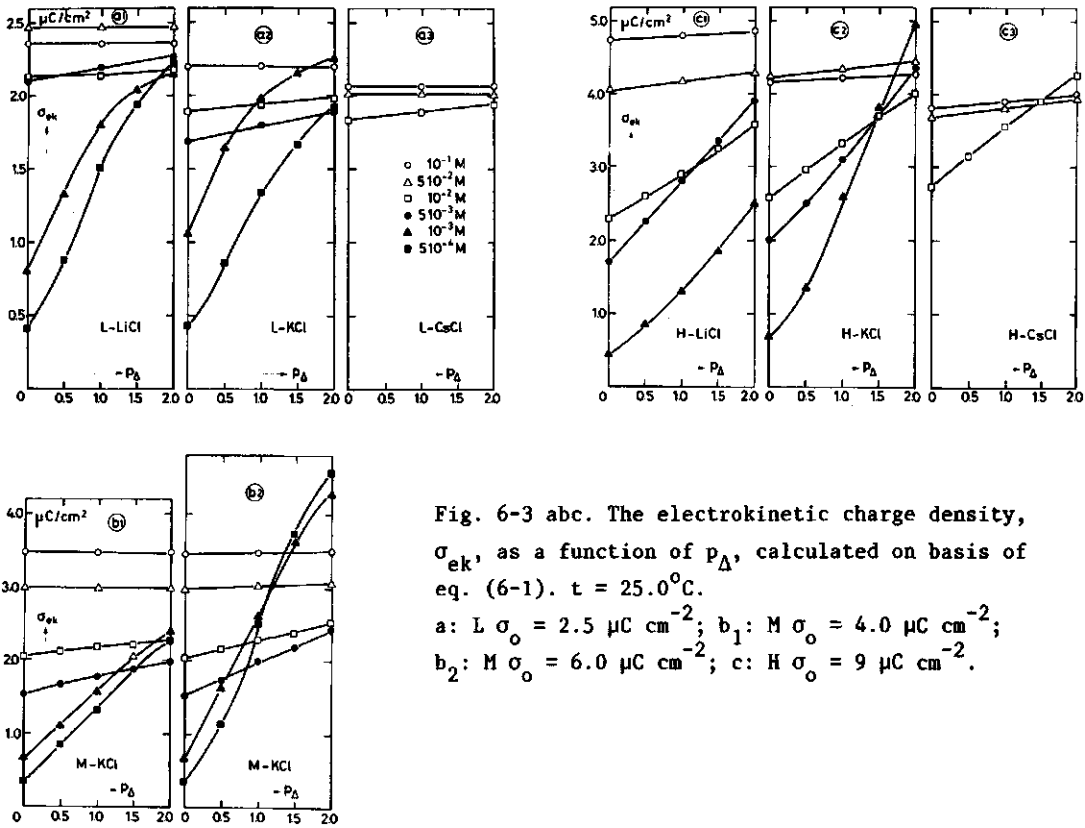

Fig. 6-3 abc. The electrokinetic charge density, σ_{ek}, as a function of p_Δ, calculated on basis of eq. (6-1). t = 25.0°C.
a: L σ_o = 2.5 μC cm^{-2}; b_1: M σ_o = 4.0 μC cm^{-2}; b_2: M σ_o = 6.0 μC cm^{-2}; c: H σ_o = 9 μC cm^{-2}.

An attempt will be made to draw some general conclusions from the $\sigma_{ek}(p_\Delta)$-results:

I The effect of p_Δ on $\sigma_{ek}(p_\Delta)$ is only substantial at low ionic strength; charge transfer in the Δ-layer ($p_\Delta > 0$) enhances $\sigma_{ek}(p_\Delta)$.

II At high ionic strengths an alkali-ion specificity in σ_{ek} is observed, analogous to the plugs (see table 6-1). Remarkably enough, at low

ionic strengths (below about 10^{-2}M, this trend reverses for $p_\Delta = 0$. This effect is especially visible for H and is much more pronounced than for the plug results. This contradiction is also consistent for $p > 0$, assuming equal p_Δ for all alkali-ions. Furthermore, in nearly all cases, $\sigma_{ek}(p_\Delta)$-curves for LiCl and KCl, drawn in one figure, do not intersect at identical ionic strengths in the studied p_Δ-range. To obtain the same sequence in σ_{ek} as observed at high c $\{\sigma_{ek}^{Li}(c, p_\Delta^{Li}) \geq \sigma_{ek}^{K}(c, p_\Delta^{K} = p_\Delta^{Li})\}$ at concentrations where the outward shift of the shear surface becomes clear, one is forced to take substantially higher p_Δ^{Li} than the corresponding p_Δ^{K} -values.

III The mutual intersections of the $\sigma_{ek}(p_\Delta)$-curves for some comparable concentrations of the same counterion, may be used to detect p_Δ. For that purpose, for fixed p_Δ, σ_{ek}-c curves are constructed from the σ_{ek}-p_Δ results presented in fig. 6-3. For p_Δ-values exceeding those corresponding with the intersections the σ_{ek}-c characteristics always become unrealistic. Suppose that at low ionic strengths the charge distribution and the position of the shear plane are independent of the nature of the counterion, thus $\sigma_{ek}(\sigma_o, p_\Delta^{K}) = \sigma_{ek}(\sigma_o, p_\Delta^{Li})$. Then we get for H at 10^{-2}M $p_\Delta^{Li} = 1.2$, $p_\Delta^{K} = 0.6$ and $p_\Delta^{Cs} = 0.3$. Suppose further that p_Δ^{Li} remains constant for lower c's; this results in $p_\Delta^{K} = 0.9$ at $5\ 10^{-3}$M and $p_\Delta^{K} = 0.6$ at 10^{-3}M. The same procedure for L, starting from the intersection of the curves for KCl at $5\ 10^{-3}$ and 10^{-3}M, gives $p_\Delta^{K} = 0.65$. At $5\ 10^{-3}$M this value cannot be matched with a p_Δ^{Li} -value; at 10^{-3}M we get $p_\Delta^{Li} = 0.95$ and at $5\ 10^{-4}$M $p_\Delta^{Li} = 0.6$. Especially for H this example seems to indicate the trend $p_\Delta^{Li} > p_\Delta^{K} > p_\Delta^{Cs}$; the ionic mobility for Li^+ in the Δ-layer probably hardly deviates from the bulk value (see section 5.8), for K^+ and Cs^+ a lower mobility is quite possible. It is not only experimental errors that hamper a more accurate discussion of this problem but also several other factors, viz.,

a) all effects of the actual double layer that have not been accounted for, have been assigned to the factors p_Δ and $\Delta(\tilde{\psi}_d, \tilde{\zeta})$;
b) the value of σ_o is to some extent arbitrary;
c) the irreversible charging phenomenon; the relatively low p_Δ^{Li} -value for L partly results, because a σ_o-value has been used that corresponds to the treated case;
d) a possible alkali-specificity on charging and the position of the shear plane.

IV From the analysis of all the $\sigma_{ek}(\sigma_o, p_\Delta^{M})$ results the conclusion may be drawn, that upon decreasing the ionic strength the same dra-

matic 'immobilization' of the electrokinetic charge occurs as observed for the plugs (see table 6-1). Only assuming a substantial increase of p_Δ upon decreasing c over a short range would make the peculiar results less drastic. However, for a more extended concentration range a regular and monotonous variation of σ_{ek} with c could then not be obtained.

V It is important, especially in the view of the charging phenomenon, to get some insight into the influence of σ_o on the $\sigma_{ek}(p_\Delta)$ characteristics for $p_\Delta > 0$. For obvious reasons, the $\tilde{u}(\sigma_{ek}, p_\Delta=0)$-c characteristic is independent of σ_o. In order to examine the influence of σ_o in case $p_\Delta \neq 0$, we assume that M has a 50% higher σ_o-value than obtained from surface charge density characterization (M: σ_o = 4μC cm^{-2}). The results are presented in fig. 6-3b. From a comparison of figures b_1 (4 μC cm^{-2}) and b_2 (6 μC cm^{-2}) we notice a remarkably small influence for $c > 10^{-2}$M; the increase of σ_{ek} upon increasing p_Δ becomes slightly more prominent. It becomes clear from the shift of the intersection points at the low ionic strengths to low p_Δ-values and the appearance of new intersection points that the chosen σ_o-value is rather high. A very inconsistent σ_{ek}-c behaviour is already observed for $p_\Delta > 0.5$. It is clear that for L the observed unrealistic trend in p_Δ^K and p_Δ^{Li} as a function of c can be improved by a better choice of σ_o.

Charging effect: several experiments were performed to detect the charging effect and the influence of the time of equilibration on e.m. Latex samples, covering an extended c-range (10^{-4}-5 10^{-2}M) were measured promptly after preparation and subsequently at distinct time intervals (1 hour). Other samples were first equilibrated at 5 10^{-2}M KCl during several days. After dilution to lower concentrations (10^{-3}, 5 10^{-4}, 10^{-4}M) the existence of a possible time dependency was investigated. In both cases no time dependency was observed. Only the treated samples showed a slightly increased mobility at 5.10^{-4} and 10^{-4}M KCl (5 à 10%). However, the change was not significant for an interpretation in terms of the D-S theory.

6.6 *Summary*

Electrophoretic mobilities of PS latices are described and interpreted in terms of the W.L.O. theory and the D-S theory. The latter theory allows the study of the effects of charge transfer in the boundary layer and a change in ionic mobility on it, in a κa-region where the relaxation effect of the double layer is substantial. Evidence was obtained

for the presence of conduction between shear plane and particle surface. Qualitatively, the alkali-specificity on surface conductance was confirmed; in passing from Li^+ to Cs^+ the average ionic mobility in the Δ-layer seems to decrease. Apparently, the substantial decrease of the electrokinetic charge density (thus the increase in discrepancy between ζ and ψ_d) upon decreasing ionic strength is a typical feature of latex systems. This means that with decreasing ionic strength the hydrodynamic plane moves away from the surface. One may note that ζ-values become rather independent of ψ_d at low c. The influence of anomalous conduction on the shape of the $\sigma_{ek}(p_\Delta)$-c graphs shows that, especially at very low ionic strengths, the decrease of σ_{ek} becomes less drastic for $p_\Delta > 0$ as compared to the results according W.L.O. and from our plugs. In the region of not too high ionic strengths, a combined study of electrophoresis and surface conductance of dilute dispersions may be an attractive method to ascertain for other systems the presence of a stagnant liquid layer, for estimating its thickness, and for verifying the effect of concentration polarization on electrophoresis under conditions of anomalous surface conduction.

6.7 *References*

1. P.H. Wiersema, Thesis, Utrecht, Netherlands, 1964; P.H. Wiersma, A.L. Loeb, J.Th.G. Overbeek, J. Colloid Interface Sci. 22, 78 (1966)
2. D.C. Henry, Proc. Roy. Soc. London A 133, 106 (1931)
3. J.Th.G. Overbeek, Adv. Colloid Sci. 3, 97 (1950)
4. F. Booth, Proc. Roy. Soc. London A 203, 514 (1950)
5. S.S. Dukhin, B.V. Derjaguin, 'Electrokinetic Phenomena', in 'Surface and Colloid Science', E. Matijević, Ed., Vol. 7 (1974)
6. S.S. Dukhin, V.N. Shilov, Kolloidn. Zh. 31, 706 (1969)
7. S.S. Dukhin, N.M. Semenikhin, Kolloidn. Zh. 32, 360 (1970)
8. N.M. Semenikhin, S.S. Dukhin, Kolloidn. Zh. 38, no. 1 (1976)
9. N.M. Semenikhin, Kolloidn. Zh. 38, 69 (1976); 38, 74 (1976)
10. R.H. Ottewill, J.N. Shaw, J. Electroanal. Chem. 37, 133 (1972)
11. F. Booth, Trans. Faraday Soc. 44, 955 (1948)
12. D.C. Henry, Trans. Faraday Soc. 44, 1021 (1948)
13. D.E. Brooks, J. Colloid Interface Sci. 43, 687 (1973)
14. G.E. van Gils, H.R. Kruyt, Kolloid-Beih. 45, 60 (1936)
15. A. Watillon, J. Stone-Masui, J. Electroanal. Chem. 37, 143 (1972)
16. M.H. Wright, A.M. James, Kolloid-Z.u.Z. Polymere 251, 745-751 (1973)
17. J.H. Schenkel, J.A. Kitchener, Trans. Faraday Soc. 56, 161 (1960)

CHAPTER 7

SOME ASPECTS OF THE LOW FREQUENCY DISPERSION OF THE ELECTRICAL RESISTANCE

7.1 *Introduction*

In chapter 3 it was shown that measurements of the electrical resistance may not only be complicated by electrode polarization, but also by a slow dielectric polarization. It appeared that the four electrode technique satisfactorily overcomes the difficulty of electrode polarization. A second advantage of this technique is that it enables to detect any intrinsic relaxation of the system in a time domain corresponding with an ultra low frequency range (below about 1 Hz), normally not covered in dielectric research[1]. The streaming current measurements indicated the presence of a dispersion at extremely low frequencies for all the plugs at electrolyte concentrations below about 10^{-3}M. The frequency dispersion range appeared to be sensitive to the ionic strength; within one concentration decade both the relaxation time(s) and the conductivity increment increased substantially with decrease of the salt concentration. These findings are of particular interest with regard to the observed Δ-layer anomaly (preceding chapters), which takes place in the same concentration range. The main purpose of this chapter is to trace the possible mechanism underlying the low frequency dispersion.

7.2 *Analysis of the low frequency dispersion**

We consider that the streaming current retardation data can be advantageously analysed by a direct numerical transformation into the dependence of the complex impedance $Z = Z' + iZ''$ on frequency. Since both the imaginary part Z" and the real part Z' are calculated, this procedure has the advantage that Cole-Cole plots can be constructed by plotting Z' against Z". These plots afford to establish such factors as the number of dispersion processes taking place together with the involved relaxation times or relaxation time-distributions, and provide an independent check on the d.c. resistance determined from streaming current and streaming potential results.

The conversion into the frequency domain was achieved with the Laplace transform procedure[3]. Some results for plug M at 25.0°C are presented in fig. 7-1a,b. In fig.a Z' data as obtained by direct measurement have been included for $\nu \geq 80$ Hz. These data, presented as the dashed

* The author is much indebted to Dr.K.J. Peverelli for evaluating the transformation procedure and presenting the computer solutions.

lines, have not been corrected for electrode polarization. The Z' results show two distinct dispersions viz. a slow frequency dispersion with a single loss peak covering the frequency range of the transformation and a second dispersion covering the kHz range. Fig.b illustrates Cole-Cole plots for the first dispersion range. These plots deviate from the semicircular locus, indicating a distribution of relaxation times. The deviations from the Cole-Cole plot at the high-frequency side may be a result of slight overlap with the second dispersion range. In the same figure the mean relaxation times, τ_{rel}, are given, as they are obtained from the loss peak frequency, ν_{rel}, with $2\pi\nu_{rel}\tau_{rel} = 1$. Both the conductance increment $\Delta Z' (= Z'_{\omega=0} - Z'_{\omega=\infty})$ and τ_{rel} increase substantially with decreasing salt concentration, in a concentration range where such changes are not expected.

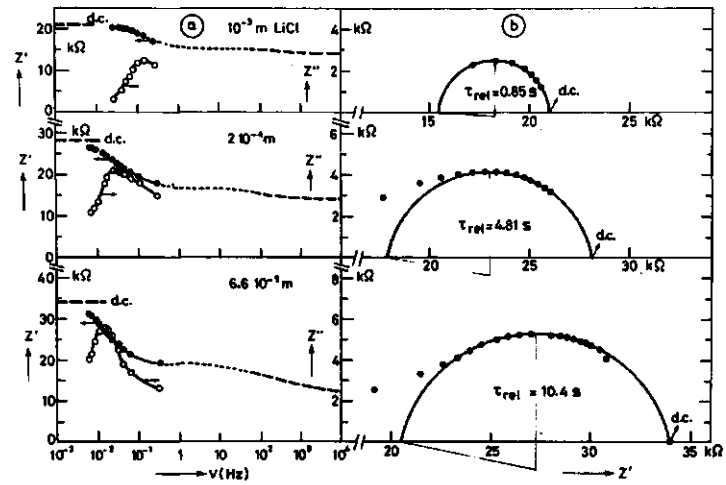

Fig.7-1a, b. a) Variation of the real, Z' ●, and the imaginary part, Z'' ○, of the impedance for three LiCl concentrations at 25.0°C. Plug M. The dashes cover the frequency range, inwhich the data ($\nu \geq 80$Hz) have not been corrected for electrode polarization. b) Cole-Cole plots of the data in fig.a.

For the study of relaxation phenomena in colloid suspensions *dilute* latex systems have frequently been employed (e.g. Springer[4]) and various mechanisms have been proposed for the interpretation of these phenomena. At first sight, theories incorporating the presence of two phases in the system and properties of the double layer are eminently suitable to account for the observed dielectric properties. The counter ions, localized to the surface by electrostatic attraction, can diffuse easily along this surface; thus, they will be displaced tangentially by an external field causing the induction of a dielectric dipole moment for the particles. All theories based upon this Schwarz - Schurr model and the modifications in which the Maxwell - Wagner effect is incorporated predict a relaxation time which is related to the particle radius, a, and the diffusion coefficient of the counter ions in the double layer, D_c, but are independent of parameters such as the ionic strength and the surface

charge density: $\tau_{rel} = a^2/2D_c$. The Dukhin - Shilov theory[4,5], which incorporates that the diffusion polarization actually occurs in the diffuse double layer, results in somewhat higher τ_{rel}-values. The theories based upon the relaxation of the ion atmosphere predict for our system a relaxation time of about 50 μs which is at variance with the observed relaxation times of the *first dispersion* by several orders of magnitude. The important conclusion ensues that some of the mechanisms proposed in those theories must be rejected, since they cannot predict the formidable change in τ_{rel} and the conductance increment with c. It is recalled that the results of the dilute suspensions are in better agreement with the calculated relaxation time (section 5.7.2). Extended experimental results on dilute latex systems by Springer[4] point to a nearly electrolyte concentration independent relaxation time of the same order as calculated on basis of the presented formula[4]. Probably, the results of the *second dispersion* (see fig.7-1a) can be ascribed to a pure double layer polarization. The effect of double layer interaction at the contact points of the particles in the plug occasions that in the alternating electric field the redistribution of ions is not confined to the region close to one particle. This may cause a shift of the whole dispersion range to lower frequencies and the appearance of the spread in relaxation times.

Yet another cause for the first dispersion has to be considered. An alternating current through the plug periodically disturbes the ion concentrations at the plug surfaces (transport number effect). As a consequence, an additional voltage drop across the plug occurs, which is out of phase with the current. This diffusion polarization[8,9] acts on the total impedance of the system like a parallel combination of a resistance and a capacitance, both proportional to $\nu^{-\frac{1}{2}}$. However, the streaming current retardation plots showed that the time range of this process is sufficiently longer than that of the intrinsic dispersion process (see section 3.5.1). Only the part of the intrinsic effect related to the longer period of the intrinsic effect may be slightly influenced by the transport number effect. Apparently, the causes for the low frequency dispersion must be related to parameters associated with the hairy layer (section 5.8.1.1). This implies that two typical aspects of that layer have to be considered viz. the presence of ion-paired groups and the protruded polystyrene chains.

The ion-paired groups, probably located deep within the Δ-layer and/or buried in the periphery of the particles can only participate in the conduction current at an increased frequency. The counter ions may be made to prefer a particular position by an external field and thus

the fixed site-counter ion dipole would be polarized. The order of magnitude of the relaxation time pertaining to the fixed site-counter ion polarization process can be estimated in the following way:

If the dipoles were spheres of radius a rotating in a uniform viscous fluid with a viscosity, η, τ_{rel} will be given by (e.g. Smyth[10], p.59): $\tau_{rel} = 4\pi\eta a^3/kT$. For the fixed site-counter ion dipole, which rotates around a fixed pole, τ would be higher than predicted by the foregoing equation, but probably not by an order of magnitude. If we suppose that the counter ion radius is about ½a and that its diffusibility in the Δ-layer is idendical to that in solution, the Einstein-Stokes relation leads to $D_c = kT/\frac{1}{2}a6\pi\eta$. Combining this with the expression for τ_{rel} we have:

$$\tau_{rel} \cong a^3/3D_c \qquad (7\text{-}1)$$

Even when D_c is a factor of 10^3 smaller than in an electrolyte solution, τ will be in the range 10^{-6}-10^{-7}s when a is about 0.6nm. It seems, therefore, that this process only plays a role in the dielectric loss at frequencies much higher than observed for the second dispersion.

Another interesting possibility is that the "partially dissolved" polystyrene molecules, constituting the Δ-layer, are responsible for the slow dispersion. The chains bearing the end charges are capable to oscillate in an alternating electrical field. This model was used by Goring et al." to explain a giant low frequency dispersion observed on plugs of different fibrous materials at frequencies below 100 Hz. The electrical resistance component must be related to the hydrodynamic resistance to conformational changes if the chains and the capacitance to the restoring force generated when the molecule is displaced from its equilibrium position. The heterodispersity in lengths and intermolecular interactions (patch concept) lead to the distribution of relaxation times (depressed semicircular arc). Upon increase of the ionic strength the terminal charges are more effectively shielded and the Δ-layer shrinks. The decrease of the mean chain length is probably connected with the shift of τ_{rel} to shorter values and the decrease of the conductivity increment (e.g. Sakamoto et al.[1]).

It is obvious that for $\nu \to 0$ two mechanisms contribute to a depression of the plug conductance viz. the diffuse double layer polarization and a slightly deformed Δ-layer in which the somewhat streched chains result in a more effective polarization field. For $\nu >> \nu_{rel}$ (first dispersion region), thus e.g. for ν's coinciding with the relaxation of the diffuse double layer, the Δ-layer can be considered as totally 'rigid'. It is

noted that the sequence in charge density is hardly reflected in the relaxation times. At identical ionic strengths we observed the slight trend τ_{rel} (M) $\gtrsim \tau_{rel}$ (L) > τ_{rel} (H) with no distinct effect of the kind of counter ion.

At this stage the question arises if the substantial additional polarization contribution of the Δ-layer to the d.c. resistance could invalidate the description of the anomalous charge distribution presented and discussed in the preceeding chapters. In chapter 5 the charge distribution was calculated according to the H-B model using d.c. streaming current and d.c. resistance values. In table 7-1 we have summarized some calculations of the charge distribution at ν=0.32 Hz, the upper limit of ν attainable with the four electrode technique, and at ν=10 kHz at which the second dispersion is almost surpassed while electrode polarization effects are supposedly small. In all calculation bulk values of the involved quantities were used. The results show a remarkable small effect of polarization on σ_{ek}, which was calculated from $I_{s,ac}$ according to the procedure described in section 4.5 d. These results confirm once more that due to a substantial anomalous conduction, thus at low Rel(I_s) values, the hydrodynamically induced polarization field can be neglected. In the calculation of σ_Δ the conductivity increment was converted into an increase in the interfacial conduction (see section 5.8). The substantial increase of the conductivity ratio $\bar{K}/K$ shifts the applicability of the Bruggeman model to higher concentrations. The relatively high σ_Δ values at ν=10 kHz are, therefore, partly due to the attainment of the limits of the H-B model. However, calculations according to the Street-model show almost the same substantial increase in σ_Δ with increase in ν, which clearly demonstrates the considerable effect of the hairy layer on the polarization field.

Table 7-1. Variation of the charge distribution with frequency for the three latex samples at 25.0°C.

c(KCl)	$-\sigma_{ek}$ μC/cm²			$-\sigma_\Delta$ μC/cm²		
M	d.c.	0.32 Hz	10 kHz	d.c.	0.32 Hz	10 kHz
L(VB)						
$1.25\ 10^{-3}$	0.90	0.90	-	1.13	1.13	-
$7.65\ 10^{-3}$	0.76	0.79	0.90	1.44	1.52	1.63
10^{-4}	0.24	0.39	0.50	3.07	5.42	7.24
M(VIIIB)						
10^{-3}	0.63	0.73	1.18	4.13	4.84	7.34
$2\ 10^{-4}$	0.20	0.33	0.56	4.85	8.93	16.7
$4\ 10^{-5}$	0.11	0.19	0.33	-	-	-
H(VIIB)						
$5\ 10^{-3}$	1.86	1.86	2.11	4.27	4.27	4.87
10^{-3}	0.90	0.90	1.18	5.71	5.71	6.82
$2.65\ 10^{-4}$	0.37	0.51	0.72	6.61	9.50	13.0

7.3 *The influence of the thorium ions on the frequency dispersion*

Goring et al.[11] suggested that upon removal of the electrical charges the low frequency dispersion would disappear. Results with thorium ions seemed to confirm this statement. We checked this with a M-plug using a 10^{-4}M $ThCl_4$ /10^{-4}M KCl (pH=3.9) solution. At t=0 the plug which was in complete equilibrium with a 10^{-3}M LiCl solution (K=1.136 $10^{-4}\Omega^{-1}cm^{-1}$), was permeated with the thorium solution (K=1.71 $10^{-4}\Omega^{-1}cm^{-1}$). A constant pressure difference of 30 cm Hg was applied during more than 200 h. All pertinent parameters were intermittently measured together with R(80Hz). From the results in fig.7-2 an initial sharp decrease of I_s and E_s is noticed, indicating the decrease of the electrokinetic charge density. The zeta-potential changed from -67.7 mV at t=0 to -6.5 mV after about 200 h permeation. The resistance initially decreases to a minimum that is reached when the interstitial pore liquid had been replaced about 6 times; subsequently, it increases slowly to a value about twice the resistance at t=0. The difference between the a.c. and d.c. resistance at t=0 points to the substantial low frequency dispersion. During permeation, this dispersion gradually disappears, indicating the destruction of the Δ-layer. From the results we may conclude that two effects are operative. The decrease in R is for a large part caused by an exchange

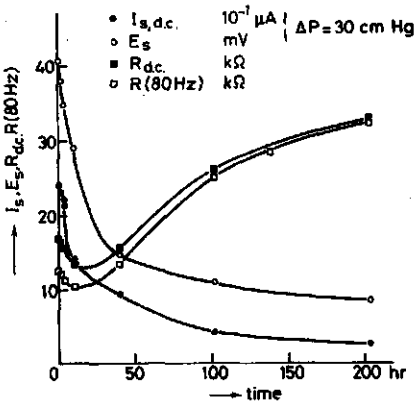

Fig. 7-2. Change of the electrokinetic quantities during permeation of plug VIII A(M) with a 10^{-4}M $ThCl_4$/10^{-4}M KCl (pH=3.9) solution. At t=0 the plug was in equilibrium with 10^{-3}M LiCl. t=25.0°C.

of Li^+- with the K^+-ions in the Δ-layer and for a small part a result of the increase in the specific conductivity of the interstitial liquid. The transport of the thorium ions into the inner part of the Δ-layer is probably obstructed sterically and/or by repulsion due to effectively positively charged terminal group-counterion pairs. The eventual neutralization of the outermost end charges induces some rearrangement and salting-out of the "dissolved chains", facilitating a further penetration of the thorium ions in the Δ-layer. Simultaneous with the gradual

salting-out of the Δ-layer the dispersion effect shifts to higher frequencies (decrease of the mean chain length) and disappears, whereas the surface conductance also becomes less. A complete interpretation of the observed phenomena is complex, but it is clear that the combined measurement of low frequency dispersion and electrokinetics is a potentially useful approach to the study of interfacial phenomena. To that purpose methods of correcting for electrode polarization must be developed for plug systems to make also the high frequency range accessible.

7.4 *Summary*

The relaxation behaviour of the polystyrene plugs seems to be governed by two phenomena, one occurring on a time-scale of seconds and one in the microsecond range. An analysis of the relaxation time shows that the slow relaxation process must be related with the 'hairy Δ-layer', whereas the faster relaxation process could be attributed to relaxation of the counter ion atmosphere. Evidence that the substantial polarization originates from the protruded polystyrene chains was obtained from the fact that the dispersion effect disappeares upon a relatively small increase of the ionic strength, whereas the relaxation time decreases by a factor of 10. Furthermore, a kinetic experiment in which the electrokinetic quantities and the frequency dispersion were followed while a plug was permeated with a thorium solution, showed that the slow frequency dispersion and the surface conductance are closely related with the terminal charges which were distributed over the Δ-layer.

7.5 *References*

1. M. Sakamoto, H. Kanda, R. Hayakawa and Y. Wada. Biopolymers, 15. 879 (1976)
2. N.E. Hill. Dielectric properties and molecular behaviour, T.M. Sugden (Ed.), Van Nostrand Reinhold Company Ltd., London (1969)
3. K.J. Peverelli, Thesis, Wageningen (1979), chapter 3
4. M.M. Springer, Thesis, Wageningen (1979)
5. S.S. Dukhin and V.N. Shilov, Dielectric phenomena and the double layer in disperse systems and polyelectrolytes, Wiley, New York, (1974)
6. Ref. 5, p. 78
7. See ref. 3; p. 51
8. K.J. Vetter, Electrochemical Kinetics, Academic Press, 1967, p. 200
9. J.R. Segal, J. Theoret. Biol. 14, 11 (1967)
10. C.P. Smyth, Dielectric behaviour and structure. Mc Graw-Hill Book Co., N.Y. (1955), p. 56
11. D.A.I. Goring, G.J. Biefer and S.G. Mason, Can. J. Research, B 28, 339 (1950)

SUMMARY

This thesis presents a systematic experimental and theoretical study on electrokinetic and electroconducting properties of disperse systems. The increasing interest in transport processes through charged porous systems has recently brought about a corresponding growth of models and theories since real systems are extremely complex. Monodisperse polystyrene latex seems to constitute a good geometrical model system to theoretically and experimentally assess the influence of the interfacial properties of the dispersed particles and the overall properties of the dispersed system.

The preparation and characterization of the polystyrene latices are dealt with in chapter 2. The concentrated dispersions (plugs), with a volume fraction of the solid in the order of 0.6, were obtained by centrifugation of the latex samples as described in chapter 3.

Chapter 3 recalls the basic principles of the theory of irreversible thermodynamics which are relevant in connection with the determination and mutual dependency of electrokinetic quantities. All possible forms of polarization, viz. concentration polarization at the electrodes and/or at the plug surfaces, ohmic polarization and intrinsic polarization of the plug, are studied with a 4-electrode equipment. The main features of these polarization phenomena are:

(i) concentration polarization at the plug-solution interface (negative adsorption) may cause transient streaming potential or an apparent non-linear electro-osmotic flow-current relationship, when this cause is not properly recognized, the results can, e.g., erroneously be interpreted in terms of special transitions in the water structure at the interface.

(ii) the retardation behaviour of the streaming current is caused by concentration polarization at the current-processing electrodes and/or is a result of a slow intrinsic relaxation process.

(iii) the current-voltage characteristics may be obscured by induced concentration polarization processes (transport number effect) but also by slow intrinsic polarization processes.

The employment of this new technique has led to the correct measurement of the pertinent phenomenological coefficients. Furthermore, it enables to obtain the time-dependency of a possibly present slow intrinsic polarization process and the transport number in the plug.

A theoretical and experimental study also shows how to evaluate the phenomenological coefficients in case various forms of polarization take

place simultaneously. The 4-electrode technique also enables to determine the concentration change at the low pressure side of a plug during permeation. A quantitative expression has been derived which interrelates the ionic strenght outside the plug, the electrolyte concentration in the porous phase and the volume flow.
Finally, the time-dependency of the depletion process is used to calculate effective charge densities (dynamic negative adsorption method) which appear to be completely consistent with the electrokinetic results (chapter 4).

Chapter 4 summarizes and discusses the basic geometric models. The electrokinetic and hydrodynamic data are then presented and discussed in relation to these various models. Special attention is given to the electroviscous effect and the concept of anomalous conduction. To that purpose theoretical predictions for the cell and the capillary model of Levine are made suitable or are extended to the concept of anomalous conduction.

The main features of the electrodynamic and hydrodynamic results are:

- the severe restriction to low potentials causes the cell model to be less usefull than Levine's capillary model;
- a mutual comparison of various theoretical models demonstrates the effect of polarization in concentrated dispersions; when surface conduction is not negligible, porous systems are even polarized under streaming current conditions, which may lead to an apparent lyotropic sequence in the streaming current;
- our latex plugs show a strong deviation from 'model behaviour'. The experimental data are interpreted in terms of an outward shift of the shear surface when decreasing the electrolyte concentration, coinciding with a change in the double layer structure. The boundary layer thicknesses evaluated from the hydrodynamic and from the electroviscous retardation results both show the same concentration dependency. The difference between the absolute values is related to the structure of the double layer.

Chapter 5 is concerned with the conversion of experimental data on the conduction of concentrated and dilute dispersions into double layer characteristics. A very clear view on the applicability on the various theoretical formulae is obtained. The conductivity of dilute dispersions can quite reasonably be described by an equation that allows for concentration polarization according to the Dukhin - Semenikhin theory, provided that the experimental conditions are chosen such that the particles are fully polarized. For concentrated systems, the concentration polari-

zation mechanism is suppressed by short-circuiting of the interacting double layers near the contact points of the particles. This keeps the conductivity finite as the ionic strength approaches zero; consequently all polarization models finally underestimate the conductivity of a concentrated dispersion upon decreasing ionic strength, especially when the concentration polarization according to Dukhin - Semenikhin is incorporated. The 'classical' Bruggeman equation proves to be most usefull for the evaluation of double layer properties. The influence of the decrease in concentration polarization upon concentrating a particle dispersion is also noticed from the shift of the isoconductivity point to higher electrolyte concentrations.

Also in chapter 5, the combined information on the influence of the nature of the counter ions, the temperature and the surface charge density on the surface conductance is used to analyse the structure of the electrical double layer of our model system. The main conclusions are:

- the counter charge effective in the electric conduction remains more or less constant upon variation of the ionic strength whereas the 'hydrodynamically immobilized' part of the counter charge increases sharply upon diluting the electrolyte;
- the hydrodynamic and electroviscous data indicate a shift of the shear plane upon decreasing ionic strength;
- contacting polystyrene with a medium of high ionic strength causes an increase in the titration charge density (charging phenomenon);
- a alkali-specificity is noticed for the surface conductance and the activation energy of conductance.

The 'hairy layer' model (Δ-layer) is used to explain these peculiar findings. Arguments are given that protruding polystyrene chains with terminal charges are present and that they are distributed in patches. Increase of ionic strength causes the thickness of the hairy patches to shrink; the shear surface enveloping the end-groups of the most protruded chains shifts inwardly and the counter ions originally accommodated between the headgroups become electrokinetically 'visible'. Furthermore, ion-paired groups in the innermost regions of the boundary layer are activated and contribute to the surface conductance. Irreversible structural rearrangements in the Δ-layer are responsible for the fact that upon subsequent dilution of the electrolyte a larger fraction of the end-groups remains active.

The concentration dependent surface diffusion of ions, the amount of specific adsorption and the observed alkali-specificity are strongly related to the shrinkage of the Δ-layer and the evoked permittivity change within that layer.

In chapter 6 the effect of concentration polarization on electrophoresis under conditions of anomalous conduction is verified with the theory of Dukhin and Semenikhin. Several procedures are discussed to obtain information about the boundary layer thickness and the average mobility of the ions inside the shear surface. The results are in line with the concept of the concentration dependent boundary layer thickness formulated in the preceding chapters. In passing from Li^+ to Cs^+ the average ionic mobility in that layer seems to decrease.

Chapter 7 presents an account of the dielectric dispersion occurring on a time-scale of seconds. The slow relaxation process is closely related with the 'hairy boundary' layer. The effect of salting out the hairy layer on the relaxation time and the conductivity increment confirms the proposed hairy layer model.

In conclusion, this study shows, that electrokinetic investigations on concentrated dispersed systems, in combination with electrophoresis, are very useful in studying electrokinetic transport processes. Admittedly, our latex system, due to its simple geometry of dispersed spheres, is an idealized model for systems that are as complex as porous plugs or membranes. However, the presented results are of considerable help in visualizing the immensely complex transport processes and the present shortcomings in their theoretical description.

Acknowledgements

This investigation was carried out in the Laboratory for Physical and Colloid Chemistry of the Agricultural University, Wageningen.

The author is much indepted to Dr. B.H. Bijsterbosch for his encouragement and criticism during this study.

Appreciation is also expressed for the helpful discussions with other faculty members.

The valuable assistance of the following staff personnel is also gratefully acknowledged: Mr. R.A.J. Wegh, Mrs. P. Bosman-van Dulm, Mr. S. Maasland, Mr. H. van Beek, Mr. G. Buurman.

The computer programs written by Ir. P.R.M. van de Kamp and Dr. K.J. Peverelli were very helpful in analyzing portions of the data.

Dr. R.J. Akers was kind enough to correct the English text of this thesis.

Samenvatting

In dit proefschrift wordt een experimenteel en theoretisch onderzoek beschreven naar de elektrokinetiek, als techniek voor de bestudering van de kolloïdchemische eigenschappen van disperse systemen. De toenemende belangstelling voor de transportprocessen die in geladen systemen plaatsvinden, heeft vooral de laatste tijd geleid tot een sterke ontwikkeling van modeltheorieën. Monodisperse polystyreenlatices vormen een goed gedefinieerd geometrisch modelsysteem voor een experimenteel en theoretisch onderzoek naar het onderlinge verband tussen enerzijds de elektrische eigenschappen van de deeltjes, van het dispersie middel en van de dubbellaag bij de wand van de deeltjes en anderzijds de elektrische eigenschappen van de dispersie. In hoofdstuk 2 zijn de bereiding en karakterisering van negatief geladen polystyreenlatices beschreven. De bereiding van geconcentreerde systemen (proppen) vindt men in hoofdstuk 3.

In hoofdstuk 3 worden enkele basis principes van de theorie van de irreversibele thermodynamica behandeld die relevant zijn voor de bepaling van de elektrokinetische grootheden en hun onderlinge samenhang. Alle mogelijke vormen van polarisatie, te weten concentratiepolarisatie aan de elektroden en/of aan de grensvlakken van de prop, weerstandspolarisatie en intrinsieke polarisatie van de prop, zijn bestudeerd met een 4-elektrode opstelling. De belangrijkste kenmerken van deze polarisatieverschijnselen zijn:

- concentratiepolarisatie aan het grensvlak prop-vloeistof (negatieve adsorptie) kan een verloop in de stromingspotentiaal teweegbrengen of aanleiding geven tot een schijnbaar niet-lineaire elektro-osmotische vloeistofflux-elektrische stroom karakteristiek. Indien de oorzaak niet is onderkend kunnen dergelijke resultaten onjuist worden geïnterpreteerd, bijvoorbeeld in termen van een verandering van de waterstructuur aan het grensvlak;
- de stromingsstroomretardatie wordt veroorzaakt door concentratiepolarisatie aan de stroomvoerende elektroden en/of is het resultaat van een intrinsiek relaxatie proces;
- de stroom-spanningskarakteristiek kan sterk beïnvloed worden door teweeggebrachte polarisatieprocessen (transportgetal effect), maar ook door trage intrinsieke polarisatieprocessen.

Het invoeren van de 4-elektroden techniek heeft ertoe geleid dat de fenomenologische coëfficiënten volledig correct bepaald kunnen worden, ondanks de genoemde polarisatieprocessen. De nieuwe techniek biedt bovendien de mogelijkheid om het relaxatiegedrag van een mogelijk aanwezig langzaam intrinsiek polarisatieproces vast te leggen alsmede de transportgetallen

in een prop of membraan op eenvoudige wijze te bepalen. Veel theoretisch en experimenteel werk is besteed aan de ontwikkeling van methoden om de fenomenologische coëfficiënten te bepalen onder de omstandigheid dat meer polarisatieprocessen gelijktijdig optreden. De 4-elektrodentechniek maakt het tevens mogelijk concentratieveranderingen aan de lage drukkant te volgen als functie van de tijd tijdens het doorspoelen van een selectief systeem. Er is een kwantitatieve uitdrukking afgeleid, die het verband legt tussen de zoutconcentraties in en buiten de prop en de volume flux. De effectieve ladingsdichtheid is berekend uit de gemeten tijdsafhankelijkheid van het uitputtingsproces aan de lage drukkant van het prop grensvlak (dynamische negatieve adsorptie methode, hoofdstuk 4). De resultaten zijn volledig in overeenstemming met de elektrokinetische ladingsdichtheden die berekend zijn uit de stromingsstroom en de elektroforese experimenten.

Hoofdstuk 4 is gewijd aan de fundamentele geometrische modellen. Hierbij is speciale aandacht gegeven aan het elektrovisceus effect en het concept van anomale geleiding. De belangrijkste kenmerken van het elektrodynamische en elektrokinetische onderzoek zijn:

- het cel model is minder bruikbaar dan Levine's capillair model door de beperking tot lage waarden van de potentiaal;
- aan de hand van diverse theoretische modellen is de invloed van polarisatie op de elektrokinetiek van geconcentreerde systemen gedemonstreerd. Als de oppervlaktegeleiding niet verwaarloosbaar is, kunnen poreuze systemen ook onder stromingsstroom condities polariseren en schijnbaar aanleiding geven tot een lyotrope reeks in de stromingsstroom;
- de dubbellaag eigenschappen van het model systeem wijken vooral bij lage zoutconcentratie sterk af van het model gedrag. De waarnemingen steunen het model waarin het afschuifvlak naar buiten verplaatst wordt en de dubbellaag structuur binnen het afschuifvlak sterk verandert bij afnemende zoutconcentratie;
- de dikte van de grenslaag, berekend uit de hydrodynamische experimentele gegevens en uit het elektrovisceus effect, is sterk afhankelijk van de zoutconcentratie. De verschillen tussen de dikten, verkregen met de beide methoden, zijn in verband gebracht met de structuur van de dubbellaag in de grenslaag.

Hoofdstuk 5 is toegespitst op het omzetten van de experimentele resultaten van het elektrische geleidingsvermogen van verdunde en geconcentreerde dispersies in dubbellaag grootheden. Dit biedt een duidelijk beeld van de toepasbaarheid van diverse theoretische formules. Een formule waarin het concentratie-polarisatie concept van Dukhin en Semenikhin

is opgenomen, beschrijft het specifiek geleidingsvermogen van verdunde dispersies goed. Het is hierbij uiterst belangrijk, dat de experimentele gegevens verkregen zijn onder omstandigheden waarbij de deeltjes maximaal gepolariseerd zijn. Zo blijkt het effect van de concentratiepolarisatie sterk af te nemen voor geconcentreerde dispersies ten gevolge van 'kortsluiting' van overlappende dubbellagen bij de contactpunten van de deeltjes. De geleiding wordt bij daling van de zoutconcentratie dan ook constant, zelfs wanneer de zoutconcentratie daalt tot nul; hieruit kan verklaard worden waarom alle polarisatiemodellen het specifieke geleidingsvermogen van een geconcentreerde dispersie onderschatten bij lage zoutconcentratie. De klassieke Bruggeman vergelijking blijkt het meest bruikbaar voor de omzetting naar de dubbellaag grootheden. Het opschuiven van het isoconductieve punt naar een hogere zoutconcentratie bij toename van de deeltjes-concentratie wijst eveneens op de afname van het concentratiepolarisatie effect.

De informatie over de dubbellaag van het model systeem is aanzienlijk uitgebreid met de gegevens, verkregen uit het onderzoek naar de invloed van het type tegenion, temperatuur en ladingsdichtheid op de oppervlaktegeleiding. De belangrijkste conclusies zijn:

- de tegenlading, berekend uit het geleidingsvermogen, is nagenoeg onafhankelijk van de zoutconcentratie, terwijl het hydrodynamische immobiele deel van de tegenlading sterk toeneemt bij daling van de zoutconcentratie;
- de titratie ladingsdichtheid neemt toe als het polystyreen op hoge zoutconcentratie wordt gebracht (oplaad effect);
- de oppervlakte geleiding en de activeringsenergie van het specifiek geleidingsvermogen zijn ion-specifiek.

Het 'hairy-layer' model (Δ-laag) is gebruikt om al deze eigenaardigheden te verklaren. Bij een lage zoutconcentratie steken de polystyreen ketens (haren) met de geladen sulfaatgroepen naar buiten. Deze ketens zijn groepsgewijs verdeeld over het oppervlak. Neemt de zoutconcentratie toe, dan schrompelen de harige delen op het oppervlak in. Het afschuifvlak, dat samenvalt met de eindgroepen die het meeste uitsteken, schuift naar binnen en de tegenionen, die zich tussen de geladen groepen in de Δ-laag bevinden, worden 'elektrokinetisch zichtbaar'; tevens zullen ionenparen binnenin de Δ-laag geactiveerd worden en bijdragen aan de geleiding. Irreversibele conformatie veranderingen in de Δ-laag hebben tot gevolg dat een groter deel van de eindgroepen actief blijft bij een daaropvolgende afname van de zoutconcentratie.

In hoofdstuk 6 is het gecombineerde effect van concentratie polarisatie en anomale geleiding op de elektroforese geverifieerd met de theo-

rie van Dukhin en Semenikhin. Voor het verkrijgen van informatie over de dikte van de grenslaag en de gemiddelde beweeglijkheid van de ionen in die laag zijn diverse procedure besproken. De experimentele resultaten passen volledig in het beeld dat de propmetingen hebben opgeleverd. De gemiddelde beweeglijkheid van de ionen in de Δ-laag blijkt af te nemen in de volgorde Li^+,K^+,Cs^+.

In hoofdstuk 7 wordt het diëlektrische gedrag van de polystyreen proppen behandeld, dat zich afspeelt op de tijdschaal van seconden. Het langzame relaxatieproces staat in nauw verband met de 'harige grenslaag'. De invloed van het uitzouten van de Δ-laag op de relaxatietijd en de frequentie-afhankelijkheid van de geleiding bevestigen het 'hairy-layer' model.

Op basis van deze studie kan worden geconcludeerd dat elektrokinetisch onderzoek naar geconcentreerde systemen in combinatie met de elektroforese techniek zeer waardevol is bij een onderzoek van elektrokinetische transport processen. Het is vanzelfsprekend dat het latex-systeem een te geïdealiseerd geometrisch model systeem is voor uiterst ingewikkelde systemen als proppen en membranen. Echter, de resultaten van dit onderzoek geven een duidelijk beeld van de buitengewoon complexe transportprocessen en de huidige tekortkomingen in de theoretische beschrijvingen ervan.

LIST OF SYMBOLS AND ABBREVIATIONS

Symbols and abbreviations that appear infrequently or in one section only are not listed.

Abbreviations

B	Bruggeman
B-M	Bjerrum - Manegold
D-S	Dukhin - Semenikhin
e.m.	electrophoretic mobility
H-B	Henry - Booth
ICP	isoconductance point
K-C	Kozeny - Carman
M	Maxwell
M-T	Meredith - Tobias
n.a.	negative adsorption
Pe	Peclet number
Re	Reynolds number
S	Slawinski
W	Wagner
WLO	Wiersema - Loeb - Overbeek

Symbols

a	particle radius
a	capillary radius; the subscripts K-C and B-M indicate the models to which the radii apply
a_i	activity of species i
a_s	solute activity
A	cross-sectional area of the plug or centrifuge tube; electrode surface area
b	radius of the unit cell
c, c_o	electrolyte concentration
$\bar{c}_+$	mean-molar concentration of the cations
$\bar{c}_-$	mean-molar concentration of the anions
c_i	molar concentration of species i
c_p	mean-molar concentration of neutral salt in the porous phase
c_p^{he}	hydrodynamically effective c_p
$\bar{c}_s$	mean solute concentration: eq. (3-1)
c_{ICP}	electrolyte concentration under isoconductance conditions
C	cell constant

C_p	cell constant of the plug
D	diffusion coefficient
D_c	diffusion coefficient of the counter ion
D_{em}	particle diameter obtained by electron microscopy
D_H	particle diameter in the model of Happel
D_{K-C}	particle diameter in the model of Kozeny - Carman
D^o	surface diffusion coefficient
$D_\Delta^\pm$	coefficients of ion diffusion in the boundary layer
$E(i,j)$	potential difference: $E_j - E_i$
$E(i,j)_t$	potential difference at time t
E_A	activation energy
E_c	Nernst contribution to potential difference
E_D	liquid junction (diffusion) potential
E_m	membrane potential
E_s	streaming potential
F	structural resistance coefficient (formation factor); the subscripts B, M, M-T, S and W indicate the models to which the factors apply
F_a	Faraday constant
F_c	correction factor: eq. (4-12)
G	correction factor: eq. (4-10)
h	thickness of the plug
H	correction factor: section 4.4b
ΔH^*	activation enthalpy
$I_\pm, I_+, I_-$	functions in the diffuse double layer theory for spherical particles
I_o, I_1	modified Bessel functions of the first kind of zero and first order, resp.
I, i	electrical current
$I(i,j')_t$	electrical current through the electrodes i and j' at time t
$I(i)_t$	streaming current at time t: eq. (3-73)
I_m	instantaneous value of the streaming current
I_s	streaming current
$I_{s,ac}$	alternating streaming current
J_v	volume flux through the porous system
J_v'	convection velocity
J_s	salt flux
J_s'	salt flux per unit area
J_i	flux of species i
k	Boltzmann constant
k^*	permeability coefficient

k^*_H	permeability coefficient according to Happel: eq. (4-25)
K	specific conductivity of the electrolyte
$\bar{K}$	specific conductivity of the disperse system
K'	specific conductivity of the particle
K_s	specific excess conductivity: $K_s = K_p - K$
K_p	specific conductivity of the pore liquid in a plug
K_c	Kozeny constant
L_{ij}	phenomenological coefficient: table 3-1
L_p	filtration coefficient
$m^{\pm}$	dimensionless parameters: eq. (6-1)
m	$= m^+ = m^-$
p	volume fraction
$p^{\pm}_{\Delta}$	$= D^{\pm} / D^{\pm}_{\Delta}$: dimensionless parameter
p_{Δ}	$= p^+_{\Delta} = p^-_{\Delta}$
ΔP	(hydrostatic) pressure difference
r	radial distance in cylindrical or spherical coordinates
R	gas constant
R	dimensionless radial coordinate: κr (section 4.4)
R_d	diffusion resistance
R_e	external resistance
R_m	resistance determined from E_s and I_m
R_p	plug resistance
R_s	shunt resistance
t	time; temperature
T	absolute temperature
t_i	transport number of species i, with i = 1,2,3 for cation, anion and water, resp.
$\tilde{t}^a_i$	apparent transport number of species i
UX^{-1}	electrophoretic mobility
$\ddot{u}_{ef}$	dimensionless electrophoretic mobility
v, v_o	sedimentation velocity
x,y	rectangular coordinates
X	fixed charge density: section 3.3.2
z_i	valence of ionic species i
Z	impedance
Z',Z"	real and imaginary part of Z, resp.
α	efficiency factor
β	electro-osmotic permeability: section 3.2
β^*	dimensionless parameter defined by eq. (4-13)
γ	correction factor: section 4.4b

Δ_{ev}	boundary layer thickness as inferred from the electroviscous effect
$\Delta_{G-C}, \Delta(\psi_d, \zeta)$	layer thickness defined by eq. (5-41)
Δ_h	hydrodynamically effective layer thickness
ε	porosity
ε_o	absolute permittivity of free space
ε_r	relative permittivity
ζ	zeta-potential; electrokinetic potential
$\tilde{\zeta}$	$= F_a\zeta/RT$
ζ_a	apparent zeta-potential
ζ_c	corrected zeta-potential
η	viscosity
κ	Debye - Hückel reciprocal distance
$\tilde{\kappa}$	double layer parameter defined by eq. (4-27)
κ^*	electrical conductance at zero flow
κ^σ	specific surface conductance
κ^σ_{ek}	specific surface conductance beyond the plane of shear
κ^σ_Δ	specific surface conductance inside the plane of shear
κ^σ_t	total specific surface conductance
Λ	molar conductivity of the electrolyte solution
Λ_o	ibid. at infinite dilution
$\Lambda_\pm$	molar conductivity of cations and anions
$\Lambda^\Delta_\pm$	molar conductivity of cations and anions in the boundary layer
μ	dipole moment; the subscripts D-S and H-B indicate the models to which the dipole moment apply
$\Delta\mu_s$	difference in chemical potential of salt across the porous system
ν	frequency of the applied field
ν_i	number of ions of species i in one mole of salt
$\Delta\pi_s$	difference in osmotic pressure across the porous system
ρ	density
σ	reflection coefficient
σ^*	parameter defined by eq. (3-22)
σ_+, σ_-	counter charge density due to cations and anions, resp.
σ_o	surface charge density
σ_t	total charge density effective in conduction
σ_{ek}	electrokinetic charge density
σ_Δ	Δ-layer charge density
τ	parameter defined by eq. (3-21)
τ_{rel}	relaxation time
$\psi(x), \psi(r)$	potential distribution

ψ_d	diffuse double layer potential
$\tilde{\psi}$	reduced potential $F_a\psi/RT$
ω	solute permeability (chapter 3)
ω	angular frequency
ω_{cr}	critical angular frequency
ω'	solute permeability per unit area (chapter 3)
ω^*	solute permeability parameter (chapter 3)